e-ISSN 2586-9396

Current Applied Science and Technology

Vol. 21 No. 3
July - September 2021

KING MONGKUT'S INSTITUTE OF TECHNOLOGY LADKRABANG

Advisory Board

Current Applied Science and Technology or CAST, formerly KMITL Science and Technology Journal published by King Mongkut's Institute of Technology Ladkrabang (KMITL), has been established since its inception as KMITL Science Journal in 2001. The journal has been dedicated to publishing advanced and applied knowledge in the form of high-quality research and review articles covering the main areas of Biotechnology, Environmental Science, Agricultural Technology, Food Science and other fields related to Applied Science and Technology. Special issues devoted to important topics in advanced science and technology will occasionally be published.

The journal is an open access peer-reviewed and double blinded journal using Online Journal System (OJS) publishing online academic research and review articles. Previously, articles were published in print on a regular basis (two issues per year) since 2001 and since 2010 onward the articles have been published both in print and electronic forms starting from volume 10. In 2017, the journal title has been changed from *KMITL Science and Technology Journal* to *Current Applied Science and Technology* (CAST) (e-ISSN 2586-9396) to be more identifiable to the international scientific community according to the suggestion of Thai-Journal Citation Index Centre. The journal has been published online only since volume 17(2) (July-December, 2017). In addition, the journal has attracted researchers from other countries more than 22% according to the data. Because of more demands on publication in CAST, the editorial board has decided to publish online original academic research and review articles four issues per year (January-March, April-June, July-September and October-December) from 2021 onward.

Furthermore, the advisory board and editorial board comprises honorable and well-known members from around the world in which 50% of editorial board members are from various countries like U.K., Norway, Japan, India, China, Canada, Estonia and Egypt. Only 25% of Thai editorial board members are from the publisher organization and 25% from other publisher organizations. Most of advisory and editorial board members have high H-index according to SCOPUS.

The journal is also committed to maintaining the high level of integrity in the content published and has a Conflict of Interest policy in place. The journal uses plagiarism detection software to screen the submissions. The journal has been working closely with Thai-Journal Citation Index Centre to ensure that the journal complies with international standard of SCOPUS.

Current Applied Science and Technology (CAST)

(formerly KMITL Science and Technology Journal)

Editor

Dusanee Thanaboripat
King Mongkut's Institute of Technology Ladkrabang, Thailand

Editorial Board

CONTENTS

Review article:

Carbon Footprint of Mangosteen Farm Level Evaluation in Eastern Thailand

Narong Pleerux[1]* and Narissara Aimkuy[2]

[1]Faculty of Geoinformatics, Burapha University, Chon Buri, Thailand
[2]Regional Office of Agricultural Economics 6, Chon Buri, Thailand

Received: 4 July 2020, Revised: 30 November 2020, Accepted: 30 December 2020

Abstract

The study of the carbon footprint (CF) of agricultural crops provides important information that can help achieve low-carbon agriculture, but there are still very few studies on CF for farmed fruit. This research emphasized CF calculation for mangosteen crops at the farm level. The study was carried out on 55 mangosteen farms that belong to the Tambol Troknong Community Enterprise in the Khlung District of Chanthaburi Province, Thailand. The findings revealed that the product CF average was 1.71 ± 1.38 kg CO_2eq/kg, and the farm CF was 15,623.41 ± 16,981.27 kg CO_2eq/ha. The total CF was determined from six sources, including the application of substances such as fertilizers (organic and inorganic), pesticide and herbicide, as well as from the use of electricity and fuel. We found that most of the CF was direct emissions from electricity usage, which accounted for as much as 85.33% of the total CF. Thus, this research provides important information on the CF and level of production inputs. We developed guidelines for reducing greenhouse gas emissions from mangosteen production in the area.

Keywords: carbon footprint; life cycle assessment; greenhouse gas emission; GIS; spatial pattern
DOI 10.14456/cast.2021.34

1. Introduction

The issues of sustainable agriculture and climate change have become global concerns [1]. The concept of environmentally friendly farming has long been introduced, and it has been formulated as a policy to encourage farmers to save our Earth throughout the production chain by reducing the use of chemical fertilizers, pesticides, and herbicides. Such reduction is safer for consumers and can reduce production costs. It is well known that agriculture is one of the chief sources of greenhouse gas (GHG) [2], therefore, the great importance in sustainable agriculture is the investigation of the carbon footprint (CF) of plants [3]. CF in crop production is the amount of greenhouse gases released throughout the plant-production chain calculated in the form of carbon dioxide equivalent. Because it provides insights for farmers to more effectively view their crop-production practices, the study of CF is crucial. It helps farmers to be more aware of production factors related to farming and to plan to use them properly in the production system. Carbon labeling on the product can be a useful

*Corresponding author: Tel.: (+66) 822313386 Fax: (+66) 38102379
E-mail: narong_p@buu.ac.th

way to inform consumers of the amount of GHG expected to be released during the production process. Consumers can then choose to buy low-carbon products, which help promote low-GHG-emission agriculture, and reduces the impact on the environment [4, 5].

Life Cycle Assessment (LCA) principles are taken into account in CF calculations throughout the production process, e.g., production inputs, transport, distribution, and product-scraps disposal. CFs are used in agriculture, especially when growing crops such as beans and grains (rice, wheat, and corn) [6-10], potatoes and sugarcane [11], and organic vegetables [12, 13]. In previous studies, however, CF calculation was not applied to horticulture because of the long production time and harvest periods involved. It requires more time to record the data and the assessment is more difficult than for grain and field crops. Particularly in Thailand, there are only a few studies on the CF of horticulture. The Tambol Troknong Community Enterprise (TTCE) is located in Khlung District, Chanthaburi Province where it is one of high-quality mangosteen plants in Thailand. Previous studies investigated the CF of mangosteen production during the 2013 and 2016 production year and were focused on the calculation of CF for all member farms in TTCE [14, 15]. Therefore, in our study, we aimed to calculate the CF from mangosteen production by participating members of the Tambol Troknong Community Enterprise (TTCE) in the Khlung District, Chanthaburi Province. We focused on the 2019 production year. Using LCA cradle-to-gate principles, we covered the entire production process, obtaining relevant factors from production through harvest. Our research results provide insights into CF sources and level of emissions from mangosteen production at each farm. Also, the findings will be beneficial to farmers in governing factors involved in farming production, leading to effective reduction of costs and GHG emissions. Moreover, about 70% of TTCE's mangosteen production is exported to foreign countries. The major export markets are China, Korea and Japan. The trend of global trade has begun to focus on environmentally conscious and non-global warming goods or products. It is clear that our research can be seen as being part of a long-term plan for the benefit of exports to avoid problems with CF-related trade barriers that may occur in the future.

2. Materials and Methods

2.1 Study area

The study was carried out on 55 TTCE member farms in the Troknong subdistrict, Khlung District, Chanthaburi Province. The research project covered a total area of 4,361 ha (Figure 1). The Troknong subdistrict in Thailand is an area that has been chosen to be a green agricultural city. It is a good source of high-quality mangosteen plants and fruit. Most of the mangosteen products from this area are selected for export to foreign countries.

2.2 Boundaries of mangosteen farms

The process of delineating the boundaries of participating mangosteen farms initially included downloading satellite-image data for the Troknong subdistrict in 2019 from Google Earth and assigning a coordinate system for the image. Then the boundaries of the 55 mangosteen farms were digitized from the satellite imagery. Finally, all the farms' attribute data (farmers' names, addresses, areas, and other information) were created.

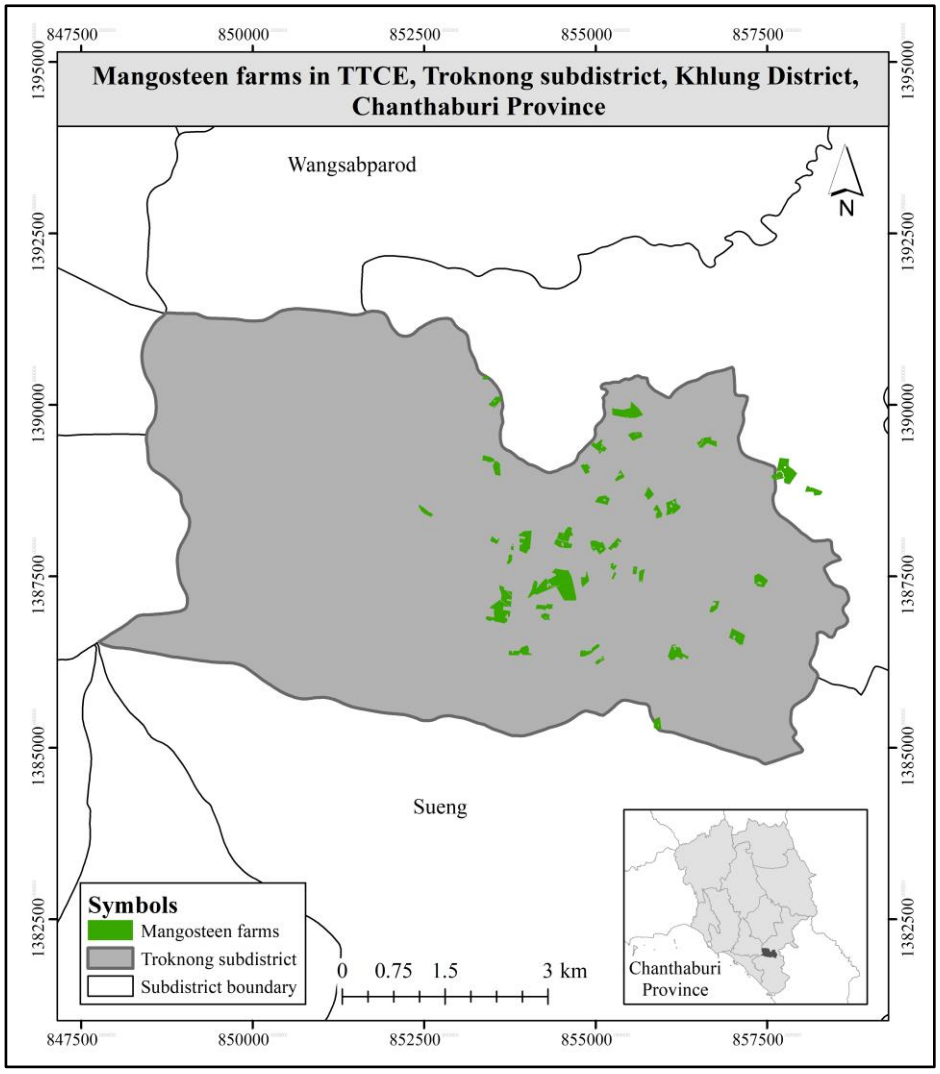

Figure 1. Study area: 55 mangosteen farms in Tambol Troknong Community Enterprise (TTCE), in Troknong subdistrict, Khlung District, Chanthaburi Province, Thailand

2.3 System boundary

This study aimed to investigate GHG emissions from mangosteen production at the farm level using LCA cradle-to-gate principles. We collected primary data on farm inputs, machinery (electric water pump and lawn mower), and transportation (inputs and yields) based on the actual records of the 2019 production year. The data included quantitative inputs (organic fertilizer, inorganic fertilizer, pesticide and herbicide, other substances, electricity, and fuel) [9, 16], outputs (products and wastes), and farm operation data that covered growth stages of mangosteens: shoot development (August-October 2018), inflorescence development (November-December 2018), flowering (January-February 2019), fruit development (March 2019), and fruit maturation (April-July 2019). The system boundary of CF calculation is illustrated in Figure 2.

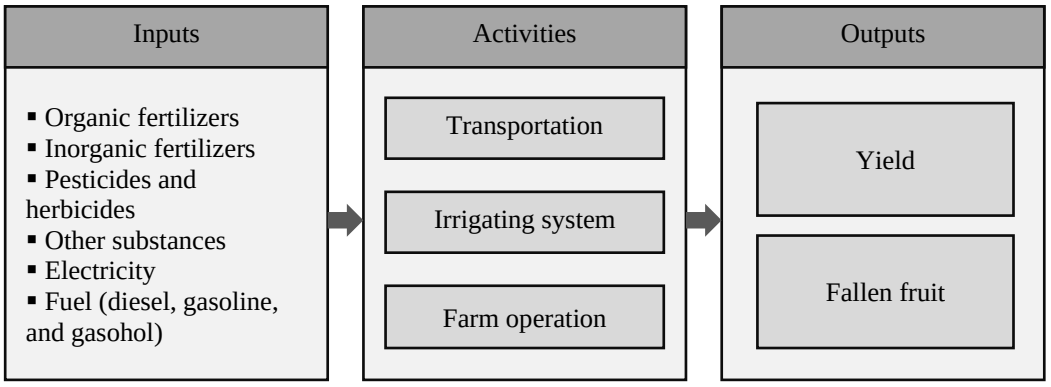

Figure 2. System boundary of the life-cycle CFs of mangosteens

In addition, on all 55 participating farms, it was specified that the trees must have fruits, and during the study period, farmers must not change land use (e.g., they were not permitted to cut down mangosteen trees and replace them with other crops). The CF was divided into two types: product carbon footprint (PCF) and farm carbon footprint (FCF). In this study, global warming potential (GWP) was assessed based on the direct and indirect emissions of carbon dioxide (CO_2) involved in mangosteen production activity for each farm [12].

2.4 Calculation of mangosteens' carbon footprint (CF)

CF calculations for mangosteen production were primarily based on the cradle-to-gate LCA concept, which covered the entire production cycle. This encompassed the entire production process in 2019 from the procedure to obtain the relevant factors related to fruit harvest. The data used in the CF calculation were obtained from in-depth interviews of the 55 farmers participating in the research project. The interview form was divided into six main groups of factors or usages affecting production: organic fertilizer, inorganic fertilizer, pesticide and herbicide, other substances, electricity, and fuel; the form was also designed to acquire other basic information such as number of mangosteen trees, production statistics, and the amount of wasted (fallen) fruit.

CF results are shown as carbon equivalent (kg CO_2eq) and are divided into two forms, product carbon footprint (PCF) and farm carbon footprint (FCF). PCF is defined as CF value per production unit (kg CO_2eq/kg) and FCF is CF value per unit area (kg CO_2eq/ha) [8, 16]:

$$PCF_n = \sum I_i \times EF_i \quad (1)$$

$$FCF_n = PCF \times Y_n \quad (2)$$

where I is the material or energy input (as kg/kg, l/kg, or kWh/kg), i is the kind of material or energy input, EF is GHG emission factor (kg CO_2eq/kg), Y is the yield per unit area of mangosteen production (kg/ha), and n is the number of farms.

Both PCF and FCF were calculated and shown on a base map using ArcGIS Desktop 10.0 software. Values for GHG emission factors from the Thailand Greenhouse Gas Management Organization in 2019 [17] were used in the CF calculations (Table 1).

Table 1. Greenhouse gas emission factors for calculating carbon footprint in mangosteen production

Material or energy usage	Emission factor	Material or energy usage	Emission factor
Chicken manure	0.32 kg CO_2eq/kg	Dolomite	0.03 kg CO_2eq/kg
Pig manure	0.26 kg CO_2eq/kg	Paraquat	3.23 kg CO_2eq/l
Cow manure	0.25 kg CO_2eq/kg	Glyphosate	16.00 kg CO_2eq/l
OF (pellet)	0.25 kg CO_2eq/kg	Abamectin	3.23 kg CO_2eq/l
OF (liquid)	0.18 kg CO_2eq/kg	Imidacloprid	3.23 kg CO_2eq/l
IF 15-15-15	1.50 kg CO_2eq/kg	Cypermethrin	3.23 kg CO_2eq/l
IF 8-24-24	1.14 kg CO_2eq/kg	Methomedfos	3.23 kg CO_2eq/l
IF 13-13-21	1.35 kg CO_2eq/kg	Chlorpyrifos	3.23 kg CO_2eq/l
IF 16-16-16	1.61 kg CO_2eq/kg	Surfactant	3.23 kg CO_2eq/l
IF 46-0-0	3.67 kg CO_2eq/kg	Flower-bud hormone	3.23 kg CO_2eq/l
IF 17-17-17	1.71 kg CO_2eq/kg	Zinc (liquid)	2.91 kg CO_2eq/l
IF 18-0-8	1.48 kg CO_2eq/kg	Mangosteen fermented water	0.89 kg CO_2eq/l
IF 20-15-15	1.91 kg CO_2eq/kg	Diesel fuel	2.74 kg CO_2eq/l
IF 18-4-5	1.53 kg CO_2eq/kg	Gasoline	2.24 kg CO_2eq/l
Sulfur powder	0.11 kg CO_2eq/kg	Gasohol fuel	2.24 kg CO_2eq/l
Hormone powder	0.25 kg CO_2eq/kg	Electricity	0.69 kg CO_2eq/kWh

Note: OF is organic fertilizer and IF is inorganic fertilizer.

3. Results and Discussion

3.1 Basic data

Mangosteen (*Garcinicmangostana* L.) is a large tropical evergreen tree with 6-25 m tall. The temperature range for growing and producing fruits is 25-35 °C, a relative humidity 75-85%, and soil with a pH of 5.5-6.5. Mangosteen trees may reach fruit – bearing in as little as 7 years. At age 30-45 years in full maturity, trees as old as 100 years still produce fruit [18].

According to a survey and data collection on all 55 mangosteen farms in 2019, a total combined area of 92.74 ha was planted with 11,023 mangosteen trees, which corresponds to an average planting density of 118.86 trees per hectare. The average age of the trees was 32 years. The youngest tree was 9 years (farm number 55) and the oldest tree was 71 years (farm number 4). Total useful yield was 855,067 kg; if fallen fruit (31,120 kg) was included, average yield was 9,555.85 kg/ha. Mangosteen cultivation averaged 76.79% in mixed orchards and 23.21% in single plantations. Five types of soil were found on the 55 mangosteen farms: sandy loam (64.29%), loam (21.43%), loamy clay (7.14%), sandy clay (5.36%), and clay (1.78%).

As for the production inputs used on the 55 mangosteen farms, we found that organic fertilizers and inorganic fertilizers totaled 165,047.45 kg and 29,379.25 kg, respectively; pesticides and herbicides totaled 681.65 l; and other substances amounted to 13,035 kg. As for energy consumed, electricity use was 1,576,882.02 kWh (for watering the mangosteen trees), and fuels (diesel, gasoline, and gasohol) totaled 1,296.71 l, which the farmers used the four-wheel trucks to transport inputs and yields (Table 2). Each farm transported inputs from store to farm and yields from farm to market. The average transport distance was 65.45 km; farm number 11 had the shortest distance of 36 km, and farm number 13 had the longest distance of 206 km. As this farm (number 13) had the most cultivated area of 7.36 ha, a large amount of production inputs was needed, and

Table 2. Inputs, output, and waste from mangosteen production in 2019

Item	Quantity	Unit
Input		
Organic fertilizers	165,047.45	kg
Inorganic fertilizers	29,379.25	kg
Pesticides and herbicides	681.65	l
Other substances	13,035.00	kg
Electricity	1,576,882.02	kWh
Fuels	1,296.71	l
Output		
Yield	855,067.00	kg
Waste		
Fallen fruit	31,120.00	kg

the yields were correspondingly large. Therefore, it had the greatest total distance of transport compared to other farms.

3.2 Product carbon footprints (PCFs) and farm CFs of mangosteen

From the PCF calculation for mangosteens, the mean and standard deviation were computed as 1.71 ± 1.3 kg CO_2eq/kg. There were 22 farms or 40% that were <0.89 kg CO_2eq/kg, which was the CF value for the standard 1-kg mangosteen [17]. When considering the PCF value for each farm, we found that farm number 16 had the lowest PCF, equivalent to 0.06 kg CO_2eq/kg. This farm has 35 mangosteen trees on 0.32 ha with a yield of 3,140 kg. The main reason why this farm had the lowest PCF was that it used very low amounts of inputs, especially energy usage in the form of electricity. Because it is near a waterfall (304 m), the farmers dug a channel to divert water from the waterfall into the mangosteen plantation without first having to pump water into a pond. This resulted in less electricity use and therefore very low PCF values compared to other farms of equal area (e.g., farm numbers 15 and 32 with PCFs of 1.72 and 2.63 kg CO_2eq/kg, respectively). Farm number 15 had very high electricity use, as it has 100 mangosteen trees (almost triple the number on farm number 16), so more water had to be pumped to irrigate the trees, whereas farm number 32 had very high organic fertilizer use (13.71 times more than farm number 16), despite the fact that there were only 50 mangosteen trees being grown on the farm. Farm number 50 had the highest PCF, equivalent to 4.72 kg CO_2eq/kg. It had 128 mangosteen trees on 1.28 ha with a yield of 5,564 kg, or 4,346.88 kg/ha (2.26 times less than farm number 16). Data for this farm (number 50) showed that the farm had higher production inputs but lower yields than did farm number 16. The main reason was that this farm was further from irrigation water (1,000 m), with other mangosteen farms separating it from the water source. Therefore, the farmers had to pump water into the pond on the farm before watering the mangosteen trees, resulting in higher electricity usage and PCFs than other farms. Farm number 13 was the largest farm with an area of 7.36 ha. It had the highest number of 800 trees with yield of 85,000 kg, equivalent to 11,548.91 kg/ha, which was 2.66 times more than farm number 50 because there was a good management system applied to farm number 13. It used less electricity than farm number 50 despite having more areas and trees. As a result, this farm (number 13) had a PCF value of only 0.32 kg CO_2eq/kg (Figure 3).

The mean and standard deviation for FCF for all 55 farms combined was 15,623.41 ± 16,981.27 kg CO_2eq/ha. With the lowest PCF and a yield equal to 9,812.50 kg/ha, farm number 16 also had the lowest FCF (636.48 kg CO_2eq/ha) of any of the farms. Farm number 26 had the highest FCF (79,354.76 kg CO_2eq/ha) and one of the highest PCFs (4.57 kg CO_2eq/kg), but its high yield (17,357 kg/ha) ranked it fourth among all 55 farms. Farm number 3 has the highest yield (19,062.50

kg/ha), but its FCF was low (11,818.80 kg CO_2eq/ha) because the PCF was only 0.62 kg CO_2eq/kg. Farm number 55 has the lowest yield (1,444.71 kg/ha), but its FCF was 28,797.90 kg CO_2eq/ha, while its PCF was almost the highest of all (4.60 kg CO_2eq/kg). The main reason was the use of electricity to pump large quantities of water to the mangosteen trees. However, it had much lower yield than other farms, resulting in a very high CF of 1 kg of mangosteen (Figure 3).

Figure 3 presents the relationship between the PCF and the FCF in the same direction, when the PCF was high, the FCF was high as well. However, when considering the top five PCF values, it was found that there were three farms that did not correlate in the same direction: farm number 50 (PCF = 4.72 kg CO_2eq/kg, FCF = 20,517.20 kg CO_2eq/ha), farm number 23 (PCF = 4.42 kg CO_2eq/kg, FCF = 11,301.10 kg CO_2eq/ha), and farm number 55 (PCF = 4.60 kg CO_2eq/kg, FCF = 28,797.90 kg CO_2eq/ha), since all three farms had very low yields with 2,556.82, 4,346.88, and 1,444.71 kg/ha, respectively. In particular, farm number 55 had the lowest yield compared to other farms. This shows that these farms used large quantities of inputs, but produced low yields and also high CFs. Therefore, these farms may need to be improved and planned for the use of inputs properly such as timing and volumes for watering the mangosteen trees, soil examination for fertilizers that is consistent with soil properties.

In the 2019 production year, TTCE had a total CF of 1.40×10^6 kg CO_2eq/yr. The total mangosteen production was 886,187 kg, which was equal to 0.25% of the total mangosteen production in Thailand, which was 351,760,000 kg [19]. We roughly estimated the CF of the remaining 99.75% of the country's mangosteen production in 2019 to have been 5.55×10^8 kg CO_2eq/yr.

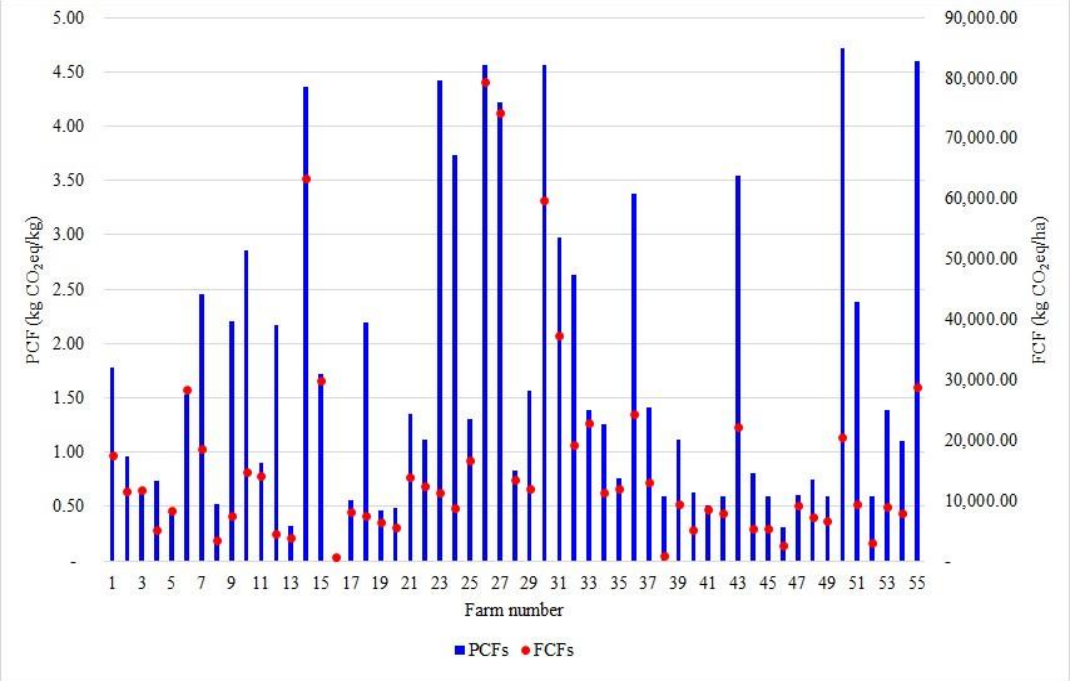

Figure 3. Product and farm carbon footprints of mangosteens in the production year 2019

The inputs used in mangosteen production were organic fertilizer, inorganic fertilizer, pesticide and herbicide, other substances, electricity, and fuel. When calculating the proportion of inputs that contributed towards CF from the production of 1 kg of mangosteen, we found that electricity was highest (85.33%); it was used mainly for pumping water to the mangosteen trees. During the dry season (November-February), no rain fell in the area, but the mangosteen trees still needed water, especially during February continuing into March, when the trees needed water to nourish the young fruit and support their growth. The farmers had to meet this demand by pumping water from wells or irrigation canals using electricity. As a result, a large amount of electricity was used, and that had an impact on CF. The inputs with the next-highest impacts were organic fertilizer and inorganic fertilizer, accounting for 8.92% and 4.67%, respectively. Even if the inorganic fertilizer had a higher emission factor than organic fertilizer, the amount of organic fertilizer used (165,047.45 kg) was 5.62 times higher than that of inorganic fertilizer (29,379.25 kg), thereby making the proportion of organic fertilizer greater than inorganic fertilizer which was an advantage that farmers in TTCE used organic fertilizers rather than inorganic fertilizers. This is because organic fertilizer has a much lower emission factor than inorganic fertilizer. Most importantly, organic fertilizer leaves no residue and can affect the health of consumers (Figure 4).

Regarding other input amounts, we found that the farmers used only small amounts, each <1%, and thus had little impact on CFs. Pesticide and herbicide used were 0.53% and other substances used (such as flower-bud hormone and zinc) were only 0.21%. Fuel including diesel, gasoline, and gasohol, which were mostly used in trucks to transport mangosteens and inputs, amounted to 0.34%. It can be seen that farmers used fuel only for transportation, as fuel is expensive. When they wanted to pump water to the mangosteen trees, they chose to use an electric water pump, which was cost-effective rather than using fuel (Figure 4).

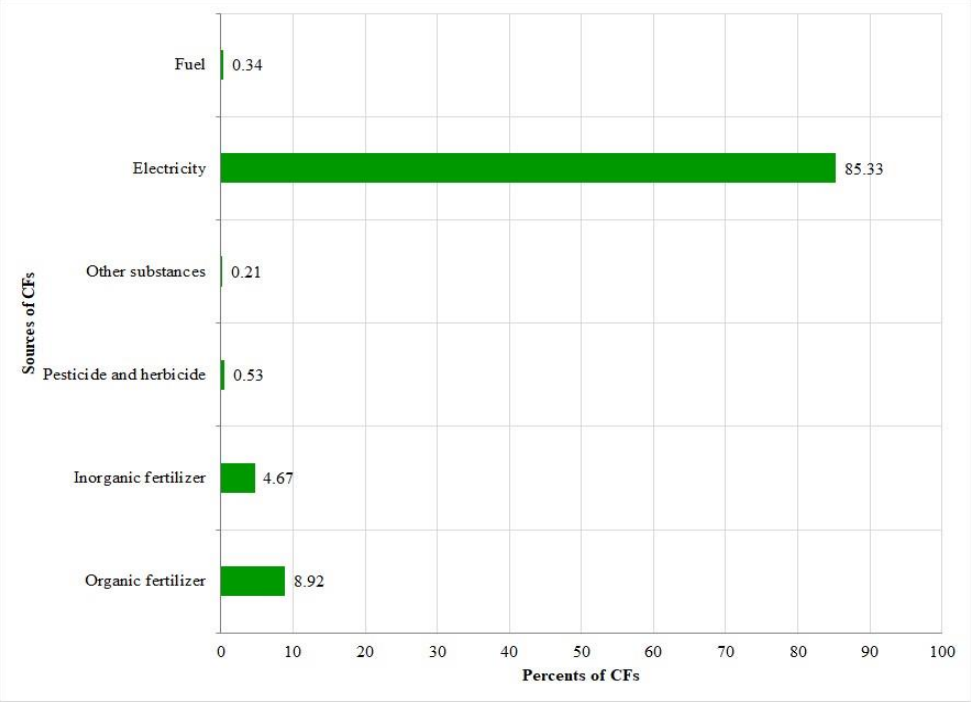

Figure 4. Proportions of carbon footprint sources per kilogram of mangosteen production by TTCE (55 participating farms) in the production year 2019

3.3 Spatial pattern of PCFs

The spatial distribution of PCFs for the mangosteen farms was unpredictable, meaning that those with low or high PCFs were scattered throughout the subdistrict (Figure 5). At the north end of the subdistrict and near the waterfall (304 m) that it used, farm number 16 had the lowest PCF (0.06 kg CO_2eq/kg). Farm number 46, in the middle of the subdistrict and also close to water sources (50 m), had a higher PCF (0.31 kg CO_2eq/kg), similar to that of farm number 32 (0.32 kg CO_2eq/kg), which was also central in the subdistrict and close to water sources (65 m). Farm number 50, in the southwestern part of the subdistrict and away from water sources (1,000 m), had the highest PCF (4.72 kg CO_2eq/kg). We, therefore, concluded that farms with low or high PCF were not related to the location or to the distance from the water source, although the distance from the water source did affect electricity usage when pumping water to the mangosteen trees. For farms near water sources or irrigation canals, the farmers could divert or pump water directly, but for those far from water sources, they first had to pump water into holding ponds. Accordingly, farms that were far from water sources likely used more electricity than those near water sources, thereby affecting the CF.

The distribution of low to high PCFs calculated from the production of 1 kg of mangosteen (kg CO_2eq/kg) (Figure 5) shows that they were dispersed across the area with unpredictable patterns. Most TTCE farmers watered their mangosteen trees in accordance with patterns that were previously practiced, on a definite schedule and with a set amount of irrigation, regardless of weather conditions. They did not use rain-forecast data to plan watering their crops. Occasionally it rained when they were watering the mangosteen trees, thereby causing the trees to receive higher amounts of water than necessary. Watering the trees required electricity use, which directly impacted CF. Another important factor affecting the distribution pattern of PCF is soil type. Based on a survey of the TTCE mangosteen farms, most of the soils on the farms were sandy loam; four other types were loam, loamy clay, sandy clay, and clay. The different soil types would also have affected water consumption on mangosteen farms.

We compared PCFs for the 55 different farms with those of the standard PCF (0.89 kg CO_2eq/kg) set by the Thailand Greenhouse Gas Management Organization [17]. We classified the 55 farms as follows: Of the 28 mangosteen farms that were close to water sources or irrigation canals, 11 farms had PCFs lower than those standard values, and the other 17 exceeded the standard values. Of the 27 mangosteen farms that were far from water sources or irrigation canals, 10 farms had PCFs lower than the standard PCFs, and the other 17 exceeded the standard values (Figure 5). Thus, whether the farms were near or far from water sources apparently had little or no effect on the PCF for each farm. PCF mainly depended on the watering pattern, soil types, and number of mangosteen trees planted on each farm.

4. Conclusions

Agriculture is one of the causes of the CF. When investigating the origin and quantity of CF for mangosteen production on a farm basis, the results of this study can be used to determine ways to more usefully reduce CF in the production process. According to data for the 55 TTCE mangosteen farms, the average PCF (1.55 kg CO_2eq/kg) was higher than the standard PCF set in 2016. The main cause of the higher CFs was electricity use to pump water to the mangosteen trees. Therefore, one way to reduce CF is to reduce water use, but watering must be in line with the needs of the mangosteen trees by introducing the farmers to proper knowledge and technology so that they can improve the crop-watering pattern or schedule. For instance, they can use the Meteorological

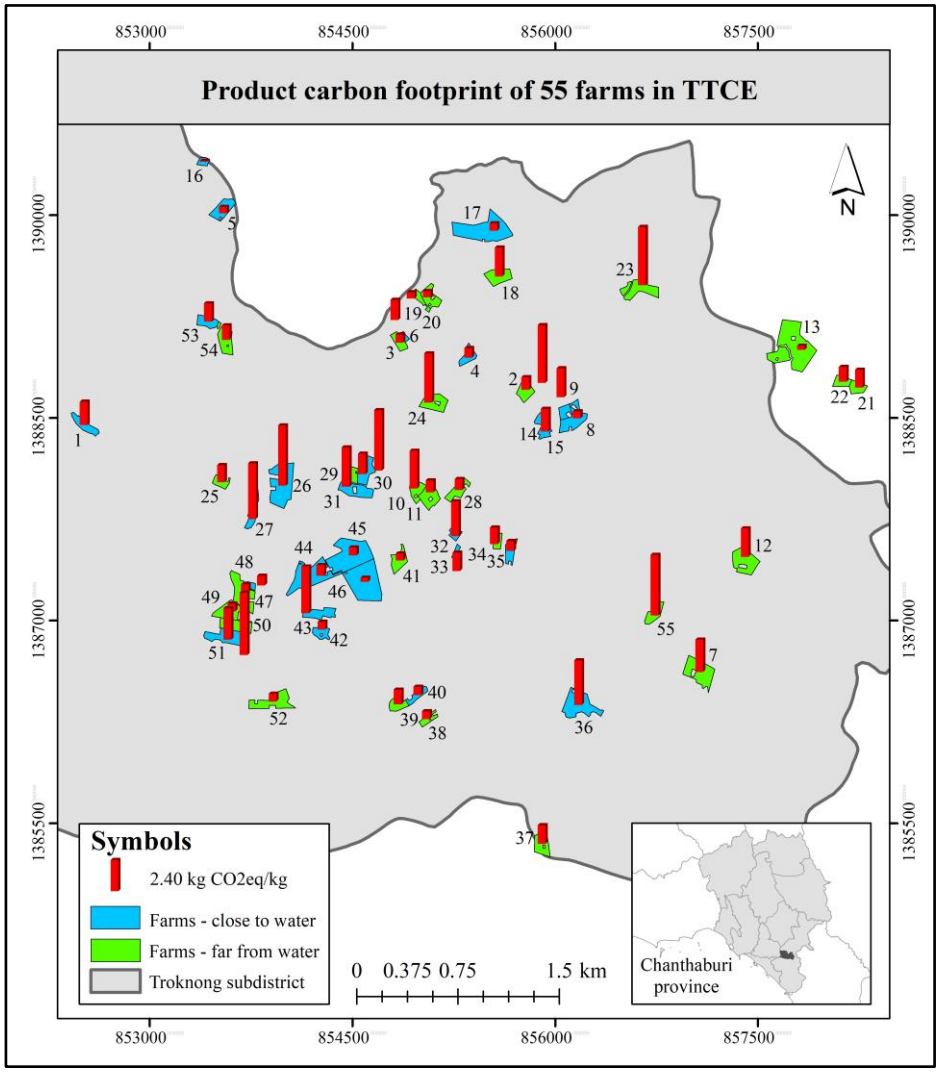

Figure 5. Product carbon footprints (PCFs) of 55 farms in TTCE in the production year 2019

Forecast Rainfall Application to help them plan the water supply for the mangosteen trees. This would help them provide amounts and timing of water application that are consistent with the weather and that do not exceed the water needs of the mangosteen trees. This can also result in saving electricity, time, labor, and costs, thereby ultimately reducing CF.

Because the production period is longer than that of crops such as rice and other cereal grains, and it takes a long time to collect the data, and there are very few studies on the CF from horticulture. In particular, the study of the mangosteen CF is new, and the only prior studies in Thailand were done on TTCE plantations and were the first CF studies in the production years 2013 and 2016 done by the Regional Office of Agricultural Economics 6. This ongoing research collected data on the mangosteen farms in the 2019 production year. It provides important information forecasting the trend of CF change in each production year and helps in determining ways to

sustainably reduce CF. It also raises farmers' awareness of using the right amounts of inputs and having the least environmental impact. Another potential benefit is that it will help prevent future trade barriers from countries around the world. We, therefore, consider the CF study of TTCE mangosteen production to be a long-term effort that is in line with the changing system of global trade, which is becoming more environmentally conscious of the global-warming issue.

5. Acknowledgements

This research project was financed by Thailand Research Fund (TRF). Most grateful thanks to the farmers in Tambol Troknong Community Enterprise for the data and Prof. Dr. Aree Wiboonpongse for valuable comments and insightful suggestions.

References

[1] Wang, L., Li, L., Cheng, K. and Pan, G., 2019. Comprehensive evaluation of environmental footprint of regional crop production: A case study of Chizhou City, China. *Ecological Economics*, 164, 1-12.

[2] Ruviaro, C.F., Gianezini, M., Brandão, F.S., Winck, C.A. and Dewes, H., 2012. Life cycle assessment in Brazilian agriculture facing worldwide trends. *Journal of Cleaner Production*, 28, 9-24.

[3] Smith, P., Haberl, H., Popp, A., Erb, K., Lauk, C., Harper, R., Tubiello, F.N., Pinto, A.S., Jafari, M., Sohi, S., Masera, O., Böttcher, H., Berndes, G., Bustamante, M., Ahammad, H., Clark, H., Dong, H., Elsiddig, E.A., Mbow, C., Ravindranath, N.H., Rice, R.W., Abad, C.R., Romanovskaya, A., Sperling, F., Herrero, M., House, J.I. and Rose, S., 2013. How much land-based greenhouse gas mitigation can be achieved without compromising food security and environmental goals?. *Global Change Biology*, 19, 2285-2302.

[4] Gan, Y.T., Liang, C., Chai, Q., Lemke, R.L., Campbell, C.A. and Zentner R.P. , 2014. Improving farming practices reduces the carbon footprint of spring wheat production. *Nature Communication*, 5, 1-13.

[5] Röös, E. and Tjärnemo, H., 2011. Challenges of carbon labelling of food products: a consumer research perspective. *British Food Journal*, 11, 982-996.

[6] Alam, M.K., Bell, R.W. and Biswas, W.K., 2019. Decreasing the carbon footprint of an intensive rice-based cropping system using conservation agriculture on the Eastern Gangetic Plains. *Journal of Cleaner Production*, 218, 259-272.

[7] Plaza-Bonillaa, D., Nogué-Serraa, I., Raffaillacc, D., Cantero-Martíneza, C. and Justes, E., 2018. Carbon footprint of cropping systems with grain legumes and cover crops: A case-study in SW France. *Agricultural Systems*, 167, 92-102.

[8] Xu, X. and Lan, Y., 2017. Spatial and temporal patterns of carbon footprints of grain crops in China. *Journal of Cleaner Production*, 146, 218-227.

[9] Zhang, D., Shen, J., Zhang, F., Li, Y. and Zhang, F., 2017. Carbon footprint of grain production in China. *Scientific Reports*, 7, 1-11.

[10] Zhang, W., He, X., Zhang, Z., Gong, S., Zhang, Q., Zhang, W., Liu, D., Zou, C. and Chen, X., 2018. Carbon footprint assessment for irrigated and rainfed maize (*Zea mays* L.) production on the Loess Plateau of China. *Biosystem Engineering*, 167, 75-86.

[11] Liu, W., Zhang, G., Wang, X., Lua, F. and Ouyang, Z., 2018. Carbon footprint of main crop production in China: Magnitude, spatial-temporal pattern and attribution. *Science of the Total Environment*, 645, 1296-1308.

[12] Adewale, C., Reganold, J.P., Higgins, S., Evans, R.D. and Carpenter-Boggs, L., 2019. Agricultural carbon footprint is farm specific: Case study of two organic farms. *Journal of Cleaner Production*, 229, 795-805.
[13] Knudsen, M.T., Meyer- Aurich, A., Olesen, J.E., Chirinda, N. and Hermansen, J.E., 2014. Carbon footprints of crops from organic and conventional arable crop rotations – using a life cycle assessment approach. *Journal of Cleaner Production*, 64, 609-618.
[14] Regional Office of Agricultural Economics 6, 2014. *Study of Greenhouse Gas Emissions of Packed Mangosteen in Troknong Green City, Chanthaburi*. [online] Available at: http://oaezone.oae.go.th/assets/portals/15/ebookcategory/133_vijai_61/vijai_61/files/assets/basic-html/page1.html
[15] Regional Office of Agricultural Economics 6, 2017. *Study of Greenhouse Gas Emissions of Packed Durian and Mangosteen in Troknong Green City, Chanthaburi*. [online] Available at: http://oaezone.oae.go.th/assets/portals/15/ebookcategory/133_vijai_61/vijai_61/files/assets/basic-html/page1.html
[16] Yan, M., Cheng, K., Luo, T., Yan, Y., Pan, G. and Rees, R.M., 2015. Carbon footprint of grain crop production in China – based on farm survey data. *Journal of Cleaner Production*, 104, 130-138.
[17] Thailand Greenhouse Gas Management Organization, 2019. *GHG Emission Factors*. [online] Available at: http://thaicarbonlabel.tgo.or.th/admin/uploadfiles/emission/ts_f2e7bb377d.pdf
[18] Agricultural Research Development Agency (Public Organization), 2020. *Batonical Characteristics of Mangosteen*. [online] Available at: https://www.arda.or.th/kasetinfo/south/mangosteen/controller/index.php
[19] Office of Agricultural Economics, 2019. *Mangosteen: Perennial Area, Production Area, Production and Yield Per Rai in Year 2019*. [online] Available at: http://www.oae.go.th/assets/portals/1/ fileups/prcaidata/files/1mangosteen%202562.pdf

A New Approach for Stabilization of Gac Oil by Natural Antioxidants

Thi Quynh Nhu Nguyen[1,3], Van Nguyen Tran[2], Le Thi Hong Anh[3], Hoang Nhu Bui[3], Duc Duy Tran[3] and Helena Cizkova[1]*

[1]Falcuty of Food and Biochemical Technology, University of Chemistry and Technology, Prague, Czech
[2]Department of Biochemistry and Microbiology, University of Chemistry and Technology, Prague, Czech
[3]Falcuty of Food Science and Technology, University of Food Industry (HUFI), Ho Chi Minh City, Viet Nam

Received: 9 September 2020, Revised: 4 December 2020, Accepted: 7 January 2021

Abstract

Gac oil contains a high amount of unsaturated fatty acids and carotenoids that are easily degraded during production and storage. Therefore, it is necessary to have appropriate methods to limit the oxidation in gac oil that leads to undesirable by-products. Green tea and rosemary extracts exhibit excellent antioxidant activities against oxidation in vegetable oils. Here, the protective effects of green tea and rosemary extracts on gac oil were evaluated for 7 consecutive days at 60ºC. Supplementation with 4000 mg/kg green tea and rosemary extracts significantly improved oil stability by reduction of 35 and 47% peroxide values; produced higher carotenoid content of about 0.31 and 0.35 mg/g; and maintaining 82 and 92% rancimat values when compared to initial samples, respectively. In comparison to BHA and BHT at 150 mg/kg, green tea extracts at 4000 mg/kg showed higher antioxidant efficacies and sensory scores.

Keywords: gac oilantioxidants; carotenoids; peroxide value; rancimat
DOI 10.14456/cast.2021.35

1. Introduction

Gac fruit (*Momordica cochinchinensis* Spreng) is widely used in traditional Asian cuisines due to its notable bright red seed aril, which is rich in β-carotene and lycopene [1]. Gac aril contains high concentration of fatty acid (22% w/w), including oleic (29%), palmitic (32%) and linoleic acids (20%) [2]. Moreover, the concentrations of β-carotene and lycopene are found in gac oil at 2.6 and 2.4 mg/g, respectively [3]. In addition, it also has a high level of vitamin E (at 330 mg/kg) which is considered to be one of the natural antioxidants that protects gac oil from oxidation [4]. Carotenoids are considered to be beneficial in decreasing the risk of certain cancers and eye diseases [5]. Gac supplements are a good source of provitamin A and and the consumption of gac products

*Corresponding author: Tel: + 420 220 443 014
E-mail: cizkovae@vscht.cz

such as “xoi gac” may be particularly beneficial to children suffering from anemia [6]. In addition, carotenoids such as α- and β-carotene can be metabolized into vitamin A and have an important role related to chronic disease prevention [7]. However, gac oil easily undergoes oxidation processes during storage and food processing that lead to nutrition degradation and unexpected rancidity [3, 8, 9] due to the high content of carotenoids and unsaturated fatty acid (about 70% of total fatty acid in the aril and half of them are polyunsaturated) [10]. Therefore, the use of antioxidants can be considered as a solution to help limit the degradation of gac oil during storage and processing.

Synthetic antioxidants, particularly butylated hydroxyanisole (BHA) and butylated hydroxytoluene (BHT) have been widely used to stabilize oils and fat due to their high antioxidant capacity and outstanding performance in the attenuation of oxidation reactions [11-13]. However, these antioxidants are considered to have adverse effects on human health [14, 15]. Consequently, replacing these synthetic antioxidants with natural antioxidants has become a focus of interest for researchers. Recently, many efforts have been made to prevent the oxidative degradation of oils through the use of natural antioxidant compounds [16, 17]. Natural antioxidants not only improve the stabilization of edible oils but they also increase the nutraceutical value of the oils. Such antioxidants are supposed to be safe and promptly accepted by consumers [18]. It has been reported that natural plant extracts (NPE) including green tea, rosemary, grapes and berries are potential antioxidants [11, 14, 16, 19-23].

Green tea and rosemary extract are widely used in fat oxidation prevention. Green tea extract contains important antioxidants including catechin, epicatechin, epicatechin gallate, epigallocatechin, and epigallocatechin gallate and other flavonoids [24]. The effect of green tea extract on the oxidation of seal blubber oil and menhaden oil under Schaal oven test at 65°C was reported. The excellent antioxidant activity of green tea extract in oil samples was demonstrated and its effectiveness was higher than those of BHA and BHT at concentrations greater than 200 ppm [25]. Green tea extract can be used to decelerate the oxidative process of fats in sponge cake products [26].

Rosemary extract is considered to be a safe type of natural antioxidant composed of carnosol and carnosic acid, the two frequently studied components for antioxidant activity. In addition, rosmarinic acid is another important antioxidant in rosemary and has been extensively studied in other plants [27]. According to Erkan *et al*. [28], rosemary extract, when compared to blackseed essential oil, had the higher phenolic content resulting in a higher antioxidant activity. Besides, many edible oils are effectively protected against several oxidative reactions when added to rosemary extract [11, 24, 29-32]. However, there have been no studies using natural antioxidants for gac oil. Gac oil is an abundant source of bio-accessible carotenoids (lycopene and β-carotene), which quickly degrade during storage. In this study, we evaluated the antioxidant efficacy of rosemary extract and green tea extract on gac oil for the first time, and compared their effectiveness with some synthetic antioxidants. These samples were assessed through peroxide value, carotenoids content and rancimat index.

2. Materials and Methods

2.1 Materials

A commercial rosemary extract was obtained from the leaves of *Rosmarinus officinalis* and it had a rosmarinic acid concentration of 60 mg/g. The green tea used was a flavoring preparation containing naturally occurring polyphenol content of 90 mg/g as gallic acid equivalent. Both the green tea and rosemary extract were provided by Vitablend Netherland. BHA and BHT were obtained from Golden Hope Nha Be edible oil company. Other chemicals including acetic acid (99.5%), potassium

dichromate (99.8%), petroleum ether (99.99%), chloroform (99.99%), sodium thiosulfate (99.99%), and potassium iodide (99.5%) were purchased from Chanu Co., Ltd., Viet Nam.

2.2 Gac oil extraction

Gac fruits were supplied by retailers in Ho Chi Minh city, Viet Nam. The fruit samples were immediately processed and gac arils were collected. Pulp, peel and seeds were discarded. The gac arils were then dried in a microwave at 630 W for 65 min [33]. A laboratory hydraulic press machine with pressures of 175 kg/cm² was used to extract the oil from the arils and the recovery oil was 90%. Finally, gac oil was deposited and filtered before storing at 4°C until analysis.

2.3 Sample preparation

In previous studies, green tea and rosemary extract at concentration of 2500-5000 mg/kg provided the best protection [34, 35]. The gac oil samples were heated to 50°C before adding antioxidants. The antioxidants were added and stirred so as to completely dissolved them in the oil samples and the stirring was continuously maintained at 55°C for 10 min. Then, the natural antioxidants (rosemary extracts, green tea extract) were added to the pre-heated gac oil samples at concentrations of 1000 and 4000 mg/kg (R1: 1000 mg/kg rosemary extract; R4: 4000 mg/kg rosemary extract; G1: 1000 mg/kg green tea extract; G4: 4000 mg/kg green tea extract).

Synthetic antioxidants (BHA and BHT) were employed at their legal limit of 150 mg/kg. According to Food and Drug Administration (FDA 2001) and European Union (Council Directive 1995), the safe usage levels range from 100 to 200 mg/kg [36-39]. The control samples (M0) had none of the antioxidants added. All the investigated samples and control samples were placed in reagent bottles and stored in an oven at 60°C [40-42]. The analyses were carried out after every 24 h.

2.4 Analytical methods

2.4.1 Peroxide value (PV)

The PV of gac oil samples was determined according to AOAC Official Method 965.33 [43]. Gac oil (5g) was placed into 250 ml Erlenmeyer flask and mixed with 30 ml of a mixture of acetic acid and chloroform (3:2, v/v). Then, 0.5 ml of saturated potassium iodide solution was added. After 1 min, 30 ml of distilled water was added and the titration process was started using sodium thiosulfate 0.01 N with a starch solution as an indicator until the solution became colorless. The results were calculated as milliequivalents of active oxygen per kg (meq/kg) of oil sample as follows:

$$\mathrm{PV(meq/kg)} = \frac{(\mathrm{S} - \mathrm{B}) \times \mathrm{N} \times 1000}{\text{Mass of sample (g)}} \quad (1)$$

S (ml): The titration amounts of 0.01 N sodium thiosulfate for the sample
B (ml): The titration amounts of 0.01 N sodium thiosulfate for blank
N: The normality of sodium thiosulfate solution.

2.4.2 Determination of carotenoid content

Total carotenoids were examined using the method described by Cenkowski *et al*. [44]. The method is based on the solubility of carotenoid in organic solvent. As carotenoids dissolve in organic

solvent, a yellow color is produced, and the color intensity of the solution is directly proportional to the content of carotenoid. Each oil sample (0.1 g) was accurately weighed in a 100 ml Becher. Then 10 ml of hexane was added to dissolve the oil. The color of the solution was measured at 460 nm by spectrophotometer and hexane was used as a blank. The standard curve was formulated by dissolving 0.1 g of β-carotene in 100 ml hexane and diluting to five different concentrations using two-fold serial dilution. The carotenoid concentrations were interpolated from the standard curve and expressed as mg/g β-carotene equivalents.

2.4.3 Antioxidant activity index

The Rancimat apparatus (Metrohom Series 679) was used to evaluate the oxidation stability of oil by determining the induction time of the treated and control oil samples. Oil samples (2.5 g) were weighed in reaction vessels and preheated for 10 min. Air (20 l/h) was bubbled through oil and temperature was adjusted to 100ºC. Reaction vessels were connected with absorption vessels containing 60 ml of deionized water via teflon tubing. During the heating of the sample with air, volatile compounds were collected in deionized water in the absorption vessels and this led to increasing water conductivity. Here, measuring electrodes were immersed in water, ensuring that they were continually measuring and recording the conductivity. The time from induction period until oil starts to become rancid is called induction period. The time taken to reach the conductivity induction times was recorded [45]. The antioxidant activity of supplemented antioxidants was expressed as a protection factor (PF), which is the ratio of induction time of the sample with and without antioxidant [46].

2.4.4 Sensory Evaluation

The samples were sensitively evaluated by 10 candidates selected from final year students who had been trained by the Faculty of Food Science and Technology, Food Industry University. Aroma, taste ad overall acceptability were assessed via a 9-point hedonic scale, the scale values of which ranged from 9 for extremely good and 1 for unacceptable [47].

2.5 Statistical analyses

The experiments were repeated three times. The results were expressed as the average of three replicates ± standard deviation. The results were analyzed by one-way ANOVA followed by the T-test using statgraphics software (Statgraphics Technologies, Inc., USA) and observed differences were considered statistically significant when $p < 0.05$.

3. Results and Discussion

3.1 The antioxidant performances of rosemary and green tea extracts

3.1.1 Peroxide values

The changes in PV of gac oil samples treated with rosemary and green tea extracts at different concentrations in 7 days are presented in Figure 1.

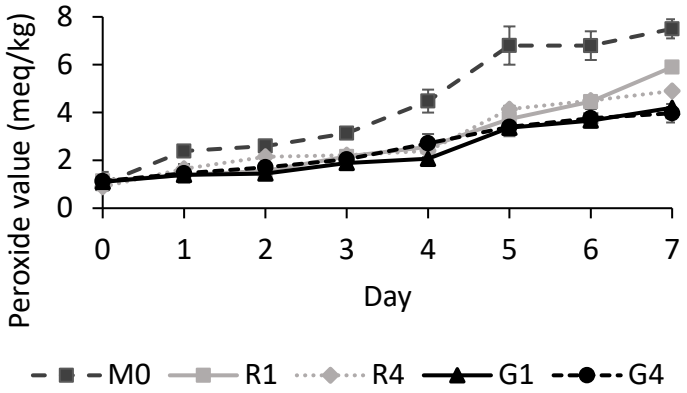

Figure 1. Peroxide value of sample treated with 1000 and 4000 mg/kg rosemary or green tea extracts for 7 days at 60ºC. M0: control sample; R1: 1000 mg/kg rosemary extract; R4: 4000 mg/kg rosemary extract; G1: 1000 mg/kg green tea extract; G4: 4000 mg/kg green tea extract

Regarding the control sample (without antioxidant), the highest PV was reached after five days of incubation (no significant PV among day 5, 6 and 7 ($p < 0.05$)). The samples treated with rosemary and green tea extracts showed significant effectiveness in reducing PV during the storage period time. Particularly, in comparison with control samples (Figure 1), the treatments with 1000 mg/kg rosemary and green tea extracts resulted in decreases of PV of 45 and 51% on day 5; and of 21 and 44% on day 7, respectively. Similar, reductions of 39 and 50% on day 5; and 35 and 47% on day 7 also observed for the supplementation of 4000 mg/kg rosemary and green tea extracts.

The oil oxidation process produces peroxides as the main initial products. Therefore, the higher the PV of the oil sample indicated, the lower the chemical stability [48]. Besides, high temperature and light are two common peroxide forming agents [49]. The peroxide value of all samples generally increased continuously over the whole 7 days of testing due to the formation of free radicals during heat treatment. These results were consistent with those obtained in previous studies [20, 40]. Malheiro *et al*. [50] studied the formation of hydroperoxide during microwave processing and its ability to prevent the formation of peroxide in the presence of tea extract.

According to Pokorny *et al*. [51], antioxidants can inhibit or retard oxidation by scavenging free radicals acting as primary antioxidant, or by a mechanism that does not involve direct scavenging of free radicals, where they act as secondary antioxidant. Based on our results, green tea extracts produced a significant reduction of peroxide value in gac oil. Green tea is notable for its phenolic compounds with antioxidant effects [52]. It is known that hydroxyl groups from aromatic rings of polyphenols react with lipid-free radicals thereby retarding lipid oxidation. Besides, polyphenols have the ability to scavenge oxygen radicals by giving an electron for the free radical in the electron transfer mechanism [53]. Green tea extract had an impressive antioxidant effect on oil stability and inhibition of hydroperoxides formation [54]. Besides, the effect of rosemary extract depends on the antioxidant activity of the extract, which is known as the phenolic content [28]. It was reported that phenolic compounds in rosemary extract can prevent transition metal ions from changing; for example, they can inhibit the change of Fe^{2+} ion into Fe^{3+} ion. Furthermore, transition metal ions at low valent states react rapidly with hydroperoxide to form alkoxy radicals in the propagation of lipid peroxidation, thus reducing induction period [55]. Comparing the effectiveness of two types of antioxidants, oil treatment with green tea extract showed greater attenuation of PV than oil treated with rosemary extract at the same concentration [22].

3.1.2 Carotenoids content

The effects of rosemary and green tea extracts on carotenoids content for 7 days at 60°C on gac oil are shown in Figure 2. In this study, the carotenoids content in the original gac oil was 2.3 ± 0.3 mg/g while in the previous study of Tran and Dang [56], about 2.0 mg/g carotenoids obtained from aril. The levels of carotenoids depend on the season, cultivar condition, harvest time, maturity and storage conditions [3].

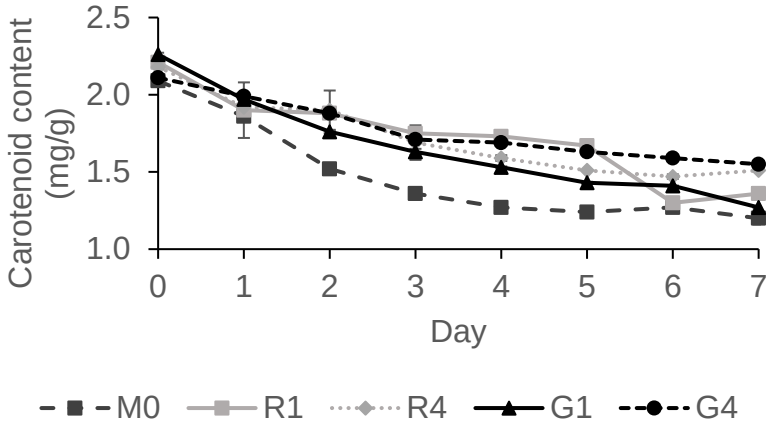

Figure 2. Carotenoids content of samples treated with 1000 and 4000 mg/kg rosemary or green tea extracts for 7 days at 60°C. M0: control sample; R1: 1000 mg/kg rosemary extract; R4: 4000 mg/kg rosemary extract; G1: 1000 mg/kg green tea extract; G4: 4000 mg/kg green tea extract

The carotenoids content predominantly decreased during the 7 days storage at 60°C may be due to thermal decomposition of carotenoids. As Mercadante [57] reported, carotenoids are easy to undergo degradation process that are induced by high temperature, low pH, light and reactive spices because they contain several conjugated double bonds. Many studies showed that heat and oxygen promote isomerization into *cis*-carotenoids which are less stable and more susceptible during storage [58-60]. Moreover, the loss of carotenoids is supposed to be related to decomposition reactions accelerated by temperature [58]. Previous work indicated that β-carotene was degraded in the first few hours of heat treatment [61]. The longer the incubation time, the more carotenoids were degraded [58, 61, 62]. Moreover, the thermal decomposition of carotenoids is dependent on the concentration of antioxidants [63]. Besides, the carotenoid contents of R1 and R4 slightly increased on day 7, compared with those observed on day 6. This was probably due to the high-temperature and long-time treatment causing the changes in oil color of these samples. Consequently, it possibly affects the carotenoid content measured by spectrophotometer at 460 nm. In addition, hydroperoxides in polyunsaturated oils may lead to formation of peroxyl or alkoxyl radial that react with β-carotene and the antioxidants protected β-carotene from degradation [62].

However, the samples supplemented by rosemary and green tea extract presented notably higher carotenoids concentrations compared to control sample in the last days of storage period. Particularly, for with 4000 mg/kg rosemary and green tea extract treatment, the carotenoids contents were higher than control by about 0.31 and 0.35 mg/g, respectively, at the day 7 of storage. Our results suggest the protective capability of natural antioxidants for carotenoids in gac oil at all testing concentrations. The higher concentrations (4000 mg/kg) of rosemary extract and green tea extract

showed higher carotenoid remaining, especially in the case of prolonging incubation time. According to Misharina and Kiseleva [63], the efficiency of inhibition of carotenoid autoxidation depended in a complex way on the concentration of antioxidants. Rosemary extract inhibited autoxidation in proportion to its concentration. In addition, rosemary extract and green tea extract also illustrated the effective inhibitory effects on β-carotene changes in buffalo homogenates lipid [64].

3.1.3 Rancimat value

Rancimat test is considered to be a rapid, economic, easy to handle and reproducible method that provides direct evidence for the tendency against oxidative rancidity of oil [65]. Therefore, it can be used as an effective and quick tool to assess the quality of fats and oils [66-68]. The longer induction times reflect the higher resistance to oxidation or good efficiency of the supplementing antioxidants [69]. The effect of rosemary and green tea extract on maintaining rancimat value was illustrated in Figure 3.

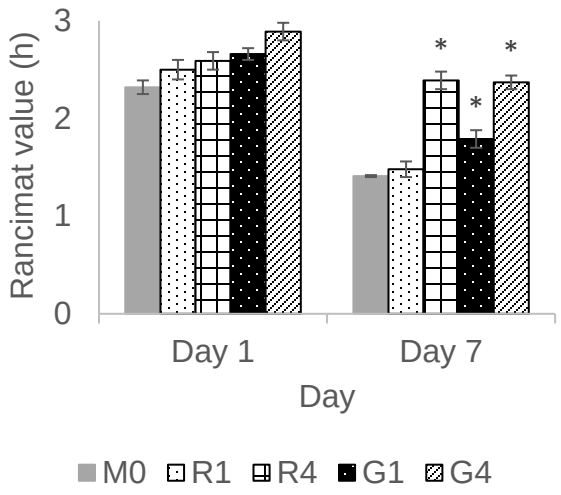

Figure 3. Rancimat values of samples treated with 1000 and 4000 mg/kg rosemary or green tea extracts for 7 days at 60ºC. *Significance at $P < 0.05$. M0: control sample; R1: 1000 mg/kg rosemary extract; R4: 4000 mg/kg rosemary extract; G1: 1000 mg/kg green tea extract; G4: 4000 mg/kg green tea extract

The rancimat values were not significantly different for all samples pre-treated with rosemary and green tea extracts at all concentrations on day 1. Nevertheless, after 7 days storage at 60ºC, the green tea and rosemary pre-treatments at 4000 mg/kg presented rancimat values of 2.37 ± 0.07 and 2.39 ± 0.09 (h), respectively, while 1.41 ± 0.01, 1.48 ± 0.08 and 1.790 ± 0.09 (h) were detected for the control sample, pre-treatment with rosemary and green tea extracts at 1000 mg/kg. Notably, after 7 days incubation, the rancimat values of the samples supplemented with green tea and rosemary extracts at 4000 mg/kg maintained at 82 and 92% compared to their initial samples. Similar results were reported by Burkow *et al*. [70] that increased antioxidant concentration gave increased induction times for all the antioxidant systems tested, based on rancimat measurements.

Rosemary extract and green tea extract addition significantly increased significantly induction time values [71], especially for high concentrations of 5000 mg/kg [35].

3.2 The comparison of natural green tea and rosemary extracts with synthetic antioxidants

3.2.1 Peroxide value, carotenoids content and rancimat value

The protective effects of natural antioxidants (4000 mg/kg rosemary and green tea extract) in comparison with synthetic antioxidants (150 mg/kg BHT and BHA) for gac oil are demonstrated in Table 1.

Table 1. Peroxide value, carotenoids content and rancimat values of samples treated with BHA, BHT, rosemary and green tea extracts after 7 days storage at 60°C

Sample	Quality index			Protection factor
	Peroxide value (meq/ kg)	Carotenoid content (mg / g)	Rancimat value (h)	
Control	7.50 ± 0.40^{e}	1.20 ± 0.04^{e}	1.41 ± 0.01^{c}	1.00 ± 0.01^{c}
BHA 150 mg/kg	4.36 ± 0.01^{b}	$1.48 \pm 0.02^{a,b}$	2.31 ± 0.01^{a}	1.64 ± 0.01^{a}
BHT 150 mg/kg	4.71 ± 0.06^{c}	$1.43 \pm 0.01^{a,b}$	2.38 ± 0.08^{a}	1.69 ± 0.06^{a}
Rosemary extract 1000 mg/kg	5.90 ± 0.03^{d}	$1.36 \pm 0.01^{c,d}$	1.48 ± 0.08^{c}	1.05 ± 0.06^{c}
Rosemary extract 4000 mg/kg	4.90 ± 0.07^{c}	$1.51 \pm 0.00^{a,b}$	2.39 ± 0.09^{a}	1.70 ± 0.06^{a}
Green tea extract 1000 mg/kg	$4.20 \pm 0.03^{a,b}$	$1.27 \pm 0.01^{d,e}$	1.81 ± 0.09^{b}	1.27 ± 0.06^{b}
Green tea extract 4000 mg/kg	3.97 ± 0.07^{a}	1.55 ± 0.01^{a}	2.37 ± 0.07^{a}	1.68 ± 0.05^{a}

Note: Data are expressed as mean values ± standard deviation of three independent experiments. Similar or shared superscript letters in the same column (e.g., a and a,b) show that there are no significant differences between samples treated with/without antioxidants based on post-hoc test. Different superscript letters (e.g., a and b) show the statistical difference ($p \leq 0.05$) between the tested groups.

The data clearly showed that the protective ability of these natural antioxidants against oxidative reactions of gac oil as measured by PV, carotenoids content and rancimate value were similar to synthetic antioxidants. In particular, supplementation with green tea extract resulted in lower PV than treatments with BHT or BHA. The protection factors of added antioxidants were also calculated (Table 1). As expected from the induction time, there were no significant differences between the protection factors calculated for BHT, BHA, and green tea and rosemary extracts at 4000 mg/kg. According to Nogala-Kalucka *et al*. [46], rosemary extract gave a markedly greater protection factor than α, δ, γ-tocopherol, and BHT at 100 mg/kg for triacylglycerols in rapeseed oil. In other studies, the protection factors were 1.1, 1.3, 1.2 and 1.2 for α, γ-tocopherol, BHT and BHA at 200 mg/kg in peanut oil, respectively, whereas rosemary extract gave values of 1.3-1.4 depending on the percentage of carnosic acid [72]. The differences may be due to the different concentrations of added antioxidants, active components contained in the extracts, and the type of oil used in these studies.

Wanasundara and Shahidi [25] demonstrated that green tea extract at 1000 mg/kg showed the better protection than did α-tocopherol, BHA and BHT, as indicated by lower records of PV. In addition, green tea extract also showed a superiority of protection against oxidation in comparison

to rosemary extract [22]. Rosemary extract also exhibited powerful antioxidant activity, almost equal to that of synthetic antioxidants (BHA and BHT) [40]. However, the opposite result observed for the oil stored at 20 ± 2ºC indicates that the antioxidant effectiveness of rosemary extract was better than that of green tea extract although both antioxidants managed to retard the oxidation process in the initial storage at higher concentration of 2500 mg/kg [35].

In some previous reports, Unten *et al*. [73] demonstrated the suppressive effect of tea polyphenols on the degradation of β carotene in both water-soluble and oily systems. Mohamed [64] also demonstrated that green tea, which is rich in flavanols, had a higher ability to inhibit the decomposition of β carotene than did rosemary extract.

According to Yang *et al*. [74], the induction time value of oil with combined rosemary extract was significantly higher than that with added synthetic antioxidants, which suggested the higher antioxidant effectiveness of rosemary extract against deterioration compared to synthetic antioxidants. Similar results obtained for ghee, both green tea and rosemary extracts at 0.5% concentration gave induction time value higher than BHA [34].

3.2.2 Sensory analysis

The sensory scores of all samples generally decreased after 7 days of incubation at 60ºC (Table 2). At day 1, no significant differences in taste, aroma and overall acceptability found among treatments with BHA and BHT were found. However, rosemary and green tea treatments had an effect on odor in gac oil, which was evaluated by the assessors. The higher concentration of these plant extracts markedly decreased the sensory scores of samples. After 7 days, rosemary treatment (4000 mg/kg) showed the worst results in overall acceptability while lower concentration (1000 mg/kg) resulted in better sensory scores. Green tea (4000 mg/kg) showed the highest overall acceptable by the assessors than BHT, BHA and the other treatment samples.

Table 2. Changes in sensory properties of gac oil after 7 days storage at 60ºC

Sample	Day	Taste	Aroma	Overall acceptability
Control	1	$7.3 \pm 0.5^{b,c}$	7.9 ± 0.3^{a}	$7.7 \pm 0.5^{a,b}$
BHA 150 mg/kg	1	$7.3 \pm 0.7^{b,c}$	6.8 ± 0.4^{b}	$7.3 \pm 0.5^{b,c}$
BHT 150 mg/kg	1	$7.4 \pm 0.5^{b,c}$	6.9 ± 0.3^{b}	$7.1 \pm 0.3^{c,d}$
Rosemary extract 1000 mg/kg	1	8.1 ± 0.9^{a}	7.9 ± 0.9^{a}	7.9 ± 0.6^{a}
Rosemary extract 4000 mg/kg	1	6.6 ± 0.5^{d}	6.8 ± 0.8^{b}	6.8 ± 0.4^{d}
Green tea extract 1000 mg/kg	1	$7.7 \pm 0.8^{a,b}$	7.5 ± 0.5^{a}	$7.7 \pm 0.8^{a,b}$
Green tea extract 4000 mg/kg	1	$7.1 \pm 0.3^{c,d}$	6.8 ± 0.6^{b}	$6.9 \pm 0.6^{c,d}$
Control	7	6.7 ± 0.5^{c}	$6.9 \pm 0.3^{a,b}$	$7.1 \pm 0.6^{b,c}$
BHA 150 mg/kg	7	6.7 ± 0.7^{c}	6.6 ± 0.5^{b}	$6.7 \pm 0.7^{c,d}$
BHT 150 mg/kg	7	6.7 ± 0.9^{c}	6.6 ± 0.7^{b}	$6.7 \pm 0.5^{c,d}$
Rosemary extract 1000 mg/kg	7	7.9 ± 0.9^{a}	7.3 ± 0.5^{a}	$7.3 \pm 0.7^{a,b}$
Rosemary extract 4000 mg/kg	7	6.3 ± 0.7^{c}	$6.8 \pm 0.8^{a,b}$	6.4 ± 0.7^{d}
Green tea extract 1000 mg/kg	7	$6.9 \pm 0.6^{b,c}$	6.5 ± 0.7^{b}	$6.6 \pm 0.7^{c,d}$
Green tea extract 4000 mg/kg	7	$7.5 \pm 0.8^{a,b}$	7.3 ± 0.5^{a}	7.7 ± 0.7^{a}

Note: Data are expressed as mean values ± standard deviation of three independent experiments. Similar or shared superscript letters in the same column (e.g., a and a,b) show that there are no significant differences treated with/without antioxidants based on post-hoc test. Different superscript letters (e.g., a and b) show the statistical difference ($p \leq 0.05$) between the tested groups.

According to Pourashouri *et al*. [75], a low percentage of rosemary extract addition had no effects on sensory evaluation but treatments with higher concentrations gave higher score for off-flavor. Moreover, these volatile including aldehydes, hydrocarbons and sulphuric compounds usually emerge during storage time due to lipid peroxidation [76]. Based on Table 1, green tea supplementation at 4000 mg/kg, which resulted in the lowest PV, contributed to it having highest overall acceptability scores when compared to the other treatments after the storage. Although some reports suggested that there was a slight increase in rancid odor when rosemary and green tea extracts were used [75, 77]. Overall, these plant extracts prevent alterations caused by oxidation which may affect the sensory scores of gac oil.

4. Conclusions

For the first time, the effects of two types of natural antioxidants, rosemary extract and green tea extract, on gac oil were carried on. Supplementation with rosemary and green tea extracts at 4000 mg/g significantly improved the quality of the gac oil through a decrease in peroxide value and maintenance of carotenoid during storage. A comparison between natural and synthetic antioxidants (BHA and BHT) was also performed to evaluate suitable antioxidants for gac oil. Both rosemary and green tea extracts showed impressive results for gac oil protection against oxidation. Although rosemary and green tea somewhat have an off-odor effect on gac oil, these results propose the possibility of replacing BHA and BHT by green tea and rosemary extract. Green tea seems to be a promising candidate in gac oil preservation.

5. Acknowledgements

This study was financed by Ho Chi Minh City University of Food Industry (HUFI).

References

[1] Vuong, L.T., Franke, A.A., Custer, L.J. and Murphy, S.P., 2006. *Momordica cochinchinensis* Spreng. (gac) fruit carotenoids reevaluated. *Journal of Food Composition and Analysis*, 19(6-7), 664-668.

[2] Kubola, J., Meeso, N. and Siriamornpun, S., 2013. Lycopene and beta carotene concentration in aril oil of gac (*Momordica cochinchinensis* Spreng) as influenced by aril-drying process and solvents extraction. *Food Research International*, 50(2), 664-669.

[3] Dang, T.T.N., Pham, N.B., Nguyen, T.H. and Thai, K.P., 2010. Changes in lycopene and beta carotene contents in aril and oil of gac fruit during storage. *Food Chemistry*, 121(2), 326-331.

[4] Vuong, L.T. and King, J.C., 2003. A method of preserving and testing the acceptability of gac fruit oil, a good source of β-carotene and essential fatty acids. *Food and Nutrition Bulletin*, 24(2), 224-230.

[5] Johnson, E.J., 2002. The role of carotenoids in human health. *Nutrition in Clinical Care*, 5(2), 56-65.

[6] Vuong, L.T., Dueker, S.R. and Murphy, S.P., 2002. Plasma β-carotene and retinol concentrations of children increase after a 30-d supplementation with the fruit *Momordica cochinchinensis* (gac). *The American Journal of Clinical Nutrition*, 75(5), 872-879.

[7] Rao, A.V. and Rao, L.G., 2007. Carotenoids and human health. *Pharmacological Research*, 55(3), 207-216.

[8] Bouaziz, M., Fki, I., Jemai, H., Ayadi, M. and Sayadi, S., 2008. Effect of storage on refined and husk olive oils composition: Stabilization by addition of natural antioxidants from Chemlali olive leaves. *Food Chemistry*, 108(1), 253-262.
[9] Shahidi, F., Wanasundara, P.K.J.P.D. and Wanasundara, U.N., 1997. Changes in edible fats and oils during processing. *Journal of Food Lipids*, 4, 199-231.
[10] Vuong, L.T., 2000. Underutilized β-carotene-rich crops of Vietnam. *Food and Nutrition Bulletin*, 21(2), 173-181.
[11] Cruz, R.G.D., Beney, L., Gervais, P., Lira, S.P.D., Vieira, T.M.F.D.S. and Dupont, S., 2019. Comparison of the antioxidant property of acerola extracts with synthetic antioxidants using an in vivo method with yeasts. *Food Chemistry*, 277, 698-705.
[12] Domingos, A.K., Saad, E.B., Vechiatto, W.W.D., Wilhelm, H.M. and Ramos, L.P., 2007. The influence of BHA, BHT and TBHQ on the oxidation stability of soybean oil ethyl esters (biodiesel). *Journal of the Brazilian Chemical Society*, 18(2), 416-423.
[13] Gertz, C., Klostermann, S. and Kochhar, S.P., 2000. Testing and comparing oxidative stability of vegetable oils and fats at frying temperature. *European Journal of Lipid Science and Technology*, 102(8-9), 543-551.
[14] Khatib, S., Harnafi, M., Touiss, I., Bekkouch, O., Amrani, S. and Harnafi, H., 2018. Phenolic extract of basil prevents lipid oxidation in sunflower oil, beef and turkey meat: A comparison with synthetic antioxidant BHA. *American Journal of Food and Nutrition*, 5(3), 66-75.
[15] Li, C., Cui, X., Chen, Y., Liao, C. and Ma, L.Q., 2019. Synthetic phenolic antioxidants and their major metabolites in human fingernail. *Environmental Research*, 169, 308-314.
[16] Aydeniz B. and Yilmaz, E., 2016. Performance of different natural antioxidant compounds in frying oil. *Food Technology and Biotechnology*, 54(1), 21-30.
[17] Spitalniak-Bajerska, K., Szumny, A., Kucharska, A.Z. and Kupczyński, R., 2018. Effect of natural antioxidants on the atability of linseed oil and fish stored under anaerobic conditions. *Journal of Chemistry*, 2018, https://doi.org/10.1155/2018/9375085.
[18] Pokorný, J., 1991. Natural antioxidants for food use. *Trends in Food Science & Technology*, 2, 223-227.
[19] Ahn, J.H., Kim, Y.P., Seo, E.M., Choi, Y.K. and Kim, H.S., 2008. Antioxidant effect of natural plant extracts on the microencapsulated high oleic sunflower oil. *Journal of Food Engineering*, 84(2), 327-334.
[20] Almeida-Doria, R. and Regitano-D'arce, M.A.B., 2000. Antioxidant activity of rosemary and oregeno ethanol extract in soybean oil under thermal oxidation. *Food Science and Technology*, 20(2), 237-239.
[21] Caleja, C., Barros, L., Antonio, A.L., Oliveira, M.B.P.P. and Ferreira, I.C.F.R., 2017. A comparative study between natural and synthetic antioxidants: Evaluation of their performance after incorporation into biscuits. *Food Chemistry*, 216, 342-346.
[22] Chen, Z.Y., Wang, L.Y., Chan, P.T., Zhang, Z., Chung, H.Y. and Liang, C., 1998. Antioxidative activity of green tea catechin extract compared with that of rosemary extract. *Journal of the American Oil Chemists' Society*, 75(12), 1141-1145.
[23] Pires, M.A., Munekata, P.E.S., Villanueva, N.D.M., Tonin, F.G., Baldin, J.C., Rocha, Y.J.P. Carvalho, L.T., Rodrigues, I. and Trindade, M.A., 2017. The antioxidant capacity of rosemary and green tea extracts to replace the carcinogenic antioxidant (BHA) in chicken burgers. Journal of Food Quality, 2017, https://doi.org/10.1155/2017/2409527
[24] Taghvaei, M. and Jafari, S.M., 2015. Application and stability of natural antioxidants in edible oils in order to substitute synthetic additives. *Journal of Food Science and Technology*, 52(3), 1272-1282.
[25] Wanasundara, U.N. and Shahidi, F., 1998. Antioxidant and pro-oxidant activity of green tea extracts in marine oils. *Food Chemistry*, 63(3), 335-342.

[26] Zbikowska, A., Kowalska, M., Rutkowska, J., Kozłowska, M. and Onacik-Gür, S., 2017. Impact of green tea extract addition on oxidative changes in the lipid fraction of pastry products. *Acta Scientiarum Polonorum Technologia Alimentaria*, 16(1), 25-35.
[27] Etter, S.C., 2004. *Rosmarinus officinalis* as an antioxidant. *Journal of Herbs, Spices & Medicinal Plants*, 11(1-2), 121-159.
[28] Erkan, N, Ayranci, G. and Ayranci, E., 2008. Antioxidant activities of rosemary (*Rosmarinus Officinalis* L.) extract, blackseed (*Nigella sativa* L.) essential oil, carnosic acid, rosmarinic acid and sesamol. *Food Chemistry*, 110(1), 76-82.
[29] Kmiecik, D., Korczak, J., Rudzińska, M., Michałowska, A.G. and Heś, M., 2009. Stabilization of phytosterols in rapeseed oil by natural antioxidants during heating. *European Journal of Lipid Science and Technology*, 111(11), 1124-1132.
[30] Martínez, M.L., Penci, M.C., Ixtaina, V., Ribotta, P.D. and Maestri, D., 2013. Effect of natural and synthetic antioxidants on the oxidative stability of walnut oil under different storage conditions. *LWT - Food Science and Technology*, 51 (1), 44-50.
[31] Rahila, M.P., Surendra Nath, B., Laxmana Naik, N., Pushpadass, H.A., Manjunatha, M. and Franklin, M.E.E. 2018. Rosemary (*Rosmarinus officinalis* Linn.) extract: A source of natural antioxidants for imparting autoxidative and thermal stability to ghee. *Journal of Food Processing and Preservation*, 42(2), https://doi.org/10.1111/jfpp.13443
[32] Yanishlieva N.V. and Marinova, E.M., 2001. Stabilisation of edible oils with natural antioxidants. *European Journal of Lipid Science and Technology*, 103(11), 752-767.
[33] Kha, T.C., Nguyen, M.H., Roach, P.D. and Stathopoulos. C.E., 2013. Effects of Gac aril microwave processing conditions on oil extraction efficiency, and-βcarotene and lycopene contents. *Journal of Food Engineering*, 117(4), 486-491.
[34] Gandhi, K., Pawar, N., Kumar, A. and Arora, S., 2013. Effect of vidarikand (extracts) on oxidative stability of ghee: A comparative study. *Research and Reviews: Journal of Dairy Science and Technology*, 2(1), 1-10.
[35] Ixtaina, V.Y., Nolasco, S.M. and Tomás, M.C., 2012. Oxidative stability of chia (*Salvia hispanica* L.) seed oil: Effect of antioxidants and storage conditions. *Journal of the American Oil Chemists' Society*, 89(6), 1077-1090.
[36] EFSA, 2011. Scientific opinion on the re-evaluation of butylated hydroxyanisole - BHA (E 320) as a food additive. *EFSA Journal*, 9(10), https://doi.org/10.2903/j.efsa.2011.2392
[37] EFSA, 2012. Scientific opinion on the re ‐ evaluation of butylated hydroxytoluene BHT (E 321) as a food additive. *EFSA Journal*, 10(3), https://doi.org/10.2903/j.efsa.2012.2588
[38] Ng, K.l., Tan, G.H. and Khor, S.M., 2017. Graphite nanocomposites sensor for multiplex detection of antioxidants in food. *Food Chemistry*, 237, 912-920.
[39] Tang, J., Mao, Y., Guo, J., Li, Z., Zhang, C. and Jin, B., 2018. Simultaneous determination of TBH2Q and BHA antioxidants in food samples using eosin Y film modified electrode. *Food Analytical Methods*, 11(12), 3380-3390.
[40] Chen, X., Zhang, Y., Zu, Y., Yang, L., Lu, Q. and Wang, W., 2014. Antioxidant effects of rosemary extracts on sunflower oil compared with synthetic antioxidants. *International Journal of Food Science & Technology*, 49(2), 385-391.
[41] Sadeghi, E., Karami, F. and Etminan, A., 2016. The Effect of *Ferulago angulata* (Schlecht) boiss essential oil on stabilization of sunflower oil during accelerated storage. *Journal of Food Processing and Preservation*, 41(1), https://doi.org/10.1111/jfpp.12745.
[42] Xie, C., Ma, Z.F., Li, F., Zhang, H., Kong, L., Yang, Z. and Xie, W., 2018. Storage quality of walnut oil containing lycopene during accelerated oxidation. *Journal of Food Science and Technology*, 55(4), 1387-1395.
[43] Hortwitz, W., 2002. *AOAC Official Method 965.33, Peroxide Value of Oils and Fats*. 17th ed. Gaithersberg: AOAC Int.

[44] Cenkowski, S., Yakimishen, R., Przybylski, R. and Muir, W.E., 2006. Quality of extracted sea buckthorn seed and pulp oil. *Canadian Biosystems Engineering*, 48, 3.9-3.16.
[45] Shahidi, F. and Zhong, Y., 2005. *Lipid Oxidation: Measurement Methods*. [online] Available at: https://doi.org/10.1002/047167849X.bio050.
[46] Nogala-Kalucka, M., Korczak, J., Dratwia, M., Lampart-Szczapa, E., Siger, A. and Buchowski, M., 2005. Changes in antioxidant activity and free radical scavenging potential of rosemary extract and tocopherols in isolated rapeseed oil triacylglycerols during accelerated tests. *Food Chemistry*, 93(2), 227-235.
[47] Storer, R.C., 1988. *ASTM Standards on Sensory Evaluation of Materials and Products.* Philadelphia: American Society for Testing and Materials.
[48] Naghshineh, M., Ariffin, A.A, Ghazali, H.M., Mohammad, A.S. and Mirhosseini, H., 2010. Effect of saturated/unsaturated fatty acid ratio on physicochemical properties of palm olein-olive oil blend. *Journal of the American Oil Chemists' Society*, 87(3), 255-262.
[49] Gharby, S., Harhar, H., Guillaume, D., Haddad, A., Matthäus, B. and Charrouf, Z., 2011. Oxidative stability of edible argan oil : A two-year study. *LWT - Food Science and Technology*, 44(1), 1-8.
[50] Malheiro, R., Rodrigues, Manzke, G., Bento, A., Pereira, J.A. and Casal, S., 2013. The use of olive leaves and tea extracts as effective antioxidants against the oxidation of soybean oil under microwave heating. *Industrial Crops and Products*, 44, 37-43.
[51] Pokorny, J., Yanishlieva, N. and Gordon, M., 2001. *Antioxidants in Food. Practical Applications*. Cambridgr: Woodhead Publishing Ltd.
[52] Namal Senanayake, S.P.J., 2013. Green tea extract: Chemistry, antioxidant properties and food applications – A review. *Journal of Functional Foods*, 5(4), 1529-1541.
[53] Lavelli, V., Vantaggi, C., Corey, M. and Kerr, W., 2010. Formulation of a dry green tea-apple product: Study on antioxidant and color stability. *Journal of Food Science*, 75(2), 184-190.
[54] Mildner-Szkudlarz, S., Zawirska-Wojtasiak, R., Obuchowski, W. and Gośliński, M., 2009. Evaluation of antioxidant activity of green tea extract and its effect on the biscuits lipid fraction oxidative stability. *Journal of Food Science*, 74(8), S362-370.
[55] Klancnik, A., Guzej, B., Kolar, M.H., Abramovic, H. and Mozina, S.S., 2009. In vitro antimicrobial and antioxidant activity of commercial rosemary extract formulations. *Journal of Food Protection*, 72(8), 1744-1752.
[56] Tran, T.Y.N. and Dang, Q.T., 2016. Enzyme assisted extraction of gac oil (*Momordica cochinchinensis* Spreng) from dried aril. *Journal of Food and Nutrition Sciences*, 4(1), 1-6.
[57] Mercadante, A.Z., 2008. Carotenoids in foods: Sources and stability during proocessing.In: Socaiu, C., ed. *Food Colorants Chemical and Functional Properties*. Boca Raton: CRC Press, pp. 213-240.
[58] Achir, N., Randrianatoandro, V.A. Bohuon, P., Laffargue, P. and Avallone, S., 2010. Kinetic study of β-carotene and lutein degradation in oils during heat treatment. *European Journal of Lipid Science and Technology*, 112(3), 349-361.
[59] Çinar, I., 2004. Carotenoid pigment loss of freeze-dried plant samples under different storage conditions. *LWT - Food Science and Technology*, 37 (3), 363-367.
[60] Zepka, L.Q. and Mercadante, A.Z., 2009. Degradation compounds of carotenoids formed during heating of a simulated cashew apple juice. *Food Chemistry*, 117(1), 28-34.
[61] Zeb, A. and Murkovic, M., 2011. Carotenoids and triacylglycerols interactions during thermal oxidation of refined olive oil. *Food Chemistry*, 127(4), 1584-1593.
[62] Yi, J., Fan, Y., Yokoyama, W., Zhang, Y. and Zhao, L., 2016. Thermal degradation and isomerization of β-carotene in oil-in-water nanoemulsions supplemented with natural antioxidants. *Journal of Agricultural and Food Chemistry*, 64 (9), 1970-1976.

[63] Misharina, T.A. and Kiseleva, V.I., 2019. Inhibition of autoxidation of paprika carotenoids by plant antioxidants. *Applied Biochemistry and Microbiology*, 55 (2), 182-188.
[64] Mohamed, H.M.A., 2011. Antioxidant synergy effect of rosemary aqueous extract and green tea flavanol-rich concentrate for superior rrotection of buffalo meatloaves. *Lucrări Ştiinţifice-Universitatea de Ştiinţe Agricole şi Medicină Veterinară Iaşi*, 56, 242-252.
[65] Laubil, M.W. and Bruttel, P.A., 1986. Determination of the oxidative stability of fats and oils: Comparison between the active oxygen method (AOCS Cd 12-57). *Journal of the American Oil Chemists' Society*, 63(6), 792-795.
[66] Farhoosh, R. and Moosavi, S.M.R., 2007. Rancimat test for the assessment of used frying oils quality. *Journal of Food Lipids*, 14(3), 263-271.
[67] García-Moreno, P.J., Pérez-Gálvez, R., Guadix, A. and Guadix, E.M., 2013. Influence of the parameters of the Rancimat test on the determination of the oxidative stability index of cod liver oil. *LWT - Food Science and Technology*, 51(1), 303-308.
[68] Kowalski, B., Ratusz, K., Kowalska, D. and Bekas, W., 2004. Determination of the oxidative stability of vegetable oils by differential scanning calorimetry and Rancimat measurements. *European Journal of Lipid Science and Technology*, 106 (3), 165-169.
[69] Womeni, H.M., Djikeng, F.T., Anjaneyulu, B., Karuna, M.S.L., Prasad, R.B.N. and Linder, M., 2016. Oxidative stabilization of RBD palm olein under forced storage conditions by old Cameroonian green tea leaves methanolic extract. *NFS Journal*, 3, 33-40.
[70] Burkow, I.C., Vikersveen, L. and Saarem, K., 1995. Evaluation of antioxidants for cod liver oil by chemiluminescence and the rancimat method. *Journal of the American Oil Chemists' Society*, 72(5) 553-557.
[71] Hamidioglu, I., Salaseviciene, A. and Zaborskiene, G., 2019. Effects of natural herbal extracts on hemp (*Cannabis sativa* L.) oil quality indicators. *Foods Raw Materials*, 7(1), 35-41.
[72] Hudson, B.J.F., 1990. *Food Antioxidants.* Dordrecht: Springer Netherlands.
[73] Unten,L., Koketsu, M. and Kim, M., 1997. Antidiscoloring activity of green tea polyphenols on β-carotene. *Journal of Agricultural and Food Chemistry*, 45 (6), 2009-2012.
[74] Yang, Y., Song, X., Sui, X., Qi, B., Wang, Z., Li, Y. and Jiang, L., 2016. Rosemary extract can be used as a synthetic antioxidant to improve vegetable oil oxidative stability. *Industrial Crops and Products*, 80, 141-147.
[75] Pourashouri, P., Shabanpour, N., Hashem Abad Z.N. and Zahiri, S., 2016. Antioxidant effects of wild pistacia (*P. atlantica*), rosemary (*Rosmarinus officinalis* L.) and green tea extracts on the lipid oxidation rate of fish oil-in-water emulsions. *Turkish Journal of Fisheries and Aquatic Sciences*, 16(3), 729-737.
[76] Al-Hijazeen, M. and Al-Rawashdeh, M., 2019. Preservative effects of rosemary extract (*Rosmarinus officinalis* L.) on quality and storage stability of chicken meat patties. *Food Science and Technology*, 39(1), 27-34.
[77] Gorji, S.G., Calingacion, M., Smyth H. and Fitzgerald, M., 2019. Effect of natural antioxidants on lipid oxidation in mayonnaise compared with BHA, the industry standard. *Metabolomics*, 15(8), https://doi.org/10.1007/s11306-019-1568-4

Current Applied Science and Technology Vol. 21 No. 3 (July-September 2021)

An Improved Protocol for High Quantity and Quality of Genomic DNA Isolation from Human Peripheral Blood

Eric Tzyy Jiann Chong, Lucky Poh Wah Goh, Keh Kheng Png and Ping-Chin Lee*

Biotechnology Programme, Faculty of Science and Natural Resources,
Universiti Malaysia Sabah, Sabah, Malaysia

Received: 7 August 2020, Revised: 30 November 2020, Accepted: 8 January 2021

Abstract

DNA isolation is the most essential step in molecular studies. The quantity and quality of the isolated DNA may subsequently influence the reliability and reproducibility of experimental data especially those involving downstream analysis such as polymerase chain reaction (PCR). In this study, we report an improved protocol for isolating high quantity and quality of genomic DNA from human peripheral blood that is as competitive to commercial kits. The concentration of the genomic DNA isolated using the improved protocol was >100 ng/µl and the A_{260}/A_{280} absorbance ratio was ranged within 1.604-1.861. When the DNA integrity was measured using Fragment Analyzer™, the isolated genomic DNA was highly intact with a genomic quality number of ≥7.0. The isolated genomic DNA was adequate for further molecular analyses including standard PCR and real-time PCR. More importantly, the improved protocol is able to isolate the genomic DNA of *Plasmodium* parasites that infected human red blood cells, thus enabling them to be correctly identified up to the species level using multiplex PCR.

Keywords: DNA isolation; human blood; polymerase chain reaction; *Plasmodium* parasites
DOI 10.14456/cast.2021.36

1. Introduction

Molecular study often involves the isolation of nucleic acids such as DNA. Hence, the quantity and the quality of the isolated DNA are extremely important for reproducible and reliable of experiment data in subsequent molecular analyses including standard polymerase chain reaction (PCR) and real-time PCR. For instance, contaminants such as polysaccharides, organic solvents, proteins, and detergents that are co-isolated with the DNA are reported to inhibit a PCR amplification [1, 2]. In addition, DNA with co-isolated contaminants may also lead to a higher cycle threshold value of the targeted gene in a real-time PCR application, which may then result in an incorrectly interpreted real-time PCR data [3].

There are multiple choices of commercial DNA isolation kits currently available in the market that can isolate a high quality of DNA. However, the commercial kits commonly have a limited number of reactions and are relatively expensive which may not be affordable by some laboratories, especially those in low-income countries. Therefore, an efficient and economic

*Corresponding author: Tel.: (+6) 088320000 ext. 100101 Fax: (+6) 088435324
E-mail: leepc@ums.edu.my

alternative DNA isolation method is crucial. We addressed this particular issue with an improved protocol that can effectively and economically isolate high quantity and quality of DNA from human peripheral blood, and empirically validated the protocol using molecular analyses such as standard PCR and real-time PCR.

2. Materials and Methods

2.1 Human blood sample collection

Three ml of peripheral blood sample was collected from volunteers into a BD Vactutainer® blood collection tube with spray-coated K_2EDTA by an experienced phlebotomist. A total of 100 volunteers were recruited in this study with informed consent. The ethical approval for this study was obtained from the Universiti Malaysia Sabah Medical Research Ethics Committee with a reference number: JKEtika 1/15 (7).

2.2 Genomic DNA isolation

Three ml of the collected blood was mixed with 7 ml of chilled 1X Red Cell Lysis Buffer (containing 1.6M of sucrose, 5% of Triton X-100, 25mM of magnesium chloride hexahydrate, and 60mM of Tris hydrochloride) in a Falcon tube and centrifuged at 2500 xg for 5 min at 4°C. The supernatant containing the lysed red blood cells was discarded and the color of the precipitated pellet was observed. The red blood cell lysis step was repeated until the pellet became light pink to white color. Subsequently, the pellet was re-suspended by adding 20 µl of 1 mg/ml Proteinase K, 80 µl of 5X Proteinase K buffer, 20 µl of 20% sodium dodecyl sulfate solution, and 150 µl of sterile distilled water containing 1 µg/ml of RNase, and incubated overnight at 37°C. The next day, the whole mixture content was treated with 100 µl of 5M sodium chloride solution and 250 µl of phenol: chloroform: isopropanol (1:1:1 v/v/v, pH 8.05-8.35) solution. After vortexing and centrifuging at 13,000 rpm for 10 min, the aqueous phase of the mixture was transferred into a microcentrifuge tube containing 500 µl of absolute ethanol. The tube was vigorously shaken until a white clump was formed and was centrifuged at 13,000 rpm for 3 min. The excess absolute ethanol was discarded and the pellet was washed with 500 µl of 70% ethanol. After centrifuged at 13,000 rpm for 2 min, the excess 70% ethanol was discarded and the pellet was air-dried for 5 min at room temperature. Finally, the pellet was re-suspended with 100 µl of 1X TE Buffer (containing 10mM of Tris and 1mM of ethylenediaminetetraacetic acid).

2.3 Quantity and quality of the isolated genomic DNA

The concentration and purity of the isolated genomic DNA were measured using the NanoPhotometer® P-Class (Implen, Germany). Unpaired t-test (https://www.graphpad.com/quickcalcs/ttest1.cfm) was utilized to compare the means of DNA purity between current protocol and other commercial kits as reported by Lee *et al*. [4], including the QIAamp® Blood Mini Kit (Qiagen, Germany), MagNA Pure LC Nucleic Acid Isolation Kit I (Roche Diagnostics, Germany) and Magtration-Magnazorb DNA common kit-200N (Precision System Science Co. Ltd., Japan). In addition, the Standard Sensitivity Genomic DNA Analysis Kit (Advanced Analytical Technologies Inc., USA) was used to measure the integrity of the isolated genomic DNA using the Fragment Analyzer™ Automated Capillary Electrophoresis System (Advanced Analytical Technologies Inc., USA) which represented with a genomic quality number (GQN). GQN of 1 indicates that the genomic DNA is highly degraded and GQN of 10 indicates that the genomic DNA is highly intact.

2.4 Standard PCR

A standard PCR amplifying the cytochrome P450 family 2 subfamily E member 1 (*CYP2E1*) gene sequence that containing the T7678A variant was performed by using the isolated genomic DNA as a template (~100 ng/reaction). The detailed procedure is as previously described by Chong *et al*. [5].

2.5 Real-time PCR

Genotyping targeting the rs3751723 single nucleotide polymorphism (SNP) of the iroquois homeobox 3 (*IRX3*) gene was performed using a real-time PCR and the isolated genomic DNA served as a template (~100 ng/reaction). The detailed procedure is as previously described by Chong *et al*. [6].

3. Results and Discussion

A total of 100 DNA samples isolated using the improved protocol were subjected to quantity and quality measurements (Table 1). The concentration of the isolated DNA ranged between 102 ng/µl and 305 ng/µl. When the purity of the isolated DNA was measured, the A_{260}/A_{280} absorbance ratio ranged from 1.604 to 1.861. The absorbance values did not deviate far from the ideal ratio of 1.800 for genomic DNA [7]. Therefore, the isolated genomic DNA using the improved protocol is able to provide sufficient quantity and quality for reliable data in the subsequent molecular analyses.

Table 1. Results of genome DNA isolated using the current improved protocol in this study

Sample	DNA conc. (ng/µl)	A_{260}/A_{280}	GQN
1	179	1.646	8.2
2	173	1.769	8.1
3	177	1.703	9.7
4	176	1.645	8.5
5	113	1.633	9.1
6	193	1.618	8.7
7	188	1.604	8.1
8	127	1.749	8.1
9	138	1.660	8.6
10	119	1.703	9.2
11	305	1.755	7.3
12	255	1.827	8.7
13	214	1.723	7.2
14	187	1.765	7.9

Table 1. Results of genome DNA isolated using the current improved protocol in this study (cont.)

Sample	DNA conc. (ng/µl)	A_{260}/A_{280}	GQN
15	172	1.776	8.1
16	152	1.701	9.5
17	133	1.675	7.3
18	134	1.661	9.3
19	112	1.695	8.9
20	140	1.826	9.9
21	188	1.671	7.0
22	136	1.751	8.3
23	134	1.759	8.1
24	198	1.754	9.1
25	115	1.715	9.3
26	110	1.861	7.0
27	102	1.659	8.5
28	199	1.663	7.5
29	109	1.618	8.5
30	169	1.797	7.4
31	208	1.717	8.5
32	152	1.801	9.0
33	218	1.845	8.4
34	154	1.642	9.5
35	239	1.755	8.1
36	172	1.646	8.9
37	144	1.718	9.2
38	147	1.648	8.6
39	168	1.689	7.2
40	165	1.636	9.0
41	180	1.762	8.5
42	214	1.755	7.4
43	171	1.670	8.5
44	260	1.638	8.0

Table 1. Results of genome DNA isolated using the current improved protocol in this study (cont.)

Sample	DNA conc. (ng/µl)	A_{260}/A_{280}	GQN
45	170	1.678	8.5
46	184	1.642	8.8
47	182	1.657	7.8
48	193	1.681	8.5
49	174	1.640	7.8
50	183	1.616	8.8
51	104	1.658	8.8
52	108	1.666	9.6
53	216	1.812	8.3
54	179	1.791	8.1
55	195	1.776	9.0
56	201	1.719	8.2
57	186	1.729	8.3
58	120	1.788	8.7
59	129	1.669	7.8
60	134	1.639	9.3
61	226	1.795	8.4
62	253	1.768	8.5
63	130	1.772	7.4
64	136	1.771	7.3
65	125	1.728	7.1
66	128	1.753	7.9
67	258	1.756	7.6
68	134	1.789	8.9
69	132	1.632	8.3
70	287	1.783	8.1
71	141	1.778	8.6
72	126	1.684	9.0
73	131	1.785	7.9

Table 1. Results of genome DNA isolated using the current improved protocol in this study (cont.)

Sample	DNA conc. (ng/µl)	A_{260}/A_{280}	GQN
74	245	1.729	8.5
75	299	1.743	9.3
76	108	1.667	8.4
77	181	1.684	8.3
78	173	1.629	8.2
79	199	1.646	8.3
80	174	1.778	7.8
81	178	1.775	7.8
82	192	1.756	8.4
83	169	1.829	7.8
84	118	1.621	7.1
85	199	1.710	8.2
86	177	1.660	9.5
87	178	1.691	9.2
88	195	1.683	7.7
89	147	1.664	9.3
90	182	1.691	8.3
91	156	1.702	7.3
92	165	1.669	8.8
93	184	1.678	9.2
94	175	1.690	7.8
95	176	1.626	7.3
96	166	1.665	8.8
97	150	1.716	10.0
98	175	1.628	8.7
99	194	1.640	7.7
100	185	1.678	7.9
Mean ± S.D.	171.47 ± 42.93	1.71 ± 0.06	8.37 ± 0.70
Range (min-max)	102-305	1.604-1.861	7-10

When compared with other commercial kits that use different isolation principles, the mean of DNA purity using the current protocol was similar to those isolated using the Magtration-Magnazorb DNA common kit-200N (p = 0.724), but statistically different to those isolated using the QIAamp® Blood Mini Kit and MagNA Pure LC Nucleic Acid Isolation Kit I (both p-values <0.001) (Table 2). The mean differences were mainly because of the different technologies utilized in isolating the DNA, the number of DNA samples isolated, and variations in sample handling during the extraction process. However, when a scatter plot of the DNA purity values was mapped (Figure 1), most of the purity values overlapped despite the different protocols utilized in isolating the DNA from human blood, suggesting that DNA isolation using the current improved protocol is as competitive to other commercial kits, yet is much more cost-effective and economical when compared to the commercial kits. However, given the advantage of cost-effective, the limitation of the current protocol is time consuming (~10 h) as compared to commercial kits which have shorter processing times (< 2 h).

Figure 2 shows a representative of 11 genomic DNA analyzed using the Fragment Analyzer™ in this study. The isolated genomic DNA using the improved protocol was highly intact with a genomic quality number (GQN) ranging from 7.0 to 10.0 (Table 1). Although the influence of GQN in subsequent molecular analyses is rarely reported, a previous study reported that nucleic acid with an integrity number <5.0 is unreliable for subsequent analysis such as real-time PCR [8].

Besides that, the isolated genomic DNA was molecularly validated using a standard PCR, and our study showed that the *CYP2E1* gene sequence containing the T7678A variant was successfully amplified (Figure 3). In addition, the isolated genomic DNA in this study could also be

Table 2. Comparison of DNA purity isolated from different protocols

Genomic DNA isolation protocol	Isolation principle	Time required	No. of samples tested	Purity range (mean ± SD)	*p*-value	Reference
Current protocol	Salting-out	10 h	100	1.60-1.86 (1.71 ± 0.06)	-	This study
QIAamp® Blood Mini Kit (Qiagen, Germany)	Spin-column	20-40 min	22	1.59-2.04 (1.84 ± 0.09)	<0.001*	Lee *et al.* [4]
MagNA Pure LC Nucleic Acid Isolation Kit I (Roche Diagnostics, Germany)	Magnetic-bead	< 2 h	22	1.60-1.97 (1.88 ± 0.08)	<0.001*	Lee *et al.* [4]
Magtration-Magnazorb DNA common kit-200N (Precision System Science Co. Ltd., Japan)	Magnetic-based	25-40 min	22	1.56-1.90 (1.70 ± 0.08)	0.724	Lee *et al.* [4]

*Statistically significant when compared to the current protocol (p <0.05).

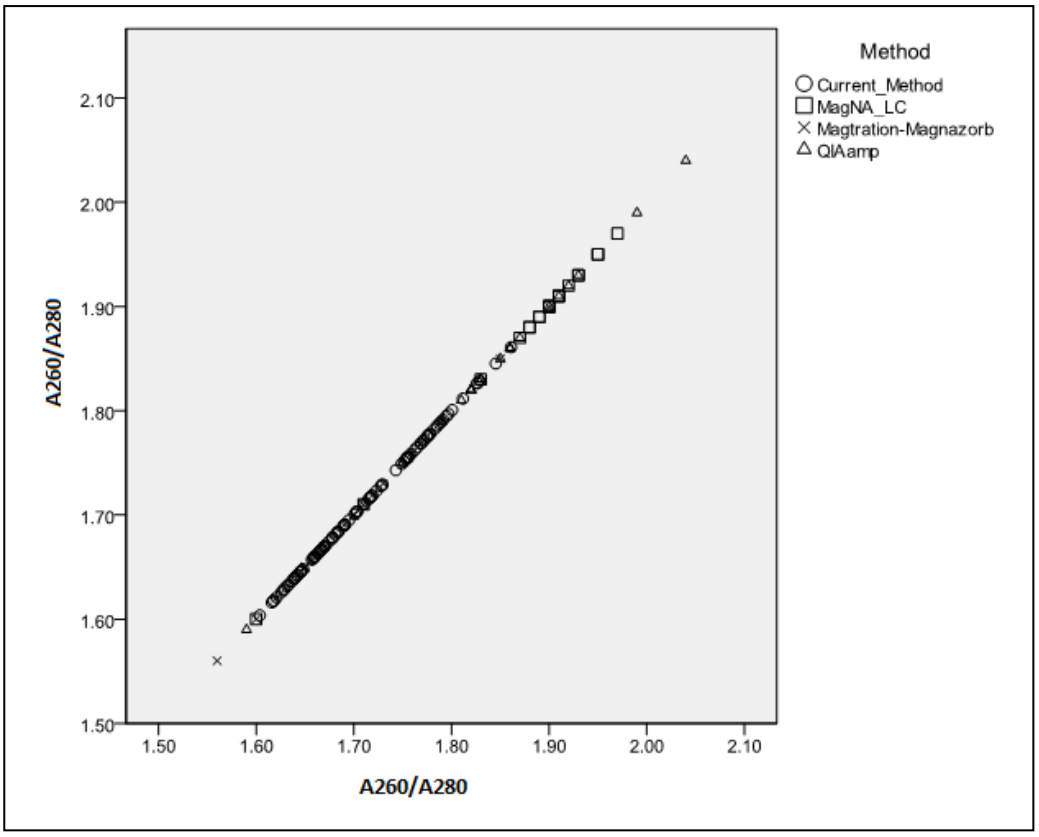

Figure 1. Scattered plot showing the overlapping of purity values between DNA isolated using the current protocol and those reported using other commercial kits

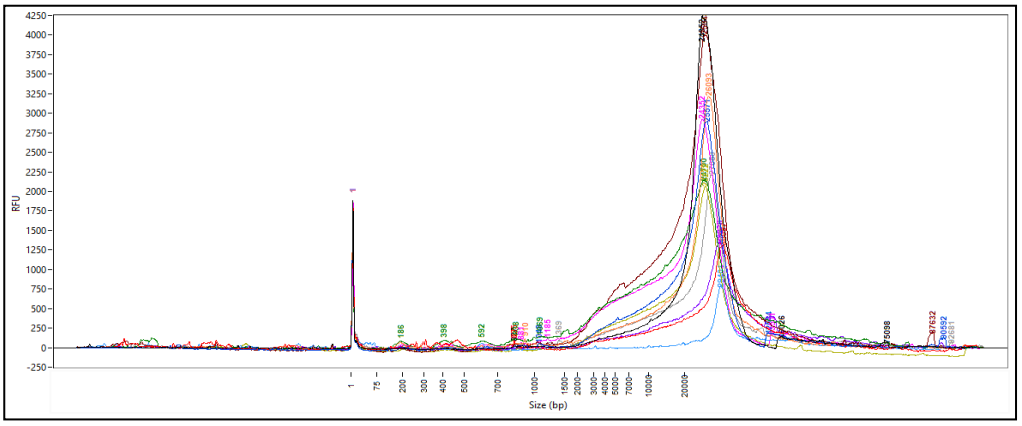

Figure 2. Overlay electropherogram of 11 isolated genomic DNA samples analyzed using the Fragment Analyzer™

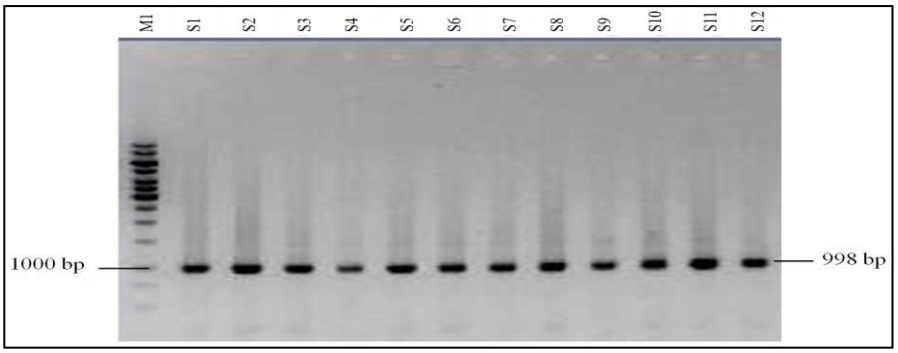

Figure 3. The *CYP2E1* gene sequence containing the T7678A variant was successfully amplified (998 bp). M1: Thermo Scientific GeneRuler^{TM} 1 kb DNA Ladder. S1-S12: DNA samples isolated using the improved protocol

used to generate reliable data for genotyping analysis in real-time PCR. For example, the rs3751723 SNP of the *IRX3* was effectively genotyped using the isolated genomic DNA in this study and could be precisely distributed into the homozygous wild-type, heterozygous, and homozygous variant groups (Figure 4). Both findings indicated that the improved method can maintain the intactness of the genomic DNA throughout the isolation process with a very minimal amount of protein contamination.

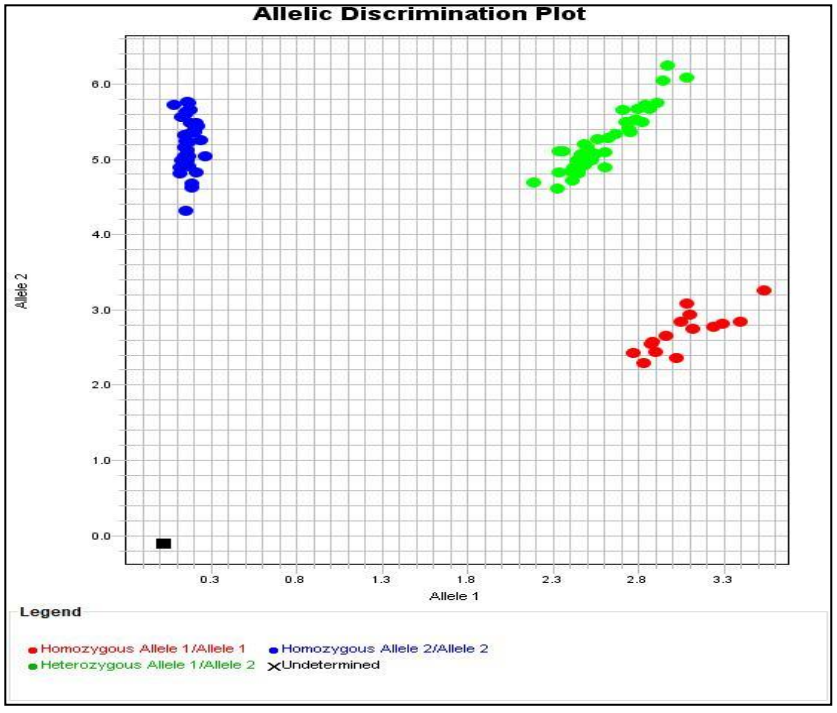

Figure 4. The rs3751723 SNP of the *IRX3* gene was effectively genotyped from DNA samples isolated using the improved protocol

More interestingly, our improved protocol is able to isolate the genomic DNA of *Plasmodium* species that infected the red blood cells, and being correctly identified up to the species level when applied with the PlasmoNex™ system [9], even for a mix-species infection (Figure 5). This finding is obviously important as the malaria incidences, especially those infected with the fatal *Plasmodium knowlesi* species, are evidently increasing in the Southeast Asia countries [10-12]. Therefore, the improved DNA isolation protocol in this study could provide consistent data in *Plasmodium* species detection for effective and rapid malaria treatment.

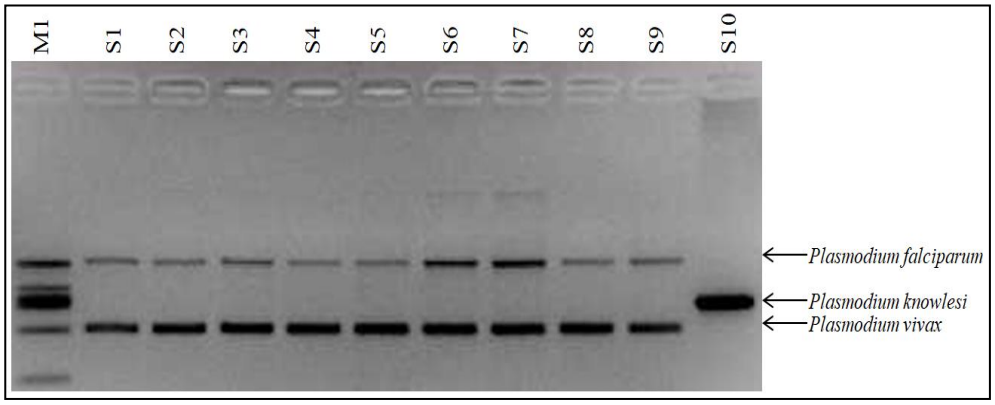

Figure 5. The *Plasmodium* species was correctly identified using the PlasmoNex™ system. M1: PlasmoNex™ DNA Marker. S1-S10: *Plasmodium* DNA samples isolated using the improved method

4. Conclusions

In conclusion, we report here an improved protocol to effectively and economically isolate high quantity and quality of genomic DNA from human peripheral blood, and the present protocol is as competitive to other commercial kits. The isolated genomic DNA is competent for subsequent molecular analyses including standard PCR and real-time PCR. More essentially, this improved protocol is capable to isolate the genomic DNA of *Plasmodium* species and being accurately diagnosed up to the species level in a multiplex PCR.

5. Acknowledgements

We would like to thank all volunteers who participated in this study. This study is supported by Universiti Malaysia Sabah (SDK207-2020 and GUG0128-1/2017).

References

[1] Lorenz, T.C., 2012. Polymerase chain reaction: basic protocol plus troubleshooting and optimization strategies. *Journal of Visualized Experiments*, 63, 3998, https://doi.org/10.3791/3998

[2] Holden, M.J., Blasic, J.R., Bussjaeger, L., Kao, C., Shokere, L.A., Kendall, D.C., Freese, L. and Jenkins, G.R., 2003. Evaluation of extraction methodologies for corn kernel (*Zea mays*) DNA for detection of tract amounts of biotechnology-derived DNA. *Journal of Agriculture and Food Chemistry*, 51, 2468-2474.

[3] Kubista, M., Andrade, J.M., Bengtsson, M., Forootan, A., Jonák, J., Lind, K., Sindelka, R., Sjöback, R., Sjögreen, B., Strömbom, L., Ståhlberg, A. and Zoric, N., 2006. The real-time polymerase chain reaction. *Molecular Aspects of Medicine*, 27, 95-125.

[4] Lee, J.H., Park, Y., Choi, J.R., Lee, E.K. and Kim, H.S., 2010 Comparisons of the three automated systems for genomic DNA extraction in a clinical diagnostic laboratory. *Yonsei Medical Journal*, 51, 104-110.

[5] Chong, E.T.J., Lee, C.C., Chua, K.H., Chuah, J.A. and Lee, P.-C., 2014. *Rsa*I but not *Dra*I polymorphism in *CYP2E1* gene increases the risk of gastrointestinal cancer in Malaysians: a case-control study. *BMJ Open*, 4(1), https://doi.org/10.1136/bmjopen-2013-004109

[6] Chong, E.T.J., Abdul, A.N.F. and Lee, P.-C., 2018. Association of *IRX3* rs3751723 polymorphism with the risk of overweight and obesity: case-control study and meta-analysis. *Meta Gene*, 16, 50-56.

[7] Desjardins, P. and Conklin, D., 2010. NanoDrop microvolume quantitation of nucleic acids. *Journal of Visualized Experiments*, 45, 2565, https://doi.org/10.3791/2565

[8] Fleige, S. and Pfaffl, M.W., 2006. RNA integrity and the effect on the real-time qRT-PCR performance. *Molecular Aspects of Medicine*, 27, 126-139.

[9] Chew, C.H., Lim, Y.A.L., Lee, P.C., Mahmud, R. and Chua, K.H., 2012. Hexaplex PCR detection system for identification of five human *Plasmodium* species with an internal control. *Journal of Clinical Microbiology*, 50, 4012-4019.

[10] Goh, X.T., Lim, Y.A.L., Vythilingam, I., Chew, C.H., Lee, P.C., Ngui, R., Tan, T.C., Yap, N.J., Nissapatorn, V. and Chua, K.H., 2013. Increased detection of *Plasmodium knowlesi* in Sandakan division, Sabah as revealed by PlasmoNex™. *Malaria Journal*, 12, 264, https://doi.org/10.1186/1475-2875-12-264

[11] William, T., Jelip, J., Menon, J., Anderios, F., Mohammad, R., Mohammad, T.A.A., Grigg, M.J., Yeo, T.W., Anstey, N.M. and Barber, B.E., 2014. Changing epidemiology of malaria in Sabah, Malaysia: increasing incidence of *Plasmodium knowlesi*. *Malaria Journal*, 13, 390, https://doi.org/10.1186/1475-2875-13-390

[12] Lee, P.C., Chong, E.T.J., Anderios, F., Lim, Y.A.L., Chew, C.H. and Chua, K.H., 2015. Molecular detection of human *Plasmodium* species in Sabah using PlasmoNex™ multiplex PCR and hydrolysis probes real-time PCR. *Malaria Journal*, 14, 28, https://doi.org/10.1186/s 12936-015-0542-5

Effects of Preharvest Boron, Calcium Sulfate Treatment and Postharvest Calcium Chloride Peduncle Infiltration on Chilling Injury Alleviation of Queen Pineapple cv. Sawi Fruit

Pannipa Youryon[1] and Suriyan Supapvanich[2]*

[1]Department of Agricultural Technology, King Mongkut's Institute of Technology Ladkrabang, Prince of Chumphon Campus, Chumphon, Thailand
[2]Department of Agricultural Education, Faculty of Industrial Education and Technology, King Mongkut's Institute of Technology Ladkrabang, Ladkrabang, Bangkok, Thailand

Received: 22 September 2020, Revised: 23 December 2020, Accepted: 13 January 2021

Abstract

The aim of this study was to determine the incorporative effects of preharvest boron (B) or calcium sulfate ($CaSO_4$) application and postharvest calcium chloride ($CaCl_2$) peduncle infiltration on chilling injury (CI) alleviation of Queen pineapple during commercial cold storage (13°C). Pineapple fruits were sprayed with 0.25% B four times a month after one month of anthesis, or $CaSO_4$ (100 kg per 400 m^2) was applied during fruit development. The fruits were harvested after 135 days of flower induction. Both preharvest B and treated fruits were then peduncle-infiltrated with 2% $CaCl_2$ for 3 days and stored at cold temperature (CT) for 14 days. Control fruits were not peduncle-infiltrated with $CaCl_2$.Visual appearance of half cut fruit, CI score, the amount of fruit having CI, colour attributes, browning index (BI) value and electrolyte leakage (EL) of tissue adjacent to the core were determined after storage at CT for 7 or 14 days, followed by leaving at room temperature (RT), 28 ± 1°C, for 2 days. The results show that the incorporative application of preharvest $CaSO_4$ with $CaCl_2$ peduncle infiltration ($CaSO_4$+$CaCl_2$) alleviated CI, delayed decrease in lightness (L^*) and chroma values, and also increased BI and total colour difference (ΔE^*) values during storage compared with control and the incorporative application of preharvest B with $CaCl_2$ treatment (B + $CaCl_2$). The treatment with $CaSO_4$ + $CaCl_2$ lowered CI severity and the amount of fruit having CI when compared to B + $CaCl_2$ and control treatments, respectively. Both treatments had no effect on the hue value over the storage period. Therefore, $CaSO_4$ + $CaCl_2$ treatment is an alternative method for alleviating CI of Queen pineapples.

Keywords: Queen pineapple; $CaSO_4$; boron; $CaCl_2$; chilling injury
DOI 10.14456/cast.2021.37

*Corresponding author: E-mail: suriyan.su@kmitl.ac.th

1. Introduction

Pineapple (*Ananas comosus* L. Merr) is recognized as one of commercial fruits in Thailand. It has been commercially grown around the country to serve the pineapple product industry and for fresh consumption. Two pineapple groups, Smooth Cayenne and Queen, have been commercially cultivated. Smooth Cayenne pineapples are mostly grown to supply the pineapple processing industry and Queen pineapples are mainly produced for fresh consumption [1]. Regarding physiological disorders of pineapples during storage, internal browning or heart blackening is a main disorder that limits the quality and consumption acceptability of both Smooth Cayenne and Queen pineapples. The disorder symptoms generally appear during refrigerated storage, and are referred to as chilling injury [2, 3]. These symptoms sometimes occur in the fruit stored at room temperature. Compared to Smooth Cayenne pineapples, Queen pineapples are more susceptible to internal browning disorder, especially during cold storage [4, 5]. Om-arun and Siriphanich [6] reported that no internal browning incidence was found in Smooth cayenne pineapple fruit during cold storage for 3 weeks whilst internal browning incidence in Queen pineapple fruit appeared within 7 days after storage at 13°C [7, 8].

Recently, most previous work has been concerned with postharvest applications including anoxia treatment [9], plant regulator application [10] and calcium peduncle infiltration [8] alleviating internal browning of Queen pineapples. Our previous work showed that calcium peduncle infiltration was an effective postharvest treatment that could alleviate the internal browning of Queen pineapple cv. Sawi during refrigerated storage [7, 8, 11, 12]. However, there have been no studies of incorporative preharvest treatment and postharvest calcium peduncle infiltration ameliorating internal browning disorder of pineapples. Nitrogen, potassium and calcium are often required as plant nutrients in the production of pineapple [13]. Moreover, boron has also been suggested as a key element for pineapple fruit formation and development of quality [13, 14]. Lack of boron can cause malformed fruit, broken core, separation and cracking of fruitlets and reduced sugar content [13]. Boron also plays a crucial role in retaining plasma membrane integrity and protecting membrane against oxidative stress [14]. Gypsum has been fertilized as a calcium source to prevent calcium deficiency during pineapple fruit development. Silva *et al*. [15] reported that the application of calcium sources such as lime, gypsum and basaltic dust increased calcium content in soil and reduced internal translucency of pineapple fruit. They also suggested that gypsum fertilization did not affect soil pH compared to lime. Kumari and Deb [16] suggested that the foliar application of 0.5 or 1.0% of boron (B) could improve the quality of 'Mauritius' pineapple. Moreover, Poovarodom and Boonplang [17] reported that the preharvest application of gypsum and 0.25% B spray could alleviate physiological disorders affecting quality of mangosteen fruit. Thus, we were interested in investigating the combinative effects of preharvest application of B or gypsum and postharvest calcium peduncle infiltration to inhibit internal browning symptom of Queen pineapples during refrigerated storage.

2. Materials and Methods

2.1 Plant materials and experiments

Queen pineapple 'Sawi" fruits were cultivated at King Mongkut's Institute of Technology Ladkrabang, Prince of Chumphon campus demonstration farm. Ammonium sulfate granular 21-0-0 fertilizer was applied to the pineapple plants every two months. The 16-month-old plants were flowered by spraying with 25 µl l^{-1} of ethephon in aqueous solution containing 2% urea and 0.04% calcium carbonate. This was in contrast to the work of Poovarodom and Boonplang [17] in which

preharvest treatments of $CaSO_4$ and B were applied. After one month of anthesis, the pineapple fruits were sprayed with 0.25% of boron (B) every month until the fruits were harvested (4 times), or $CaSO_4$ (100 kg per 400 m^2) was applied to the pineapple plant one month after anthesis. The untreated pineapples were used as control. The fruits were harvested after 135 days of flower induction when fruit peels were yellow to about 25%. Regarding our previous work, 2% $CaCl_2$ peduncle infiltration was recommended as an effective approach to alleviate internal translucency and browning of Queen pineapple cv. 'Sawi' [7, 11], whereas the application of $CaCl_2$ at concentrations higher than 2% caused browning incidence in the fruit stem [18]. Fifty fruits per treatment were taken. The fruits were cleaned using an air-blaster. Both preharvest B and $CaSO_4$ treated pineapples were peduncle-infiltrated with 2% $CaCl_2$ at 13°C for 3 days and then continuously stored at 13°C for 14 days. In the control treatment, the fruits were stored at 13°C without $CaCl_2$ peduncle infiltration. The fruits were sampled every 7 days. Before investigation on various parameters, the fruits were left at room temperature (RT) (28 ± 1°C) for 2 days. Various biological parameters such as visual appearance of half-cut fruit, colour attributes, chilling injury (CI) severity score, browning index (BI) value, the amount of fruit having CI and electrolyte leakage (EL) value of tissue adjacent to the core were monitored. Fifty fruits (50 replicates) were used to evaluate CI incidence, including CI severity score, and the amount of fruit having CI. Five replicates per treatment (10 fruits per replicate) were used to determine colour attributes, BI, and EL values.

2.2 Visual appearance and colour attribute measurements

Vertically half-cut pineapple fruits were used to determine internal browning and translucency appearance caused by CI. Visual browning appearance of the tissue adjacent to the core was presented by photographs. L^*, hue and chroma values of the tissue were measured using a HunterLab MiniScan@ XE Plus (Hunter Associates Laboratory Inc., USA). The total colour difference (ΔE^*) value of tissue adjacent to the core compared with the fruit at initial day (0) was calculated using the equation shown below.

$$\Delta E* = \sqrt{\left(L_0{}^{*2} - L_x{}^{*2}\right) + \left(\mathrm{hue}_0{}^2 - \mathrm{hue}_x{}^2\right) + \left(\mathrm{chroma}_0{}^2 - \mathrm{chroma}_x{}^2\right)}$$

2.3 CI score measurement

CI severity score was evaluated using a 5-point ranking test. Ten trained panellists were used to evaluate the CI severity score. The simplified CI scores ranged from 0 to 5: 0 = no symptom; 1 = small translucent spots turning brown (less than 5%); 2 = 5-10% CI symptom; 3 = 11-20% CI symptom; 4 = 21-30% CI symptom; and 5 = more than 30% CI symptom, were used.

2.4 BI measurement

BI of the fruit tissues was assessed using the method described by Supapvanich *et al*. [19] with slight modification. A 10 g sample of tissue adjacent to the core was homogenised with 30 ml of 60% (v/v) ethanol and then stirred for 1 h. The homogenate was filtered through Whatman No. 1 filter paper and the wavelength absorbance of filtrate was measured at 420 nm. Data were expressed as OD_{420} g^{-1} fresh weight (OD_{420} g^{-1}).

2.5 EL measurement

EL of tissue adjacent to the core was determined using the method of Youryon *et al*. [8]. Fifteen disks (7.5 mm diameter per disk) of tissue adjacent to the core of pineapple fruit were rinsed with de-ionized water and dried using a Whatman No.1 filter paper. The disks were immersed in 30 ml of de-ionized water for 30 min and the conductivity of solution (EC_{sample}) was measured using a conductivity meter. Afterwards, the sample was frozen at -20°C for 24 h. After thawing, the sample was boiled for 30 min and after the temperature of sample had dropped to room temperature, the conductivity of solution was again measured and recorded as total conductivity (EC_{total}). The EL value of each sample was calculated by comparing with total conductivity of the sample.

2.6 Statistical analysis

The experiments were performed using a completed randomized design (CRD) and statistical data were analysed using the Analysis of Variances (ANOVA). Significant differences between data were compared using the Duncan's new multiple range test (DMRT) at $P < 0.05$.

3. Results and Discussions

3.1 Visual appearance

It is commonly recognized that translucency and browning of tissue adjacent to the core are the symptoms of CI in pineapples during cold storage. Figure 1 shows the visual appearance of half-cut Queen pineapple 'Sawi' fruits treated with B + $CaCl_2$ or $CaSO_4$ + $CaCl_2$ during storage. It was found that after storage at CT for 7 days followed by leaving at RT for 2 days, the control fruits had more CI incidence than fruits treated with B+$CaCl_2$ or $CaSO_4$ + $CaCl_2$. The lowest CI incidence was found in the fruit treated with $CaSO_4$ + $CaCl_2$. After cold storage for 14 days followed by leaving at RT for 2 days, $CaSO_4$ + $CaCl_2$ treated fruits had IB incidence much lower than other treatments. The highest CI incidence was found in the control fruits. The result shows that $CaSO_4$ + $CaCl_2$ could alleviate CI symptom of Queen pineapple during commercial cold storage at 13°C. Youryon *et al*. [7] suggested that the more uptake of Ca in the core of pineapple fruits, the more alleviation of internal translucency and browning were caused by chilling stress during cold storage. Youryon *et al*. [8] explained that Ca could possibly strengthen cell wall structure and maintain membrane function. Youryon and Wongs-Aree [11] reported that the postharvest application of 2 or 3% of $CaCl_2$ alleviated CI more than 1% $CaCl_2$. The recent study confirms that calcium application could better alleviate CI of Queen pineapple as the fruit treated with $CaSO_4$ + $CaCl_2$ had lower internal translucency and browning than the fruit treated with B + $CaCl_2$ and control.

3.2 CI incidence

Table 1 shows the CI severity score and the percentage of fruit having CI symptoms. The CI severity score of the pineapple fruits increased as the storage period increased. The highest CI severity score was found in control fruit followed by B + $CaCl_2$ and $CaSO_4$ + $CaCl_2$ treated fruits, respectively. At the end of 14 days storage, the CI severity score of both control and B+$CaCl_2$ treated fruit was 4.8 and 4.6, respectively, while that of $CaSO_4$ + $CaCl_2$ treated fruit was only 2.80. The amount of fruit without CI symptom found in $CaSO_4$ + $CaCl_2$ treated fruits was about 70% and 16.7% after storage for 7 and 14 days, respectively. Moreover, CI symptom was detected in all control fruits after storage

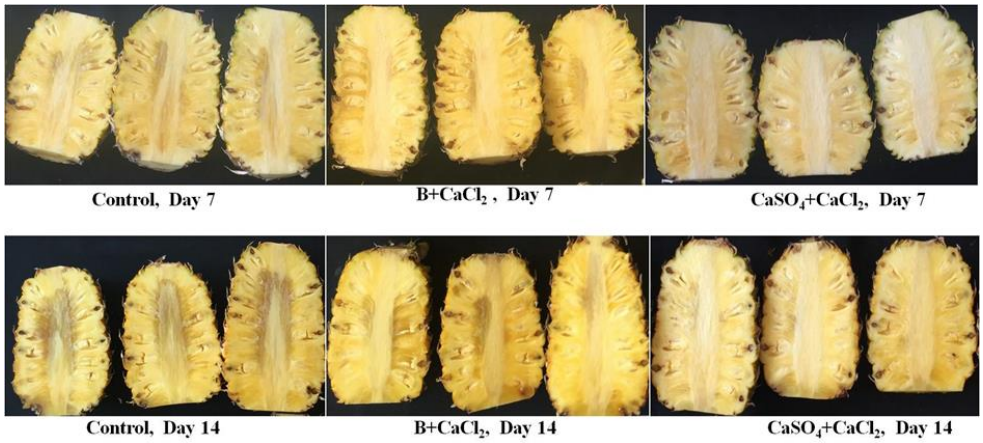

Figure 1. Visual appearance of half-cut Queen pineapple fruits preharvest-treated with B, $CaSO_4$ and postharvest $CaCl_2$ peduncle infiltration after cold storage at 13°C for 7 and 14 days

Table 1. CI severity score and percentage of fruit with CI of Queen pineapple fruits preharvest treated with boron or $CaSO_4$ followed by postharvest $CaCl_2$ peduncle infiltration after storage at CT for 7 and 14 days and by storage at RT for 2 days

Treatments	Storage time (d)	CI severity score	Percentage of fruit with CI (%)		
			no CI	< 3 score	≥ 3 score
Control	7 (CT)+2(RT)	3.00^{b}	0	50	50
	14(CT)+2(RT)	4.80^{a}	0	30	70
$B+CaCl_2$	7 (CT)+2(RT)	1.80^{c}	30	50	20
	14(CT)+2(RT)	4.60^{a}	0	30	70
$CaSO_4+CaCl_2$	7 (CT)+2(RT)	0.20^{d}	70	10	20
	14(CT)+2(RT)	2.80^{b}	16.7	33.3	50

Data are shown as means (n = 50).
Different superscript letters shown in the same column indicated a significant difference at $P < 0.05$.

at CT for 7 and 14 days. The fruits treated with 30 % of B + $CaCl_2$ had CI symptom after storage for 7 days and all of the B+$CaCl_2$ treated fruit had CI after storage for 14 days. After cold storage for 7 days, the CI score of the control fruit was significantly higher than that of other treated fruits ($P < 0.05$). The lowest CI score was observed in $CaSO_4$ + $CaCl_2$ treated fruits and was significantly lower than that of other treated fruits ($P < 0.05$). After cold storage for 14 days, CI scores of the control and $CaSO_4$ + $CaCl_2$ treated fruits were similar while that of $CaSO_4$ + $CaCl_2$ treated fruits was significantly lower ($P < 0.05$). The CI severity score was concomitant with the CI incidence and the changes in colour attributes as shown in Figures 1 and 2. These results suggest that the treatment of B + $CaCl_2$ treatment could alleviate CI of the pineapple fruit when compared to the control, but the efficiency was less than that of $CaSO_4$ + $CaCl_2$ treatment. It is commonly recognized that B functions to maintain plant cell wall strength through its binding to the pectin polysaccharides

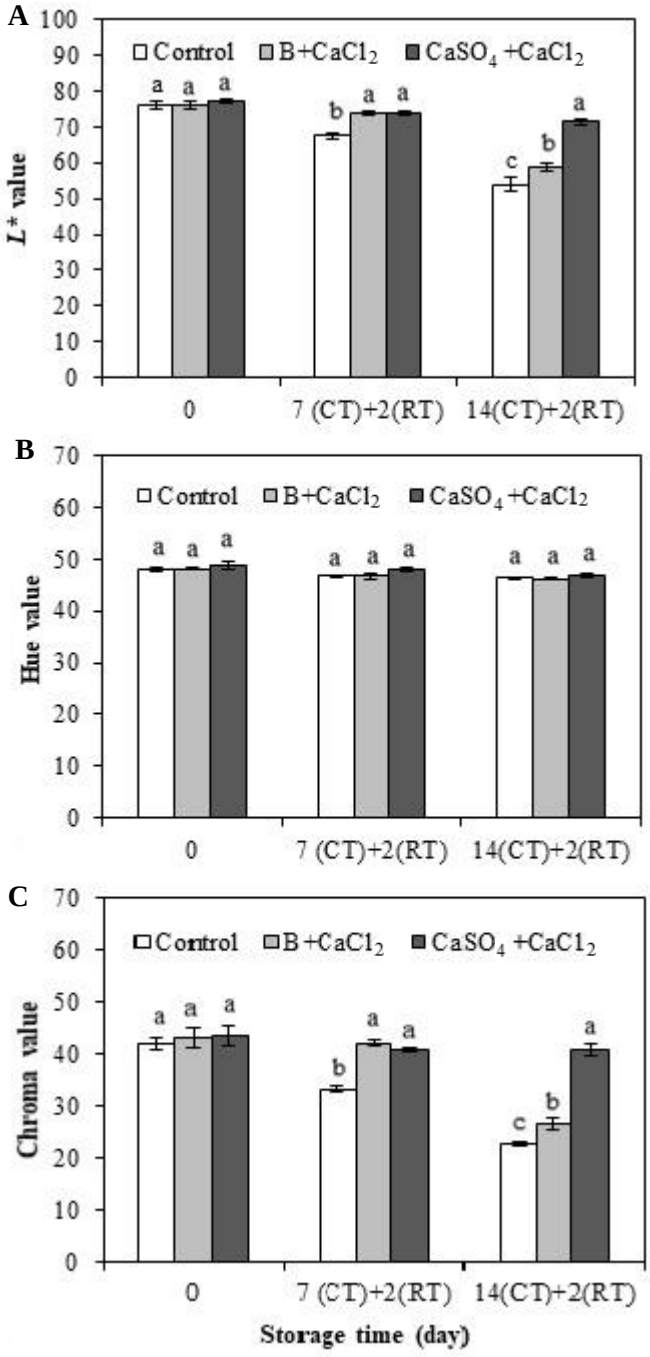

Figure 2. *L** (A), hue (B) and chroma (C) values of tissue adjacent to the core of Queen pineapple fruits preharvest treated with boron or $CaSO_4$ followed by postharvest $CaCl_2$ peduncle-infiltration after CT for 7 and 14 days and by leaving at RT for 2 days. Vertical bars represent standard deviation (SD) of means (n = 5). The different letters within the same day of storage are significantly different at $P < 0.05$.

that B functions to maintain plant cell wall strength through its binding to the pectin polysaccharides in collaboration with Ca^{2+} [20]. The treatment of $CaSO_4$ + $CaCl_2$ could alleviate severity of CI incidence as well as induce the chilling stress tolerance of the fruit rather than B + $CaCl_2$ alone. Hewajulige *et al*. [21] also reported that the concentration of Ca^{2+} in tissue of pineapple fruit was positively related to CI symptom, where Ca^{2+} concentration in the fruit core was lower than that in flesh and shell. These results also confirm that the concentration of Ca^{2+} in tissues influenced the CI tolerance of Queen pineapple fruit [11].

3.3 Colour attributes of tissue adjacent to the core

The changes in colour attributes of tissue adjacent to the core of Queen pineapple fruits treated with B + $CaCl_2$ and $CaSO_4$ + $CaCl_2$ are shown in Figure 2. After cold storage for 7 days followed by leaving at RT for 2 days, L^* and chroma values of control fruits were significantly lower than those of B + $CaCl_2$ and $CaSO_4$ + $CaCl_2$ treated fruits ($P < 0.05$). However, both L^* and chroma values of B + $CaCl_2$ and $CaSO_4$ + $CaCl_2$ treated fruits were similar. After cold storage for 14 days followed by leaving at RT for 2 days, both L^* and chroma values of the control fruits had evidently decreased and were significantly lower than those of B + $CaCl_2$ and $CaSO_4$ + $CaCl_2$ treated fruits ($P < 0.05$). When compared to $CaSO_4$ + $CaCl_2$ treated fruits, L^* and chroma values of B + $CaCl_2$ treated fruits were significantly lower ($P < 0.05$). While, hue values of all treatments remained constant throughout the storage periods. The hue value of tissue adjacent to the core was approximately 47.33, which presented as yellow colour. These results suggest that $CaSO_4$ + $CaCl_2$ treatment can prevent the losses of L^* and chroma value of tissue adjacent to the core better than B + $CaCl_2$ treatment. Many previous work suggested that the increase in internal translucency and browning of tissue adjacent to the core of pineapples was concomitant with the reduction of L^* value [3, 8, 10]. Moreover, we found that the reduction of chroma value was also related with the increase in CI symptom of Queen pineapple during cold storage. It is typically acknowledged that chroma value represents the intensity of colour. Therefore, the occurrence of internal translucency (Figure 1) was concomitant with the decrease of chroma value of tissue adjacent to the core of pineapples.

3.4 Browning index and total colour difference value of tissue adjacent to the core

BI and ΔE^* values of the pineapples are shown in Figure 3. Both parameters of the control fruits evidently increased and were significantly higher than those of B + $CaCl_2$ and $CaSO_4$ + $CaCl_2$ treated fruits over the storage ($P < 0.05$). After storage at CT for 7 days followed by RT for 2 days, both BI and ΔE^* values of B + $CaCl_2$ or $CaSO_4$ + $CaCl_2$ treated fruits were similar. After storage at CT for 14 days followed by RT for 2 days, both BI and ΔE^* values of B + $CaCl_2$ increased significantly higher than those of $CaSO_4$ + $CaCl_2$ treated fruits. These results indicate that $CaSO_4$ + $CaCl_2$ treatment could maintain colour and prevent browning incidence of tissue adjacent to the core of the pineapples during cold storage. It is commonly recognized that browning incidence occurred in tissue adjacent to the core of pineapple is caused by the reaction of PPO and phenolic compounds, namely enzymatic browning reaction. Hewajulige *et al.* [21] suggested that the severity of black heart or internal browning incidence in pineapples was associated with low calcium content in tissue adjacent to the core compared to pulp and peel. Hopfinger *et al.* [22] suggested that preharvest Ca treatment increased Ca concentration in fruit and decreased browning enzyme activity. Moreover, previous work reported that postharvest calcium treatment could alleviate internal browning of tissue adjacent to the core of Queen pineapples due to the decrease in PPO activity [7, 8, 10, 12]. The recent results indicated that preharvest $CaSO_4$ treatment incorporated with postharvest $CaCl_2$ application effectively alleviated internal browning incidence when compared to preharvest B treatment incorporated with postharvest $CaCl_2$ peduncle infiltration.

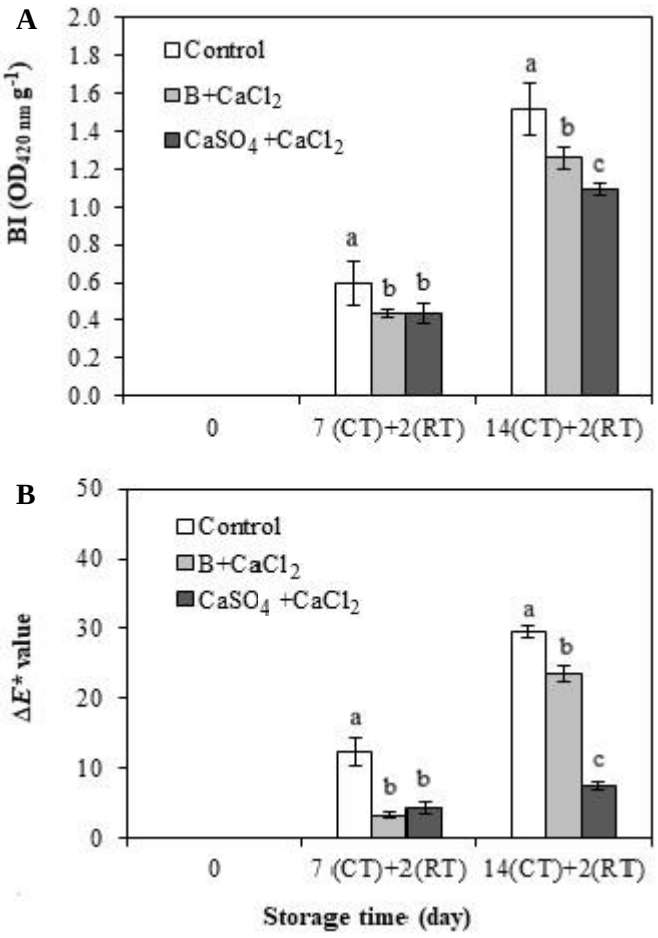

Figure 3. BI (A) and Δ*E** (B) values of tissue adjacent to the core of Queen pineapple fruits preharvest treated with boron or $CaSO_4$ followed by postharvest $CaCl_2$ peduncle-infiltration after CT for 7 and 14 days and by leaving at RT for 2 days. Vertical bars represent standard deviation (SD) of means (n = 5). The different letters within the same day of storage are significantly different at $P < 0.05$.

3.5 EL of tissue adjacent to the core

Figure 4 shows EL value of tissue adjacent to the core during storage. EL value of all treatments increased during the storage period. The highest EL value was found in the control fruits and it was significantly higher than that of B + $CaCl_2$ and $CaSO_4$ + $CaCl_2$ treated fruits ($P < 0.05$). $CaSO_4$ + $CaCl_2$ treatment controlled the increase in EL of tissue adjacent to the core better than B + $CaCl_2$ treatment. These results indicate that the treatment of $CaSO_4$ + $CaCl_2$ could alleviate the membrane dysfunction and thus inhibit the increase in EL value during the storage period. It is commonly recognized that CI is an oxidative stress caused by chilling temperature. The factors indicating CI incidence is EL value which associated with increased membrane lipid oxidation caused by chilling

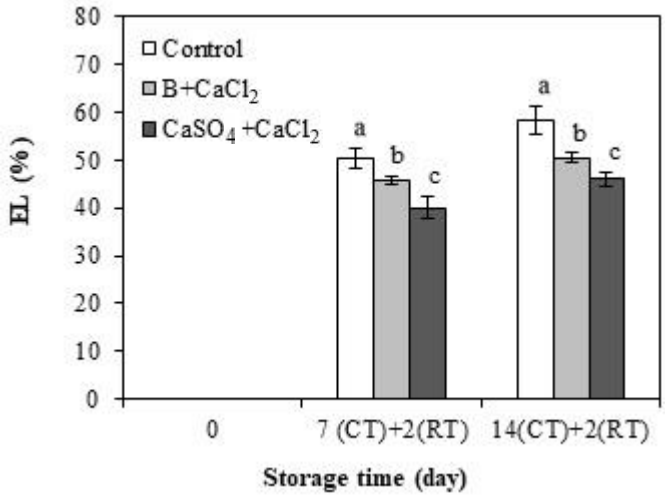

Figure 4. EL value of tissue adjacent to the core of Queen pineapple fruits preharvest treated with boron or $CaSO_4$ followed by postharvest $CaCl_2$ peduncle infiltration after CT for 7 and 14 days followed by RT for 2 days. Vertical bars represent standard deviation (SD) of means (n = 5). The different letters within the same day of storage are significantly different at $P < 0.05$.

temperature [23]. Picchioni *et al*. [24] stated that Ca in plant tissue plays a role in strengthening cell wall structure as well as regulating protein kinase signalling and inducing membrane integrity. Thus, the treatment of $CaSO_4$ + $CaCl_2$ may increase the Ca concentration in tissue adjacent to the core in a superior way to the treatment of B + $CaCl_2$, leading to prevent the increase in EL value. Thus, Ca application helps to maintain membrane integrity of pineapples. Regarding the cell wall and membrane strengthening by Ca treatment, the breakdown of tissue structure is low, leading to lower translucency incidence and to prevent the release of PPO [25]. The recent study showed that the lower EL value of $CaSO_4$ + $CaCl_2$ treated fruits was concomitant with lower CI incidence (Figure 1 and Table 1), higher L^* and chroma values (Figure 2) and lower BI and ΔE^* values (Figure 3) compared to B + $CaCl_2$ and control treatments, respectively.

4. Conclusions

The applications of preharvest B, $CaSO_4$ and postharvest $CaCl_2$ peduncle infiltration could alleviate CI of Queen pineapple cv. 'Sawi' fruits during commercial cold storage. $CaSO_4$ + $CaCl_2$ treatment could inhibit the increase in internal browning incidence. The treatment also maintained the membrane integrity of tissue adjacent to the core due to the lowered EL value when compared to B + $CaCl_2$ treatment. Our results suggest that $CaSO_4$ + $CaCl_2$ treatment is an alternative approach for alleviating CI of postharvest Queen pineapple during cold storage.

5. Acknowledgements

We thank National Research Council of Thailand for fully financial support of this project.

References

[1] Quyen, D.T.M., Jommwong, A. and Rachtanapun, P., 2013. Influence of storage temperature on ethanol content, microbial growth and other properties of queen pineapple fruit. *International Journal of Agriculture and Biology*, 15, 207-214.

[2] Paull, R.E. and Rohrbach, K.G., 1985. Symptom development of chilling injury in pineapple fruit. *Journal of the American Society for Horticultural Science*, 110, 100-105.

[3] Hong, K., Xu, H., Wang, J., Zhang, L., Hu, H., Jia Z. and Gong, D., 2013. Quality changes and internal browning developments of summer pineapple fruit during storage at different temperature. *Scientia Horticulturae*, 151, 68-74.

[4] Wijeratnam, R.S.W, Abeyesakere, M. and Surjani, P., 1993. Studies on black heart disorder in pineapple varieties grown in Sri Lanka. *Acta Horticulturae*, 334, 317-324.

[5] Pusittigul, I., Kondo, S. and Siriphanich, J., 2012. Internal browning of pineapple (*Ananas comosus* L.) fruit and endogenous concentrations of abscisic acid and gibberellins during low temperature storage. *Scientia Horticulturae*, 146, 45-51.

[6] Om-arun, N. and Siriphanich, J., 2005. Hydrogen peroxide and ascorbic acid contents, superoxide dismutase and catalase activities in Smooth Cayenne and Queen pineapples during cold storage. *Acta Horticulturae*, 682, 611-616.

[7] Youryon, P. Wongs-Aree, C., McGlasson, W.B., Glahan. S. and Kanlayanarat, S., 2013. Alleviation of internal browning in pineapple fruit by peduncle infiltration with solutions of calcium chloride or strontium chloride under mild chilling storage. *International Food Research Journal*, 20(1), 239-246.

[8] Youryon, P., Supapvanich, S., Kongtrakool, P. and Wongs-Aree, C., 2018. Calcium chloride and calcium gluconate peduncle infiltrations alleviate the internal browning of Queen pineapple in refrigerated storage. *Horticulture, Environment, and Biotechnology*, 59, 205-213.

[9] Techavuthiporn, C., Boonyaritthongchai, P. and Supabvanich, S., 2017. Physicochemical changes of "Phulae" pineapple fruit treated with short term anoxia during ambient storage. *Food Chemistry*, 228, 388-393.

[10] Sangprayoon, P., Supapvanich, S., Youryon, P., Wongs-Aree, C. and Boonyaritthongchai, P., 2019. Efficiency of salicylic acid or methyl jasmonate immersions on internal browning alleviation and physicochemical quality of Queen pineapple cv, "Sawi" fruit during cold storage. *Journal of Food Biochemistry*, 43 (12), e13059, https://doi.org/10.1111/jfbc.13059

[11] Youryon, P., and Wongs-Aree, C., 2015. Postharvest application of calcium chloride affects internal browning reduction during low temperature storage of 'Sawi' pineapple. *Acta Horticulturae*, 1088, 197-200.

[12] Youryon, P., Supapvanich, S. and Wongs-Aree, C., 2019. Internal browning alleviation of Queen pineapple cv. 'Sawi' under cold storage using salicylic acid or abscisic acid peduncle infiltration. *The Journal of Horticultural Science and Biotechnology*, 94 (6), 744-752.

[13] Ramos, M.J.M., Monnerat, P.H., de Carvalho, A.J.C., Pinto, J.L.A. and da Silva, J.A., 2006. Nutritional deficiency in 'Imperial' pineapple in the vegetative growth phase and leaf nutrient concentration. *Acta Horticulturae*, 702, 133-139.

[14] Cakmak, I. and Römheld, V., 1997. Boron deficiency-induced impairments of cellular functions in plants. *Plant Soil*, 193, 71-83.

[15] Silva, J.A., Hamasaki, R., Paull, R., Ogoshi, R., Bartholomew, D.P., Fukuda, S., Hue, N.V., Uehara, G. and Tsuji, G.Y., 2006. Lime, gypsum, and basaltic dust effects on the calcium nutrition and fruit quality of pineapple. *Acta Horticulturae*, 702, 123-131.

[16] Kumari, U. and Deb, P., 2018. Effect of foliar application of zinc and boron on quality of pineapple cv. Mauritius. *Journal of Pharmacognosy and Phytochemistry*, 7(6), 1166-1168.

[17] Poovarodom, P. and Boonplang, N., 2010. Soil calcium application and pre-harvest calcium and boron sprays on mangosteen fruit quality attributes. *Acta Horticulturae*, 868, 359-366.
[18] Pusittigul, I., Siriphanich, J. and Juntee, C., 2014. Role of calcium on internal browning of pineapples. *Acta Horticulturae*, 1024, 329-338.
[19] Supapvanich, S., Pimsaga, J. and Srisujan, P., 2011. Physiochemical changes in fresh-cut wax apple (*Syzygium samarangenese* [Blume] Merrill & L.M. Perry) during storage. *Food Chemistry*, 127, 912-917.
[20] Matoh, T. and Kobayashi, M., 1998. Boron and calcium, essential inorganic constituents of pectic polysaccharides in higher plant cell walls. Journal of Plant Research, 111(1), 179-190.
[21] Hewajulige, I.G.N., Wijeratnam, S.W., Wijeratnam, R.L.C. and Abeysekere, M., 2003. Fruit calcium concentration and chilling injury during low temperature storage of pineapple. *Journal of the Science of Food and Agriculture*, 83(14), 1451-1454.
[22] Hopfinger, J.A., Poovaiah, B.W. and Patterson, M.E., 1984. Calcium and magnesium interactions in browning of 'Golden Delicious' apples with bitter pit. *Scientia Horticulturae*, 23, 345-351.
[23] Kukura, J.L., Beelman, R.B., Peifer, M. and Walsh, R., 1998. Calcium chloride added to irrigation water of mushrooms (*Agaricus bisporus*) reduces postharvest browning. *Journal of Food Science*, 63(3), 454-457.
[24] Picchioni, G.A., Watada, A.E., Conway, W.S., Whitaker, B.D. and Sams, C.E., 1998. Postharvest calcium infiltration delays membrane lipid catabolism in apple fruit. *Journal of Agricultural and Food Chemistry*, 46, 2452-2457.
[25] Taranto, F., Pasqualone, A., Mangini, G., Tripodi, P., Miazzi, M. M., Pavan, S. and Montemurro, C., 2017. Polyphenol oxidases in crops: Biochemical, physiological and genetic aspects. *International Journal of Molecular Sciences*, 18(2), 377, https://doi.org/10.3390/ijms18020377

Current Applied Science and Technology Vol. 21 No. 3 (July-September 2021)

Autonomous Mobile Robot Using Vision System and ESP8266 Node MCU Board

Napassadol Singhata*

Department of Automation and Robotic Engineering, Faculty of Engineering, Rajamangala University of Technology Krungthep, Bangkok, Thailand

Received: 9 June 2020, Revised: 21 October 2020, Accepted: 19 January 2021

Abstract

This paper proposes an automated mobile robot indoor system. A web camera sensor is equipped to detect the current location of the vehicle. The web camera is located above to capture the object and environment for mapping. The images come from the web camera via a USB interface to the computer. The image processing method is used to determine the position of the mobile robot for giving the input of path planning. The microcontroller obtains interactive actions with the combinations of image processing and suitable path planning to control the direction of the mobile robot. The experimental results show that the vision system can interact with the microcontroller. The robot can move automatically from the starting point to the goal.

Keywords: vision system; autonomous vehicle; mobile robot; microcontroller; image processing
DOI 10.14456/cast.2021.38

1. Introduction

Nowadays, service transportation indoor systems repeat passages that involve traveling short and these are controlled by humans. It is necessary that service transportation systems can recognize traffic signals and signs on the way [1]. Operators control the vehicles enabling the vehicles to get to their targets safely [2, 3]. Many researchers have been trying to create technology that can make transportation more convenient [4] and part of this has been the creation of autonomous robots that can travel to the destination safely [5] and improve the lifestyles of their users [6]. There are different systems that can be used to make self-driving vehicles [7] in order to replace human operations. The system is controlled by an interactive interface and reaches autonomous navigation by extracting the appropriate mapping information [8] for better convenience, safety, and efficiency on the road [9]. A sensor is one important part that measures physical input from its environment to convert into a signal for the perception of a vehicle if the sensor is suitable to handle these tasks. It is able to complete the identification [10 -12] and allows a vehicle to go to the target with precision [13]. Considering the key role of self-driving in the automatic mobile robot, it seems that the perception sensors are necessary for a mobile robot to automatically self-drive [14]. These types of systems also need improved vehicle navigation system [15], location system [16], electronic map, path planning [17]. Furthermore, better vehicle speed control is crucial for overall vehicle control [18].

*Corresponding author: Tel.: (086) 4259561
E-mail: napassadol.s@mail.rmutk.ac.th

Speed control is complex due to the large amount of information that needs to be dealt with, and usually a single sensor is unable to efficiently perceive the mass information. However, an additional performance of the automatic mobile robot based on those factors is necessary.

In order to develop a self-driving mobile robot for indoors, choosing a suitable method for mapping is very important for the navigation of an autonomous driving robot [19]. There are several methods to guide the mobile robot to reach the goal [20]. Magnetic tape is an easy way to guide the mobile robot for tracking. It is attached to the floor and helps the robot to identify the surrounding area for navigating mobile robots. The mobile robot often seems to be confused about moving when something is obstructed on the road or when the magnetic tape is lost. Lidars are often used and they play an important role in system navigation. Many researchers use a Lidar to perceive the surrounding environment and establish the electronic map [21-23]. Lidar is a remote sensing method that uses light in the form of a pulsed laser to measure ranges to the object. It is not appropriate for some tasks that are too sensitive to laser light and the laser beams may harm the human eye in cases where the beam is too powerful. A vision system is one innovation that can be applied in visual perception [24, 25]. To provide more information than conventional sensors [26, 27], the accuracy of data collected can be improved by methods based on image processing advanced sensory tools [28], particularly with respect to physical measurement [29]. Vision system helps to automatically locate [30], navigate [31], judge motion [32], and perform path planning [33] for the mobile robot on the way to its destination. Such vision systems can provide better convenience, safety, and efficiency for transportation systems.

This paper presents a mapping method with image processing that identifies the current position of the mobile robot for path planning. The autonomous mobile robot is controlled by an ESP8266 Node MCU board. The microcontroller interfaces with the vision system to control the direction of the mobile robot for autonomous driving. The computer shows electric graphic mapping in real-time. The system is also designed for path planning for navigation of the mobile robot on the computer [34]. The vision system not only provides a graphic map via the image processing method but it also navigates and guides the robot to the goal based on the path planning. The system also helps autonomous mobile robots reduce the use of multiple sensors and is considered to be one of the best options to reduce production costs [35].

2. Materials and Methods

2.1 The operation system

This section describes the design of an autonomous mobile robot for indoors. Considering the key role of the components in self-driving vehicle, the system consists of three parts, as follows: 1) a navigation system that requires the current location of the vehicle and position of destination, 2) a path planning facility, and 3) vehicle control. In this research, the vehicle system consists of two parts: 1) a vision system and 2) a mobile robot system as shown in Figure 1. The whole process of the system consists of four steps.

1) A web camera captures the images and sends the information to a computer.

2) A computer determines the vehicle location which is obtained by image processing. The vehicle location and destination position are inputs of path planning to guide the robot to go to the goal. The path planning signal is sent to a microcontroller.

3) The microcontroller receives the path planning signal and converts it for wheel control of the mobile robot. There are four functions as follows: Forward, Turn Left, Turn Right, and Stop.

4) The mobile robot is moved from starting to reach a goal by command of the microcontroller.

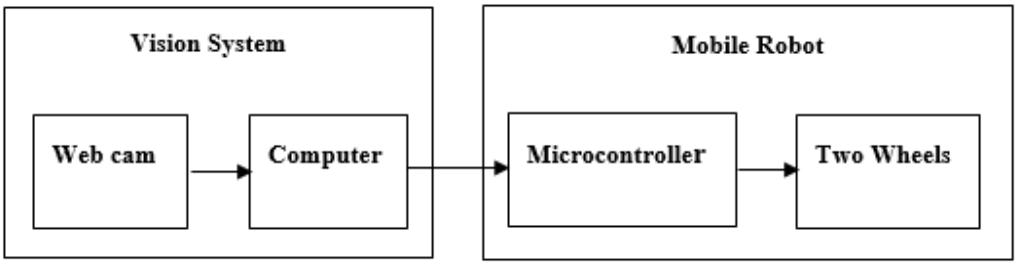

Figure 1. Block diagrams of the design of an autonomous mobile robot system

2.2 Vision system

The vision system consists of a web camera and a computer. The computer is used for image processing and designed path planning for the mobile robots. The computer is the central interface between the web camera and the microcontroller.

2.2.1 Web camera

The web camera is attached to a tripod stand. The web camera is installed from above as shown in Figure 2. The tripod stand is 127 cm high. The field of view (FOV) of the camera covers the area in 1280x960 pixels (122 × 32 cm). The configuration of the web camera is set up. There are brightness, contrast, exposure, sharpness, saturation, and white balance settings. The resolution of the web camera is 1600X896 pixels with 30 fps for capturing. The information is sent to the computer and the image is processed using the image processing method with LabVIEW software.

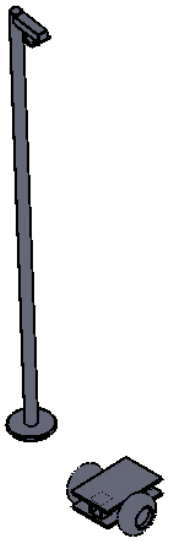

Figure 2. An autonomous mobile robot system

2.2.2 Object extraction from red plane

The RGB color image is an input signal of the computer. RGB (Red, Green, Blue) is the basic physical color of the object. The color of the robot is orange. This characteristic is distinguished from the scene. The object is separated from the scene by using red plane extraction and then the information is sent to thresholding.

2.2.3 Thresholding

Thresholding plays an important role in segmentation techniques and involves the separation of the object from the scene. The scene is changed to black color background. The object becomes more distinct. This process quickly determines the object and leads to finding the correct object.

2.2.4 Image matching

The image matching technique is used to evaluate the effect of the object by comparing the source image and the input image. The image matching process finds the existence of a pattern within a source image and it proceeds via the four steps as follows:

1) The object is captured as a source image to identify and reference patterns for matching

2) The web camera captures the image to send to the computer. The input image is compared across the source image to identify similar features that provide a matching of pairs between the source image and the input image.

$$(A1, B1) \leftrightarrow (A2, B2) \tag{1}$$

Where (A1, B1) is a feature in the source image and (A2, B2) is a matching feature in the input image.

3) The angle orientation parameter is set up to allows an automated way to detect images of an object in 360 degrees

4) The graphical interface is set up, and the trajectory of the robot is displayed in the graphic map. The computer updates the current location of the vehicle movement and reports the current position to the path planning.

2.2.5 Navigation system

The main purpose of the path planning is to guide the robot to its goal by locating the mobile robot's position relative to the destination position. The current position of the mobile robot is obtained by image processing. The mobile robot's position and the destination position can be derived by using the parameters as follows:

$$[(Xd - Xc), (Yd - Yc)] \leq \pm 100 \tag{2}$$

The design path planning consists of four terms as follows:

1) The mobile robot goes straight in the Y- axis direction until the distance between the mobile robot's position and target position is less than or equal to ±100 pixels.

2) The mobile robot turns to the right when the result of distance in the Y axis direction between the target and the mobile robot (Yd – Yc) has a positive value.

3) The mobile robot turns to the left when the result of distance in the Y axis direction between the target and the mobile robot (Yd – Yc) has a negative value.

4) The mobile robot moves forward in the X- axis direction until the distance between the mobile robot's position and target position is less than or equal to ±100 pixels and then it stops.

The computer processes the information and sends data to the microcontroller at the same time, which requests for commands to be executed as mobile robot movement. The program displays the mobile robot trajectory graphic within a given position in the pixels of the monitor as shown in Figure 3. Therefore, the vision system not only shows a graphic map by the image processing method but also navigates to guide the robot to go to the goal as directed by path planning.

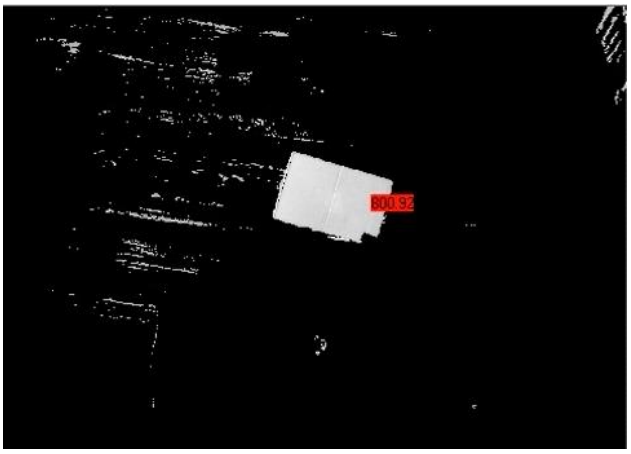

Figure 3. Tracking by using the image processing

2.3 Mobile robot system

2.3.1 The mobile robot's structure

The mobile robot's structural dimensions are 320 mm long, 250 wide, and 280 mm tall. The robot has an orange color for image processing detection. There are four wheels on the mobile robot. Two wheels of the mobile robot are attached to DC motors and the two additional wheels are attached to the rear of a vehicle to assist when the robot performs the turn. The DC motors are connected to a L298N board. The L298N board is used to generate a PWM signal from the microcontroller.

2.3.2 Microcontroller

The microcontroller mainly controls the speed and direction of the mobile robot. Generally, the function of the microcontroller is to receive the mobile robot's status perception from many sensors. The control signal carries directional information including environment perception to control the wheels and drives the robot to reach the goal. In this research, the ESP8266 NodeMCU microcontroller board is used to interface with the vision system. Starting point, path planning, and goal are fed as inputs into the vision system and then passed to the microcontroller. The microcontroller executes those instructions to control the mobile robot's direction and speed according to the path planning program. The ESP8266 NodeMCU is installed on the mobile robot to control the wheels. A diagram of all physical connections between the ESP8266 NodeMCU board and the several peripherals is shown in Figure 4. The described physical connections between ESP8266. This diagram obviously presents that the marked position is linked to I/O of the ESP8266 NodeMCU board.

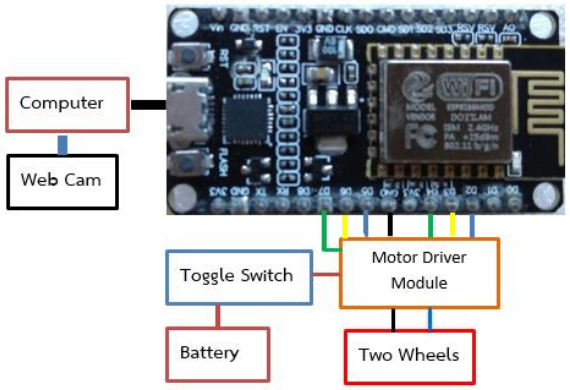

Figure 4. The physical connections between ESP8266 and each block of the proposed system

The path planning obtains information about the mobile robot's location and destination from image processing, which is designed to facilitate a car's movements and navigation from the starting point to the goal. The microcontroller utilizes path planning from the computer to control two wheels of a mobile robot into four functions: 1) Forward, 2) Turn left, 3) Turn right, and 4) Stop. The two wheels of the mobile robot are directly used for direction control in which four function datasets have been provided in Table 1.

Table 1. Control direction wheels of the mobile robot

Function	Left Motor	Right Motor
Forward	High (CW)	High (CW)
Turn Left	LOW	High (CW)
Turn Right	High (CW)	LOW
Stop	LOW	LOW

The stop toggle switch connects the digital inputs of the ESP8266 Node MCU board and the L298N motor driver module, which is used to stop in an emergency case. The ESP8266 Node MCU board is connected to the computer via a USB serial port. This whole process is summarized in Figure 5.

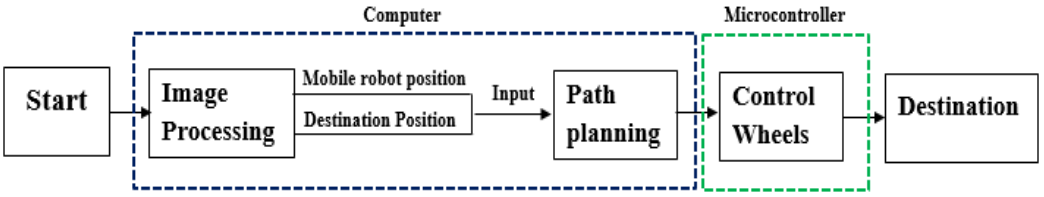

Figure 5. Blocks diagram of the mobile robot system

3. Results and Discussion

3.1 Test 1: Four corner of starting

There are four corners for starting: 1) The upper left corner, 2) The upper right corner, 3) The lower left corner, and 4) The lower right corner. The robot is required to autonomously execute a movement from four corners to the goal at point (800,400) as shown in Figure 6. A simulation was performed to evaluate the performance in order to reduce and eliminate errors before the test. The result of the trajectory to control the mobile robot is shown in Figures 7.

The image processing method used to determine the position of the robot by setting the web camera is attached above the mobile robot and the mobile robot executes the commands via the microcontroller. The trajectory of the robot is displayed in data as shown in Figure 8. The accurate trajectory followed the mobile robot movement. When the mobile robot is placed at the upper left corner (a, b) and the lower right corner (g, h), the mobile robot can go straight in the Y-axis direction then turn to the left and go straight to reach the goal by executing the command in range within ± 100 pixels. When the mobile robot is placed at the upper right corner (c, d) and the lower left corner (c, d), the mobile robot can go straight in the Y-axis direction then turn to the right and go straight to reach the goal by executing the command in range within ± 100 pixels.

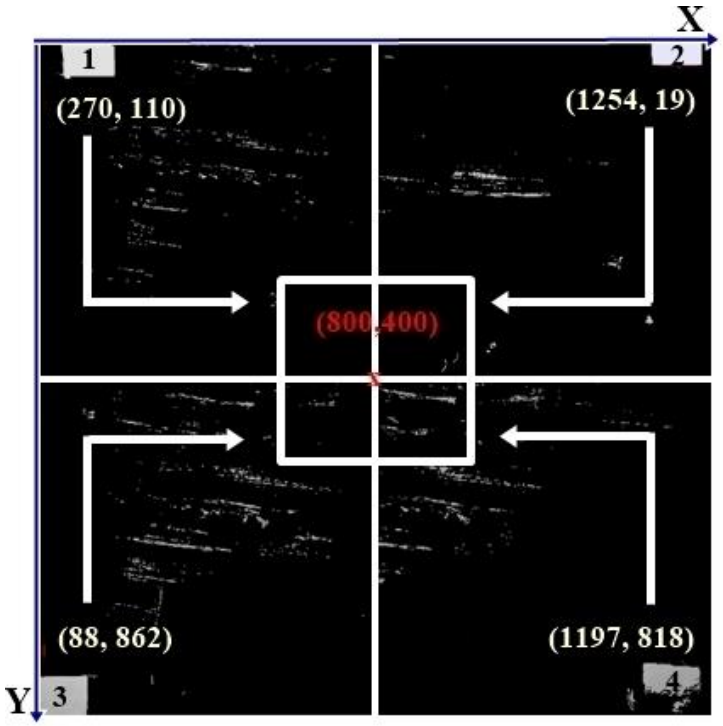

Figure 6. The trajectory of an autonomous mobile robot of four cornner of starting

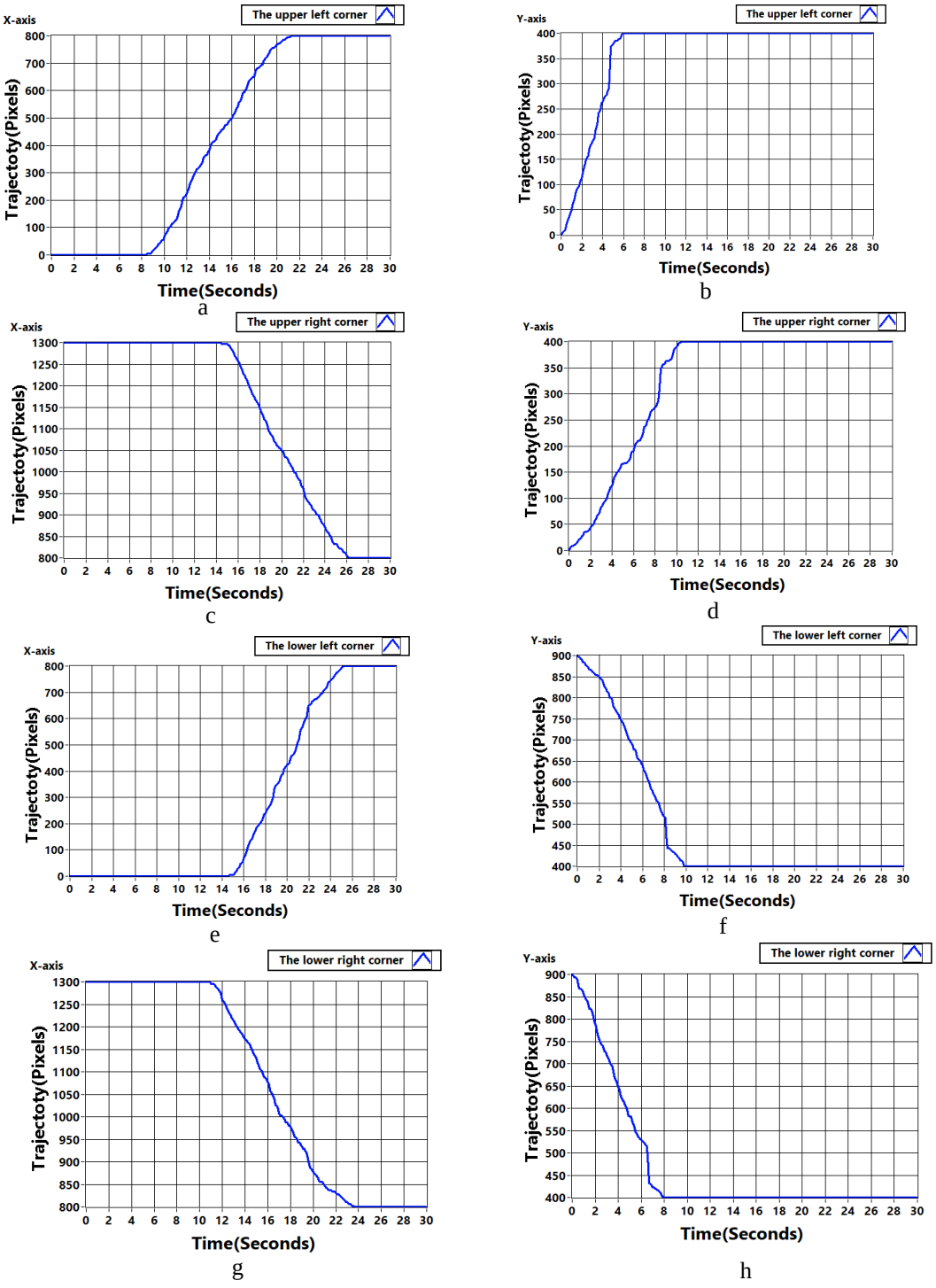

Figure 7. The trajectory simulation of an autonomous mobile robot at four corners

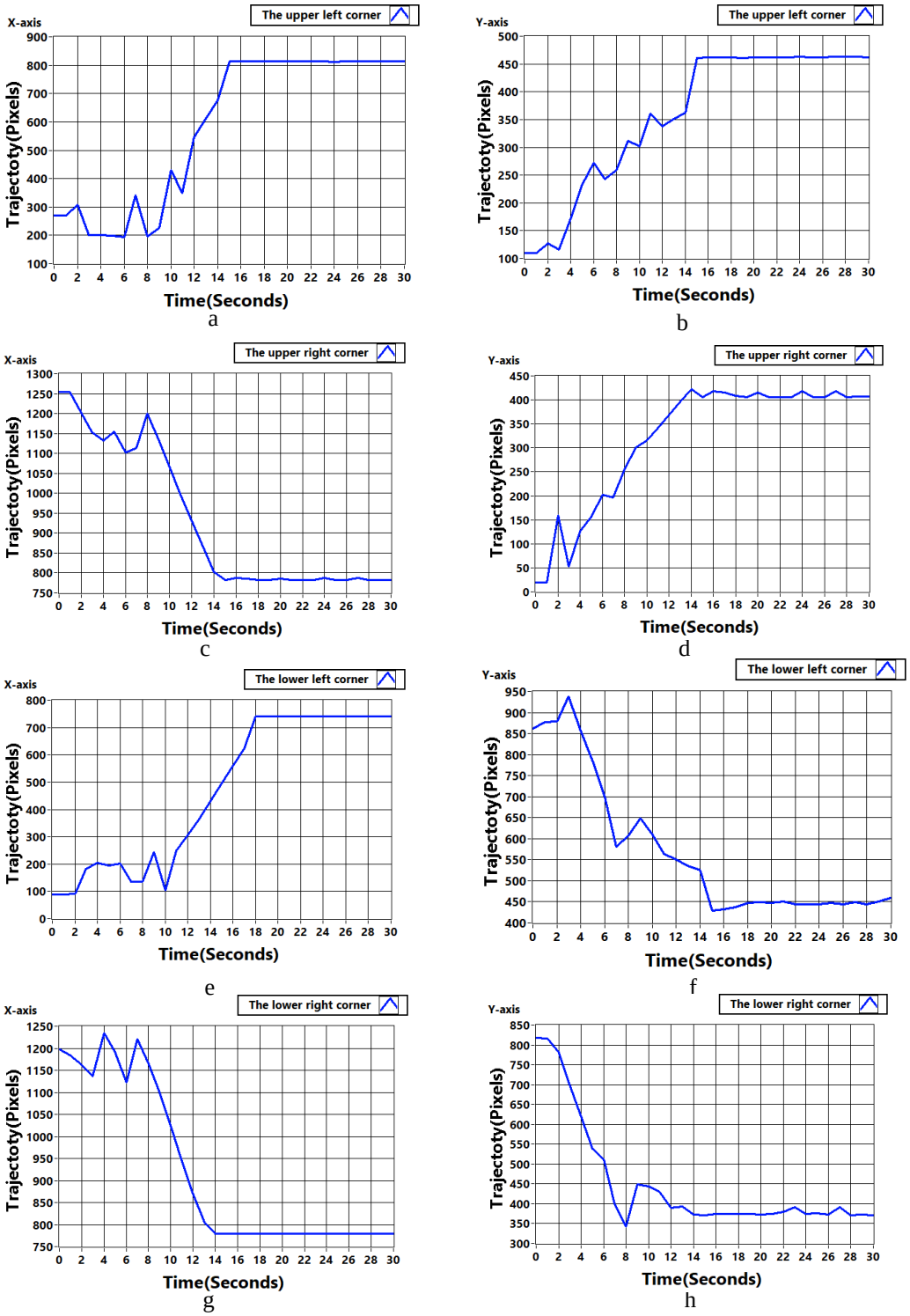

Figure 8. The trajectory of an autonomous mobile robot at four corners

3.2 Test 2: Two points of goal

To ensure that it confirmed the autonomous vehicle movement, the mobile robot was required to autonomously execute a movement from the upper left corner to the goal at point (300,800) and (110,450) as shown in Figure 9.

The simulations evaluated the performance as shown in Figure 10. The mobile robot moved straight from the upper left corner to go to the point (300,800) as shown in Figure 11 (a, b). When the goal has changed as shown in Figure 11 (c, d), the mobile robot was able to move straight along

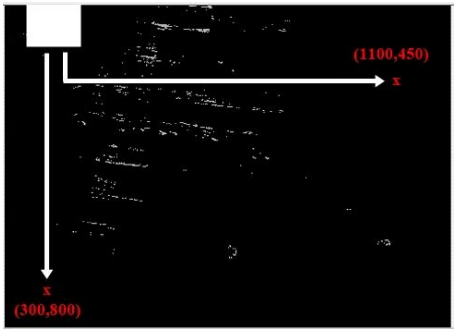

Figure 9. The trajectory of an autonomous mobile robot from the upper left corner to the goal

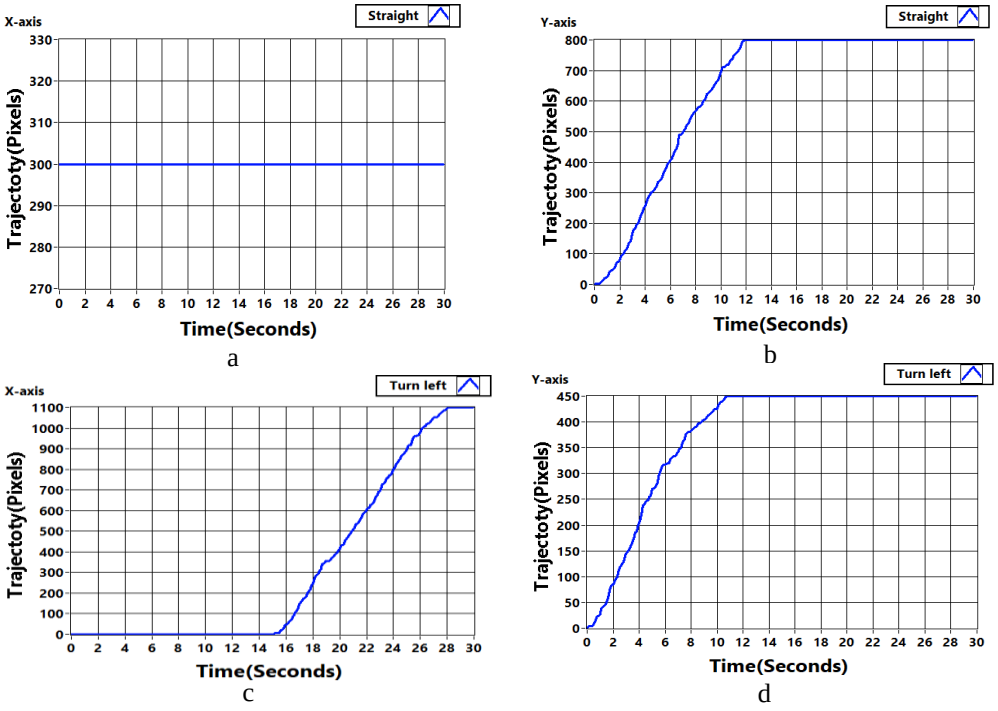

Figure 10. The trajectory simulation from the upper left corner to the point of goal

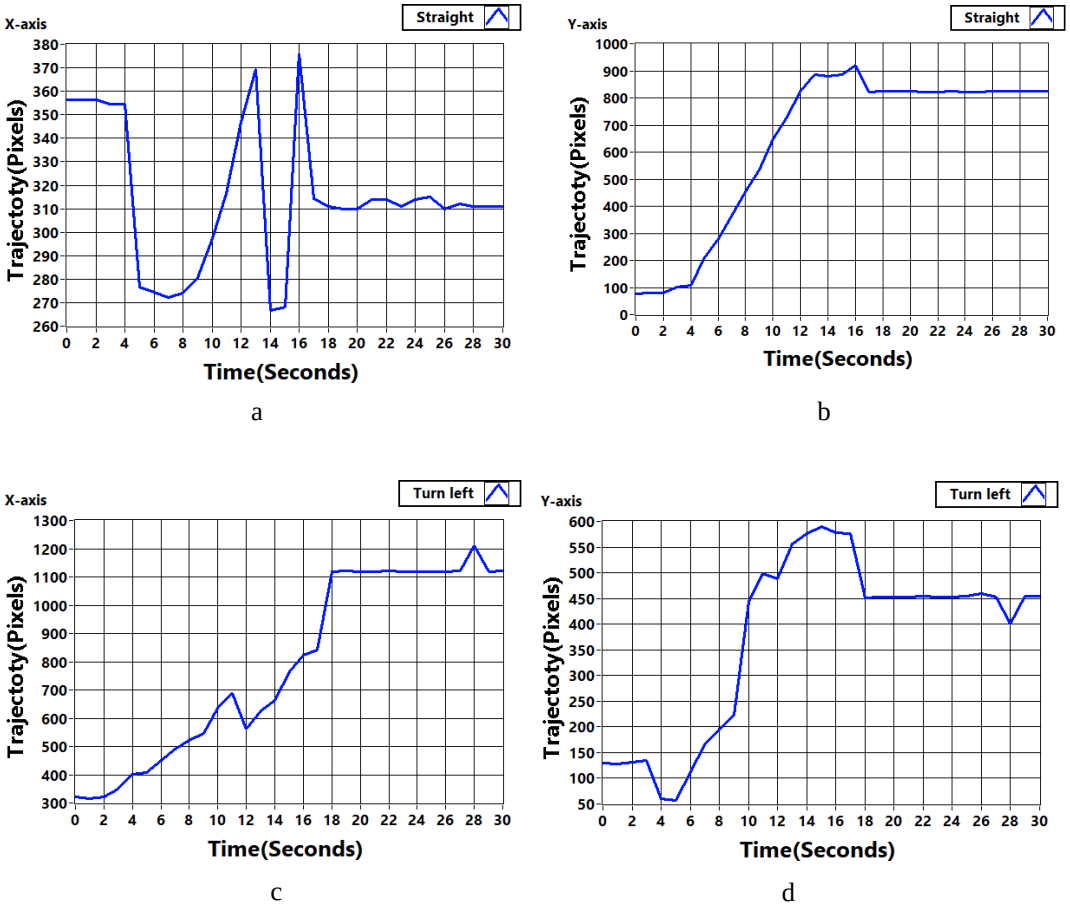

Figure 11. The trajectory of an autonomous mobile robot from the upper left corner

the y-axis direction then the mobile robot turned to the left on the x-axis direction and went straight to the point (1100,450). The overall trajectory was executed fully and autonomously, and the robot successfully arrived at the goal. These experiments with the automated mobile robot using the microcontroller under vision system navigation demonstrated that the system was sensitive and responsive enough to automatically move the mobile robot, which arrived at the goal successfully.

Table 2 shows that the movements of the mobile robot simulation and experiment had an average error rate of (X, Y) position of 7.51%, 1.63%, 9.00%, 4.26%, 3.01% and 1.18%, respectively. This indicates that the image processing method by setting the web camera above the robot interfacing with the microcontroller was able to take control of the autonomous vehicle movement.

Table 2. Function of movement the mobile robot

Function	X Sim (px)	Y Sim (px)	X Test (px)	Y Test (px)	AVG Error (%)
The upper left corner	800	400	813	462	7.51
The upper right corner	800	400	786	406	1.63
The lower left corner	800	400	740	444	9.00
The lower right corner	800	400	779	378	4.26
Straight	300	800	310	310	3.01
Turn left	1100	450	1119	453	1.18

4. Conclusions

These results confirm that the path planning can be programmed and designed for autonomous navigation in the vision system. The vision system can be interacted with the microcontroller to move the vehicle to the destination successfully. In this research, the area is limited to the coverage of the field of view of the camera. This method has been designed to support the system operation, enabling the mobile robot to automatically move to the destination by only using a web camera sensor. The mobile robot was enhanced and became more accurate upon the resolution of the camera, light intensity and light stability. The mobile robot system was not only controlled by an interactive interface but also achieved autonomous navigation by extracting the appropriate mapping information. In future work, we will develop and design a vehicle system that is able to avoid obstruction in various situations.

References

[1] Farag, W., 2018. Recognition of traffic signs by convolutional neural nets for self-driving vehicles. *International Journal of Knowledge Based and Intelligent Engineering Systems*, 22(3), 205-214.

[2] Elbagoury, B. M., Maskeliunas, R. and Salem, A. B. M. M., 2018. A Hybrid Liar/Radar-based deep learning and vehicle recognition engine for autonomous vehicle precrash control. *Eastern-European Journal of Enterprise Technologies*, 5(9), 6-17.

[3] Zhou, Z., Akhtar, Z., Man, KL. and Siddique, K., 2019. A deep learning platooning-based video information-sharing internet of things framework for autonomous driving systems. *International Journal of Distributed Sensor Networks*, 15(11), https://doi.org/10.1177/1550147719883133

[4] Boukerche, A., Siddiqui, A.J. and Mammeri, A., 2017. Automated vehicle detection and classification: Models, methods, and techniques. *ACM Computing Surveys*, 50(5), 62, https://doi.org/10.1145/3107614

[5] Li, B., Zheng, S. and Qiu, M., 2018. Research on picking identification and positioning system based on IOT. *International Journal of Online and Biomedical Engineering*, 14(7), 149-160.

[6] Visconti, P., de Fazio, R., Costantini, P., Miccoli, S. and Cafagna, D., 2019. Arduino-based solution for in-car abandoned infants' controlling remotely managed by smartphone application. *Journal of Communications Software and Systems*, 15(2), 89-100.
[7] Müller, M., Casser, V., Lahoud, J., Smith, N. and Ghanem, B., 2018. Sim4CV: A photo-realistic simulator for computer vision applications. *International Journal of Computer Vision*, 126(9), 902-919.
[8] Wong, C.-C., Chen, H.-C., Lee, C.-T., Wang, C.-C. and Feng, H.-M., 2019. High interactive sensory robot system design in the indoor autonomous services applications. *Journal of Intelligent and Fuzzy Systems*, 36(2), 1259-1271.
[9] Gwak, J., Jung, J., Oh, R.D., Park., M., Ramimov, M.A.K. and Ahn, J., 2019. A review of intelligent self-driving vehicle software research. *KSII Transactions on Internet and Information Systems*, 13(11), 5299-5320.
[10] Guillaumin, M., Küttel, D. and Ferrari, V., 2014. ImageNet auto-annotation with segmentation propagation. *International Journal of Computer Vision*, 110(3), 328-348.
[11] Han, Y., Jiang, T., Ma, Y. and Xu, C., 2018. Pretraining convolutional neural networks for image-based vehicle classification. *Advances in Multimedia*, 2018, https://doi.org/10.1155/2018/3138278
[12] Zhang, B., Zhou, Y., Pan, H. and Tillo, T., 2014. Hybrid model of clustering and kernel autoassociator for reliable vehicle type classification. *Machine Vision and Applications*, 25(2), 437-250.
[13] Martinez-Guanter, J., Agüera, P., Agüera, J. and Pérez-Ruiz, M., 2019. Spray and economics assessment of a UAV-based ultra-low-volume application in olive and citrus orchards. *Precision Agriculture*, 21(1), 226-243.
[14] Wang, K., Yan, F., Zou, B., Tang, L., Yuan, Q. and Lv, C., 2019. Occlusion-free road segmentation leveraging semantics for autonomous vehicles. *Sensors*, 19(21), 4711, https://doi.org/10.3390/s19214711
[15] Ravankar, A., Ravankar, A.A., Kobayashi, Y., Hoshino, Y. and Peng, C.-C., 2018. Path smoothing techniques in robot navigation: State-of-the-art, current and future challenges. *Sensors*, 18(9), 3170, https://doi.org/10.3390/s18093170
[16] Layek, M.A., Chung, T.C. and Huh, E.-N., 2019. Remote distance measurement from a single image by automatic detection and perspective correction. *KSII Transactions on Internet and Information Systems*, 13(8), 3981-4004.
[17] Zhao, J., Liang, B. and Chen, Q., 2018. The key technology toward the self-driving car. *International Journal of Intelligent Unmanned Systems*, 6(1), 2-20.
[18] Yenkaya, S., Yenkaya, G. and Düven, E., 2013. Keeping the vehicle on the road: A survey on on-road lane detection systems. *ACM Computing Surveys*, 46(1), https://doi.org/10.1145/2522968.2522970.
[19] Ilias, B., Shukor, A.S., Yaacob, S., Adom, A.H. and Razali, M.H.M., 2014. A nurse following robot with high speed kinetic sensor. *ARPN Journal of Engineering and Applied Sciences*, 9(12), 2454-2459.
[20] Wong, C.-C., Chen, H.-C., Lee, C.-T., Wang, C.-C. and Feng, H.-M., 2019. High interactive sensory robot system design in the indoor autonomous services applications. *Journal of Intelligent and Fuzzy Systems*, 36(2), 1259-1271.
[21] Ouyang, Z.-H., Cui, S.-A., Zhang, P.-F., Wang, S.-F., Dai, X. and Xia, Q., 2020. Iterative closest point (ICP) performance comparison using different types of Lidar for indoor localization and mapping. *Lasers in Engineering (Old City Publishing)*, 47(4-6), 221-232.
[22] Sidharta, H.A., Sidharta, S. and Sari, W.P., 2019. 2D mapping and boundary detection using 2D LIDAR sensor for prototyping autonomous PETIS (programable vehicle with integrated sensor). *Kinetik*, 4(2), 107-114.

[23] Rivai, M., Hutabarat, D. and Nafis, Z.M.J., 2020. 2D mapping using omni-directional mobile robot equipped with LiDAR. *Telecommunication Computing Electronics and Control*, 18(3), https://doi.org/10.12928/telkomnika.v18i3.14872

[24] Mohammed, S.K.K. and Maqbool, T.T., 2018. Android board based intelligent car anti-theft system through face recognition using GSM and GPS. *Journal of Applied Information Science*, 6(2), 1-5.

[25] Okarma, K. and Fastowicz, J., 2019. Adaptation of full-reference image quality assessment methods for automatic visual evaluation of the surface quality of 3D prints. *Elektronika Ir Elektrotechnika*, 25(5), 57-62.

[26] Chiu, C.-C., Ku, M.-Y. and Wang, C.-Y., 2010. Automatic traffic surveillance system for vision-based vehicle recognition and tracking. *Journal of Information Science and Engineering*, 26(2), 611-629.

[27] Ospina, R.E., Cardona, S.D. and Bacca-Cortes, B., 2017. Software tool for thermographic inspection using multimodal fusing of thermal and visible images. *Ingeniería y Competitividad*, 19(1), 53-68.

[28] Bargoti, S. and Underwood, J.P., 2017. Image segmentation for fruit detection and yield estimation in apple orchards. *Journal of Field Robotics*, 34(6), 1039-1060.

[29] Franchetti, B., Ntouskos, V., Giuliani, P., Herman, T., Barnes, L. and Pirri, F., 2019. Vision based modeling of plants phenotyping in vertical farming under artificial lighting. *Sensors*, 19(20), 4378, https://doi.org/10.3390/s19204378

[30] Esau, T., Zaman, Q., Groulx, D., Farooque, A., Schumann, A. and Chang, Y., 2018. Machine vision smart sprayer for spot-application of agrochemical in wild blueberry fields. *Precision Agriculture*, 19(4), 770-788.

[31] Shinkuma, R., Nishio, T., Inagaki, Y. and Oki, E., 2020. Data assessment and prioritization in mobile networks for real-time prediction of spatial information using machine learning. *EURASIP Journal on Wireless Communications and Networking*, 2020, 92, https://doi.org/10.1186/s13638-020-01709-1

[32] Gomes, S.L., Rebouças, E.D., Neto, E.-C., Papa, J.P., Albuquerque, V.H., Filho, P.P.R. and Tavares, J.M., 2017. Embedded real-time speed limit sign recognition using image processing and machine learning techniques. *Neural Computing and Applications*, 28(1), 573-584.

[33] Zhan, W., Xiao, C., Wen, Y., Zhou, C., Yuan, H., Xiu, S., Zhang, Y., Zou, X., Lu, X. and Li, Q., 2019. Autonomous visual perception for unmanned surface vehicle navigation in an unknown environment. *Sensors*, 19, 2216, https://doi.org/10.3390/s19102216.

[34] Xu, Y., Fang, G., Chen, S., Zou, J.L. and Ye, Z., 2014. Real-time image processing for vision-based weld seam tracking in robotic GMAW. *International Journal of Advanced Manufacturing Technology*, 73(9-12), 1413-1425.

[35] Cubero, S., Aleixos, N., Albert, F., Torregrosa, A., Ortiz, C., García-Navarrete, O. and Blasco, J., 2014. Optimised computer vision system for automatic pre-grading of citrus fruit in the field using a mobile platform. *Precision Agriculture*, 15(1), 80-94.

Current Applied Science and Technology Vol. 21 No. 3 (July-September 2021)

Tyrosinase Inhibiting Extracts from Coastal Plants as Potential Additives in Skin Whitening Formulations

Win Yee Lim[1], Eric Wei Chiang Chan[2], Chia Wei Phan[3] and Chen Wai Wong[1]*

[1]Department of Biotechnology, Faculty of Applied Sciences, UCSI University, Kuala Lumpur, Malaysia
[2]Department of Food Science with Nutrition, Faculty of Applied Sciences, UCSI University, Kuala Lumpur, Malaysia
[3]Department of Pharmaceutical Life Sciences, Faculty of Pharmacy, University of Malaya, Kuala Lumpur, Malaysia

Received: 6 July 2020, Revised: 23 September 2020, Accepted: 19 January 2021

Abstract

Coastal plants produce more secondary metabolites than normal terrestrial plants and this means that they may possess many bioactive compounds that are worth studying. The study described antioxidant, *in vitro* tyrosinase inhibition activity and cytotoxicity of six coastal plants including *Sonneratia alba, Rhizophora apiculata, Syzygium grande, Rhizophora mucronata, Hibiscus tiliaceus* and *Bruguiera gymnorhiza*. Leaves of these coastal plants were sequentially extracted using dichloromethane (DE), ethyl acetate (EE), acetone (AE) and methanol (ME). Most AE and ME extracts exerted high free radical scavenging activity which ranged from 124 to 454 mg AA/g extract. However, *R. apiculata, R. mucronata* and *H. tiliaceus* showed stronger *in vitro* tyrosinase inhibition, in which *H. tiliaceus* DE exhibited the lowest IC_{50} value, followed by *R. mucronata* DE and *R. apiculata* ME. Tested with B16F1 murine melanoma cells, 9 out of 24 extracts studied for 24 h incubation and 4 out 24 extracts for 72 h incubation showed low cytotoxic. Tyrosinase inhibiting extracts with low cytotoxicity such as *H. tiliaceus* are potential additives in skin-whitening formulations and should be further studied for their melanogenesis inhibition.

Keywords: Malaysian coastal plants; antioxidant; anti-tyrosinase; cytotoxicity; B16F1 murine melanoma cell
DOI 10.14456/cast.2021.48

1. Introduction

Coastal forests are considered a vital natural heritage of Malaysia as much of Malaysia's rural population living along its 4,675 km coastline are dependent on coastal forests for their livelihood. The role of mangroves, as nursery and feeding areas, was well documented by Jusoff [1] and

*Corresponding author: Tel.: (+603) 9101 8880 Fax: (+603) 9102 3606
E-mail: wongcw@ucsiuniversity.edu.my

Neamsuvan *et al*. [2]. Despite their great diversity and ecological function, coastal forests are under constant threat of being converted into oil palm estates [3].

Coastal forests occur in relatively harsh condition characterised by high salinity and intense UV radiation. In order to survive in difficult environment, coastal plants produce more secondary metabolites than normal terrestrial plants [4, 5]. This makes the coastal plants good candidates for bioprospecting which can provide an additional reason for preserving coastal forests. Such efforts are in line with Goals 9 and 14 of the UN Sustainable Development Goals. Wood from coastal plants, including the trunk and the woody roots of mangroves, are often used for firewood and charcoal production, construction of dwellings as well as production of furniture, boats, and fishing gear. The leaves are often discarded as waste and they can be safely harvested without felling the tree. Thus, the leaves of the coastal plants have been used for the study of their bioactivity.

Six coastal plants including *Sonneratia alba*, *Rhizophora apiculata*, *Syzygium grande*, *Rhizophora mucronata*, *Hibiscus tiliaceus* and *Bruguiera gymnorhiza* were used in this study (Figure 1). *Sonneratia alba*, also known as Mangrove apple, belongs to family Sonneratiacea. It has rounded and leathery leaves and can be found in the Pacific [6]. *Rhizophora apiculata* and *R. mucronata* are the major species of *Rhizophora*. In Malaysia, *R. apiculata* and *R. mucronate*, locally known as Bakau minyak and Bakau kurap, are the famous mangrove plant widely used in charcoal industry [5].

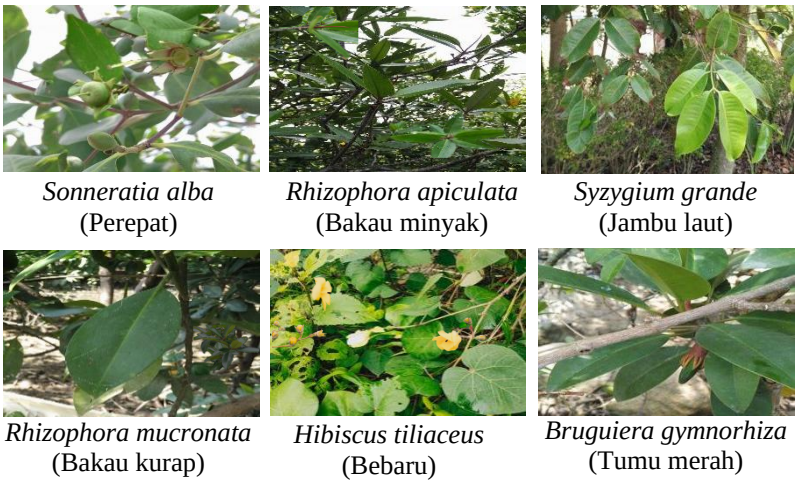

Figure 1. Photos of selected coastal plants taken from the field

Sonneratia grande, also known locally as Sea apple or Jambu laut, is a common coastal plant that is often used for roadside plantings. *Hibiscus tiliaceus*, or Sea hibiscus, is an evergreen plant which normally grows up to 3-10 meters in height [7]. *Bruguiera gymnorhiza* or Tumu merah is a widespread mangrove species in the Pacific [6]. Some parts, like fruits, leaves and shoots of these chosen coastal plants, are edible. Some of these coastal plants were reported to have medicinal and bioactive properties such as antimicrobial, anti-tumour and anti-depressant activities. This may be related to the wealth of bioactive phytochemicals such as flavonoids, triterpenes, phenols and hydrocarbons present in the selected plants [5, 7].

Tyrosinase is an important enzyme which catalyzes the initial steps of melagenic pathway. It is involved in the formation of ortho-quinone, which then undergoes other reactions and forms melanin, causing skin darkening [8]. To prevent the formation of melanin, tyrosinase inhibition is

the safest way to inhibit melanogenesis. In the literature, antioxidant and anti-tyrosinase properties of several coastal plants, for example, biflavonoids isolated from *Garcinia subelliptica* exhibited strong anti-tyrosinase activity [9, 10]. Possible tyrosinase inhibition ability of the coastal plants may add to the growing body of knowledge on the therapeutic application of coastal forests and promote their conservation.

Solvent extraction is a common technique for sample preparation and involves separation of compounds [11]. The abundant phytochemicals found in these coastal plants can be separated by using different extraction solvents. In this study, we intend to compare the antioxidant and anti-tyrosinase activities of leaves from selected Malaysian coastal plants extracts using different extraction solvent. Leaves are ideal for bioprospecting as they can be safely harvested without felling the tree. The safety of the plant extracts will also be determined based on the cytotoxicity of the extracts on B16F1 murine melanoma cells.

2. Materials and Methods

2.1 Plant Materials

Six coastal plants were chosen for this study: *Sonneratia alba* Sm., *Rhizophora apiculata* Blume., *Syzygium grande* (Wight) Walp., *Rhizophora mucronata* Lam., *Hibiscus tiliaceus* Linn., and *Bruguiera gymnorhiza* (L.) Lam. They were sampled from the vicinity of Pulau Indah and Teluk Gong, Selangor, Malaysia and authenticated by a botanist, Dr. H.T. Chan. All reagents and solvents used in this study were of analytical grade.

2.2 Plant extraction and preparation

The mangrove leaves were dried in an oven at 50°C and ground into powder. For the determination of mode of inhibition of the plants, methanol (300 ml) was used to extract the powdered leaf samples (15 g) followed by continuous swirling for 1 h at room temperature. This was done at a 20:1 (v/w) solvent to sample ratio. For subsequent analysis for determining the tyrosinase inhibition, antioxidant properties and cell viability, a sequential extraction was used to fractionate the phytochemicals according to polarity. The sequential extraction used the following solvents in order: dichloromethane (DE), ethyl acetate (EE), acetone (AE) and methanol (ME), using the same solvent to sample ratio of 20:1 (v/w). All extracts were dried using a rotary evaporator to yield an amorphous solid. The extracts were oven-dried until constant weight and stored at room temperature. A stock solution of 10 mg/ml of each dried extract was then prepared using DMSO and used for the following tests and assays.

2.3 Phenolic contents

2.3.1 Total phenolic contents

Extracts of four types of solvents were analysed for total phenolic content (TPC) and total flavonoid content (TFC). Total phenolic content (TPC) was assayed using Folin-Ciocalteu (FC) assay with modification [12]. Extracts (21 µl) were mixed with 105 µl of FC reagent (10 times dilution) and 84 µl of sodium carbonate (7.5%, w/v). After 30 min incubation in the dark, absorbance was measured at 765 nm and the result was expressed as gallic acid equivalent (GAE) in mg/g of sample. The standard equation for gallic acid was $y = 0.0054x$ ($R^2 = 0.9997$).

2.3.2 Total flavonoid contents

Total flavonoid content (TFC) was evaluated using the aluminium chloride assay [13]. Extracts (21 µl) were mixed with 63 µl of methanol, 42 µl of 1% aluminum chloride, 42 µl of 0.1M potassium acetate and 42 µl of ultra-pure water. The assay solutions were incubated at room temperature for 10 min and absorbance was measured at 415 nm. Total flavonoid content was expressed as quercetin equivalent (QE) in mg/g plant material. The standard equation for quercetin was $y = 0.0031x$ ($R^2 = 0.9996$).

2.4 Antioxidant assay

Antioxidant activity of the extracts was examined depending on the ferrous ion chelatig ability (FIC) and free radical scavenging activity using 2,2-diphenyl-1-picrylhydrazyl (DPPH) assay.

2.4.1 Ferrous ion chelating (FIC) ability

FIC ability was measured using the ferrozine assay as described by Chan *et al.* [14]. $FeSO_4$ (0.2 mM, 35 µl) was mixed with different dilutions of extracts (140 µl), followed by ferrozine (0.5 mM, 35 µL). Absorbance (A) was measured at 562 nm after 10 min. Sample blanks comprised appropriate dilutions of sample with $FeSO_4$ but did not have ferrozine added. Chelating ability of extracts (%) was calculated as $(1 - A_s/A_c) \times 100$ (s = sample, c = control). FIC ability was expressed as chelating efficiency concentration (CEC_{50}) in mg/ml.

2.4.2 DPPH assay

The free radical scavenging (FRS) activity of samples was determined following Chan *et al*. [12] with modification. Different dilutions of extracts (70 µl) were added to 140 µl of DPPH (5.9 mg/100 ml methanol). Absorbance was measured at 517 nm after 30 min incubation in the dark and IC_{50} was expressed as ascorbic acid antioxidant capacity (AEAC) in mg ascorbic acid (AA)/g, and calculated as $IC_{50}(a)/IC_{50}(s) \times 10^3$ (a = ascorbate, s = sample).

2.5 Determination of mode of inhibition of the coastal plants

Mode of inhibition of methanol extracted samples was assessed using modified dopachrome method with 3,4-dihydroxy-L-phenylalanine (L-DOPA) as substrate [14]. The assay was conducted in a 96-well microtiter plate using a plate reader to measure absorbance (A) at 475 nm with 700 nm as reference. Forty µl of sample (125-500 µg/ml) in 80 µl of phosphate buffer (0.1M, pH 6.8), 40 µl of mushroom tyrosinase (31 units/ml), and 40 µl of L-DOPA (2.5-10 mM) were mixed and absorbance was measured spectrophotometrically at 20 s intervals up to 300 s. Lineweaver-Burk plot was plotted for both enzyme activities without inhibitors and with inhibitors. K_i value and types of inhibition for each inhibitor was identified based on the Lineweaver-Burk plot.

2.6 *In vitro* tyrosinase inhibition assay

Tyrosinase inhibition activity (TIA) of total 24 samples was assessed using the dopachrome method which was mentioned earlier with slight modification [15]. Samples were dissolved in 50% dimethyl sulphoxide (DMSO) and 40 µl of sample was added to 80 µl of 0.1 M phosphate buffer at pH 6.8 with 40 µl of mushroom tyrosinase (31 units/ml). After incubated at 37°C for 1 min, 40 µl of L-DOPA (2.5 mM) was added and absorbance was measured at 475 nm with 700 nm as reference after a 30-min incubation. Each sample was accompanied by a blank that had all the components except

L-DOPA. Results in percentage inhibition (%) were expressed as half-maximal inhibition (IC_{50}) value. Kojic acid was used as a positive control.

2.7 Cell viability assay

The B16F1 murine melanoma cell lines (ATCC® CRL-6323™), obtained from the American Type Culture Collection (USA), were cultured in DMEM supplemented with 5% fetal bovine serum and 1% penicillin (10,000 µg/ml)/ streptomycin (10,000 µg/ml). The cells were placed in CO_2 incubator at 37°C to reach a confluent monolayer.

Cell viability assay of all the samples was performed using 3-(4,5-imethylthiazol-2-yl)-2,5- diphenyltetrazolium bromide (MTT) as described by Sharif *et al*. [16] with modification. Cells were first seeded in a 96-well plate with 10,000 cells in 0.2 ml growth medium per well and were placed overnight in the incubator. The cells were treated with plant extracts (100 µg/ml) for 24 h and 72 h. Viability of the cells was determined by adding MTT solution (0.5 mg/ml) followed by incubation for 3 h. DMSO was used to solubilise the MTT derivatives and absorbance was measured at 570 nm. A negative control was included to determine cell growth in the absence of any treatment. Cells viability (%) was calculated as (A_{570} of treated cells/A_{570} of control) x 100 and the results were expressed as half-maximal inhibitory concentration (IC_{50}) values.

2.8 Statistical analysis

All experiments were done in triplicate (n = 3) and results were expressed as mean ± standard deviation (SD). Analysis of variance (ANOVA) was analysed using the Tukey Honestly Significant Difference (HSD) test with significant difference at $p < 0.05$. Correlation between different variables were expressed as Pearson's correlation. All the analysis was done using IBM SPSS Statistics 22.

3. Results and Discussions

3.1 Extraction efficiency

All coastal plant leaf sample were extracted with solvents of increasing polarity which were DE, EE, AE and ME (with polarity index 3.1, 4.4, 5.1 and 5.1, respectively) [17]. By using these solvents, compounds of varying polarity were extracted. Methanol extracts were found to obtain higher yield than all other extracts. Methanol extracts of all the coastal plants, except for *S. grande* and *H. tiliaceus*, exhibited more than 15% yield while the other extracts exhibited less than 5% yield. This may be due to the high solubility parameter of methanol in which most of the leftover compounds were soluble and extracted in methanol [17]. Despite having the same polarity index, acetone is less able to extract polar compounds as it only has a single carbonyl oxygen as a hydrogen bond acceptor and no hydrogen bond donor.

3.2 Phenolic contents

Phenolic contents assays include total phenolic contents and total flavonoid contents of the coastal plant extracts as shown in Table 1.

Table 1. Phenolic content and antioxidant activity of coastal plant extracts

Coastal Plants	Extract	Phenolic contents		Antioxidant activity	
		TPC (mg GAE/g)	TFC (mg QE/g)	CEC_{50} (mg/ml)	AEAC (mg AA/g)
Sonneratia alba	DE	22.92 ± 2.22^{dA}	58.31 ± 5.81^{bC}	0.215 ± 0.02^{aD}	9.472 ± 0.13^{dC}
	EE	56.88 ± 2.51^{cA}	75.73 ± 6.65^{aA}	0.179 ± 0.02^{bE}	40.71 ± 0.84^{cB}
	AE	383.0 ± 15.8^{aA}	30.84 ± 2.03^{cC}	0.097 ± 0.01^{cE}	190.9 ± 10.0^{bC}
	ME	186.8 ± 13.4^{bA}	11.26 ± 1.06^{dB}	0.129 ± 0.01^{cE}	357.1 ± 31.1^{aB}
Rhizophora apiculata	DE	8.025 ± 0.72^{dD}	54.62 ± 4.78^{bC}	0.348 ± 0.02^{cB}	17.62 ± 0.59^{cA}
	EE	41.73 ± 2.96^{cB}	75.48 ± 7.30^{aA}	0.979 ± 0.05^{aB}	36.22 ± 1.20^{cC}
	AE	122.0 ± 11.8^{bD}	54.84 ± 5.10^{bA}	0.983 ± 0.08^{aB}	123.6 ± 4.56^{bD}
	ME	184.7 ± 12.3^{aA}	11.82 ± 1.08^{cB}	0.582 ± 0.04^{bC}	327.7 ± 20.3^{aB}
Syzygium grande	DE	15.43 ± 1.31^{dB}	46.48 ± 4.24^{aC}	0.433 ± 0.01^{aA}	9.802 ± 0.43^{cC}
	EE	46.23 ± 2.79^{cB}	49.67 ± 3.65^{aC}	0.048 ± 0.00^{dF}	27.78 ± 2.19^{cD}
	AE	234.4 ± 17.6^{aB}	45.31 ± 4.32^{aB}	0.316 ± 0.01^{bD}	352.6 ± 15.2^{bA}
	ME	172.0 ± 15.5^{bAB}	11.74 ± 1.14^{bB}	0.115 ± 0.01^{cE}	453.6 ± 46.0^{aA}
Rhizophora mucronata	DE	10.21 ± 0.90^{dCD}	12.23 ± 8.94^{cD}	0.297 ± 0.03^{cC}	9.239 ± 0.33^{dC}
	EE	58.98 ± 3.20^{cA}	53.37 ± 5.01^{aBC}	1.232 ± 0.07^{aA}	51.54 ± 3.98^{cA}
	AE	203.4 ± 14.9^{aC}	34.23 ± 2.92^{bC}	0.812 ± 0.05^{bC}	260.1 ± 20.6^{aB}
	ME	156.7 ± 15.6^{bB}	10.89 ± 0.88^{cB}	0.878 ± 0.05^{bA}	175.0 ± 15.4^{bC}
Hibiscus tiliaceus	DE	10.87 ± 1.07^{dC}	85.36 ± 8.12^{aA}	0.096 ± 0.01^{cE}	11.64 ± 0.88^{dB}
	EE	31.12 ± 3.04^{cC}	62.08 ± 5.29^{bB}	0.468 ± 0.03^{bD}	15.28 ± 0.20^{cE}
	AE	55.31 ± 1.88^{bE}	45.12 ± 3.75^{cB}	0.933 ± 0.05^{aB}	34.70 ± 0.84^{bE}
	ME	150.8 ± 8.29^{aBC}	5.740 ± 0.68^{dC}	0.403 ± 0.03^{bD}	153.0 ± 3.15^{aC}
Brugueira gymnorhiza	DE	14.14 ± 1.25^{cB}	70.49 ± 6.84^{aB}	0.199 ± 0.02^{dD}	8.990 ± 0.26^{cC}
	EE	26.62 ± 1.61^{bC}	54.49 ± 5.28^{bBC}	0.693 ± 0.02^{cC}	15.16 ± 0.29^{cE}
	AE	139.2 ± 10.7^{aD}	54.06 ± 5.34^{bA}	1.266 ± 0.06^{aA}	143.7 ± 7.24^{bD}
	ME	130.9 ± 5.60^{aC}	17.25 ± 1.86^{cA}	0.787 ± 0.06^{bB}	155.7 ± 6.23^{aC}

Values represented mean ± SD (n = 3), $p < 0.05$. Within each column of each species, different superscript letters (a-d) and (A-F) indicates significant difference of different plant extracts at $p < 0.05$. Abbreviations: DE = dichloromethane extract, EE = ethyl acetate extract, AE = acetone extract, ME = methanol extract, TPC = total phenolic contents, TFC = total flavonoid contents, CEC_{50} = chelating efficiency concentration, AEAC = ascorbic acid antioxidant capacity

3.2.1 Total phenolic content (TPC)

Natural antioxidants are widely found in medicinal plants in the form of phenolic compounds. According to Table 1, *R. mucronata* AE showed the highest TPC value (364 mg GAE/g extract),

followed by *S. grande* AE (300 mg GAE/g extract) and *H. tiliaceus* ME (261 mg GAE/g extract). Significant difference was observed when different extraction solvents were used.

Most AE and ME showed high total phenolic content which was more than 50 mg GAE/g extract. This is in accordance with Barchan *et al.* [18] in which polar solvents were more effective in extracting phenolic compounds. This indicates that most phenolic compounds are more polar. Leaves of *H. tiliaceus* and *S. grande* were said to possess higher TPC values than the other plants such as *Hibiscus sabdariffa*, which ranged from 18-30 mg GAE/g extract [19] as well as *Psidium guayaquilense and Psidium rostratum*, which ranged from 6-9 mg GAE/g extract [20]. This suggested that these coastal plants could be a good source of phenolic compounds and antioxidants.

3.2.2 Total flavonoid content (TFC)

For TFC values, the three extracts with the highest TFC values were *H. tiliaceus* DE (85 mg QE/g extract), *S. alba* EE (76 mg QE/g extract) and *R. apiculata* EE (75 mg QE/g extract). For all the coastal samples except *S. grande*, significant difference was obtained for different solvents used. However, no significant difference was observed between different coastal plants using the same extraction solvent.

Flavonoids are regarded as one of the main types of phenolic compounds. However, in contrast with the TPC, most of the ME and AE showed lower TFC values. This indicates that the phenolic compounds of the extracts could be other types of phenolic compounds [21]. The TFC values are comparable to those reported in the leaves of *Eupatorium adenophorum*, which ranged from 19-32 mg QE/g extract and *Cucumis melo*, which was 30 mg QE/g extract [22, 23].

3.3 Antioxidant activity

The antioxidant activity of coastal samples was accessed by FIC assay (CEC_{50}) and DPPH assay (AEAC), and the results are summarised in Table 1. In terms of FIC activity, *S. grande* EE extract showed the lowest CEC_{50}, which was 0.05 mg/ml, followed by *S. alba* AE and *H. tiliaceus* DE, which both exhibited CEC_{50} of 0.10 mg/ml. No fixed pattern was observed for CEC_{50} value of coastal plants extracted by different solvents. For DPPH assay, *S. grande* ME, *S. alba* ME and *S. grande* AE exhibited the top three highest radical scavenging activities with AEAC of 454, 357 and 353 mg AA/g extract, respectively. Most of the AE and ME showed higher antioxidant activity in DPPH assay, which was similar to TPC assay. The antioxidant properties of most of the extracts were comparable to those reported by Silva and Sirasa [24] which ranged from 1-27 mg AA/g.

Phenolic compounds are well known for antioxidant activity due to their capacity to act as reducing agents, hydrogen donors and singlet oxygen quenchers [25]. In correlation analysis, AEAC was positively correlated with TPC with correlation coefficient of r = 0.965 (Figure 2). This indicates that the ability to quench DPPH free radicals increases when phenolic content increases, but levels off to a flat plateau at high phenolic content. While AEAC have weak negative correlation with TFC (r = -0.632) which indicates that flavonoids contributed less or no antioxidant power to the antioxidant capacity of coastal plant extracts. TPC have a weak correlation with TFC (r = -0.534), which might be because flavonoids are just a group of phenolic compounds that consist of other compounds such as phenolic acid, tannins and lignans [26].

However, there was no correlation between AEAC and CEC_{50} (r = -0.087). This might be due to the potential of the phytochemicals to act as free radical quencher but this does not necessarily equal to their ability as metal ion chelator. This could be further examined as no relationship was obtained between CEC_{50} with TPC (r = -0.029) and TFC (r = 0.038). This finding was in accordance with the results reported by Ngo *et al.* [27].

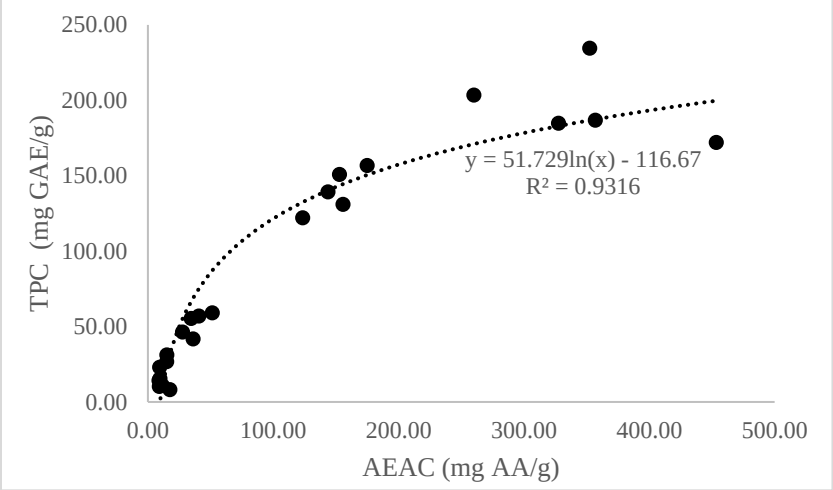

Figure 2. Correlation graph of total phenolic content (TPC) and free radical scavenging (FRS) activity of different coastal plant extracts

3.4 *In vitro* tyrosinase inhibition assay

Table 2 summarises the *in vitro* tyrosinase inhibition activity based on IC_{50} values, and types of inhibition of plant extracts. Tyrosinase inhibition percentage increased in dose-dependent manner as inhibition percentage increased with increased extract concentration. Lower IC_{50} value indicates higher tyrosinase inhibition capacity. It was found that *H. tiliaceus* DE inhibited the tyrosinase enzyme the most with the lowest IC_{50} value (0.13 mg/ml), followed by *R. mucronata* DE (0.15 mg/ml) and *R. apiculata* ME (0.28 mg/ml). Tyrosinase inhibition properties of these three extracts were comparable with α-mangostin reported by Hassan *et al.* [28], but they were much lower than positive control (kojic acid) used in this study. All EE exhibited low inhibition towards tyrosinase, which suggested that ethyl acetate is not a good solvent for extracting tyrosinase inhibiting compounds.

In general, antioxidants were said to be possible tyrosinase inhibitor as they can prevent the initial reaction of tyrosinase by reacting with oxygen. They can also reduce *o*-quinone back to *o*-diphenol [29]. However, there was no correlation between antioxidant and anti-tyrosinase activity (r = -0.271). For example, *H. tiliaceus* DE which is the best tyrosinase inhibitor among all the extracts, exhibited low AEAC (12 mg AA/g extract). This indicates that the tyrosinase inhibiting compounds may not possess antioxidant properties. Melecchi *et al.* [30] reported on a number of compounds in dichloromethane fractionated extract from *H. tiliaceus*. However, bioactivity guide fractionation and structural elucidation would be required to link these compounds to specific bioactivity.

In terms of type of inhibition, inhibitors can be categorized into competitive, non-competitive, uncompetitive as well as mixed inhibitors. This can be determined by the Lineweaver-Burk plot in which the plot of *H. tiliaceus* was shown in Figure 3. Competitive inhibitors commonly bind to enzymes at the substrate binding site, preventing the interaction of the enzymes with substrates while non-competitive inhibitors bind enzymes at the site other than active site to inhibit the enzyme. Uncompetitive inhibition occurs when inhibitors bind to enzyme-substrate complex and enhance the binding of substrates to enzymes, results in decreasing of the rate of reaction. Mixed inhibitors resemble the activities of both competitive and uncompetitive inhibitors [31].

Table 2. *In vitro* tyrosinase inhibition activity of different coastal plant extracts expressed in IC_{50} value (mg/ml) and the type of inhibition identified.

Coastal plant	DE	EE	AE	ME	K_i (mg/ml)	Type of inhibition
Sonneratia alba	0.60 ± 0.05^{bA}	1.78 ± 0.06^{aB}	0.55 ± 0.04^{bC}	0.65 ± 0.06^{bC}	0.45	Un-competitive
Rhizophora apiculata	0.60 ± 0.03^{bA}	1.21 ± 0.11^{aD}	0.64 ± 0.06^{bB}	0.28 ± 0.02^{cE}	0.14	Non-competitive
Syzygium grande	0.44 ± 0.04^{bcB}	1.94 ± 0.05^{aA}	0.38 ± 0.02^{cD}	0.48 ± 0.03^{bD}	0.38	Un-competitive
Rhizophora mucronata	0.15 ± 0.01^{cC}	1.37 ± 0.14^{aC}	0.66 ± 0.04^{bB}	0.79 ± 0.04^{bB}	0.33	Non-competitive
Hibiscus tiliaceus	0.13 ± 0.01^{cC}	0.74 ± 0.07^{aE}	0.54 ± 0.04^{bC}	0.46 ± 0.05^{bD}	0.60/0.20	Mixed
Brugueira gymnorhiza	0.62 ± 0.02^{cA}	1.48 ± 0.05^{aC}	1.30 ± 0.08^{bA}	1.30 ± 0.08^{bA}	0.62	Un-competitive
Control (kojic acid)	0.01 ± 0.00					

Values represent mean ± SD (n = 3), $p < 0.05$. Within each column of each species, different superscript letters (a-c) and (A-E) indicates significant difference of different solvents and types of plant at $p < 0.05$. Abbreviations: DE = dichloromethane extract, EE = ethyl acetate extract, AE = acetone extract, ME = methanol extract

Rhizophora apiculata and *R. mucronata* are non-competitive inhibitors and *H. tiliaceus* is a mixed-type inhibitor. Non-competitive inhibitor may be good for the future application as it works regardless of substrate concentration whereas mixed-type inhibitor indicates that there may be more than one type of inhibitors (active compounds) in the extracts [32]. Among all the coastal plants, *R. apiculata* was found to exhibit lowest K_i value (0.14 mg/ml) which indicated the strongest binding towards the enzyme. This may be because *R. apiculata* non-competitively inhibited the enzyme, binding to a site other than the active site [33].

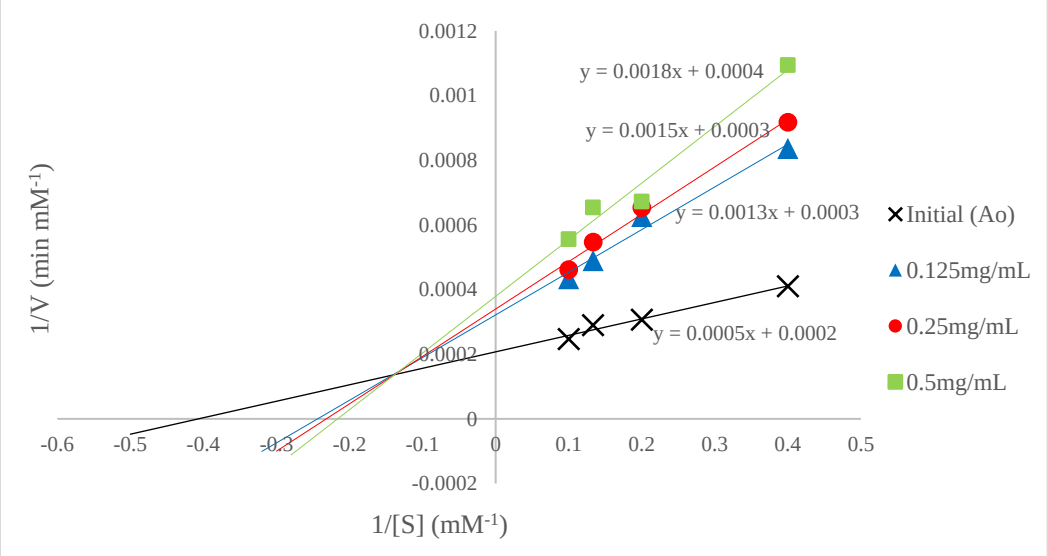

Figure 3. Tyrosinase inhibitory effect of *Hibiscus tiliaceus*

3.5 Cell viability assay

No studies of cytotoxicity on B16F1 murine melanoma cells have been done on the selected coastal plants. It is necessarily to determine the cytotoxicity of the extracts because they may lead to inflammation. The cytotoxicity of all the extracts were screened against B16F1 murine melanoma cells for 24 and 72 h, and the results obtained were reported in Figure 4. In the study of cytotoxicity of the extracts, higher cell viability was preferred. From the results of 24 h, it was noticed that 9 out of 24 extracts had more than 80% cell viability which is considered as low cytotoxic. The most promising extracts for 24 h were *H. tiliaceus* ME (111%), *R. apiculata* DE (99%) and *H. tiliaceus* EE (96%). For MTT assay for 72 h, only 4 out of 24 extracts exhibited more than 80% cell viability.

From anti-tyrosinase study, *R. apiculata* ME, *R. mucronata* DE and *H. tiliaceus* DE were more potent inhibitors, however, only *H. tiliaceus* DE had more than 80% cell viability for 24 h which is good to be further studied. Interestingly, *R. apiculata* ME showed an increased cell viability (83%) for 72 h. Weak positive correlation was obtained for cell viability of 24 h and 72 h ($r = 0.573$), which inferred that not all samples had decresed cell viability from 24 h to 72 h. This was explained by Prakash *et al.* [34], whose work indicated that the variation in cytotoxicity was with respect to the mechanism of the plant extract.

Some extracts such as *R. apiculata* ME and *S. alba* AE exhibited cytotoxic potential towards melanoma cells with IC_{50} value lower than 100 µg/ml. This is comparable with *Kalanchoe laciniata* (322-639 µg/ml) and *Bryophyllum pinnatum* (552 µg/ml) which were addressed by Sharif *et al.* [16]. Therefore, it is recommended to extend the study on these extracts for their anti-carcinogenic effect.

a)

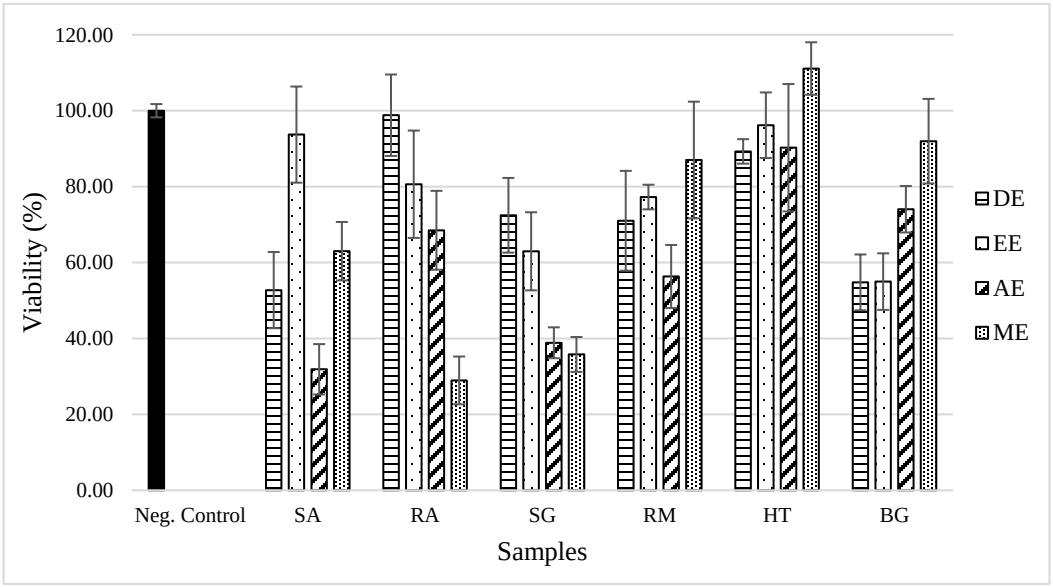

b)

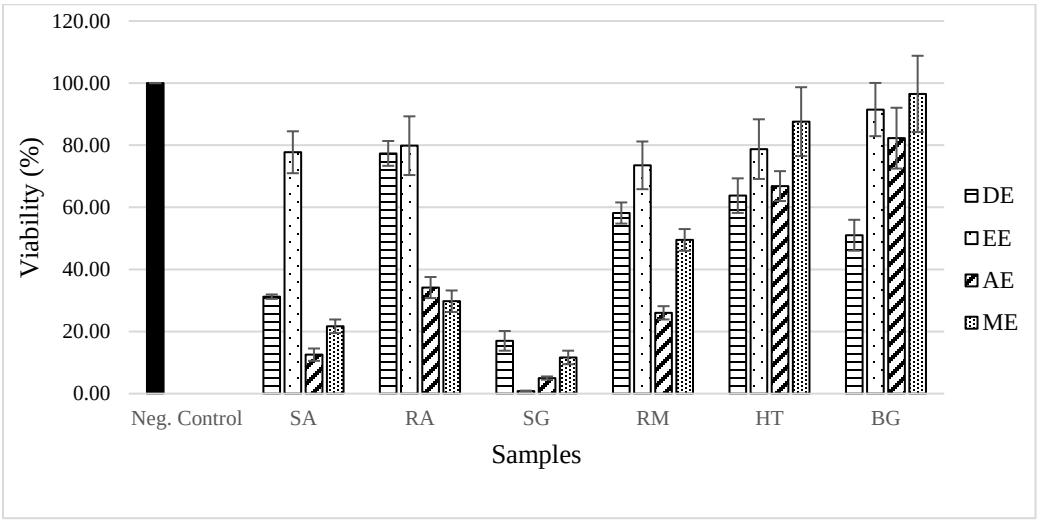

Figure 4. Cell viability in percentage against samples in 100 µg/ml for: a) 24 h and b) 72 h Abbreviations: SA = *S. alba*, RA = *R. apiculata*, SG = *S. grande*, RM = *R. mucronata*, HT = *H. tiliaceus*, BG = *B. gymnorhiza*, DE = dichloromethane extract, EE = ethyl acetate extract, AE = acetone extract, ME = methanol extract. Values represent mean ± SD (n = 3), $p < 0.05$

4. Conclusions

In summary, different bioactive constituents from the six selected coastal plants were extracted with different solvents according to their polarity. It can be concluded that AEAC of the extracts was positively correlated with TPC. Most of the AEs and MEs showed high TPC and DPPH radical scavenging activity, but did not show high TFC and FIC abilities. *Hibiscus tiliaceus* DE, *R. mucronata* DE and *R. apiculata* ME were found to possess high anti-tyrosinase properties. Out of these three extracts, *H. tiliaceus* DE exhibited the lowest cytotoxicity on B16F1 murine melanoma cells, and is thus considered the safest to use. Tyrosinase-inhibiting extracts with low cytotoxicity are potential additives in skin-whitening formulations and should be further studied for their melanogenesis inhibition, and subsequent pre-clinical skin irritation and absorption studies.

5. Acknowledgements

The authors would like to thank Dr H.T. Chan from International Society for Mangrove Ecosystems, Faculty of Agriculture, University of the Ryukyus, Japan who helped for the determination of coastal plants. The author would also like to express their gratitude to the Centre of Excellence for Research, Value Innovation and Entrepreneurship (CERVIE) for the financial support of this study under Pioneer Scientist Incentive Fund (PSIF) with the code of Proj-In-FAS-052, UCSI University, Malaysia.

References

[1] Jusoff, K., 2013. Malaysian mangrove forests and their significance to the coastal marine environment. *Polish Journal Environmental Studies*, 22(4), 979-1005.

[2] Neamsuvan, O., Singdam, P., Yingcharoen, K. and Sengnon, N., 2012. A survey of medicinal plants in mangrove and beach forests from Sating Phra Peninsula, Songkhla Province, Thailand. *Journal of Medicinal Plant Research*, 6(12), 2421-2437.

[3] Shevade, V.S., 2019. Loboda TV oil palm plantations in Peninsular Malaysia: determinants and constraints on expansion. *PLoS ONE*, 14(2), https://doi.org/10.1371/journal.pone.0210628

[4] Dahibhate, N.L., Saddhe, A.A. and Kumar, K., 2019. Mangrove plants as a source of bioactive compounds: A review. *The Natural Products Journal*, 9(2), 86-97.

[5] Balasubramanian, V., Rajesh, P., Rajaram, R. and Rajesh Kannan, V., 2015. A review on *Rhizophora* genus: therapeutically important perspective phytochemical constituents. *Bioactive Phytochemicals: Perspectives for Modern Medicine*, 3, 211-230.

[6] Chan, H.T. and Baba, S., 2009. *Manual on Guidelines for Rehabilitation of Coastal Forests Damaged by Natural Hazards in the Asia-pacific Region.* Okinawa: International Society for Mangrove Ecosystems (ISME) and International Tropical Timber Organisation (ITTO).

[7] Lim, T.K., 2014. *Edible Medicinal and Non Medicinal Plants: Volume 8, Flowers*. New York: Springer Science & Business.

[8] Ramsden, C.A. and Riley, P.A., 2014. Tyrosinase: The four oxidation states of the active site and their relevance to enzymatic activation, oxidation and inactivation. *Bioorganic and Medicinal Chemistry*, 22(8), 2388-2395.

[9] Reddy, A.R.K. and Grace, J.R., 2016. *In vitro* evaluation of antioxidant activity of methanolic extracts of selected mangrove plants. *Medicinal and Aromatic Plants*, 5(3), https://doi.org/ 10.4172/2167-0412.1000250

[10] Masuda, T., Yamashita, D., Takeda, Y. and Yonemori, S., 2005. Screening for tyrosinase inhibitors among extracts of seashore plants and identification of potent inhibitors from *Garcinia subelliptica*. *Bioscience, Biotechnology and Biochemistry*, 69(1), 197-201.
[11] Chen, H.Z. and Wang, L., 2017. *Technologies for Biochemical Conversion of Biomass*. London: Academic Press.
[12] Chan, E.W.C., Ng, S.M., Sim, B.W.K., Tan, H.C. and Lo, Z.L., 2017. Antioxidant, anti-tyrosinase and anti-quorum sensing activities of four mangrove tree species vs. green tea. *Journal of Applied Pharmaceutical Science*, 7(7), 225-229.
[13] Chang, C.C., Yang, M.H., Wen, H.M. and Chern, J.C., 2002. Estimation of total flavonoid content in propolis by two complementary colorimetric methods. *Journal of Food and Drug Analysis*, 10(3), 178-182.
[14] Chan, E.W.C., Lim, Y.Y., Chong, K.L., Tan, J.B.L. and Wong, S.K., 2010. Antioxidant properties of tropical and temperate herbal teas. *Journal of Food Composition and Analysis*, 23, 185-189.
[15] Cui, H.X., Duan, F.F., Jia, S.S., Cheng, F.R. and Yuan, K., 2018. Antioxidant and tyrosinase inhibitory activities of seed oils from *Torreya grandis* Fort. ex Lindl. *BioMed Research International*, 2018, https://doi.org/10.1155/2018/5314320
[16] Sharif, A., Akhtar, M.F., Akhtar, B., Saleem, A., Manan, M., Shabbir, M., Ashraf, M., Peerzada, S., Ahmed, S. and Raza, M., 2017. Genotoxic and cytotoxic potential of whole plant extracts of *Kalanchoe laciniata* by Ames and MTT assay. *EXCLI Journal*, 16, 593-601.
[17] Dutkiewicz, M., 1900. Classification of organic solvents based on correlation between dielectric β parameter and empirical solvent polarity parameter. *Journal of the Chemical Society, Faraday Transactions*, 86(12), 2237-2241.
[18] Barchan, A., Bakkali, M., Arakrak, A., Pagán, R. and Laglaoui, A., 2014. The effects of solvents polarity on the phenolic contents and antioxidant activity of three *Mentha* species extracts. *International Journal of Current Microbiology and Applied Sciences*, 3(11), 399-412.
[19] Zhen, J., Villani, T.S., Guo, Y., Qi, Y.D., Chin, K., Pan, M.H., Ho, C.T., Simon, J.E. and Wu, Q.L., 2016. Phytochemistry, antioxidant capacity, total phenolic content and anti-inflammatory activity of *Hibiscus sabdariffa* leaves. *Food Chemistry*, 190, 673-680.
[20] María, R., Shirley, M., Xavier, C., Jaime, S., David, V., Rosa, S and Jodie, D., 2018. Preliminary phytochemical screening, total phenolic content and antibacterial activity of thirteen native species from Guayas province Ecuador. *Journal of King Saud University – Science*, 30(4), 500-505.
[21] Minatel, I.O., Borges, C.V., Ferreira, M.I., Gomez, H.A.G., Chen, O.C.Y. and Lima, G.P.P., 2017. Phenolic compounds: functional properties, impact of processing and bioavailability. In: M. Soto-Hernandez, M. Palma-Tenango and M.R. Garcia-Mateos, eds. *Phenolic Compounds – Biological Activity*. Croatia: InTech.
[22] Gopalasatheeskumar, K., Kumar, G.A., Sengottuvel, T., Devan, V.S. and Srividhya, V., 2019. Quantification of total phenolic and flavonoid content in leaves of *Cucumis melo* var. *agrestis* using UV-spectrophotometer. *Asian Journal of Research in Chemistry*, 12(6), 335-337.
[23] Tripathi, Y.C. and Saini, N., 2019. Total phenolic, total flavonoid content and antioxidant efficacy of leaves of *Eupatorium adenophorum*. *International Journal of Pharma and Bio Sciences*, 10(2), 157-166.
[24] Silva, K.D.R.R. and Sirasa, M.S.F., 2018. Antioxidant properties of selected fruit cultivars grown in Sri Lanka. *Food Chemistry*, 238, 203-208.
[25] Sadeghi, Z., Valizadeh, J., Shermeh, O.A. and Akaberi, M., 2015. Antioxidant activity and total phenolic content of *Boerhavia elegans* (choisy) grown in Baluchestan, Iran. *Avicenna Journal of Phytomedicine*, 5(1), 1-9.
[26] Gan, R.Y., Chan, L.C., Yang, Q.Q., Li, H.B., Zhang, D., Ge, Y.Y., Gunaratne, A., Ge, J. and Corke, H., 2019. Bioactive compounds and beneficial functions of sprouted grains. *In:* H.

Feng, B. Hemzer, J.W. DeVries, eds. *Sprouted Grains: Nutritional Value, Production and Applications.* India: Elsevier Inc., pp.191-246.

[27] Ngo, T.V., Scarlett, C.J., Bowyer, M.C., Ngo, P.D. and Vuong, Q.V., 2017. Impact of different extraction solvents on bioactive compounds and antioxidant capacity from the root of *Salacia chinensis* L. *Journal of Food Quality*, 2017, https://doi.org/10.1155/2017/9305047

[28] Hassan, W.N.A.W., Zulkifli, R.M., Basar, N., Che Yunus, M.A. and Ahmad, F., 2015. Antioxidant and tyrosinase inhibition activities of α- mangostin and *Garcinia mangostana* Linn. pericarp extracts. *Journal of Applied Pharmaceutical Science*, 5(09), 37-40.

[29] Gögüs, F., Fadıloğlu, S. and Soysal, Ç., 2009. Biological Oxidation: Enzymatic and Nonenzymatic Browning Reactions and Control Mechanisms. In: F. Yildiz, ed. *Advances in Food Biochemistry*. Boca Raton: CRC Press, pp. 341-382.

[30] Melecchi, M.I.S., Péres, V.F., Dariva, C., Zini, C.A., Abad, F.C., Martinez, M.M. and Caramão, E.B., 2006. Optimization of the sonication extraction method of *Hibiscus tiliaceus* L. flowers. *Ultrasonics Sonochemistry*, 13, 242-250.

[31] Copeland, R.A., 2013. *Evaluation of Enzyme Inhibitors in Drug Discovery: A Guide for Medicinal Chemists and Pharmacologists.* 2nd ed. Ontario: John Wiley & Sons, Inc.

[32] Lim, W.Y., Cheun, C.F. and Wong, C.W., 2019. Inhibition of enzymatic browning in sweet potato (*Ipomoea batatas* (L.)) with chemical and natural anti-browning agents. *Journal of Food Processing and Preservation*, 43(11), https://doi.org/10.1111/jfpp.14195

[33] Lim, W.Y. and Wong, C.W., 2018. Inhibitory effect of chemical and natural anti-browning agents on polyphenol oxidase from ginger (*Zingiber officinale* Roscoe). *Journal of Food Science and Technology*, 55(8), 3001-3007.

[34] Prakash, S., Ramasubburayan, R., Ramkumar, V.S., Kannapiran, E., Palavesam, A. and Immanuel, G., 2016. *In vitro* − Scientific evaluation on antimicrobial, antioxidant, cytotoxic properties and phytochemical constituents of traditional coastal medicinal plants. *Biomedicine and Pharmacotherapy*, 83, 648-657.

Current Applied Science and Technology Vol. 21 No. 3 (July-September 2021)

A Class of Continuous Solutions of a Fourth Order Polynomial-like Iterative Equation

Suppharerg Thangroongvongthana[1]*, Vichian Laohakosol[2] and Sukrawan Mavecha[1]

[1]Department of Mathematics, Faculty of Science, King Mongkut's Institute of Technology Ladkrabang, Bangkok, Thailand
[2]Department of Mathematics, Faculty of Science, Kasetsart University, Bangkok, Thailand

Received: 15 July 2020, Revised: 11 January 2021, Accepted: 22 January 2021

Abstract

Using the so-called characteristic method, continuous solutions of the fourth order polynomial-like iterative equation

$$f^4(x)+a_3f^3(x)+a_2f^2(x)+a_1f(x)+a_0x=0$$

were determined subject to certain natural conditions on its characteristic roots. The result so obtained complements earlier work in the cases of second and third order equations.

Keywords: polynomial-like iterative equation; continuous solution; characteristic root
DOI 10.14456/cast.2021.39

1. Introduction

For $n\in N$, the n^{th} iterate of a function f is defined by

$$f^n(x)=f(f^{n-1}(x)),\ f^0(x)=x\ .$$

A polynomial-like iterative equation is a functional equation of the form

$$f^n(x)+a_{n-1}f^{n-1}(x)+...+a_0x=F(x)\ , \tag{1.1}$$

where $a_i\in R\ \ (i=0,1,2,...,n-1)$, F is a given function, and $f:R\to R$ is an unknown function. The homogeneous case of (1.1) (i.e., when $F(x)=0$)

$$f^n(x)+a_{n-1}f^{n-1}(x)+...+a_0x=0 \tag{1.2}$$

is of interest here. There have appeared a number of recent works [1-4] attempting to solve (1.2) using a technique mimicking that of Euler for solving linear differential equations with constant coefficients, which proceeds by assuming a solution of the form e^{rx}. Substituting this into the differential equation and simplifying, an algebraic equation in r, called its characteristic equation

*Corresponding author: Tel.: +66 838214391
E-mail: suppharerg@gmail.com

is obtained. Solving the characteristic equation yields linearly independent solutions of the differential equation, and the general solution follows by taking a linear combination of these independent solutions. In the case of iterative equation (1.2), we consider, instead, a continuous solution of the form $f(x) = rx$. Substituting into (1.2), we get an algebraic equation (in r)

$$r^n - a_{n-1}r^{n-1} - \ldots - a_1 r - a_0 = 0,$$

which, by abuse of language, is also called the *characteristic equation of (1.2)* and its roots are called its *characteristic roots*. Let $r_1, \ldots, r_n$ be all the characteristic roots. Using symmetric functions relations involving roots and coefficients, the iterative equation (1.2) is equivalent to

$$f^n(x) - (\sum_{i=1}^{n} r_i) f^{n-1}(x) + (\sum_{i<j}^{n} r_i r_j) f^{n-2}(x) + \ldots + (-1)^n r_1 r_2 \ldots r_n x = 0. \quad (1.3)$$

At the outset, we make several preliminary observations and define conventions to be adopted throughout the entire investigation here.

- The coefficient a_0 is always nonzero.
  (For otherwise, one of the characteristic roots is zero yielding the trivial solution function $f \equiv 0$ which must always be ruled out.)
- Any function solution $f : R \to R$ of (1.2) is injective.
  (If $x, y \in R$ are such that $f(x) = f(y)$, then $f^k(x) = f^k(y)$ for all $k \in N$ and (1.2) implies that $a_0 x = a_0 y$. Since $a_0 \neq 0$, we get $x = y$.)
- Any continuous function solution $f : R \to R$ of (1.2) is strictly monotone and surjective.
  (Since f is continuous and 1-1, clearly, it is strictly monotone. To show that f is onto, we consider only the case f is strictly increasing as the other case is similar. Suppose f is not onto on R. By its continuity, the range must be of the form $f(R) = I$, where $I \neq R$ is an interval, which can take one of the three shapes : $(-\infty, a)$, $(-b, a)$ or $(-b, \infty)$, for finite values $-b < a$. From $f : R \to f(R) := I$, we see that $f^2 : R \to f(I) \subseteq I, \ldots, f^n : R \to f(I) \subseteq I$.
  From (1.2), we get
  $$|a_0 x| = |f^n(x) + a_{n-1} f^{n-1}(x) + \ldots + a_1 f(x)|.$$
  For the cases $I := (-\infty, a)$ or $I := (-b, a)$, letting $x \to \infty$, we see that the left-hand side $\to \infty$, while the right-hand expression (since the range of the function is bounded) is bounded, which is contradiction.
  For the case $I := (-b, \infty)$, letting $x \to -\infty$, the left-hand side $\to \infty$, the right-hand side is bounded, which is again a contradiction.)
- Since $a_0 \neq 0$ and f is bijective, the inverse function $f^{-1} : R \to R$ exists and the original iterative equation (1.3) is equivalent to the dual equation
  $$f^{-n}(x) - (\sum_{i=1}^{n} \frac{1}{r_i}) f^{-(n-1)}(x) + (\sum_{i<j}^{n} \frac{1}{r_i r_j}) f^{-(n-2)}(x) + \ldots + (-1)^n \frac{1}{r_1 r_2 \ldots r_n} x = 0 \quad (1.4)$$
  where f^{-j} denotes the j^{th} iterate of f^{-1}.

In 2004, Yang and Zhang [3] constructed all continuous solutions of the equation (1.2) when $n \geq 2$ for the hyperbolic cases subject to the condition that characteristic roots belong to following ranges:

- all characteristic roots are in the interval $(1,\infty)$: $1 < r_1 < r_2 < .... < r_n$;
- all characteristic roots are in the interval $(0,1)$: $0 < r_1 < r_2 < .... < r_n < 1$;
- all characteristic roots are in the interval $(-\infty,-1)$: $r_1 < r_2 < .... < r_n < -1$;
- all characteristic roots are in the interval $(-1,0)$: $-1 < r_1 < r_2 < .... < r_n < 0$.

- no real characteristic roots (in this case n must be even and characteristic roots form pairs of conjugate complex numbers), it is shown that (1.2) has no continuous solution.
- all characteristic roots are equal, i.e., $r_1 = ... = r_n = r$.

  (i) If $0 < r \neq 1$, then f is strictly increasing, the function

$$F^{n-1}[r](f^0) := f^{n-1}(x) + \sum_{m=1}^{n-1} (-1)^m \binom{n-1}{m} r^m f^{n-1-m}(x)$$

  is nondecreasing, $f(0) = 0$, and $F^{n-1}[r](f^0) = 0$ for even n.

  (ii) If $-1 \neq r < 0$, then f is strictly decreasing, the function $F^{n-1}[r](f^0)$ is nondecreasing (respectively, nonincreasing) for odd (respectively, even) n, $f(0) = 0$, and $F^{n-1}[r](f^0) = 0$ for even n.

  (iii) If $r = 1$, then f is strictly increasing. Additionally, $f(x) \equiv x$ if f has fixed point, otherwise, $F^{n-1}[r](f^0) \equiv a$ for all $x \in R$, where a is a real constant which equals 0 for odd n. In particular, for $n = 3$, continuous solutions of equation (1.2) are of the form $f(x) = x + c$, where c is a real constant.

  (iv) If $r = -1$, then $f(x) = -x$ for all $x \in R$.

  The subcases (i), (ii) and (iii) provide a method to reduce the order of iteration, giving equivalent equations of lower order, although it does not give the construction of the general solution in all cases.

In their work, there remain un-resolved cases when the existing characteristic roots of (1.2)

- are both positive and negative, or
- have absolute values both greater and less than 1.

In the second order case (i.e., $n = 2$), Matkowski and Weinian [1] established continuous solutions by subdividing into the following cases.

- Noncritical cases: $r_1 r_2 > 0$, $|r_1| \neq 1$ and $|r_2| \neq 1$ with all possibilities

  $1 < r_1 < r_2$, $0 < r_1 < 1 < r_2$, $0 < r_1 < r_2 < 1$,

  $r_1 < r_2 < -1$, $r_1 < -1 < r_2 < 0$, $-1 < r_1 < r_2 < 0$.
- Noncritical cases: $r_1 r_2 < 0$, $|r_1| \neq 1$, $|r_2| \neq 1$, $r_2 \neq -r_1$ with all possibilities

  $0 < -r_1 < r_2 < 1$, $0 < r_2 < -r_1 < 1$, $1 < r_2 < -r_1$, $0 < r_2 < 1 < -r_1$, $0 < -r_1 < 1 < r_2$.

- Case $|r_1| = |r_2|$: $r_1 = r_2 = r \neq 0$.
- Critical cases: there is a characteristic root with absolute value 1 with all possibilities
  $0 < r_1 < r_2 = 1$, $1 \neq r_1 < 0 < r_2 = 1$, $-1 = r_1 < 0 < r_2 \neq 1$, $-1 = r_1 < r_2 < 0$, $r_1 < r_2 = -1$.
- Case with no real roots: in this case (1.2) has no continuous solution on R.

From their work, the un-resolved case is when $r_1 = -r = -r_2$ ($r > 0$). The governing equation of this case is

$$f^2(x) = r^2 x. \tag{1.5}$$

When $r = 1$, Kuczma's Theorem 15.2 [6] shows that (1.5) has a decreasing solution depending on an arbitrary function, but $f(x) = x$ is its unique increasing solution.

When $r \neq 1$, Kuczma's Theorems 15.7 [6] and 15.9 [6] indicate that (1.5) has not only increasing continuous solutions but also decreasing ones, all of which depend on arbitrarily given functions.

In the third order case (i.e., $n = 3$), Zhang and Gong [4] in 2014 solved (1.2) for continuous solutions in the hyperbolic cases not treated in the work of Yang and Zhang. They completed the following cases:

I. The three characteristic roots have different signs. There are two possibilities.

I.1 Two positive characteristic roots $0 < r_2 < r_3$, and one negative characteristic root $r_1 < 0$. Treated cases are

- $0 < -r_1 < 1$: $0 < -r_1 < r_2 < r_3 < 1$, $0 < r_2 < -r_1 < r_3 < 1$, $0 < r_2 < r_3 < -r_1 < 1$, $0 < -r_1 < 1 < r_2 < r_3$, $0 < r_2 < -r_1 < 1 < r_3$, $0 < -r_1 < r_2 < 1 < r_3$.
- $1 < -r_1$: $1 < -r_1 < r_2 < r_3$, $1 < r_2 < -r_1 < r_3$, $1 < r_2 < r_3 < -r_1$, $0 < r_2 < 1 < -r_1 < r_3$, $0 < r_2 < 1 < r_3 < -r_1$, $0 < r_2 < r_3 < 1 < -r_1$.

I.2 One positive characteristic root $r_3 > 0$, and two negative characteristic roots $0 > r_1 > r_2$.

- $0 < r_3 < 1$: $0 < -r_1 < -r_2 < r_3 < 1$, $0 < -r_1 < r_3 < -r_2 < 1$, $0 < r_3 < -r_1 < -r_2 < 1$, $0 < r_3 < 1 < -r_1 < -r_2$, $0 < r_3 < -r_1 < 1 < -r_2$, $0 < -r_1 < r_3 < 1 < -r_2$.
- $1 < r_3$: $1 < -r_1 < -r_2 < r_3$, $1 < -r_1 < r_3 < -r_2$, $1 < r_3 < -r_1 < -r_2$, $0 < -r_1 < 1 < -r_2 < r_3$, $0 < -r_1 < 1 < r_3 < -r_2$, $0 < -r_1 < -r_2 < 1 < r_3$.

II. The three characteristic roots have the same signs. The treated possibilities are

$$0 < r_1 < 1 < r_2 < r_3,\ 0 < r_3 < r_2 < 1 < r_1,\ r_1 < r_2 < -1 < r_3 < 0,\ r_3 < -1 < r_2 < r_1 < 0.$$

The still un-resolved cases are:

- there is a characteristic root with absolute value 1.
- there is a characteristic root with multiplicity ≥ 2.

Zhang and Gong [4] also considered the 4-th order equation when the four characteristic roots have different signs lying in the following ranges:

$1 < -r_1 < r_2 < r_3 < r_4$, $1 < -r_1 < r_2 < r_4 < r_3$, $1 < -r_1 < r_4 < r_2 < r_3$, $1 < -r_1 < r_2 < -r_4 < r_3$, $1 < -r_1 < -r_4 < r_2 < r_3$, $1 < -r_4 < -r_1 < r_2 < r_3$.

2. Methodology

Following ideas from the work of Zhang and Gong [4], we determine here continuous solutions of the homogeneous equation (1.2) of order 4, i.e. the iterative equation

$$f^4(x)-(\sum_{i=1}^{4} r_i) f^3(x)+(\sum_{i<j}^{4} r_i r_j) f^2(x)-(\sum_{i<j<k}^{4} r_i r_j r_k) f(x)+r_1 r_2 r_3 r_4 x=0, \tag{1.6}$$

when the characteristic roots r_1, r_2, r_3, r_4 are subject to the restrictions:

1) $|r_i| \neq 0,1$ $(i=1,2,3,4)$, and

2) the absolute values of the chrarcteristic roots $|r_i|$ $(i=1,2,3,4)$ are all distinct.

The dual equation of (1.6) is

$$f^{-4}(x)-(\sum_{i=1}^{4} \frac{1}{r_i}) f^{-3}(x)+(\sum_{i<j}^{4} \frac{1}{r_i r_j}) f^{-2}(x)-(\sum_{i<j<k}^{4} \frac{1}{r_i r_j r_k}) f^{-1}(x)+\frac{1}{r_1 r_2 r_3 r_4} x=0. \tag{1.7}$$

To simplify our analysis, we leave out certain special cases consisting of

$$r_1<r_2<r_3<r_4<-1,\ -1<r_1<r_2<r_3<r_4<0,\ 0<r_1<r_2<r_3<r_4<1,\ 1<r_1<r_2<r_3<r_4$$

that have already been treated in Yang and Zhang [3]. In addition, the special case where all characteristic roots are not real, which has also been shown to have no continuous solution by them, is also left out.

Specifically, we solve (1.6) when the characteristic equation has

- one negative and three positive characteristic roots or
- three negative and one positive characteristic roots or
- two negative and two positive characteristic roots.

The solutions so obtained are displayed in Figures 1, 2 and 3, respectively. Though there are totally seventy subcases solved in this work, there remain two cases that are yet to be resolved for which the methods and techniques used here do not seem to work. These subcases are when

(i) all characteristic roots are positive, some being in $(0,1)$ and the others in $(1,\infty)$,

(ii) all characteristic roots are negative, some being in $(-1,0)$ and the others in $(-\infty,-1)$.

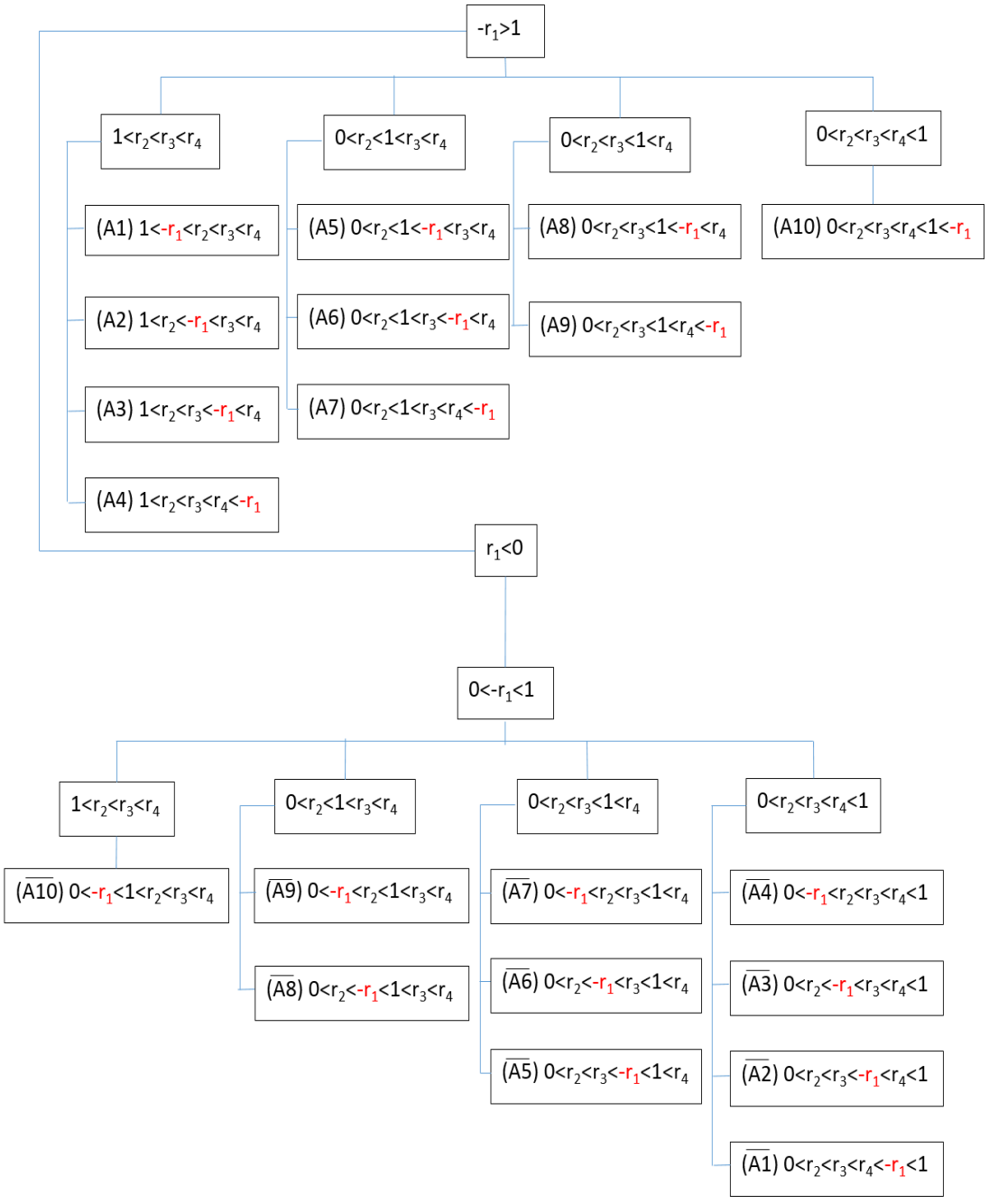

Figure 1. One negative characteristic root, r_1, and

three positive characteristic roots, $\mathbf{0 < r_2 < r_3 < r_4}$

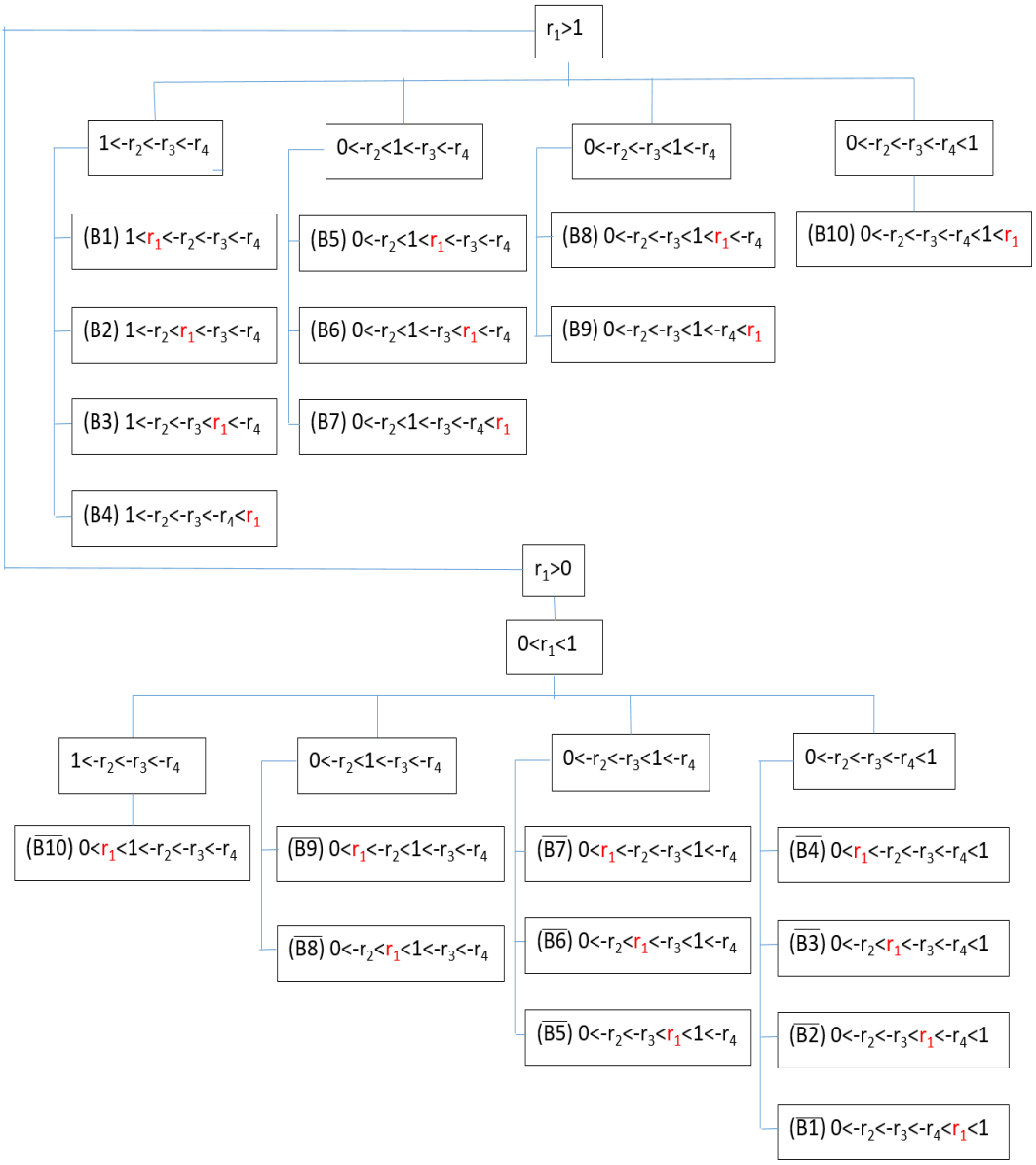

Figure 2. Three negative characteristic roots, $\mathbf{0 > r_2 > r_3 > r_4}$, and one positive characteristic root, $\boldsymbol{r_1}$

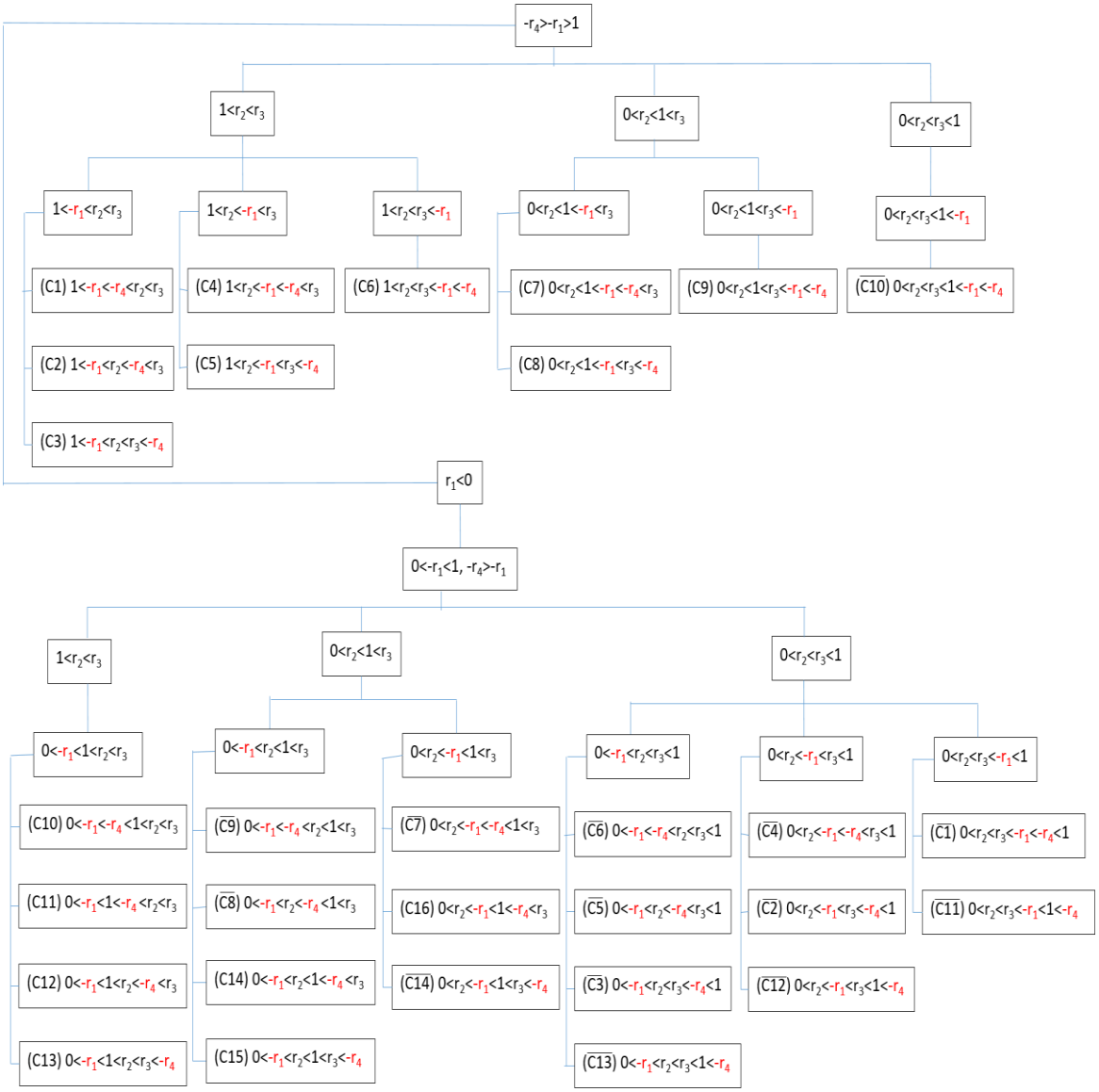

Figure 3. Two negative characteristic roots, $\mathbf{0 > r_1 > r_4}$, and two positive characteristic roots, $\mathbf{0 < r_2 < r_3}$

Detailed proofs of our results are given in the next section. Preliminary results needed throughout are displayed in the above two boxes.

To simplify the presentation, define

$$CS(x) = \{f : R \to R;\ f \text{ is a continuous solution of the iterative equation } (x)\},$$
$$CSI(x) = \{f : R \to R;\ f \text{ is a continuous strictly increasing solution of the iterative equation } (x)\},$$
$$CSD(x) = \{f : R \to R;\ f \text{ is a continuous strictly decreasing solution of the iterative equation } (x)\}.$$

To consider our continuous solutions, we need the continuous solutions from the works of Yang and Zhang [3], Matkowski and Weinian [1], and Zhang and Gong [4] as shown below.

Works of Yang and Zhang [3]

Theorem 1.1 (Theorem 2 [3]) Suppose that $1 < r_1 < ... < r_n$. If $f \in CS(1.2)$, then

(i) f is strictly increasing,

(ii) $f(0) = 0$, and

(iii) $f^{n-1}(x) - (\sum_{i=1}^{n-1} r_i) f^{n-2}(x) + (\sum_{i<j}^{n-1} r_i r_j) f^{n-3}(x) + ... + (-1)^{n-1} r_1 r_2 ... r_{n-1} x$ is nondecreasing

and $f^{n-1}(x) - (\sum_{i=2}^{n} r_i) f^{n-2}(x) + (\sum_{i<j\neq 1}^{n} r_i r_j) f^{n-3}(x) + ... + (-1)^{n-1} r_2 r_3 ... r_n x$ is non-decreasing (resp. non-increasing) for odd (resp. even) n.

Conversely, given positive numbers $x_0, ..., x_{n-1}$ such that

$$x_{n-1} - (\sum_{i\neq k}^{n} r_i) x_{n-2} + (\sum_{i<j,i,j\neq k}^{n} r_i r_j) x_{n-3} + ... + (-1)^{n-1} r_1 ... r_{k-1} r_{k+1} ... r_n \geq 0 \text{ (resp. } \leq 0),$$

if $n-k$ is even (resp. odd) and given a continuous function $f_* : [x_0, x_{n-1}] \to [x_1, x_n]$, where

$$x_n := (\sum_{i=1}^{n} r_i) x_{n-1} - (\sum_{i<j}^{n} r_i r_j) x_{n-2} + ... + (-1)^{n-1} r_1 ... r_n x_0, \text{ satisfying}$$

(I) $f_*(x_j) = x_{j+1} (0 \leq j \leq n-1)$ and

(II) Each $f_*^{n-1}(x) - (\sum_{i=1\neq k}^{n} r_i) f_*^{n-2}(x) + (\sum_{i<j\neq k}^{n} r_i r_j) f_*^{n-3}(x) + ... + (-1)^{n-1} r_1 ... r_{k-1} r_{k+1} ... r_n x,$

$k = 1, 2, ..., n$, is nondecreasing (resp. nonincreasing) on $[x_0, x_1]$ if $n-i$ is even (resp. odd), then equation (1.2) has a unique continuous solution $\phi : (o, \infty) \to (o, \infty)$ satisfying $\phi|_{[x_0, x_{n-1}]} = f_*$.

Furthermore, given f_{*1} and f_{*2} arbitrarily like f_*, the function

$$f(x) := \begin{cases} \phi_1(x), & x > 0, \\ 0, & x = 0, \\ -\phi_2(-x), & x < 0 \end{cases}$$

is a continuous solution of equation (1.2) on , where ϕ_1 and ϕ_2 are functions determined correspondingly by f_{*1} and f_{*2}.

Corollary 1.2 (Remark 4 [3]) The case that $0 < r_1 < ... < r_n < 1$ can be reduced to the case of above Theorem 1 by considering the dual equation (1.4).

Theorem 1.3 (Theorem 3 [3]) The case that $r_1 < ... < r_n < -1$. Suppose $f \in CS(1.2)$. Then
(i) f is strictly decreasing and has a unique fixed point 0;
(ii) $f^{n-1}(x) - (\sum_{i=1}^{n-1} r_i) f^{n-2}(x) + (\sum_{i<j}^{n-1} r_i r_j) f^{n-3}(x) + ... + (-1)^{n-1} r_1 r_2 ... r_{n-1} x$ is nondecreasing and

$f^{n-1}(x) - (\sum_{i=2}^{n} r_i) f^{n-2}(x) + (\sum_{i<j\neq 1}^{n} r_i r_j) f^{n-3}(x) + ... + (-1)^{n-1} r_2 r_3 ... r_n x$ is nondecreasing (resp. nonincreasing) for odd (resp. even) n.
Moreover, (1.2) has symmetric continuous solutions in the form

$$f(x) := \begin{cases} -\varphi(x), & x \geq 0, \\ \varphi(-x), & x < 0, \end{cases}$$

where $\varphi : [0,\infty) \to [0,\infty)$ is an arbitrarily given function satisfying

$$\varphi^n(x) = (\sum_{i=1}^{n} r_i)\varphi^{n-1}(x) - (\sum_{i<j}^{n} r_i r_j)\varphi^{n-1}(x) + ... + (-1)^{n-1} r_1 ... r_n x, \ x \in (0,\infty).$$

Theorem 1.4 (Theorem 4 [3]) The case that $r_1 < ... < r_n < -1$. Given real $x_0, ..., x_{n-1}$ arbitrarily, which are not all zero such that $x_{n-1} - (\sum_{i\neq k}^{n} r_i) x_{n-2} + (\sum_{i<j, i, j\neq k}^{n} r_i r_j) x_{n-3} + ... + (-1)^{n-1} r_1 ... r_{k-1} r_{k+1} ... r_n \geq 0$ (resp. ≤ 0), if n-k is even (resp. odd). Given a continuous function $f_* : \bigcup_{j=0}^{n-2} [x_j; x_{j+2}] \to \bigcup_{j=0}^{n-2} [x_{j+1}; x_{j+3}]$, where $x_k := (\sum_{i=1}^{k} r_i) x_{k-1} - (\sum_{i<j}^{k} r_i r_j) x_{k-2} + ... + (-1)^{k-1} r_1 ... r_k x_{k-n}$, for $k = n, n+1$ such that

(I) $f_*(x_j) = x_{j+1}$ $j = 0, ..., n$ and

(II) each $f_*^{n-1}(x) - (\sum_{i=1\neq k}^{n} r_i) f_*^{n-2}(x) + (\sum_{i<j\neq k}^{n} r_i r_j) f_*^{n-3}(x) + ... + (-1)^{n-1} r_1 ... r_{k-1} r_{k+1} ... r_n x,$

$k = 1, 2, ..., n$, is nondecreasing (resp. nonincreasing) on $[x_0, x_2]$ if $n - i$ is even (resp. odd), then equation (1.2) has a unique continuous solution f such that $f|_{\bigcup_{j=0}^{n-2}[x_j, x_{j+2}]} = f_*$.

Corollary 1.5 (Remark 6 [3]) The case that $-1 < r_1 < ... < r_n < 0$ can be reduced to the case of Theorem 4 by considering the dual equation (1.4).

Works of Matkowski and Weinian [1]

Theorem 1.6 (Theorem 1 [1]) Suppose $1 < r_1 < r_2$.
(i) If $f \in CS(1.2)$ for $n = 2$, then $f(0) = 0$ and f, strictly increasing, satisfies
$r_1 \leq (f(x) - f(x'))/(x - x') \leq r_2$ for $x \neq x' \in R$.
(ii) Conversely, equation (1.2) for $n = 2$ has a continuous solution depending on an arbitrary function. More precisely, for every $x_0 > 0, x_1 > 0$ and $f_0 : [x_0, x_1] \to R$ such that

$$r_1 x_0 \leq x_1 \leq r_2 x_0,$$

$$f_0(x_0) = x_1, \quad f_0(x_1) = (r_1 + r_2)x_1 - r_1 r_2 x_0,$$
$$r_1 \le \frac{f_0(x) - f_0(x')}{x - x'} \le r_2; \quad \forall x, x' \in [x_0, x_1],$$

there is a unique continuous function $p : (0,\infty) \to (0,\infty)$ satisfying equation (1.2) for $n = 2$ on $(0,\infty)$ and $p = f_0$ on $[x_0, x_1]$; for two arbitrary initial functions f_{01} and f_{02} like f_0, the function

$$f(x) := \begin{cases} p_1(x), & x > 0, \\ 0, & x = 0, \\ -p_2(-x), & x < 0. \end{cases} \tag{3.1}$$

is a continuous function of equation (1.2) for $n = 2$ on R, where p_1 and p_2 are functions like p determined as above by f_{01} and f_{02}. (3.1) gives all continuous solutions of equation (1.2) for $n = 2$ in R.

Corollary 1.7 (Page 427 [1]) The case where $0 < r_1 < r_2 < 1$ can be obviously reduced to the case of Theorem 6 by considering the dual equation (1.4) for $n = 2$.

Theorem 1.8 (Theorem 2 [1]) Suppose $0 < r_1 < 1 < r_2$.
(i) If $f \in CS(1.2)$ for $n = 2$ then f is strictly increasing. If, additionally, f has a fixed point then

$$f(x) = \begin{cases} r_i x, x \ge 0 \\ r_j x, x < 0 \end{cases} \qquad \exists i, j = 1, 2.$$

(ii) Conversely, every $f \in CS(1.2)$ for $n = 2$ without fixed points depends on an arbitrary initial function. More precisely, for $x_0 = 0$, for every $x_1 > 0$ $(resp. < 0)$ and for every function $f_0 : [x_0, x_1] \to R$ $(resp. f_0 : [x_1, x_0] \to R)$ such that

$$f_0(x_0) = f_0(0) = x_1, \quad f_0(x_1) = (r_1 + r_2)x_1,$$
$$r_1 \le (f_0(x) - f_0(x')) / (x - x') \le r_2, \quad \forall x, x' \ne 0.$$

There exists a unique continuous function $f : R \to R$ satisfying equation (1.2) for $n = 2$ and $f(x) = f_0(x)$ on $[x_0, x_1]$ (*resp.* on $[x_1, x_0]$).

Theorem 1.9 (Theorem 3 [1]) Suppose $r_1 < r_2 < -1$.
(i) If $f \in CS(1.2)$ for $n = 2$ then f is strictly decreasing with a unique fixed point 0 and satisfies the condition $r_1 \le (f(x) - f(x')) / (x - x') \le r_2$, for $x \ne x' \in R$.
(ii) Conversely, equation (1.2) for $n = 2$ has a continuous solution depending on an arbitrary function, given by $f(x) = -p(x)$ when $x \ge 0$ and $f(x) = p(-x)$ when $x < 0$ where $p : [0,\infty) \to [0,\infty)$ has been constructed in Theorem 6 as an arbitrary solution of the functional equation

$$p^2(x) = ((-r_1) + (-r_2))\, p(x) - (-r_1)(-r_2)x, \quad x \in [0,\infty).$$

Theorem 1.10 (Theorem 4 [1]) Suppose $r_1 < -1 < r_2 < 0$. Then every $f \in CS(1.2)$ for $n = 2$ is strictly decreasing and 0 is its unique fixed point, and $r_1 \le (f(x) - f(x')) / (x - x') \le r_2, \forall x \ne x'$.

Corollary 1.11 (Page 427 [1]) The case where $-1 < r_1 < r_2 < 0$ can be obviously reduce to the case of Theorem 9 by considering the dual equation (1.4) for $n = 2$.

Theorem 1.12 (Theorem 5 [1]) Suppose that $r_1 < 0, r_1 \neq -1, r_2 > 0, r_2 \neq 1$ and $r_2 \neq -r_1$. If $f \in CS(1.2)$ for $n = 2$ then $f(x) = r_1 x$ or $f(x) = r_2 x$ for $x \in R$.

Works of Zhang and Gong [4]

Lemma 1.13 (Lemma 2.5 [4]) Suppose that the characteristic equation (1.3) has n distinct roots $r_1, ..., < r_n \in C$. If $f \in CS(1.2)$, then

$$f^m = \sum_{j=1}^{n} \frac{r_j^m}{\prod_{i=1, i\neq j}^{n} (r_j - r_i)} [f^{n-1}(x) - (\sum_{k\neq j}^{n-1} r_k) f^{n-2}(x) + (\sum_{k>t\neq j}^{n-1} r_k r_t) f^{n-3}(x) + ... + (-1)^{n-1} \prod_{i\neq j}^{n-1} r_i x]$$

$$f^{-m} = \sum_{j=1}^{n} \frac{r_j^{-m}}{\prod_{i=1, i\neq j}^{n} (\frac{1}{r_j} - \frac{1}{r_i})} [f^{-(n-1)}(x) - (\sum_{k\neq j}^{n-1} \frac{1}{r_k}) f^{-(n-2)}(x) + (\sum_{k>t\neq j}^{n-1} \frac{1}{r_k r_t}) f^{-(n-3)}(x) + ... + (-1)^{n-1} \prod_{i\neq j}^{n-1} \frac{1}{r_i} x]$$

for all integers $m \geq 1$ and $i = 1, 2, ..., n$.

Lemma 1.14 (Lemma 3.1 [4]) Suppose that $0 < r_1 < 1 < r_2 < r_3$. Then for $x_0 = 0$ and arbitrarily given x_1, x_2 such that

$$x_1 > 0 \text{ and } (r_1 + r_2) x_1 < x_2 < (r_1 + r_3) x_1,$$

the sequence $(..., x_{-2}, x_{-1}; x_0, x_1, x_2, ...)$ defined by

$$x_{n+2} = (r_1 + r_2 + r_3) x_{n+1} - (r_1 r_2 + r_1 r_3 + r_2 r_3) x_n + r_1 r_2 r_3 x_{n-1}, \tag{3.2}$$

$$x_{-n} = \left(\frac{1}{r_1} + \frac{1}{r_2} + \frac{1}{r_3}\right) x_{-n+1} - \left(\frac{1}{r_1 r_2} + \frac{1}{r_1 r_3} + \frac{1}{r_2 r_3}\right) x_{-n+2} + \frac{1}{r_1 r_2 r_3} x_{-n+3}, \tag{3.3}$$

is strictly increasing and satisfies

$$\lim_{n\to+\infty} x_n = +\infty, \qquad \lim_{n\to-\infty} x_n = -\infty.$$

Lemma 1.15 (Lemma 3.2 [4]) Suppose that $0 < r_1 < 1 < r_2 < r_3$. Then for $x_0 = 0$ and arbitrarily given x_1, x_2 such that

$$x_1 < 0 \text{ and } (r_1 + r_3) x_1 < x_2 < (r_1 + r_2) x_1,$$

the sequence $(..., x_2, x_1; x_0, x_{-1}, x_{-2}, ...)$ defined by (3.2) and (3.3) is strictly decreasing and satisfies

$$\lim_{n\to+\infty} x_n = -\infty, \qquad \lim_{n\to-\infty} x_n = +\infty.$$

Theorem 1.16 (Theorem 3.1 [4]) Suppose that $0 < r_1 < 1 < r_2 < r_3$. Then all $f \in CS(1.2)$ for $n = 3$ are strictly increasing. Additionally:
(i) If f has fixed points, then 0 is the unique fixed point and

$$f(x)=\begin{cases} f_i(x), x\geq 0 \\ f_j(x), x<0 \end{cases} \qquad i,j=1,2$$

where $f_1(x)=r_1x$ and $f_2(x)$ is a solution given in Theorem 1 of Nabeya [5].

(ii) If $f(x)>x$ for all $x\in R,$ then the set of f contains both $f(x)>max(r_1x,r_ix)(i=2,3)$ constructed by Theorem 2 of [5] and

$$f(x):=\begin{cases} f_n(x), & x\in[x_n,x_{n+1}], n=0,1,..., \\ f_{-n}^{-1}(x), & x\in[x_{-n},x_{-n+1}], n=1,2,..., \end{cases}$$

where the bilateral sequence (x_i) is given in Lemma 14, and $f_n:[x_n,x_{n+1}]\to[x_{n+1},x_{n+2}]$ and $f_{-n}:[x_{-n+1},x_{-n+2}]\to[x_{-n},x_{-n+1}], n=1,2,...$ are orientation-preserving homeomorphisms defined inductively as

$$f_{n+2}(x)=(r_1+r_2+r_3)x-(r_1r_2+r_1r_3+r_2r_3)f_{n+1}^{-1}(x)+r_1r_2r_3f_n^{-1}(f_{n+1}^{-1}(x)),$$

$$f_{-n}(x)=\left(\frac{1}{r_1}+\frac{1}{r_2}+\frac{1}{r_3}\right)x-\left(\frac{1}{r_1r_2}+\frac{1}{r_1r_3}+\frac{1}{r_2r_3}\right)f_{-n+1}^{-1}(x)+\frac{1}{r_1r_2r_3}f_{-n+2}^{-1}(f_{-n+1}^{-1}(x))$$

which are uniquely determined by two given function $f_0:[x_0,x_1]\to[x_1,x_2]$ and $f_1:[x_1,x_2]\to[x_2,x_3]$.

(iii) If $f(x)<x$ for all $x\in R,$, then the set of f contains both $f(x)<max(r_1x,r_ix)(i=2,3)$ constructed by Theorem 2 of Nabeya [5] and

$$f(x):=\begin{cases} f_n(x), & x\in[x_{n+1},x_n], n=0,1,..., \\ f_{-n}^{-1}(x), & x\in[x_{-n+1},x_{-n}], n=1,2,..., \end{cases}$$

where the bilateral sequence (x_i) is given in Lemma 15, and $f_n:[x_{n+1},x_n]\to[x_{n+2},x_{n+1}]$ and $f_{-n}:[x_{-n+2},x_{-n+1}]\to[x_{-n+1},x_{-n}]$ are orientation-preserving homeomorphisms defined inductively as

$$f_{n+2}(x)=(r_1+r_2+r_3)x-(r_1r_2+r_1r_3+r_2r_3)f_{n+1}^{-1}(x)+r_1r_2r_3f_n^{-1}(f_{n+1}^{-1}(x)),$$

$$f_{-n}(x)=\left(\frac{1}{r_1}+\frac{1}{r_2}+\frac{1}{r_3}\right)x-\left(\frac{1}{r_1r_2}+\frac{1}{r_1r_3}+\frac{1}{r_2r_3}\right)f_{-n+1}^{-1}(x)+\frac{1}{r_1r_2r_3}f_{-n+2}^{-1}(f_{-n+1}^{-1}(x))$$

which are uniquely determined by two given function $f_0:[x_1,x_0]\to[x_2,x_1]$ and $f_1:[x_2,x_1]\to[x_3,x_2]$.

Corollary 1.17 (Corollary 3.1 [4]) Suppose that $0<r_3<r_2<1<r_1$. Then every $f\in CS(1.3)$ for $n=3$ is strictly increasing and f^{-1} is a solution given in Theorem 16.

Theorem 1.18 (Theorem 3.2 [4]) Suppose that $r_1<r_2<-1<r_3<0$. Then all $f\in CS(1.3)$ for $n=3$ are strictly decreasing and $x=0$ is the unique fixed point of every f. Moreover,

(i) If $x=0$ is attractive fixed point of f^2, then $f(x)=r_3x$.

(ii) If $x=0$ is repelling fixed point of f^2, then f is a solution in the class given in Theorem 3 of Nabeya [5].

Corollary 1.19 (Corollary 3.2 [4]) Suppose that $r_3 < -1 < r_2 < r_1 < 0$. Then all $f \in CS(1.3)$ for $n = 3$ are strictly decreasing with the unique fixed point 0, and the inverse f^{-1} is a solution given in Theorem 18.

From now, Zhang and Gong [4] considered all continuous solutions of equation (1.3) for $n = 3$ for one negative root and two positive roots as in Table 1 and two negative roots and one positive root as in Table 2.

Table 1. Two positive and one negative characteristic roots

$(i)\ 1 < -r_1 < r_2 < r_3$	$(iii)\ 1 < r_2 < -r_1 < r_3$	$(v)\ 1 < r_2 < r_3 < -r_1$
$(\bar{v})\ 0 < -r_1 < r_2 < r_3 < 1$	$(\bar{iii})\ 0 < r_2 < -r_1 < r_3 < 1$	$(\bar{i})\ 0 < r_2 < r_3 < -r_1 < 1$
$(ii)\ 0 < -r_1 < 1 < r_2 < r_3$	$(iv)\ 0 < r_2 < 1 < -r_1 < r_3$	$(vi)\ 0 < r_2 < 1 < r_3 < -r_1$
$(\bar{ii})\ 0 < r_2 < r_3 < 1 < -r_1$	$(\bar{iv})\ 0 < r_2 < -r_1 < 1 < r_3$	$(\bar{vi})\ 0 < -r_1 < r_2 < 1 < r_3$

Table 2. One positive and two negative characteristic roots

$(a)\ 1 < -r_1 < -r_2 < r_3$	$(c)\ 1 < -r_1 < r_3 < -r_2$	$(e)\ 1 < r_3 < -r_1 < -r_2$
$(\bar{e})\ 0 < -r_1 < -r_2 < r_3 < 1$	$(\bar{c})\ 0 < -r_1 < r_3 < -r_2 < 1$	$(\bar{a})\ 0 < r_3 < -r_1 < -r_2 < 1$
$(b)\ 0 < -r_1 < 1 < -r_2 < r_3$	$(d)\ 0 < -r_1 < 1 < r_3 < -r_2$	$(f)\ 0 < r_3 < 1 < -r_1 < -r_2$
$(\bar{b})\ 0 < r_3 < -r_1 < 1 < -r_2$	$(\bar{d})\ 0 < -r_1 < r_3 < 1 < -r_2$	$(\bar{f})\ 0 < -r_1 < -r_2 < 1 < r_3$

Theorem 1.20 (Theorem 4.1 [4]) Cases $(i)\ 1 < -r_1 < r_2 < r_3$, $(ii)\ 0 < -r_1 < 1 < r_2 < r_3$, $(iii)\ 1 < r_2 < -r_1 < r_3$ and $(v)\ 1 < r_2 < r_3 < -r_1$ in Table 1.

1) If $f \in CSI(1.3)$ for $n = 3$, then f is a function in the class given in Theorem 1 of [5].

2) If $f \in CSD(1.3)$ for $n = 3$, then $f(x) = r_1 x$.

Corollary 1.21 (Corollary 4.1 [4]) Cases $(\bar{i})\ 0 < r_2 < r_3 < -r_1 < 1$, $(\bar{ii})\ 0 < r_2 < r_3 < 1 < -r_1$, $(\bar{iii})\ 0 < r_2 < -r_1 < r_3 < 1$ and $(\bar{v})\ 0 < -r_1 < r_2 < r_3 < 1$ in Table 1.

If $f \in CS(1.3)$ for $n = 3$, then f^{-1} is a function in the class given in Theorem 20.

Theorem 1.22 (Theorem 4.2 [4]) Cases $(\bar{iv})\ 0 < r_2 < -r_1 < 1 < r_3$ and $(\bar{vi})\ 0 < -r_1 < r_2 < 1 < r_3$ in Table 1.

1) If $f \in CSI(1.3)$ for $n = 3$, then f is a function in the class given in Theorem 2 of [5].

2) If $f \in CSD(1.3)$ for $n = 3$, then $f(x) = r_1 x$.

Corollary 1.23 (Corollary 4.2 [4]) Cases $(iv)\ 0 < r_2 < 1 < -r_1 < r_3$ and $(vi)\ 0 < r_2 < 1 < r_3 < -r_1$ in Table 1.

If $f \in CS(1.3)$ for $n = 3$, then f^{-1} is a function in the class given in Theorem 22.

Theorem 1.24 (Theorem 4.3 [4]) Cases $(a)\ 1 < -r_1 < -r_2 < r_3$, $(c)\ 1 < -r_1 < r_3 < -r_2$, $(e)\ 1 < r_3 < -r_1 < -r_2$ and $(f)\ 0 < r_3 < 1 < -r_1 < -r_2$ in Table 2.

1) If $f \in CSI(1.3)$ for $n=3$, then $f(x)=r_3x$.

2) If $f \in CSD(1.3)$ for $n=3$, then f is a function in the class given in Theorem 3 of Nabeya [5].

Corollary 1.25 (Corollary 4.3 [4]) Cases $(\bar{a})\ 0<r_3<-r_1<-r_2<1$, $(\bar{c})\ 0<-r_1<r_3<-r_2<1$, $(\bar{e})\ 0<-r_1<-r_2<r_3<1$ and $(\bar{f})\ 0<-r_1<-r_2<1<r_3$ in Table 2.

If $f \in CS(1.3)$ for $n=3$, then f^{-1} is a function in the class given in Theorem 24.

Theorem 1.26 (Theorem 4.4 [4]) Cases $(b)\ 0<-r_1<1<-r_2<r_3$ and $(d)\ 0<-r_1<1<r_3<-r_2$ in Table 2.

1) If $f \in CSI(1.3)$ for $n=3$, then $f(x)=r_3x$.

2) If $f \in CSD(1.3)$ for $n=3$, then $f(x)=r_1x$ or $f(x)=r_2x$.

Corollary 1.27 (Corollary 4.4 [4]) Cases $(\bar{b})\ 0<r_3<-r_1<1<-r_2$ and $(\bar{d})\ 0<-r_1<r_3<1<-r_2$ in Table 2.

If $f \in CS(1.3)$ for $n=3$, then f^{-1} is a function in the class given in Theorem 26.

We single out from Lemma 1.13, two useful formulas for the iterates of an element in $CS(1.6)$.

Lemma 1.28 Suppose that (1.6) has four different characteristic roots $r_1, r_2, r_3, r_4 \in C$. If $f \in CS(1.6)$, then

$$f^m(x)=\sum_{j=1}^{4}\frac{r_j^m}{\prod_{i=1,i\neq j}^{4}(r_j-r_i)}[f^3(x)-(\sum_{k\neq j}^{4}r_k)f^2(x)+(\sum_{k>t,\neq j}^{4}r_kr_t)f(x)-\prod_{i\neq j}^{4}r_ix]$$

$$f^{-m}(x)=\sum_{j=1}^{4}\frac{r_j^{-m}}{\prod_{i=1,i\neq j}^{4}(\frac{1}{r_j}-\frac{1}{r_i})}[f^{-3}(x)-(\sum_{k\neq j}^{4}\frac{1}{r_k})f^{-2}(x)+(\sum_{k>t,\neq j}^{4}\frac{1}{r_kr_t})f^{-1}(x)-\prod_{i\neq j}^{4}\frac{1}{r_i}x]$$

for any integer $m \geq 0$.

3. Results and Discussion

3.1 Results

Our results are derived in accordance with those listed in Cases A, B and C. Apart from adopting the approach Zhang and Gong [4], we introduce a novel technique of using a second limiting criterion for the cases starting from (A2),(A3) (i.e., from Theorem 2.23) onwards.

Theorem 2.1 Cases (A1):$1<-r_1<r_2<r_3<r_4$, (A4):$1<r_2<r_3<r_4<-r_1$ and $(\overline{\text{A10}})\ 0<-r_1<1<r_2<r_3<r_4$.

i) If $f \in CSI(1.6)$, then f is a function given in Theorem 1.1.

ii) If $f \in CSD(1.6)$, then $f(x) = r_1 x$, the form given by Theorem 1.20.

Proof. We know that if $f \in CSI(1.6)$, then $f^{-1} \in CSI(1.7)$. If $f \in CSD(1.6)$, then $f^{-1} \in CSD(1.7)$.

Case $(A1): 1 < -r_1 < r_2 < r_3 < r_4$.

i) Let $f \in CSI(1.6)$. From Lemma 1.28, we have

$$\lim_{m\to\infty} \frac{f^{-m}(x)}{r_1^{-m}} = \frac{1}{(\frac{1}{r_1}-\frac{1}{r_2})(\frac{1}{r_1}-\frac{1}{r_3})(\frac{1}{r_1}-\frac{1}{r_4})}(f^{-3}(x) - (\frac{1}{r_2}+\frac{1}{r_3}+\frac{1}{r_4})f^{-2}(x) + (\frac{1}{r_2r_3}+\frac{1}{r_2r_4}+\frac{1}{r_3r_4})f^{-1}(x) - \frac{1}{r_2r_3r_4}x).$$

For a fixed $x \in R$, since $f^{-1}(x)$ is strictly increasing, the limiting function $\lim_{m\to\infty} \frac{f^{-m}(x)}{r_1^{-m}}$ is nondecreasing for even m and nonincreasing for odd m, which implies that it must be a constant, i.e.,

$$f^{-3}(x) - (\frac{1}{r_2}+\frac{1}{r_3}+\frac{1}{r_4})f^{-2}(x) + (\frac{1}{r_2r_3}+\frac{1}{r_2r_4}+\frac{1}{r_3r_4})f^{-1}(x) - \frac{1}{r_2r_3r_4}x = c_1 \in R, \forall x \in R. \quad (2.1)$$

Substituting (2.1) into (1.7), we get $c_1 = r_1^{-1}c_1$ implying that $c_1 = 0$, and so

$$f^{-3}(x) - (\frac{1}{r_2}+\frac{1}{r_3}+\frac{1}{r_4})f^{-2}(x) + (\frac{1}{r_2r_3}+\frac{1}{r_2r_4}+\frac{1}{r_3r_4})f^{-1}(x) - \frac{1}{r_2r_3r_4}x = 0,$$

equivalently,

$$f^3(x) - (r_2+r_3+r_4)f^2(x) + (r_2r_3+r_2r_4+r_3r_4)f(x) - r_2r_3r_4x = 0. \quad (2.2)$$

The equation (2.2) is of 3rd-order with three positive distinct characteristic roots > 1, and its solutions are as given in Theorem 1.1.

ii) Let $f \in CSD(1.6)$. From Lemma 1.28, we have

$$\lim_{m\to\infty} \frac{f^m}{r_4^m} = \frac{1}{(r_4-r_1)(r_4-r_2)(r_4-r_3)}(f^3(x) - (r_1+r_2+r_3)f^2(x) + (r_1r_2+r_1r_3+r_2r_3)f(x) - r_1r_2r_3x).$$

For a fixed $x \in R$, since $f(x)$ is strictly decreasing, the limiting function $\lim_{m\to\infty} \frac{f^m(x)}{r_4^m}$ is nondecreasing for even m and nonincreasing for odd m, which forces it to be a constant, i.e.,

$$f^3(x) - (r_1+r_2+r_3)f^2(x) + (r_1r_2+r_1r_3+r_2r_3)f(x) - r_1r_2r_3x = c_1 \in R, \forall x \in R. \quad (2.3)$$

Substituting (2.3) into (1.6), we get $c_1 = r_4c_1$ implying that $c_1 = 0$, and so

$$f^3(x) - (r_1+r_2+r_3)f^2(x) + (r_1r_2+r_1r_3+r_2r_3)f(x) - r_1r_2r_3x = 0.$$

Since the three distinct characteristic roots satisfy $1 < -r_1 < r_2 < r_3$, Theorem 1.20 gives $f(x) = r_1 x$.

Case $(A4): 1 < r_2 < r_3 < r_4 < -r_1$.

i) Assume that $f \in CSI(1.6)$. By the same proof as that of the case (A1), we obtain

$$f^3(x)-(r_2+r_3+r_4)f^2(x)+(r_2r_3+r_2r_4+r_3r_4)f(x)-r_2r_3r_4x=0.$$

Since $1<r_2<r_3<r_4$, the solution function is given by Theorem 1.1.

ii) Assume that $f\in CSD(1.6)$. By the same proof as that of the case (A1), we obtain

$$f^{-3}(x)-(\frac{1}{r_1}+\frac{1}{r_3}+\frac{1}{r_4})f^{-2}(x)+(\frac{1}{r_1r_3}+\frac{1}{r_1r_4}+\frac{1}{r_3r_4})f^{-1}(x)-\frac{1}{r_1r_3r_4}x=0,$$

equivalently,

$$f^3(x)-(r_1+r_3+r_4)f^2(x)+(r_1r_3+r_1r_4+r_3r_4)f(x)-r_1r_3r_4x=0.$$

Since $1<r_3<r_4<-r_1$, Theorem 1.20 yields $f(x)=r_1x$.

Case $(\overline{\text{A10}}):0<-r_1<1<r_2<r_3<r_4$.

The proof for this case is the same as that of the case (A1) and is omitted.

Corollary 2.2 Cases $(\overline{\text{A1}}):0<r_2<r_3<r_4<-r_1<1$, $(\overline{\text{A4}}):0<-r_1<r_2<r_3<r_4<1$ and $(\text{A10}):0<r_2<r_3<r_4<1<-r_1$.

Proof. For the case $(\overline{\text{A1}})$ since $0<r_2<r_3<r_4<-r_1<1$, we get $\frac{1}{r_2}>\frac{1}{r_3}>\frac{1}{r_4}>-\frac{1}{r_1}>1$.

The reciprocals are characteristic roots of (1.7), which is the dual equation of (1.6). Thus, its solution f^{-1} is a function given in Theorem 2.1 depending on its behavior (increasing or decreasing).

The cases $(\overline{\text{A4}}):0<-r_1<r_2<r_3<r_4<1$ and $(\text{A10}):0<r_2<r_3<r_4<1<-r_1$ are reasoned similarly.

The solution functions in the forthcoming corollaries are derived via the same arguments as in Corollary 2.2.

Theorem 2.3 Case $(\text{A7}):0<r_2<1<r_3<r_4<-r_1$.

i) If $f\in CSI(1.6)$, then f is as given in Theorem 1.16.

ii) If $f\in CSD(1.6)$, then $f(x)=r_1x$, the form given by Theorem 1.20.

Proof. i) Assume that $f\in CSI(1.6)$. By the same proof as that of the case (A1), we obtain

$$f^3(x)-(r_2+r_3+r_4)f^2(x)+(r_2r_3+r_2r_4+r_3r_4)f(x)-r_2r_3r_4x=0.$$

Since $0<r_2<1<r_3<r_4$, the solution function f is as given in Theorem 1.16.

ii) Assume that $f\in CSD(1.6)$. By the same proof as that of the case (A1), we obtain

$$f^3(x)-(r_1+r_3+r_4)f^2(x)+(r_1r_3+r_1r_4+r_3r_4)f(x)-r_1r_3r_4x=0.$$

Since $1<r_3<r_4<-r_1$, again Theorem 1.20 yields $f(x)=r_1x$.

Corollary 2.4 Case $(\overline{\text{A7}}):0<-r_1<r_2<r_3<1<r_4$.

If $f\in CS(1.6)$, then f^{-1} is a function given in Theorem 2.3.

Theorem 2.5 Case $(\overline{\text{A9}}):0<-r_1<r_2<1<r_3<r_4$.

i) If $f\in CSI(1.6)$, then f is a function given in Theorem 1.16.

ii) If $f \in CSD(1.6)$, then $f(x) = r_1 x$, the form given by Theorem 1.22.

Proof. i) Assume that $f \in CSI(1.6)$. By the same proof as the case (A1) by Lemma 1.28 (form of f^{-m}) and removing $\frac{1}{r_1}$ we obtain

$$f^3(x) - (r_2 + r_3 + r_4) f^2(x) + (r_2 r_3 + r_2 r_4 + r_3 r_4) f(x) - r_2 r_3 r_4 x = 0.$$

Since $0 < r_2 < 1 < r_3 < r_4$, then f is a function in the class given in Theorem 1.16.

ii) Assume that $f \in CSD(1.6)$. By the same proof as that of the case (A1), we obtain

$$f^3(x) - (r_1 + r_2 + r_3) f^2(x) + (r_1 r_2 + r_1 r_3 + r_2 r_3) f(x) - r_1 r_2 r_3 x = 0.$$

Since $0 < -r_1 < r_2 < 1 < r_3$, Theorem 1.22 yields $f(x) = r_1 x$.

Corollary 2.6 Case $(A9): 0 < r_2 < r_3 < 1 < r_4 < -r_1$.

If $f \in CS(1.6)$, then f^{-1} is a function given in Theorem 2.5.

Theorem 2.7 Cases $(B1): 1 < r_1 < -r_2 < -r_3 < -r_4$, $(B4): 1 < -r_2 < -r_3 < -r_4 < r_1$ and $(\overline{B10}): 0 < r_1 < 1 < -r_2 < -r_3 < -r_4$.

i) If $f \in CSI(1.6)$, then $f(x) = r_1 x$, the form given by Theorem 1.24.

ii) If $f \in CSD(1.6)$, then f is given by Theorem 1.4.

Proof. Case $(B1): 1 < r_1 < -r_2 < -r_3 < -r_4$.

i) By the same proof as in the case (A1), we obtain

$$f^3(x) - (r_1 + r_2 + r_3) f^2(x) + (r_1 r_2 + r_1 r_3 + r_2 r_3) f(x) - r_1 r_2 r_3 x = 0.$$

Since $1 < r_1 < -r_2 < -r_3$, Theorem 1.24 gives $f(x) = r_1 x$.

ii) By the same proof as in the case (A1), we obtain

$$f^3(x) - (r_2 + r_3 + r_4) f^2(x) + (r_2 r_3 + r_2 r_4 + r_3 r_4) f(x) - r_2 r_3 r_4 x = 0.$$

Since $1 < -r_2 < -r_3 < -r_4$, the solution function f is given by Theorem 1.4.

Case $(B4): 1 < -r_2 < -r_3 < -r_4 < r_1$.

i) By the same proof as in the case (A1), we obtain

$$f^3(x) - (r_1 + r_3 + r_4) f^2(x) + (r_1 r_3 + r_1 r_4 + r_3 r_4) f(x) - r_1 r_3 r_4 x = 0.$$

Since $1 < -r_3 < -r_4 < r_1$, Theorem 1.24 gives $f(x) = r_1 x$.

ii) By the same proof as in the case (A1), we obtain

$$f^3(x) - (r_2 + r_3 + r_4) f^2(x) + (r_2 r_3 + r_2 r_4 + r_3 r_4) f(x) - r_2 r_3 r_4 x = 0.$$

Since $1 < -r_2 < -r_3 < -r_4$, the solution function is given by Theorem 1.4.

Case $(\overline{B10}): 0 < r_1 < 1 < -r_2 < -r_3 < -r_4$.

i) By the same proof as in the case (A1), we obtain

$$f^3(x) - (r_1 + r_2 + r_3) f^2(x) + (r_1 r_2 + r_1 r_3 + r_2 r_3) f(x) - r_1 r_2 r_3 x = 0.$$

Since $0 < r_1 < 1 < -r_2 < -r_3$, Theorem 1.24 then yields $f(x) = r_1 x$.

ii) By the same proof as in the case (A1), we obtain

$$f^3(x) - (r_2 + r_3 + r_4) f^2(x) + (r_2 r_3 + r_2 r_4 + r_3 r_4) f(x) - r_2 r_3 r_4 x = 0.$$

Since $1 < -r_2 < -r_3 < -r_4$, the solution f is given by Theorem 1.4.

Corollary 2.8 Cases $(\overline{\text{B1}}): 0 < -r_2 < -r_3 < -r_4 < r_1 < 1$, $(\overline{\text{B4}}): 0 < r_1 < -r_2 < -r_3 < -r_4 < 1$ and $(\text{B10}): 0 < -r_2 < -r_3 < -r_4 < 1 < r_1$.

If $f \in CS(1.6)$, then f^{-1} is given by Theorem 2.7.

Theorem 2.9 Case $(\text{B7}): 0 < -r_2 < 1 < -r_3 < -r_4 < r_1$.

i) If $f \in CSI(1.6)$, then $f(x) = r_1 x$, the form given by Theorem 1.24.

ii) If $f \in CSD(1.6)$, then the solution function f is as given in Theorem 1.18.

Proof. i) By the same proof as in the case (A1), we obtain

$$f^3(x) - (r_1 + r_3 + r_4) f^2(x) + (r_1 r_3 + r_1 r_4 + r_3 r_4) f(x) - r_1 r_3 r_4 x = 0.$$

Since $1 < -r_3 < -r_4 < r_1$, Theorem 1.24 then gives $f(x) = r_1 x$.

ii) By the same proof as in the case (A1), we obtain

$$f^3(x) - (r_2 + r_3 + r_4) f^2(x) + (r_2 r_3 + r_2 r_4 + r_3 r_4) f(x) - r_2 r_3 r_4 x = 0.$$

Since $0 < -r_2 < 1 < -r_3 < -r_4$, the solution f is given by Theorem 1.18.

Corollary 2.10 Case $(\overline{\text{B7}}): 0 < r_1 < -r_2 < -r_3 < 1 < -r_4$.

If $f \in CS(1.6)$, then f^{-1} is given by Theorem 2.9.

Theorem 2.11 Case $(\overline{\text{B9}}): 0 < r_1 < -r_2 < 1 < -r_3 < -r_4$.

i) If $f \in CSI(1.6)$, then $f(x) = r_1 x$, the form given in Corollary 1.27.

ii) If $f \in CSD(1.6)$, then f is given by Theorem 1.18.

Proof. i) By the same proof as in the case (A1), we obtain

$$f^3(x) - (r_1 + r_2 + r_3) f^2(x) + (r_1 r_2 + r_1 r_3 + r_2 r_3) f(x) - r_1 r_2 r_3 x = 0.$$

Since $0 < r_1 < -r_2 < 1 < -r_3$, Theorem 1.27 yields $f(x) = r_1 x$.

ii) By the same proof as in the case (A1), we obtain

$$f^3(x) - (r_2 + r_3 + r_4) f^2(x) + (r_2 r_3 + r_2 r_4 + r_3 r_4) f(x) - r_2 r_3 r_4 x = 0.$$

Since $-r_2 < 1 < -r_3 < -r_4$, the solution function f is given by Theorem 1.18.

Corollary 2.12 Case $(\text{B9}): 0 < -r_2 < -r_3 < 1 < -r_4 < r_1$.

If $f \in CS(1.6)$, then f^{-1} is given by Theorem 2.11.

Theorem 2.13 Cases $(C1): 1 < -r_1 < -r_4 < r_2 < r_3$, $(C2): 1 < -r_1 < r_2 < -r_4 < r_3$, $(C5)\ 1 < r_2 < -r_1 < r_3 < -r_4$, and $(C6): 1 < r_2 < r_3 < -r_1 < -r_4$.

i) If $f \in CSI(1.6)$, then f is given by Theorem 1.20.

ii) If $f \in CSD(1.6)$, then f is given by Theorem 1.24.

Proof. Case $(C1): 1 < -r_1 < -r_4 < r_2 < r_3$.

i) By the same proof as in the case (A1), we obtain

$$f^3(x) - (r_2 + r_3 + r_4) f^2(x) + (r_2 r_3 + r_2 r_4 + r_3 r_4) f(x) - r_2 r_3 r_4 x = 0.$$

Since $1 < -r_4 < r_2 < r_3$, the solution f is given by Theorem 1.20.

ii) By the same proof as in the case (A1), we obtain

$$f^3(x)-(r_1+r_2+r_4)f^2(x)+(r_1r_2+r_1r_4+r_3r_4)f(x)-r_1r_2r_4x=0\ .$$

Since $1<-r_1<-r_4<r_2$, the solution f is given by Theorem 1.24.

Case $(C2):1<-r_1<r_2<-r_4<r_3$.

i) By the same proof as in the case (A1), we obtain

$$f^3(x)-(r_2+r_3+r_4)f^2(x)+(r_2r_3+r_2r_4+r_3r_4)f(x)-r_2r_3r_4x=0.$$

Since $1<r_2<-r_4<r_3$, the solution f is given by Theorem 1.20.

ii) By the same proof as in the case (A1), we obtain

$$f^3(x)-(r_1+r_2+r_4)f^2(x)+(r_1r_2+r_1r_4+r_2r_4)f(x)-r_1r_2r_4x=0\ .$$

Since $1<-r_1<r_2<-r_4$, the solution f is given by Theorem 1.24.

Case $(C5):1<r_2<-r_1<r_3<-r_4$.

i) By the same proof as in the case (A1), we obtain

$$f^3(x)-(r_1+r_2+r_3)f^2(x)+(r_1r_2+r_1r_3+r_2r_3)f(x)-r_1r_2r_3x=0.$$

Since $1<r_2<-r_1<r_3$, the solution f is given by Theorem 1.20.

ii) By the same proof as in the case (A1), we obtain

$$f^3(x)-(r_1+r_3+r_4)f^2(x)+(r_1r_3+r_1r_4+r_3r_4)f(x)-r_1r_3r_4x=0\ .$$

Since $1<-r_1<r_3<-r_4$, the solution f is given by Theorem 1.24.

Case $(C6):1<r_2<r_3<-r_1<-r_4$.

i) By the same proof as in the case (A1), we obtain

$$f^3(x)-(r_1+r_2+r_3)f^2(x)+(r_1r_2+r_1r_3+r_2r_3)f(x)-r_1r_2r_3x=0.$$

Since $1<r_2<r_3<-r_1$, the solution f is given by Theorem 1.20.

ii) By the same proof as in the case (A1), we obtain

$$f^3(x)-(r_1+r_3+r_4)f^2(x)+(r_1r_3+r_1r_4+r_3r_4)f(x)-r_1r_3r_4x=0\ .$$

Since $1<r_3<-r_1<-r_4$, the solution f is given by Theorem 1.24**.**

Corollary 2.14 Cases $(\overline{C1}):0<r_2<r_3<-r_1<-r_4<1$, $(\overline{C2}):0<r_2<-r_1<r_3<-r_4<1$, $(\overline{C5}):0<-r_1<r_2<-r_4<r_3<1$ and $(\overline{C6}):0<-r_1<-r_4<r_2<r_3<1$.

If $f\in CS(1.6)$, then f^{-1} is given by Theorem 2.13.

Theorem 2.15 Cases $(C8):0<r_2<1<-r_1<r_3<-r_4$ and $(C9):0<r_2<1<r_3<-r_1<-r_4$.

i) If $f\in CSI(1.6)$, then f is given by Corollary 1.23.

ii) If $f\in CSD(1.6)$, then f is given by Theorem 1.24.

Proof. Case $(C8):0<r_2<1<-r_1<r_3<-r_4$.

i) By the same proof as in the case (A1), we obtain

$$f^3(x)-(r_1+r_2+r_3)f^2(x)+(r_1r_2+r_1r_3+r_2r_3)f(x)-r_1r_2r_3x=0.$$

Since $0<r_2<1<-r_1<r_3$, the solution f is given by Corollary 1.23.

ii) By the same proof as in the case (A1), we obtain

$$f^3(x)-(r_1+r_3+r_4)f^2(x)+(r_1r_3+r_1r_4+r_3r_4)f(x)-r_1r_3r_4x=0\ .$$

Since $1 < -r_1 < r_3 < -r_4$, the solution f is given by Theorem 1.24.

Case $(C9): 0 < r_2 < 1 < r_3 < -r_1 < -r_4$.

i) By the same proof as in the case (A1), we obtain

$$f^3(x) - (r_1 + r_2 + r_3) f^2(x) + (r_1 r_2 + r_1 r_3 + r_2 r_3) f(x) - r_1 r_2 r_3 x = 0.$$

Since $0 < r_2 < 1 < r_3 < -r_1$, the solution f is given by Corollary 1.23.

ii) By the same proof as in the case (A1), we obtain

$$f^3(x) - (r_1 + r_3 + r_4) f^2(x) + (r_1 r_3 + r_1 r_4 + r_3 r_4) f(x) - r_1 r_3 r_4 x = 0.$$

Since $1 < r_3 < -r_1 < -r_4$, the solution f is given by Theorem 1.24.

Corollary 2.16 Cases $(\overline{C8}): 0 < -r_1 < r_2 < -r_4 < 1 < r_3$ and $(\overline{C9}): 0 < -r_1 < -r_4 < r_2 < 1 < r_3$.

If $f \in CS(1.6)$, then f^{-1} is given by Theorem 2.15.

Theorem 2.17 Case $(C10): 0 < -r_1 < -r_4 < 1 < r_2 < r_3$.

i) If $f \in CSI(1.6)$, then f is given by Theorem 1.20.

ii) If $f \in CSD(1.6)$, then f is given by Corollary 1.25.

Proof. i) By the same proof as in the case (A1), we obtain

$$f^3(x) - (r_2 + r_3 + r_4) f^2(x) + (r_2 r_3 + r_2 r_4 + r_3 r_4) f(x) - r_2 r_3 r_4 x = 0.$$

Since $0 < -r_4 < 1 < r_2 < r_3$, the solution f is given by Theorem 1.20.

ii) By the same proof as in the case (A1), we obtain

$$f^3(x) - (r_1 + r_2 + r_4) f^2(x) + (r_1 r_2 + r_1 r_4 + r_2 r_4) f(x) - r_1 r_2 r_4 x = 0.$$

Since $0 < -r_1 < -r_4 < 1 < r_2$, the solution f is given by Corollary 1.25.

Corollary 2.18 Case $(\overline{C10}): 0 < r_2 < r_3 < 1 < -r_1 < -r_4$.

If $f \in CS(1.6)$, then f^{-1} is given by Theorem 2.17.

Theorem 2.19 Cases $(C11): 0 < -r_1 < 1 < -r_4 < r_2 < r_3$ and $(C12): 0 < -r_1 < 1 < r_2 < -r_4 < r_3$.

i) If $f \in CSI(1.6)$, then f is given by Theorem 1.20.

ii) If $f \in CSD(1.6)$, then f is given by Theorem 1.26.

Proof. Case $(C11): 0 < -r_1 < 1 < -r_4 < r_2 < r_3$.

i) By the same proof as in the case (A1), we obtain

$$f^3(x) - (r_2 + r_3 + r_4) f^2(x) + (r_2 r_3 + r_2 r_4 + r_3 r_4) f(x) - r_2 r_3 r_4 x = 0.$$

Since $1 < -r_4 < r_2 < r_3$, the solution f is given by Theorem 1.20.

ii) By the same proof as in the case (A1), we obtain

$$f^3(x) - (r_1 + r_2 + r_4) f^2(x) + (r_1 r_2 + r_1 r_4 + r_2 r_4) f(x) - r_1 r_2 r_4 x = 0.$$

Since $0 < -r_1 < 1 < -r_4 < r_2$, the solution f is given by Theorem 1.26.

Case $(C12): 0 < -r_1 < 1 < r_2 < -r_4 < r_3$.

i) By the same proof as in the case (A1), we obtain

$$f^3(x) - (r_2 + r_3 + r_4) f^2(x) + (r_2 r_3 + r_2 r_4 + r_3 r_4) f(x) - r_2 r_3 r_4 x = 0.$$

Since $1 < r_2 < -r_4 < r_3$, the solution f is given by Theorem 1.20.

ii) By the same proof as in the case (A1), we obtain

$$f^3(x)-(r_1+r_2+r_4)f^2(x)+(r_1r_2+r_1r_4+r_2r_4)f(x)-r_1r_2r_4x=0\,.$$

Since $0<-r_1<1<r_2<-r_4$, the solution f is given by Theorem 1.26.

Corollary 2.20 Cases $(\overline{C11}):0<r_2<r_3<-r_1<1<-r_4$ and $(\overline{C12}):0<r_2<-r_1<r_3<1<-r_4$.
If $f\in CS(1.6)$, then f^{-1} is given by Theorem 2.19.

Theorem 2.21 Case $(C14):0<-r_1<r_2<1<-r_4<r_3$.
i) If $f\in CSI(1.6)$, then f is given by Corollary 1.23.
ii) If $f\in CSD(1.6)$, then f is given by Corollary 1.27.
Proof. i) By the same proof as in the case (A1), we obtain

$$f^3(x)-(r_2+r_3+r_4)f^2(x)+(r_2r_3+r_2r_4+r_3r_4)f(x)-r_2r_3r_4x=0.$$

Since $0<r_2<1<-r_4<r_3$, the solution f is given by Corollary 1.23.

ii) By the same proof as in the case (A1), we obtain

$$f^3(x)-(r_1+r_2+r_4)f^2(x)+(r_1r_2+r_1r_4+r_2r_4)f(x)-r_1r_2r_4x=0\,.$$

Since $0<-r_1<r_2<1<-r_4$, the solution f is given by Corollary 1.27.

Corollary 2.22 Case $(\overline{C14}):0<r_2<-r_1<1<r_3<-r_4$.
If $f\in CS(1.6)$, then f^{-1} is given by Theorem 2.21.

Theorem 2.23 Cases $(A2):1<r_2<-r_1<r_3<r_4$ and $(A3):1<r_2<r_3<-r_1<r_4$.

i) Assume that $f\in CSI(1.6)$. In the case (A2), further assume that $\lim_{m\to\infty}\frac{f^{-m}}{r_1^{-m}}$ exists.

While in the case (A3) further assume that $\lim_{m\to\infty}\frac{f^{m}}{r_1^{m}}$ exists, then the solution function f is as given in Theorem 1.6.

ii) If $f\in CSD(1.6)$, then $f(x)=r_1x$, the form given by Theorem 1.20.

Proof. Case $(A2):1<r_2<-r_1<r_3<r_4$.

Let $\lim_{m\to\infty}\frac{f^{-m}}{r_1^{-m}}=c$. From Lemma 1.28, we get

$$c=\lim_{m\to\infty}\frac{f^{-m}}{r_1^{-m}}=\frac{1}{(\frac{1}{r_1}-\frac{1}{r_2})(\frac{1}{r_1}-\frac{1}{r_3})(\frac{1}{r_1}-\frac{1}{r_4})}(f^{-3}(x)-(\frac{1}{r_2}+\frac{1}{r_3}+\frac{1}{r_4})f^{-2}(x)+(\frac{1}{r_2r_3}+\frac{1}{r_2r_4}+\frac{1}{r_3r_4})f^{-1}(x)-\frac{1}{r_2r_3r_4}x)$$

$$+\lim_{m\to\infty}\frac{(\frac{r_1}{r_2})^m}{(\frac{1}{r_2}-\frac{1}{r_1})(\frac{1}{r_2}-\frac{1}{r_3})(\frac{1}{r_2}-\frac{1}{r_4})}(f^{-3}(x)-(\frac{1}{r_1}+\frac{1}{r_3}+\frac{1}{r_4})f^{-2}(x)+(\frac{1}{r_1r_3}+\frac{1}{r_1r_4}+\frac{1}{r_3r_4})f^{-1}(x)-\frac{1}{r_1r_3r_4}x)$$

showing that

$$\lim_{m\to\infty}\frac{(\frac{r_1}{r_2})^m}{(\frac{1}{r_2}-\frac{1}{r_1})(\frac{1}{r_2}-\frac{1}{r_3})(\frac{1}{r_2}-\frac{1}{r_4})}(f^{-3}(x)-(\frac{1}{r_1}+\frac{1}{r_3}+\frac{1}{r_4})f^{-2}(x)+(\frac{1}{r_1r_3}+\frac{1}{r_1r_4}+\frac{1}{r_3r_4})f^{-1}(x)-\frac{1}{r_1r_3r_4}x)=0.$$

Thus

$$f^{-3}(x)-(\frac{1}{r_1}+\frac{1}{r_3}+\frac{1}{r_4})f^{-2}(x)+(\frac{1}{r_1r_3}+\frac{1}{r_1r_4}+\frac{1}{r_3r_4})f^{-1}(x)-\frac{1}{r_1r_3r_4}x=0,$$

or equivalently,

$$f^3(x)-(r_1+r_3+r_4)f^2(x)+(r_1r_3+r_1r_4+r_3r_4)f(x)-r_1r_3r_4x=0\,. \tag{2.4}$$

Returning to the limiting equation, we deduce that:

$$f^{-3}(x)-(\frac{1}{r_2}+\frac{1}{r_3}+\frac{1}{r_4})f^{-2}(x)+(\frac{1}{r_2r_3}+\frac{1}{r_2r_4}+\frac{1}{r_3r_4})f^{-1}(x)-\frac{1}{r_2r_3r_4}x=c_1 \tag{2.5}$$

for some constant c_1. Substituting (2.5) in (1.7), we get $c_1=r_1^{-1}c_1$ yielding $c_1=0$.
Hence,

$$f^{-3}(x)-(\frac{1}{r_2}+\frac{1}{r_3}+\frac{1}{r_4})f^{-2}(x)+(\frac{1}{r_2r_3}+\frac{1}{r_2r_4}+\frac{1}{r_3r_4})f^{-1}(x)-\frac{1}{r_2r_3r_4}x=0,$$

equivalently,

$$f^3(x)-(r_2+r_3+r_4)f^2(x)+(r_2r_3+r_2r_4+r_3r_4)f(x)-r_2r_3r_4x=0. \tag{2.6}$$

Subtracting (2.4) from (2.6), we get

$$f^2(x)-(r_3+r_4)f(x)+r_3r_4x=0.$$

Since $1<r_3<r_4$, the solution function f is given in Theorem 1.6.

i) By the same proof as that of the case (A1), we obtain

$$f^3(x)-(r_1+r_2+r_3)f^2(x)+(r_1r_2+r_1r_3+r_2r_3)f(x)-r_1r_2r_3x=0.$$

Since $1<r_2<-r_1<r_3$, the solution function is $f(x)=r_1x$, the form given by Theorem 1.20.

Case $(\mathrm{A3}):1<r_2<r_3<-r_1<r_4.$

i) By the same proof as that of the case (A2), we obtain

$$f^2(x)-(r_2+r_3)f(x)+r_2r_3x=0.$$

Since $1<r_2<r_3$, the solution function f is as given in Theorem 1.6.

ii) By the same proof as that of the case (A1), we obtain

$$f^3(x)-(r_1+r_2+r_3)f^2(x)+(r_1r_2+r_1r_3+r_2r_3)f(x)-r_1r_2r_3x=0.$$

Since $1<r_2<r_3<-r_1$, the solution function is $f(x)=r_1x$, the form given by Theorem 1.20.

Corollary 2.24. Cases $(\overline{\mathrm{A2}}):0<r_2<r_3<-r_1<r_4<1$ and $(\overline{\mathrm{A3}}):0<r_2<-r_1<r_3<r_4<1$.
Under the hypotheses of Theorem 2.23, if $f\in CS(1.6)$, then f^{-1} is given in Theorem 2.23.

Theorem 2.25. Cases $(\text{A5}): 0 < r_2 < 1 < -r_1 < r_3 < r_4$ and $(\text{A6}): 0 < r_2 < 1 < r_3 < -r_1 < r_4$.

i) Assume that $f \in CSI(1.6)$. In the case (A5), further assume that $\lim_{m\to\infty} \frac{f^{-m}}{r_1^{-m}}$ exists, while in the case (A6) further assume that $\lim_{m\to\infty} \frac{f^{m}}{r_1^{m}}$ exists. Then the solution function f is as given in Theorems 1.6 and 1.8., respectively.

ii) If $f \in CSD(1.6)$, then $f(x) = r_1 x$, the form given by Corollary 1.23.

Proof. Case $(\text{A5}): 0 < r_2 < 1 < -r_1 < r_3 < r_4$.

i) By the same proof as that of the case (A2), we get

$$f^2(x) - (r_3 + r_4) f(x) + r_3 r_4 x = 0.$$

Since $1 < r_3 < r_4$, the solution function f is as given in Theorem 1.6.

ii) By the same proof as that of the case (A1), we obtain

$$f^3(x) - (r_1 + r_2 + r_3) f^2(x) + (r_1 r_2 + r_1 r_3 + r_2 r_3) f(x) - r_1 r_2 r_3 x = 0.$$

Since $0 < r_2 < 1 < -r_1 < r_3$, by Corollary 1.23 $f(x) = r_1 x$.

Case $(\text{A6}): 0 < r_2 < 1 < r_3 < -r_1 < r_4$.

i) By the same proof as that of the case (A2), we obtain

$$f^2(x) - (r_2 + r_3) f(x) + r_2 r_3 x = 0.$$

Since $0 < r_2 < 1 < r_3$, thesolution function f is as given in Theorem 1.8.

ii) By the same proof as that of the case (A1), we obtain

$$f^3(x) - (r_1 + r_2 + r_3) f^2(x) + (r_1 r_2 + r_1 r_3 + r_2 r_3) f(x) - r_1 r_2 r_3 x = 0.$$

Since $0 < r_2 < 1 < r_3 < -r_1$, by Corollary 1.23 $f(x) = r_1 x$.

Corollary 2.26. Cases $(\overline{\text{A5}}): 0 < r_2 < r_3 < -r_1 < 1 < r_4$ and $(\overline{\text{A6}}): 0 < r_2 < -r_1 < r_3 < 1 < r_4$.

Under the hypotheses of Theorem 2.25, if $f \in CS(1.6)$, then f^{-1} is as given in Theorem 2.25.

Theorem 2.27. Case $(\overline{\text{A8}}): 0 < r_2 < -r_1 < 1 < r_3 < r_4$.

i) If $f \in CSI(1.6)$ and it $\lim_{m\to\infty} \frac{f^{-m}}{r_1^{-m}}$ exists, then f is as given in Theorem 1.6.

ii) If $f \in CSD(1.6)$, then $f(x) = r_1 x$, the form given by Theorem 1.22.

Proof. i) By the same proof as that of the case (A2), we obtain

$$f^2(x) - (r_3 + r_4) f(x) + r_3 r_4 x = 0.$$

Since $1 < r_3 < r_4$, the solution function f is given by Theorem 1.6.

ii) By the same proof as that of the case (A1), we obtain

$$f^3(x) - (r_1 + r_2 + r_3) f^2(x) + (r_1 r_2 + r_1 r_3 + r_2 r_3) f(x) - r_1 r_2 r_3 x = 0.$$

Since $0 < r_2 < -r_1 < 1 < r_3$, Theorem 1.22 gives $f(x) = r_1 x$.

Corollary 2.28. Case $(\text{A8}): 0 < r_2 < r_3 < 1 < -r_1 < r_4$.

Under the hypotheses of Theorem 2.27, if $f \in CS(1.6)$, then f^{-1} is as given by Theorem 2.27.

Theorem 2.29 Cases (B2):$1<-r_2<r_1<-r_3<-r_4$ and (B3):$1<-r_2<-r_3<r_1<-r_4$.
i) If $f\in CSI(1.6)$, then $f(x)=r_1x$, the form given by Theorem 1.24.

ii) Assume that $f\in CSD(1.6)$. In the case (B2), assume further that $\lim_{m\to\infty}\frac{f^{-m}}{r_1^{-m}}$ exists, while in the case (B3), assume further that $\lim_{m\to\infty}\frac{f^{m}}{r_1^{m}}$ exist. Then f is given by Theorem 1.9.

Proof. Case (B2):$1<-r_2<r_1<-r_3<-r_4$.

i) By the same proof as in the case (A1), we obtain

$$f^3(x)-(r_1+r_2+r_3)f^2(x)+(r_1r_2+r_1r_3+r_2r_3)f(x)-r_1r_2r_3x=0.$$

Since $1<-r_2<r_1<-r_3$, Theorem 1.24 gives $f(x)=r_1x$.

ii) By the same proof as in the case (A2), we obtain

$$f^2(x)-(r_3+r_4)f(x)+r_3r_4x=0.$$

Since $1<-r_3<-r_4$, the solution f is given by Theorem 1.9.

Case (B3):$1<-r_2<-r_3<r_1<-r_4$.

i) By the same proof as in the case (A1), we obtain

$$f^3(x)-(r_1+r_2+r_3)f^2(x)+(r_1r_2+r_1r_3+r_2r_3)f(x)-r_1r_2r_3x=0.$$

Since $1<-r_2<-r_3<r_1$, Theorem 1.24 gives $f(x)=r_1x$.

ii) By the same proof as in the case (A2), we obtain

$$f^2(x)-(r_2+r_3)f(x)+r_2r_3x=0\ .$$

Since $1<-r_2<-r_3$, the solution f is given by Theorem 1.9.

Corollary 2.30 Case $(\overline{\text{B2}})$:$0<-r_2<-r_3<r_1<-r_4<1$ and $(\overline{\text{B3}})$:$0<-r_2<r_1<-r_3<-r_4<1$.
Under the hypotheses of Theorem 2.29, if $f\in CS(1.6)$, then f^{-1} is given by Theorem 2.29.

Theorem 2.31. Cases (B5):$0<-r_2<1<r_1<-r_3<-r_4$ and (B6):$0<-r_2<1<-r_3<r_1<-r_4$.
i) If $f\in CSI(1.6)$, then $f(x)=r_1x$, the form given by Theorem 1.26.

ii) Assume that $f\in CSD(1.6)$. In the case (B5), assume further that $\lim_{m\to\infty}\frac{f^{-m}}{r_1^{-m}}$ exists, while in the case (B6), assume further that $\lim_{m\to\infty}\frac{f^{m}}{r_1^{m}}$ exists. Then the solution function f is given by Theorems 1.9 and 1.10, respectively.

Proof. Case (B5):$0<-r_2<1<r_1<-r_3<-r_4$.

i) By The same proof as in the case (A2), we obtain

$$f^3(x)-(r_1+r_2+r_3)f^2(x)+(r_1r_2+r_1r_3+r_2r_3)f(x)-r_1r_2r_3x=0\ .$$

Since $0<-r_2<1<r_1<-r_3$, Theorem 1.26 yield $f(x)=r_1x$.

ii) By The same proof as in the case (A2), we obtain

$$f^2(x)-(r_3+r_4)f(x)+r_3r_4x=0\ .$$

Since $1<-r_3<-r_4$, the solution f is given by Theorem 1.9.

Case $(B6): 0 < -r_2 < 1 < -r_3 < r_1 < -r_4$.

i) By The same proof as in the case (A2), we obtain

$$f^3(x) - (r_1 + r_2 + r_3) f^2(x) + (r_1 r_2 + r_1 r_3 + r_2 r_3) f(x) - r_1 r_2 r_3 x = 0 .$$

Since $0 < -r_2 < 1 < -r_3 < r_1$, Theorem 1.26 yield $f(x) = r_1 x$.

ii) By The same proof as in the case (A2), we obtain

$$f^2(x) - (r_2 + r_3) f(x) + r_2 r_3 x = 0 .$$

Since $0 < -r_2 < 1 < -r_3$, the solution f is given by Theorem 1.10.

Corollary 2.32. Cases $(\overline{B5}): 0 < -r_2 < -r_3 < r_1 < 1 < -r_4$ and $(\overline{B6}): 0 < -r_2 < r_1 < -r_3 < 1 < -r_4$.
Under the hypotheses of Theorem 2.31, if $f \in CS(1.6)$, then f^{-1} is given by Theorem 2.31.

Theorem 2.33. Case $(\overline{B8}): 0 < -r_2 < r_1 < 1 < -r_3 < -r_4$.

i) If $f \in CSI(1.6)$, then $f(x) = r_1 x$, the form given by Corollary 1.27.

ii) If $f \in CSD(1.6)$ and if $\lim_{m\to\infty} \frac{f^{-m}}{r_1^{-m}}$ exist, then f is given by Theorem 1.9.

Proof. i) By The same proof as in the case (A2), we obtain

$$f^3(x) - (r_1 + r_2 + r_3) f^2(x) + (r_1 r_2 + r_1 r_3 + r_2 r_3) f(x) - r_1 r_2 r_3 x = 0.$$

Since $0 < -r_2 < r_1 < 1 < -r_3$, Corollary 1.27 gives $f(x) = r_1 x$.

ii) By The same proof as in the case (A2), we obtain

$$f^2(x) - (r_3 + r_4) f(x) + r_3 r_4 x = 0.$$

Since $1 < -r_3 < -r_4$, the solution f is given by Theorem 1.9.

Corollary 2.34. Case $(B8): 0 < -r_2 < -r_3 < 1 < r_1 < -r_4$.
Under the hypotheses of Theorem 2.33, if $f \in CS(1.6)$, then f^{-1} is given by Theorem 2.33.

Theorem 2.35. Case $(C3): 1 < -r_1 < r_2 < r_3 < -r_4$.

i) If $f \in CSI(1.6)$, then f is given by Theorem 1.20.

ii) If $f \in CSD(1.6)$ and if $\lim_{m\to\infty} \frac{f^m}{r_3^m}$ exists, then $f(x) = r_1 x$, the form given by Theorem 1.12.

Proof. i) By The same proof as in the case (A2), we obtain

$$f^3(x) - (r_1 + r_2 + r_3) f^2(x) + (r_1 r_2 + r_1 r_3 + r_2 r_3) f(x) - r_1 r_2 r_3 x = 0 .$$

Since $1 < -r_1 < r_2 < r_3$, the solution f is given by Theorem 1.20.

ii) By The same proof as in the case (A2), we obtain

$$f^2(x) - (r_1 + r_2) f(x) + r_1 r_2 x = 0 .$$

Since $1 < -r_1 < r_2$, Theorem 1.12 gives $f(x) = r_1 x$.

Corollary 2.36. Case $(\overline{C3}): 0 < -r_1 < r_2 < r_3 < -r_4 < 1$.
Under the hypotheses of Theorem 2.35, if $f \in CS(1.6)$, then f^{-1} is given by Theorem 2.35.

Theorem 2.37. Case $(C4): 1 < r_2 < -r_1 < -r_4 < r_3$.

i) If $f \in CSI(1.6)$ and if $\lim_{m\to\infty} \frac{f^m}{r_4^m}$ exists, then $f(x) = r_2 x$, the form given by Theorem 1.12.

ii) If $f \in CSD(1.6)$, then f is given by Theorem 1.24.

Proof. i) By The same proof as in the case (A2), we obtain

$$f^3(x) - (r_1 + r_2) f(x) + r_1 r_2 x = 0.$$

Since $1 < r_2 < -r_1$, Theorem 1.12 gives $f(x) = r_1 x$.

ii) By The same proof as in the case (A2), we obtain

$$f^3(x) - (r_1 + r_2 + r_4) f^2(x) + (r_1 r_2 + r_1 r_4 + r_2 r_4) f(x) - r_1 r_2 r_4 x = 0.$$

Since $1 < r_2 < -r_1 < -r_4$, the solution f is given by Theorem 1.24.

Corollary 2.38. Case $(\overline{C4}): 0 < r_2 < -r_1 < -r_4 < r_3 < 1$.

Under the hypotheses of Theorem 2.37, if $f \in CS(1.6)$, then f^{-1} is given by Theorem 2.37.

Theorem 2.39. Case $(C7): 0 < r_2 < 1 < -r_1 < -r_4 < r_3$.

i) If $f \in CSI(1.6)$ and if $\lim_{m\to\infty} \frac{f^m}{r_4^m}$ exists, then $f(x) = r_2 x$, the form given in Theorem 1.12.

ii) If $f \in CSD(1.6)$, then f is given by Theorem 1.24.

Proof. i) By The same proof as in the case (A2), we obtain

$$f^2(x) - (r_1 + r_2) f(x) + r_1 r_2 x = 0.$$

Since $0 < r_2 < 1 < -r_1$, Theorem 1.12 yields $f(x) = r_2 x$.

ii) By The same proof as in the case (A2), we obtain

$$f^3(x) - (r_1 + r_2 + r_4) f^2(x) + (r_1 r_2 + r_1 r_4 + r_2 r_4) f(x) - r_1 r_2 r_4 x = 0.$$

Since $0 < r_2 < 1 < -r_1 < -r_4$, the solution f is given by Theorem 1.24.

Corollary 2.40. Case $(\overline{C7}): 0 < r_2 < -r_1 < -r_4 < 1 < r_3$.

Under the hypotheses of Theorem 2.39, if $f \in CS(1.6)$, then f^{-1} is given by Theorem 2.39.

Theorem 2.41. Case $(C13): 0 < -r_1 < 1 < r_2 < r_3 < -r_4$.

i) If $f \in CSI(1.6)$, then f is given by Theorem 1.20.

ii) If $f \in CSD(1.6)$ and if $\lim_{m\to\infty} \frac{f^m}{r_3^m}$ exists, then $f(x) = r_1 x$, the form given by Theorem 1.12.

Proof. i) By The same proof as in the case (A2), we obtain

$$f^3(x) - (r_1 + r_2 + r_3) f^2(x) + (r_1 r_2 + r_1 r_3 + r_2 r_3) f(x) - r_1 r_2 r_3 x = 0.$$

Since $0 < -r_1 < 1 < r_2 < r_3$, the solution f is given by Theorem 1.20.

ii) By The same proof as in the case (A2), we obtain

$$f^2(x) - (r_1 + r_2) f(x) + r_1 r_2 x = 0.$$

Since $0 < -r_1 < 1 < r_2$, Theorem 1.12 gives $f(x) = r_1 x$.

Corollary 2.42. Case $(\overline{C13})$: $0 < -r_1 < r_2 < r_3 < 1 < -r_4$.
Under the hypotheses of Theorem 2.41, if $f \in CS(1.6)$, then f^{-1} is given by Theorem 2.41.

Theorem 2.43. Case $(C15): 0 < -r_1 < r_2 < 1 < r_3 < -r_4$.
i) If $f \in CSI(1.6)$, then f is given by Theorem 1.22.

ii) If $f \in CSD(1.6)$ and if $\lim_{m\to\infty} \frac{f^m}{r_3^m}$ exists, then , $f(x) = r_1 x$, the for given by Theorem 1.12.

Proof. i) By The same proof as in the case (A2), we obtain

$$f^3(x) - (r_1 + r_2 + r_3) f^2(x) + (r_1 r_2 + r_1 r_3 + r_2 r_3) f(x) - r_1 r_2 r_3 x = 0.$$

Since $0 < -r_1 < r_2 < 1 < r_3$, the solution f is given by Theorem 1.22.

ii) By the same proof as in the case (A2), we obtain

$$f^3(x) - (r_1 + r_2 + r_4) f^2(x) + (r_1 r_2 + r_1 r_4 + r_2 r_4) f(x) - r_1 r_2 r_4 x = 0.$$

Since $0 < -r_1 < r_2 < 1$, Theorem 1.12 gives $f(x) = r_1 x$.

Theorem 2.44. Case $(C16): 0 < r_2 < -r_1 < 1 < -r_4 < r_3$.

i) If $f \in CSI(1.6)$ and if $\lim_{m\to\infty} \frac{f^m}{r_4^m}$ exists, then , $f(x) = r_2 x$, the form given by Theorem 1.12.

ii) If $f \in CSD(1.6)$, then f is given by Corollary 1.27.

Proof. i) By The same proof as in the case (A2), we obtain

$$f^2(x) - (r_1 + r_2) f(x) + r_1 r_2 x = 0.$$

Since $0 < r_2 < -r_1 < 1$, Theorem 1.12 yields $f(x) = r_2 x$.

ii) By The same proof as in the case (A2), we obtain

$$f^3(x) - (r_1 + r_2 + r_4) f^2(x) + (r_1 r_2 + r_1 r_4 + r_2 r_4) f(x) - r_1 r_2 r_4 x = 0.$$

Since $0 < r_2 < -r_1 < 1 < -r_4$, the solution f is given by Corollary 1.27.

3.2 General discussion

Based mainly on the ideas from the work of Zhang and Gong [4], all solution functions $f \in CSI(1.6)$ have been determined subject to the restrictions that

- the characteristic roots r_1, r_2, r_3, r_4 satisfy $|r_i| \neq 0,1$ $(i = 1,2,3,4)$,
- the absolute values of the charcteristic roots $|r_i|$ $(i = 1,2,3,4)$ are all distinct and
- the four characteristic roots have different signs.

In particular, the following cases have been completely solved.
A. One negative characteristic root $r_1 < 0$, and three positive characteristic roots $0 < r_2 < r_3 < r_4$.
B. Three negative characteristic roots $0 > r_2 > r_3 > r_4$, and one positive characteristic root $r_1 > 0$.
C. Two negative characteristic roots $0 > r_1 > r_4$, and two positive characteristic roots $r_3 > r_2 > 0$.

In certain cases an extra condition, namely, $\lim_{m\to\infty} \frac{f^m}{r_i^m}$ for some $i = 1, 2, 3, 4$, is needed to obtain the solutions.

4. Conclusions

There are totally seventy subcases solved in this work, but there remain two cases that are yet to be resolved for which the methods and techniques used here do not seem to work. These subcases are when:

(i) all characteristic roots are positive, some being in $(0,1)$ and the others in $(1,\infty)$, and

(ii) all characteristic roots are negative, some being in $(-1,0)$ and the others in $(-\infty,-1)$.

References

[1] Matkowski, J. and Weinian, Z., 1997. Method of characteristic for functional equations in polynomial form. *Acta Mathematica Sinica*, 13(3), 421-432.

[2] Matkowski, J. and Zhang, W., 2000. On linear dependence of iterates. *Journal of Applied Analysis*, 6(1), 149-157.

[3] Yang, D. and Zhang, W., 2004. Characteristic solutions of polynomial-like iterative equations. *Aequationes Mathematicae*, 67, 80-105.

[4] Zhang, P. and Gong, X., 2014. Continuous solutions of 3rd-order iterative equation of linear dependence. *Advances in Difference Equations*, 2014, 318, https://doi.org/10.1186/1687-1847-2014-318

[5] Nabeya, S., 1974. On the functional equation $f(p+qx+rf(x)) = a+bx+cf(x)$. *Aequationes Mathematicae*, 11, 199-211.

[6] Kuczma, M., 1968. *Functional Equations in a Single Varible* (*Monografic Matematyczne*). Warszwa : PWN-Polish Scientific Publishers.

Current Applied Science and Technology Vol. 21 No. 3 (July-September 2021)

Efficient Comparison of Calcium Chloride and Calcium Gluconate Immersions on Quality Maintenance and Bioactive Compounds of Ready-to-cook Baby Corns

Suriyan Supapvanich[1], Surassawadee Promyou[2] and Chairat Techavuthiporn[1]*

[1]Department of Agricultural Education, Faculty of Industrial Education and Technology, King Mongkut's Institute of Technology Ladkrabang, Ladkrabang, Bangkok, Thailand
[2]Department of Agriculture and Resources, Faculty of Natural Resources and Agro-Industry, Kasetsart University, Chalermphrakiat Sakon Nakhon Province Campus, Sakon Nakhon, Thailand

Received: 7 October 2020, Revised: 16 December 2020, Accepted: 2 February 2021

Abstract

The efficiency of calcium chloride ($CaCl_2$) or calcium gluconate (Ca-Glu) immersion on physicochemical quality and bioactive compounds of ready-to-cook baby corns during cold storage at 4 ± 1ºC for 7 d was investigated. Baby corns were immersed in 1% (w/v) $CaCl_2$, 1% (w/v) Ca-Glu or distilled water (control) for 1 min. The biological parameters such as superficial colour attributes, weight loss, texture, pectin fractions, antioxidant activities and bioactive compounds of baby corns were determined. Both calcium immersions did not affect superficial the colour attributes of the baby corn compared to the control sample during storage. Baby corn texture was maintained by calcium immersions, with $CaCl_2$ evidently better maintaining texture compared to Ca-Glu. The texture maintenance by calcium immersions was associated with the retardation of increased EDTA-soluble pectin content and decreased Na_2CO_3-soluble pectin content. Ca-Glu immersion exhibited the enhancement of antioxidant activity and the concentrations of total phenols and ascorbic acid as well as the retention of free radical scavenging activity and flavonoid content during storage. In conclusion, 1% Ca-Glu immersion is a feasible alternative for maintaining texture and enhanced nutritional value of ready-to-cook baby corns during storage.

Keywords: baby corn; calcium immersion; texture; bioactive compound
DOI 10.14456/cast.2021.40

1. Introduction

Baby corn, typically recognised as immature ear corn, (*Zea mays* L.), is a well-known and important commercial crop. Typically, baby corn is harvested after silk become visible for 1 to 3 days and the cob size is approximately 4.5 cm to 10 cm in length and 7 mm to 17 mm in diameter [1]. Baby corn contains high contents of soluble and reducing sugars and is of high nutritional values as it contains proteins, vitamins, dietary fibre and minerals, especially iron and phosphorous [2]. Baby corn is utilized commercially in both fresh and processed forms. For fresh consumption, most baby corns

*Corresponding author: E-mail: chairat.te@kmitl.ac.th

are produced from sweet corn seeds because these offer better flavour and taste than field corn seeds [1]. In Thailand, baby corn in the form of a fresh-cut vegetable, is an important vegetable product produced for export as well as domestic markets [3]. It is commonly acknowledged that baby corn is very perishable due to its high metabolic rate and moisture loss [4, 5]. Three main problems that affect the marketable quality of fresh baby corn are the loss of crispness and sweetness and the incidence of tip-browning [3, 6]. These problems are caused by high respiration rate, ear desiccation and enzymatic browning activity [3, 4]. Previous work reported that shrink wrapping and cold storage delayed senescence and browning incidence and maintained desirable appearance, texture and flavour due to the suppression of respiration rate and the prevention of moisture loss [7]. Attia *et al*. [4] reported that 1% $CaCl_2$ dip followed by wrapping with polypropylene film could extend the pleasant fresh-liked quality of baby corns stored at 5ºC due to the inhibition of browning and moisture loss and maintenance of total sugars content. Exogenous calcium application is accepted as an effective approach for maintaining physicochemical quality and prolonging shelf-life, and for delaying disease attack and senescence of postharvest fruit and vegetables [8, 9]. Calcium can also preserve texture by maintaining cell wall structure and osmotic tonicity and by reducing membrane lipid dysfunction [10]. In commercial, $CaCl_2$ has been widely used for postharvest commodities; however, it might impart undesirable bitterness to products, affecting organoleptic quality. The application of other calcium salts had been suggested by Labin-Goldscher and Edenstein [11] that calcium lactate (Ca-Lac), calcium citrate and calcium gluconate (Ca-Glu) do not provide bitter taste and enhance nutritional value. Varela *et al*. [12] reported that 1% $CaCl_2$ immersion provided a slight bitter taste in fresh-cut apple but there was no effect on the organoleptic evaluation by trained panels. Youryon *et al*. [13] reported that exogenous postharvest application of Ca-Glu could induce the formation of antioxidants and retard membrane lipid peroxidation in 'Queen' pineapple better than $CaCl_2$ application during storage at 13ºC. However, the comparison of the effects of the application of various calcium salts on physicochemical quality of ready-to-cook baby corns has not been recently studied. Thus, the aim of this study was to compare the efficiency of $CaCl_2$ and Ca-Glu immersions on physicochemical quality of ready-to-cook baby corns during short-term storage at 4 ± 1°C.

2. Materials and Methods

2.1 Raw materials and treatments

Baby corns cv. 'Pacific' were derived from a commercial corn plot at Kampangsan District, Nakhon Pathom Province, Thailand. The baby corns were harvested at 47-49 days after planting (DAP) when the length of silk was approximately 3-5 cm. The baby corns were delivered to the laboratory at Department of Agricultural Education, King Mongkut's Institute of Technology Ladkrabang (KMITL), Bangkok, within 2 h., with control of the inside temperature of container below 10°C. The baby corns were peeled and cleaned by rinsing with potable water and dipped in 100 µl l^{-1} sodium hypochlorite for 2 min. After that, the baby corns were immersed into water (control), 1% (w/v) calcium chloride ($CaCl_2$) or 1% (w/v) calcium gluconate (Ca-Glu) for 1 min. Five ears of baby corns were packed in a foam tray (83 x 135 x 15 mm in dimension) and wrapped with Linear Low-Density Polyethylene (LLDPE) film (12.7 µm thickness). The ready-to-cook baby corns were stored at 4 ± 1°C for 7 days. Physicochemical quality attributes such as visual appearance, superficial colours, weight loss, texture, pectin substances, antioxidant activities and bioactive compounds were determined during storage.

2.2 Colour, weight loss and texture measurements

Colour, weight loss and texture of the baby corns were determined at the beginning of storage (day 0) until day 7. Colour attributes were measured using a Minolta colorimeter, CR-400 (Minolta, Japan). Lightness (L^*), yellowness (b^*), hue and chroma values were recorded every day during storage. The weight of ready-to-cook baby corns during storage period was recorded daily. The percentage of fresh weight loss was calculated by comparison with the weight on initial day. The texture of the baby corns was measured using a Texture Analyser, EZ-SX (Stable Micro Systems, USA). A cutting blade was used for texture measurement (hardness) and the compression force as Newton (N) was presented. The blade was driven at speed of 0.5 mm s^{-1} to a depth of 5 mm.

2.3 Pectin substances assays

Acetone insoluble solid (AIS) of the baby corns was prepared following the procedure described by Supapvanich and Tucker [14]. The AIS was extracted with 50 mM ethylenediamine tetraacetic acid (EDTA) in 50 mM sodium acetate, pH 6.5 solution at room temperature for 12 h and then filtered through a GF/A filter paper. The filtrate was collected and the EDTA-soluble pectin fraction (soluble pectin) was precipitated using absolute ethanol. The pallet was again extracted with 50 mM sodium carbonate (Na_2CO_3) in 50 mM sodium acetate, pH 6.5, solution at 4°C for 24 h followed by ambient temperature for 2 h. The suspension was then filtered through a GF/A filter paper and the Na_2CO_3- soluble pectin fraction (insoluble pectin) in the filtrate was precipitated using absolute ethanol. Both the EDTA-soluble and Na_2CO_3- soluble pectin fractions were hydrolysed with 1 M H_2SO_4 at 95°C. Galacturonic acid content of both pectin fractions was determined using the procedure of Ahmed and Labavitch [15]. Data were expressed as mg galacturonic acid per kg (mg kg^{-1}).

2.4 Antioxidant activities

A 10 g of baby corn was extracted with 60% (v/v) ethanol solution. The extract was used to determine antioxidant activities and the concentrations of total phenols and flavonoids. Ferric reducing antioxidant potential (FRAP value) and DPPH radical scavenging activity were determined according to the procedures of Benzie and Strain [16]. FRAP value was calculated using a linear equation derived from a Trolox standard curve and presented as mmole Trolox equivalent per kg sample (mmol TE kg^{-1}). DPPH radical scavenging activity was assayed using the method of Brand-Williams *et al*. [17]. The percentage of decreased optical density (OD) at 517 nm wavelength was calculated and presented as the percentage of free radical scavenging activity (%).

2.5 Total phenols, flavonoids and total ascorbic acid assays

Total phenols concentration was determined using the method of Slinkard and Singleton [18]. The concentration of total phenols was calculated using a linear equation of gallic acid standard curve and presented as mg gallic acid equivalents per kg (mg kg^{-1}). The concentration of flavonoids was determined using the procedure according to Jia *et al*. [19]. Flavonoids concentration was reckoned using a linear equation derived from catechin standard curve. The data were expressed as mg catechin equivalents per kg fresh weight of fruit (mg kg^{-1}). Ascorbic acid in the samples was extracted using 5% cold metaphosphoric acid. The concentration of total ascorbic acid (AsA) was assayed using the procedure of Hashimoto and Yamafuji [20]. The data were expressed as mg ascorbic acid per kg fresh weight (mg kg^{-1}).

2.6 Statistical Analysis

The experiments were performed using a completely randomized design (CRD). The data were analysed using analysis of variance (ANOVA) and the Duncan's Multiple Range Test (DMRT) at $P \leq 0.05$. All data were presented as the mean of four replications (n = 4) ± standard deviation (SD).

3. Results and Discussions

3.1 Superficial colour attributes

Superficial colour including *L**, *b**, hue and chroma value of the ready-to-cook baby corns are presented in Figure 1. Superficial colours of all treatments seemed to remain constant over the storage. The averages of *L**, *b**, hue and chroma values were approximately 76.5, 32, 92.5 and 31.9, respectively. Moreover, we did not find undesirable visual appearance of the baby corns over the storage (data not shown). These results suggest that 1% $CaCl_2$ and 1% Ca-Glu immersions did not affect superficial colour of the baby corns during refrigerated storage for 7 days. It is commonly recognised that undesirable visual appearance of ready-to-cook baby corns involving discoloration is mainly caused by moisture loss during storage [21]. In this study, the change in superficial colour of the baby corns was protected by the LLDPE film package, which is recommended for fresh commodities because its good water vapour barrier properties reduce moisture loss [22].

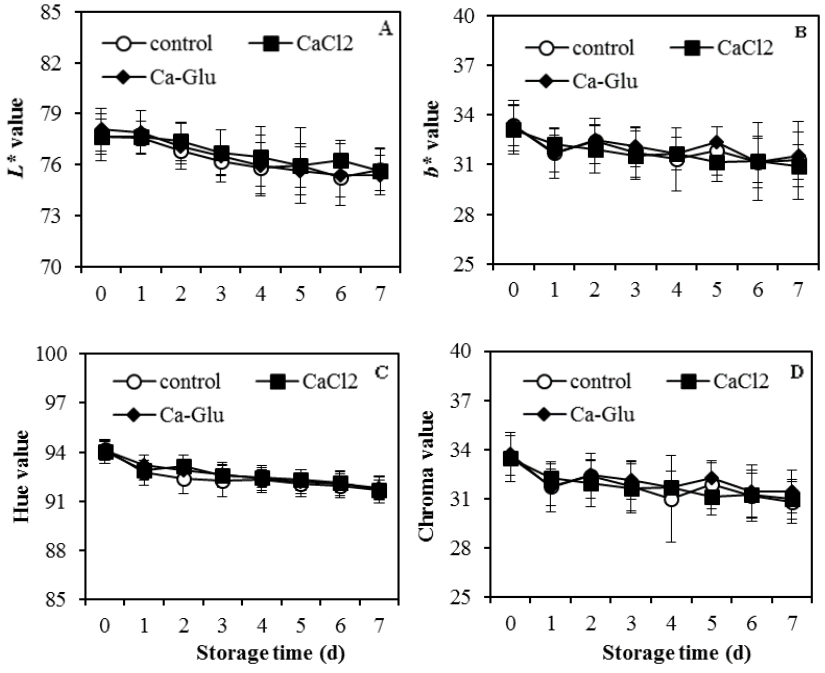

Figure 1. Colour attributes including *L** (A), *b** (B), hue (C) and chroma (D) values of baby corns treated with $CaCl_2$ and Ca-Glu compared with control samples during storage. Data are presented as mean (n = 4) with SD bar.

3.2 Weight loss and texture

Weight loss and texture change of the baby corns during storage are presented in Figure 2. It was found that an increase in weight loss was observed in all treatments during storage. The weight loss of control samples was significantly higher than that of all calcium treated samples within the first 3 days of storage period ($P < 0.05$). This might be associated with the maintenance of cell membrane function by Ca^{+} as described by Lester and Grusak [8] and Youryon *et al*. [13]. After 3 d of storage, the increased weight loss of all treatments was not significantly different over the storage ($P < 0.05$) (Figure 2A). At the end of storage, the moisture loss of all treatments was approximately 7.5%. The texture of the baby corns was measured using cutting force. Both of the calcium salts immersions could maintain texture being evidently greater than the control samples (Figure 2B). The cutting force value of control samples continuously decreased and was significantly lower than that of $CaCl_2$ and Ca-Glu treated baby corns ($P < 0.05$). $CaCl_2$ immersion maintained the texture of the baby corns better than Ca-Glu immersion. The average cutting force value of control, $CaCl_2$ and Ca-Glu treated baby corns for 7 days storage was 15.60, 16.98 and 16.29 N, respectively. The recent results revealed that both $CaCl_2$ and Ca-Glu immersions might not obviously affect the loss of fresh weight but they maintained the texture of the baby corns during storage, and especially in the case of $CaCl_2$ immersion. The loss of moisture is recognised as a main factor affecting texture change of fresh commodities [23]. The result showed that the increased weight loss during storage might not be the main factor affecting the loss of texture when the baby corns were packed in a package protecting the loss of moisture. It is commonly acknowledged that exogenous calcium application prevents the softening process of postharvest commodities due to the formation of calcium pectate structure. Calcium pectate enhances cell wall strengthening and furthermore it is not a substrate of polygalacturonase (PG), a cell wall hydrolase [23]. The recent results, the decreased weight loss of control baby corns during the first 3 days of storage was concomitant with the reduction of cutting force. Meanwhile, the weight loss of both $CaCl_2$ and Ca-Glu treated baby corns was evidently lower than that of control samples and their cutting force values were higher than control samples. However, after the third day of storage, the weight loss of all treatments was similar, which might be due to the moisture equilibrium in the package. The different effects of $CaCl_2$ and Ca-Glu immersion on texture maintenance of the baby corns might be associated with their soluble properties; $CaCl_2$ provides a higher elemental calcium content in solution than does Ca-Glu [24, 25].

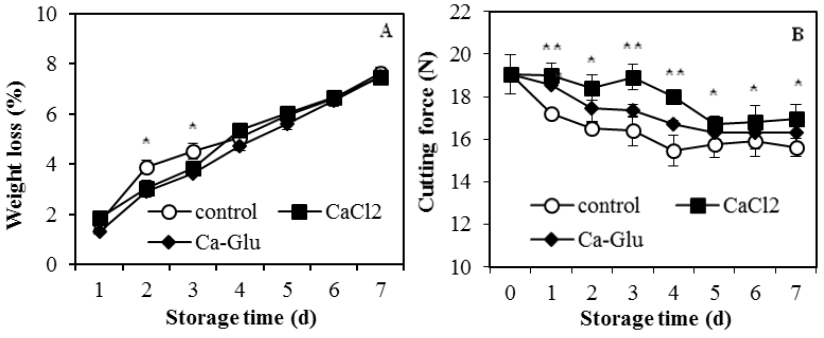

Figure 2. Weight loss (A) and texture (cutting force) (B) of ready-to-cook baby corn treated with $CaCl_2$ and Ca-Glu compared with control samples during cold storage. Data are presented as mean (n = 4) with SD bar. Significant differences between treatments are indicated with asterisks [** ($P < 0.01$); * ($P < 0.05$)].

3.3 Pectin substances

Table 1 shows the concentration of EDTA-soluble and Na_2CO_3- soluble pectin fractions of the baby corns after storage for 7 days. The EDTA-soluble pectin fraction of control samples was markedly increased whilst Na_2CO_3-soluble pectin fraction was obviously decreased when compared to those on day 0 of storage. Both calcium salt immersions delayed an increase of the EDTA-soluble and a decrease of the Na_2CO_3-soluble pectin fractions of the baby corns. $CaCl_2$ immersion showed the best result in preventing the increase of the EDTA-soluble pectin fraction as well as the decrease of the Na_2CO_3-soluble pectin fraction of the baby corns compared to Ca-Glu immersion. Changes in both the EDTA-soluble and Na_2CO_3-soluble pectin fractions were concomitant with texture changes of ready-to-cook baby corns during storage (Figure 2B). Decreased cutting force during storage was accompanied by increased EDTA-soluble pectin fraction and decreased Na_2CO_3-soluble pectin fraction. Theoretically, exogenous calcium application inhibits cell wall polymerization by the binding of Ca^{2+} with demethylated polygalacturonic backbone of pectin to form calcium pectate [23, 25]. We found that the cutting force value of $CaCl_2$ treated baby corns was evidently higher than that of Ca-Glu treated samples (Figure 2B), which was concomitant with the amounts of EDTA-soluble and Na_2CO_3-soluble pectin fractions. As described above, solubility of calcium salts is related to the elemental calcium concentration in the solution, which $CaCl_2$ provides a higher elemental calcium concentration than Ca-Glu [24, 26]. This might influence the absorption of Ca^{2+} during immersion period. Although the Ca^{2+} content in baby corn tissue was not determined, the results of texture and pectin fractions could confirm that the solubility of calcium salt influenced the texture retention of the baby corns during storage.

Table 1. The concentration of pectin substances of ready-to-cook baby corn treated with $CaCl_2$ and Ca-Glu compared with control samples during cold storage

Treatment	Storage time (d)	EDTA-soluble pectin (mg kg^{-1})	Na_2CO_3-soluble pectin (mg kg^{-1})
Control	0	190.05 ± 29.77 ^{c}	100.89 ± 8.09 ^{c}
$CaCl_2$	0	170.50 ± 24.17 ^{c}	140.84 ± 15.81^{a}
Ca-Glu	0	173.30 ± 15.03 ^{c}	118.41 ± 10.50 ^{b}
Control	7	252.84 ± 20.92 ^{a}	52.84 ± 2.40 ^{e}
$CaCl_2$	7	172.84 ± 22.56 ^{c}	110.28 ± 18.33^{bc}
Ca-Glu	7	224.50 ± 19.99 ^{b}	71.21 ± 10.64 ^{d}

Data are means (n) ± SD. Different letters in each pectin substance represent a significant difference among treatments at $P < 0.05$.

3.4 Antioxidant activities

The effects of calcium salt treatments on antioxidant activities including FRAP and DPPH radical scavenging activity are shown in Figure 3. During 3 days of storage, the decrease in FRAP was

observed for all treatments. After that, an increase in the FRAP of all treatments was observed and reached its highest value on the fifth day of storage. Ca-Glu treatments obviously enhanced FRAP more than $CaCl_2$ and control treatments. At the end of storage (day 7), the FRAP of all treatments markedly declined. However, we found that the FRAP of Ca-Glu treated baby corns was significantly higher than that of control samples ($P < 0.05$) whilst the lowest FRAP value was found in control samples. The increase in FRAP on day 5 of storage might have been related to the simulation of defence mechanism caused by chilling temperature and calcium treatment, whereas the decrease in FRAP on day 7 of storage might have been associated with deterioration process of the baby corn. The DPPH radical scavenging activity of control samples markedly declined during the storage period (Fig 3B). $CaCl_2$ immersion slightly induced DPPH radical scavenging activity during 3 days of storage and markedly declined afterwards. Meanwhile, Ca-Glu immersion could maintain DPPH radical scavenging activity during 5 days of the storage and then declined. At the end of storage, DPPH radical scavenging activity of Ca-Glu treated baby corns was significantly higher than that of other samples ($P < 0.05$). These results suggested that Ca-Glu immersion could enhance antioxidant activities in the baby corns rather than $CaCl_2$ immersion. Previous works reported that calcium application could induce antioxidant activity in plants [27]. Aghdam *et al*. [28] suggested that $CaCl_2$ stimulated antioxidant system in cornelian cherry fruits due to the inducement of phenylpropanoid-flavonoids pathways. Youryon *et al.* [13] reported that Ca-Glu treatment enhanced antioxidant system including antioxidant enzyme activities in 'Queen' pineapples more than $CaCl_2$ treatment. Among the calcium salt treatments in the present study, Ca-Glu immersion was more likely to enhance as well as maintain antioxidant activities of the baby corns than $CaCl_2$ immersion. However, the mechanism of Ca-Glu enhance DPPH scavenging activity is more superior than $CaCl_2$ treatment which is ambiguous and further studies are needed.

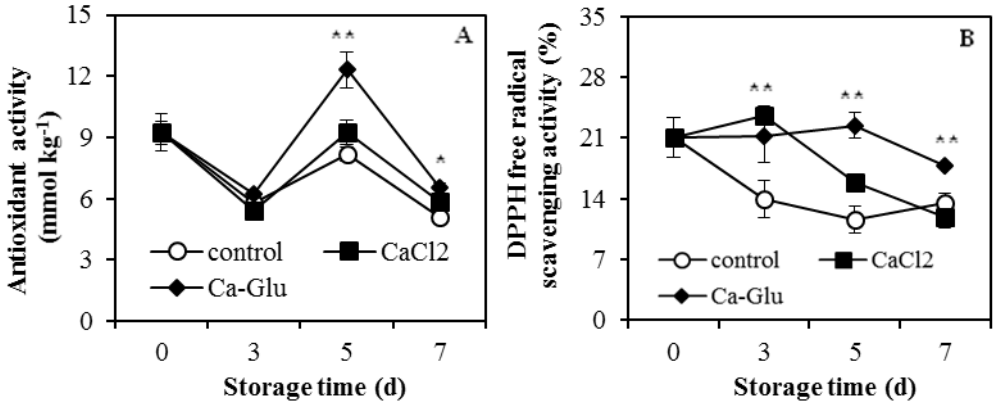

Figure 3. Antioxidant activity (FRAP) (A) and DPPH radical scavenging activity (B) of ready-to-cook baby corn treated with $CaCl_2$ and Ca-Glu compared with control samples during cold storage. Data are presented as mean (n = 4) with SD bar. Significant differences between treatments are indicated with asterisks [** ($P < 0.01$); * ($P < 0.05$)].

3.5 Bioactive compounds

Bioactive compounds such as total phenols, flavonoids and ascorbic acid concentrations of the baby corns are shown in Figure 4. The total phenols concentration of all treatments obviously increased

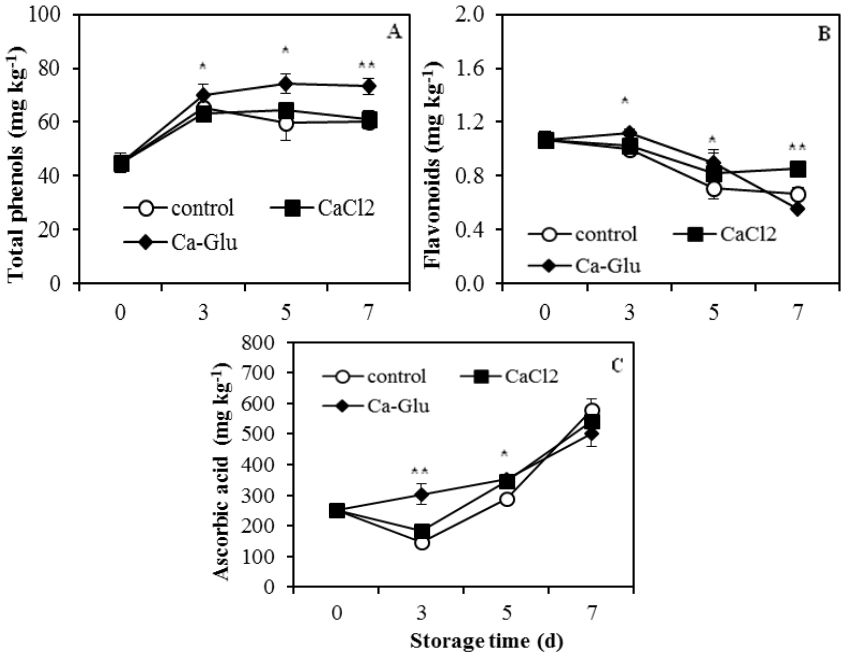

Figure 4. Total phenols (A), flavonoids (B) and ascorbic acid (C) concentrations of ready-to-cook baby corn treated with $CaCl_2$ and Ca-Glu compared with control samples during cold storage. Data are presented as mean (n = 4) with SD bar. Significant differences between treatments are indicated with asterisks [** ($P < 0.01$); * ($P < 0.05$)].

during 3 days of storage, and that of Ca-Glu treated baby corns was significantly higher than those of control and $CaCl_2$ treated samples ($P < 0.05$). After that, total phenols content of Ca-Glu and $CaCl_2$ treated samples remained constant over the storage. The total phenols concentration of control treated samples declined after 3 days of storage. At the end of storage, total phenols concentration of Ca-Glu treated baby corns was significantly higher than those of other samples ($P < 0.05$), whereas no significant difference between control and $CaCl_2$ treated samples was observed. The flavonoids content of Ca-Glu treated baby corns increased during 3 days of storage whilst that of control and $CaCl_2$ treated samples remained constant. After that, the flavonoids content of all treatments decreased. During 5 days of storage, flavonoids content of Ca-Glu treated baby corns was significantly higher than that of control samples ($P < 0.05$). At the end of storage, we found that the flavonoids concentration of $CaCl_2$ treated samples was significantly higher than other samples ($P < 0.05$). The efficiency of calcium treatment enhancing phenolic compounds has been described by Aghdam *et al.* [28] in which calcium stimulated PAL activity and then triggered the phenylpropanoid-flavonoids pathways in cornelian cherries. It is commonly acknowledged that phenolic compounds and flavonoids are synthesized through phenylpropanoid-flavonoids pathways. Many previous studies have reported the enhancement of total phenols and flavonoids contents by various calcium salt applications such as in sweet peppers [27], plums [29], cherries [28] and guavas [30]. We also found that the ascorbic acid concentration of control and $CaCl_2$ treated baby corns decreased during the first 3 d of storage, whilst increased ascorbic acid concentration was found in Ca-Glu treated samples (Figure 4C). After the third day of storage, the increment of ascorbic acid concentration was found in all treatments. On the fifth day of storage, the ascorbic acid concentration of both calcium treated baby corns was significantly higher than that of control samples ($P < 0.05$).

However, at the end of storage (day 7), no significant difference in ascorbic acid concentration of all treatments was observed. Durrani *et al*. [29] reported that the treatments with $CaCl_2$ and Ca-Glu exhibited higher retention of ascorbic acid concentration in plums when compared to untreated fruits during storage. Moreover, foliar application of calcium induced ascorbic acid content in strawberries [31]. However, the results showed that Ca-Glu immersion enhanced ascorbic acid content of ready-to-cook baby corns rather than $CaCl_2$ immersion during 3 days of storage. This might be associated with released gluconic acid which is recognised as a precursor of L-ascorbic acid biosynthesis in plants [32]. The present result also found that the higher total phenols content of Ca-Glu treated baby corn was concomitant with the higher antioxidant activities of FRAP and DPPH radical scavenging activity compared to control and $CaCl_2$ treated samples (Figure 3).

4. Conclusions

Here, our research indicated that the immersion of different calcium salts solutions showed different effects on quality maintenance and improvement of ready-to-cook baby corns during cold storage. Both the $CaCl_2$ and Ca-Glu immersions had no influence on the changes in colour attributes of ready-to-cook baby corns during 7 days storage. The texture of the ready-to-cook baby corns was preserved by immersion in both calcium salts, but $CaCl_2$ evidently maintained better texture when compared to Ca-Glu. The loss of texture was accompanied by an increased EDTA-soluble pectin fraction and decreased Na_2CO_3-soluble pectin fraction during cold storage. Based on our findings, calcium treatments could enhance as well as maintain antioxidant activities and bioactive compounds during refrigerated storage. Ca-Glu at the concentration of 1% (w/v) was likely to enhance antioxidant activity and bioactive compounds to a greater extent than was 1% $CaCl_2$ immersion.

5. Acknowledgements

This work was funded by Kasetsart University Research and Development Institute, Kasetsart University, Thailand. The grant code was KURDI29.61. We gratefully acknowledge the assistance of Dr. J. Anuchai, V. Chimsonthon, C. Kijka and A. Boonlila.

References

[1] Bar-Zur, A. and Saadi, H., 1990. Prolific maize hybrids for baby corn. *Journal of Horticultural Science*, 65(1), 97-100.

[2] Hooda, S. and Kawatra, A., 2013. Nutritional evaluation of baby corn (*Zea mays*). *Nutrition and Food Science*, 43 (1), 68-73.

[3] Meenaphan, A. and Ketsa, S., 2003. Browning of baby corn after harvest. *Acta Horticulturae*, 628, 569-574.

[4] Attia, M.M., Saleh, S. M.M. and El-Shabrawy, E.M., 2011. Effect of anti-browning agents and wrapping films on browning inhibition and maintaining quality of baby corn during storage. *Journal of Plant Production, Mansoura University*, 2 (12), 1667-1682.

[5] Singh, M., Kumar, A. and Kaur, P., 2014. Respiratory dynamics of fresh baby corn (*Zea mays* L.) under modified atmospheres based on enzyme kinetics. *Journal of Food Science and Technology*, 51(9), 1911-1919.

[6] Nik Fakurudin, N.A., Solihah, M.A. and Wan Rosli, W.I., 2013. Ultra structural description of young corn (*Zea mays* L.) ear. *Annals of Microscopy*, 13, 14-22.
[7] Risse, L.A. and McDonald, R.E., 1990. Quality of supersweet corn film overwrapped in trays. *HortScience*, 25 (3), 322-324.
[8] Lester, G. and Grusak, M.A., 1999. Postharvest application of calcium and magnesium to honeydew and netted muskmelons: effects on tissue ion concentrations, quality, and senescence. *Journal of the American Society for Horticultural Science*, 124, 545-552.
[9] Supapvanich, S., Arkajak, R. and Yalai, K., 2012. Maintenance of postharvest quality and bioactive compounds of fresh-cut sweet leaf bush (*Sauropus androgynus* L. Merr.) through hot $CaCl_2$ dips. *International Journal of Food Science and Technology*, 47, 2662-2670.
[10] Kukura, J.L., Beelman, R.B., Peiffer, M. and Walsh, R., 1998. Calcium chloride added to irrigation water of mushrooms (*Agaricus Bisporus*) reduces postharvest browning. *Journal of Food Science*, 63(3), 454-457.
[11] Labin-Goldscher, R. and Edenstein, S., 1996. Calcium citrate: a revised look at calcium fortification. *Food Technology*, 50, 96-98.
[12] Varela, P., Salvador, A. and Fiszman, S.M., 2007. The use of calcium chloride in minimally processed apples: A sensory approach. *European Food Research and Technology*, 224, 461-467.
[13] Youryon, P., Supapvanich, S., Kongtrakool, P. and Wongs-Aree, C., 2018. Calcium chloride and calcium gluconate peduncle infiltrations alleviate the internal browning of Queen pineapple in refrigerated storage. *Horticulture, Environment, and Biotechnology*, 59, 205-213.
[14] Supapvanich, S. and Tucker, G.A., 2013. The effect of 1-methylcyclopropene (1-MCP) on quality and cell wall hydrolases activities of fresh-cut muskmelon (*Cucumis melo* var reticulatus L.) during storage. *Food and Bioprocess Technology*, 6(8), 2196-2201.
[15] Ahmed, A.E.R. and Labavitch, J.M., 1977. A simplified method for accurate determination of cell wall uronide content. *Journal of Food Biochemistry*, 1, 361-365.
[16] Benzie, I.F.F. and Strain, J.J., 1996. The ferric reducing ability of plasma (FRAP) as a measure of "Antioxidant power": the FRAP assay. *Analytical Biochemistry*, 239, 70-76.
[17] Brand-Williams, W., Cuvelier, M.E. and Berset, C., 1995. Use of free radical method to evaluate antioxidant activity. *LWT-Food Science and Technology*, 28(1), 25-30.
[18] Slinkard, K. and Singleton, V.L., 1997. Total phenol analysis: automation and comparison with manual methods. *American Journal of Enology and Viticulture*, 28, 49-55.
[19] Jia, Z., Tang, M. and Wu, J., 1999. The determination of flavonoid contents in mulberry and their scavenging effects on superoxide radical. *Food Chemistry*, 64, 555-559.
[20] Hashimoto, S. and Yamafuji, K., 2001. The determination of diketo-l-glulonic acid, dehydro-l-ascorbic acid, and l-ascorbic acid in the same tissue extract by 2, 4-dinitrophenol hydrazine method. *Journal of Biochemistry*, 147, 201-208.
[21] Silva, P.D.S., Batista, C.M., Soares, M.C., Mota, W.F. and Pimenta, S., 2019. Post-harvest conservation of baby corn under controlled atmosphere and refrigeration. *Journal of Agricultural Science*, 11(15), 78-86.
[22] Mangaraj, S., Goswami, T. K. and Mahajan, P.V., 2009. Applications of plastic films for modified atmosphere packaging of fruits and vegetables: a review. *Food Engineering Reviews*, 1, 133-158.
[23] Brummell, D.A., 2006. Cell wall disassembly in ripening fruit. *Functional Plant Biology*, 33, 103-119.
[24] Kubantseva, N. and Hartel, R.W., 2002. Solubility of calcium lactate in aqueous solution. *Food Reviews International*, 18, 135-149.
[25] Trailokya, A., Srivastava, A., Bhole, M. and Zalte, N., 2017. Calcium and calcium salts. *Journal of the Association of Physicians of India*, 65, 100-103.

[26] Toivonen, P.M.A. and Brummell, D.A., 2008. Biochemical bases of appearance and texture changes in fresh-cut fruit and vegetables. *Postharvest Biology and Technology*, 48(1), 1-14.
[27] Barzegar, T., Fateh, M. and Razavi, F., 2018. Enhancement of postharvest sensory quality and antioxidant capacity of sweet pepper fruits by foliar applying calcium lactate and ascorbic acid. *Scientia Horticulturae*, 241, 293-303.
[28] Aghdam, M.S., Dokhanieh, A.Y., Hassanpour, H. and Fard, J.R., 2013. Enhancement of antioxidant capacity of cornelian cherry (*Cornus mas*) fruit by postharvest calcium treatment. *Scientia Horticulturae*, 161, 160-164.
[29] Durrani, Y., Khan, R.A., Ali, S.A., Hashmi, M., Muhammad, A., Shahid, M. and Ahmed, T., 2018. Comparative study of selected calcium salts impacts on enhancement of postharvest storage life of fresh plum fruits. *Fresenius Environmental Bulletin*, 27 (1), 46-53.
[30] Fekry, O.M., 2018. Effect of edible coating chitosan and calcium gluconate on maintaining fruit quality and marketability of guava (*Psidium guajava*) fruits during storage. *Middle East Journal of Applied Sciences*, 8 (4), 1046-1060.
[31] Singh, R., Sharma, R.R. and Tyagi, S.K., 2007. Pre-harvest foliar application of calcium and boron influences physiological disorders, fruit yield and quality of strawberry (*Fragaria ananassa* Duch.). *Scientia Horticulturae*, 112, 215-220.
[32] Isherwood, F.A., Chen, Y.T. and Mapson, L.W., 1954. Synthesis of L-ascorbic acid in plants and animals. *Biochemistry Journal*, 56 (1), 1-15.

Molecular Identification of Endophytic Fungi Associated with *Cynometra ramiflora* L. and *Wrightia pubescens* (R. Br.) Using the Internal Transcribed Spacer (ITS) Region of rDNA and Its Morphotypes

Benjamin V. Jose[1], Dana Theresa De Leon[2], Mike Andre Malonzo[3] and Jerwin R. Undan[1,2,3]*

[1]Department of Biological Sciences, College of Arts and Sciences, Central Luzon State University, Science City of Muñoz, Nueva Ecija, Philippines
[2]Tuklas Lunas Laboratory, Central Luzon State University, Science City of Muñoz, Nueva Ecija, Philippines
[3]Biotechnology and Analytical Laboratory, Central Luzon State University, Science City of Muñoz, Nueva Ecija, Philippines

Received: 20 April 2020, Revised: 15 November 2020, Accepted: 3 February 2021

Abstract

In this study, endophytic fungi from Philippine medicinal plants namely, *Cynometra ramiflora* and *Wrightia pubescens* were isolated and identified. The endophytic fungi were isolated using potato dextrose agar, and were identified by amplifying a fragment of their internal transcribed spacer (ITS) regions of rDNA using polymerase chain reaction. The identified endophytic fungi were *Colletotrichum karsti, Diaporthe longicolla, Phomopsis columnaris, D. pseudomangiferae, C. acutatum,* and *D. inconspicua.* All of the isolates belonged to phylum Ascomycota. Two isolates (*C. karsti* and *C. acutatum*) belonged to Glomerellaceae family and four isolates (*D. longicolla, P. columnaris, D. pseudomangiferae,* and *D. inconspicua*) were under the Diaporthaceae family. In addition, based on cultural morphology, the isolated endophytic fungi were described as irregular and circular morphotypes. This is the first report on the isolation of endophytic fungi associated with healthy leaves of *C. ramiflora* and *W. pubescens.*

Keywords: Cynometra ramiflora; *Wrightia pubescens*; endophytic fungi; Diaporthaceae; Glomerellaceae
DOI 10.14456/cast.2021.46

1. Introduction

Endophytic fungi are types of microorganisms inhabiting the inner tissues of plants. It has been found that a variable relationship exists between endophytes and their host plants, ranging from either mutualism or symbiosis to antagonism or slightly pathogenic [1]. Although some endophytes

*Corresponding author: Tel.: (+63) 9171031333
E-mail: jerwinundan@clsu.edu.ph

can be termed pathogens, most are in an inactive state within the host tissue. Some saprobes can also be facultative parasites. Moreover, endophytic microorganisms tend to become pathogenic when the host plant is in a stressed condition [2].

Generally, most endophytic fungi are found to be beneficial to their host plants and produce or initiate the development of important bioactive compounds that have been used in many applications [3-4]. Interestingly, the bioactive compounds of endophytes not only play an important role in ecology or environment, but also have a positive impact in the field of medicine [5].

Recently, there has been extensive research on endophytic fungi from different plants including trees, vegetables, fruits, and crops. However, less research has been conducted on the leaves of tropical plants and specifically on medicinal plants. *Cynometra ramiflora*, also known as Katong laut in Malaysia and known as Balitbitan in the Philippines, is a small erect tree known to have anticancer, antioxidant, and antiviral activities [6]. On the other hand, *Wrightia pubescens*, known as Lanete in the Philippines, is a medicinal plant that was found to have anti-inflammatory and anticancer activities [7, 8].

Among the DNA barcoding markers available, the internal transcribed spacer (ITS) regions of rDNA has been found to have the highest probability of successful identification of the broadest range of fungi [9]. rDNA-ITS was also found to have high resolution in some taxonomic groups and has been used as the standard DNA barcode for fungi and other biological groups such as algae, protist, and animals [10]. Nowadays, the ITS regions are the most accepted DNA barcode for fungi [11] and provide important information on fungal diversity [12] and uniqueness because they have the highest resolving power to discriminate closely related species [9]. Aside from morphotype determination of the endophytic fungi using the cultural characteristics, the identification of the specific endophytic fungi associated with healthy leaves of *C. ramiflora* and *W. pubescens* was also performed using the ITS region in this study.

2. Materials and Methods

2.1 Collection of samples

Healthy leaves of *C. ramiflora* and *W. pubescens* were collected in the Science City of Muñoz, Nueva Ecija, Philippines. Ten to fifteen pieces of leaves were randomly picked around the tree and placed in a clean polyethylene bag, which was immediately transported to the laboratory.

In order to remove impurities and eliminate epiphytic microorganisms, the leaves were subjected to a surface-sterilization procedure. Each plant tissue was cut with a sterile blade into 1-cm segments. Each part of the samples was thoroughly washed under running tap water, after which, the surface was sterilized by submerging the part in 75% ethanol for 2 min, 5.3% sodium hypochlorite for 5 min, and 75% ethanol for 30 sec, and finally, rinsed with sterile distilled water for 1 min. Thereafter, the samples were dried on sterile filter paper.

2.2 Media preparation and sterilization

Potato Dextrose Agar (PDA) media were prepared by dissolving 9.75 grams of PDA powder (HIMEDIA) in a 250 ml of distilled water. After sterilization, the bottled media were allowed to cool. Twenty-five ml of prepared medium was aseptically dispensed into newly sterilized dried petri dishes. They were allowed to stand up open for a few min to allow the moisture to evaporate in order to avoid contamination. These petri dishes were observed for 24 h to ensure that these were free from contaminants before inoculation.

2.3 Isolation of endophytic fungi

The freshly picked plant samples were placed aseptically into the PDA medium, with 100µl of streptomycin sulfate (30 mg/l) to inhibit the growth of bacteria, using a clean and sterile blade. The plates were incubated and monitored at room temperature approximately 20 to 25°C for 5-7 days. The isolated fungal endophyte was revived and was aseptically transferred onto new PDA plates. The cultures were incubated 27°C for 3-5 days to allow mycelia proliferation.

Once the mycelial growth from the revived culture had proliferated, a small portion of the colony was aseptically transferred using the inoculation needle onto the sterilized PDA slants in test tubes for the stock culture. The mycelia from the stock culture were inoculated using the small block of agar containing mycelial structures on sterilized PDA plates and incubated at 27°C until profuse growth was observed for morphological characterization. These cultures were incubated and stored as pure cultures readily available for molecular identification.

2.4 Genomic DNA extraction, gel electrophoresis and PCR amplification

The mycelia of endophytic fungi were scraped off using a sterile inoculating needle and were transferred immediately to 1.5 ml tube that contained 500µl cetyltrimethylammonium bromide (CTAB). The samples were ground using pipette tip. The samples were then mixed using a vortex every 5 min. Samples were then incubated at room temperature and 500µl of chloroform isoamyl-alcohol (24:1 ratio) was added and thoroughly mixed using vortex. Then, it was spun using a centrifuge at 10,000 rpm for 30 min.

The supernatant (upper phase) of each sample was transferred to a new tube (2 ml) and immediately added with the 500µl of cold isopropanol and incubated at -20ºC overnight. After incubation, the samples were spun on a centrifuge at 10,000 rpm for 10 min. The isopropanol (supernatant or the upper phase) was decanted and the pellet was washed with 500µl of 70% ethanol and it was spun on a centrifuge at 12,000 rpm for 3 min and the ethanol was removed. The addition of ethanol and spinning were repeated twice. The pellet was drained dry by inverting the tube on a paper towel to get rid of excess liquid. The pellet was dissolved in 100µl of 1× TE buffer and was incubated at room temperature for 3-4 h until pellet was dissolved completely.

The DNA quality was checked by mixing 1µl of the DNA samples with loading dye and dispensed on a well with 1% agarose gel containing 1µl of Biotium GelRed™ Nucleic Acid Gel Stain. The DNA was run for 30 min in the electrophoresis tank (ENDURO™ Horizontal Gel Electrophoresis System) with 100V along with the standard ladder. After electrophoresis, it was viewed in the gel documentation system (ENDURO™ Gel Documentation System) for imaging. The genomic DNA was diluted 1:100 µl using sterilized distilled water before rDNA-ITS amplification.

To identify the isolated fungal endophytes from the leaves of *C. ramiflora and W. pubescens*, total DNAs were run in a Polymerase Chain Reaction (PCR) machine (Applied Biosystems®, 2720 Thermal Cycler) with the primers, ITS 1F (5'-CTTGGTCATTTAGAGGAA GTAA-3') [13], and ITS 4R (5'-TCCTCCGCTTATTGATATGC-3') [14]. A volume of 1 µl of diluted DNA was mixed with PCR components (volume depends on brand's instruction). The PCR was performed fitted with a heated lid using the following PCR profile: for initial denaturation, 95°C for 1 min followed by 35 cycles of 95°C for 15 s, 50.1°C for 15 s, and 72°C for 15 s, with final extension step of 72°C for 5 min. The amplified products were checked again using gel electrophoresis system using 3µl run for 30 min in the electrophoresis tank with 100V along with the standard ladder using gel doc system and were sent to 1st BASE Laboratory at Malaysia for purification of the PCR product

and sequencing procedure. The sequences were used for BLAST (Basic Local Alignment Search Tool) [15] analysis and the related gene sequences available from NCBI (National Center for Biotechnology Information) were used for identification and phylogenetic analysis.

2.5 Phylogenetic analysis

The rDNA-ITS sequences were aligned using Clustal W provided in the default parameter of MEGA X [16]. Phylogenetic tree was constructed by applying the Neighbor-Joining (NJ) and BioNJ algorithms to a matrix of pairwise distances estimated using the Tamura-Nei model [17, 18].

3. Results and Discussion

3.1 Morphotypes of endophytic isolates from *W. pubescens* and *C. ramiflora*

There were six endophytic fungi that were isolated in this study (Figure 1). One endophytic fungus (Wp1) was isolated from *W. pubescens*, while there were five endophytic fungal isolates (Cr1, Cr2, Cr3, Cr4 and Cr6) from *C. ramiflora* . The isolated endophytic fungi were separated in three morphotypes based on their cultural characteristics as shown in Table 1.

The colony of Wp1 mycelia appeared as a white, circular form and has an entire margin. The conidia appeared hyaline, cylindrical, and aseptate as also described by Tahere *et al.* [19]. On the other hand, the isolate Cr1 appeared as a white, irregular form and undulate margin. The conidiogenous cells were hyaline and unbranched as also described by Yang *et al.* [20]. The colony of isolate Cr2 was also observed to be white, irregular form and undulate margin. The conidiogenous cells appeared hyaline with multicellular columns as reported by Farr *et al.* [21]. The colony of isolate Cr3, on the other hand, had white mycelia in a circular form and entire margin. The hyphae appeared septate hyaline and branched; currently, there has been no available concrete detailed description of

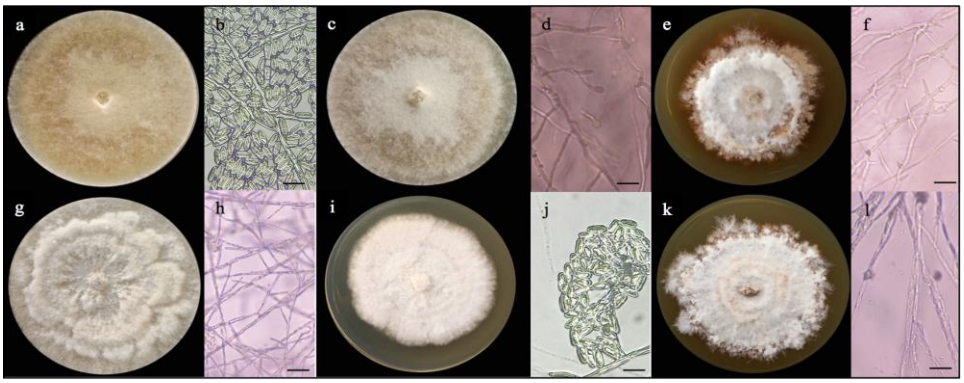

Figure 1. Morphological characteristics of the six isolates on PDA, **(**a**)** colony of *Colletotrichum karsti* (b) conidia of *C. karsti* (c) colony of *Diaporthe longicolla* (d) conidiogenous cells of *D. longicolla* (e) colony of *Phomopsis columnaris* (f) conidiogenous cells of *P. columnaris* (g) colony of *D. pseudomangiferae* (h) hyphae of *D. pseudomangiferae* (i) colony of *C. acutatum* (j) conidia of *C. acutatum* (k) colony of *D. inconspicua* (l) conidiogenous cells of *D. inconspicua* Scale bar = 1µm

Table 1. Morphotypes and cultural characteristics of the isolates on PDA

Morphotypes	Isolates	Host	Size (cm) of colony; 14 days	Shape	Color	Edge
1	Wp1	*W. pubescens*	7.6	Circular	White	Entire
	Cr3	*C. ramiflora*	>A	Circular	White	Entire
2	Cr1	*C. ramiflora*	7.2	Irregular	White	Undulate
	Cr2	*C. ramiflora*	6.0	Irregular	White	Undulate
	Cr4	*C. ramiflora*	7.0	Irregular	White	Undulate
3	Cr6	*C. ramiflora*	6.4	Irregular	Light brown to white	Filiform

Note: >A Completely covering plate

sexual morphology of this isolate so far. The colony of isolate Cr4 had white mycelia, irregular form, and undulate margin. The conidia appeared hyaline, ellipsoid, and fusiform [22]. The mycelia of the isolate Cr6, had light brown to white mycelia, irregular form, and filiform margin. The conidiogenous cells were phialidic and hyaline [23] (Figure 1 and Table 1).

3.2 Molecular identity of the endophytic fungi based on ITS gene sequence

The identity of the endophytic fungi was resolved using the rDNA-ITS region (Table 2). The isolate Wp1 was identified as *C. karsti* (KX578794.1) with 99.67% identity. The isolate Cr1 was identified as *D. longicolla* (LN552212.1) with 97.95% identity. The isolate Cr2 had 100% identity to *Phomopsis columnaris* (KU204512.1), while the isolate Cr3 was identified as *D. pseudomangiferae* (MG576128.1) with 97.72% identity. The isolate Cr5 was identified as *C. acutatum* (LC194224.1) with 99.66% identity, and lastly, the isolate Cr6 was identified as *D. inconspicua* (MF495476.1) with 98.07% identity. Similarly, the phylogenetic study based on the rDNA-ITS region revealed that the isolates belonged to three genera as delineated in the constructed phylogeny tree. Wp1, and Cr4 were from *Colletotrichum*, while Cr1, Cr3, and Cr6 belonged to *Diaporthe*, and Cr2 was in the genus *Phomopsis* (Figure 2). The molecular identification of the isolates was confirmed using their morphological description, also taking into consideration the mycelia, conidia, or their conidiogenous cells or hyphae.

Table 2. Identities of the endophytic fungi based on the ITS region

Isolates	Scientific name	%Identity	Accession number from NCBI GenBank
Wp1	*Colletotrichum karsti*	99.67%	KX578794.1
Cr1	*Diaporthe longicolla*	97.95%	LN552212.1
Cr2	*Phomopsis columnaris*	100.00%	KU204512.1
Cr3	*Diaporthe pseudomangiferae*	97.72%	MG576128.1
Cr4	*Colletotrichum acutatum*	99.66%	LC194224.1
Cr6	*Diaporthe inconspicua*	98.07%	MF495476.1

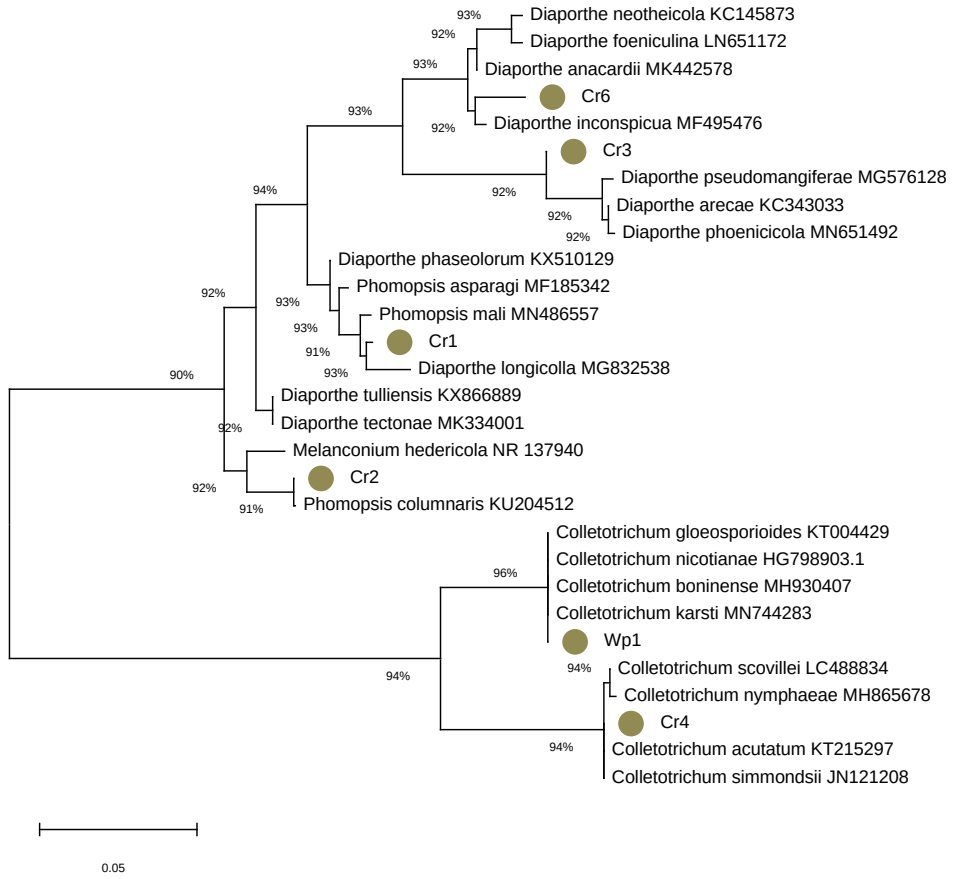

Figure 2. Phylogenetic tree based on the nucleotide sequences of rDNA-ITS region. The isolates and their phylogenetic position based on the ITS region according to neighbor joining method. The phylogeny involved 29 nucleotide sequences; the NCBI GenBank accession numbers from the reference strains are shown after the name of the strain.

Colletotrichum karsti causes anthracnose of *Capsicum anuum* in mango in northeastern Brazil [24]. In this study, *C. karsti* was found on the healthy leaves of *W. pubescens*, suggesting that it benefits the growth and development of *W. pubescens*. In the study of Gangadevi and Muthumary [25], the relative family of *C. karsti*, which is the *C. gloeosporioides*, a novel endophytic taxol-producing fungus, was isolated from the leaves of a medicinal plant, *Justicia gendarussa*. In addition, *Colletotrichium* species, in particular *C. gloesporioides*, produces taxol (163.4 μg/l), which is a secondary metabolite capable of inhibiting cell division or proliferation. Based on its taxonomy, *C. karsti* belongs to subkingdom Dikarya, phylum Ascomycota, subphylum Pezizomycotina, class Sordiaromycetes, subclass Hypocreomycetidae, order Glomerellales, family Glomerellaceae, and genus *Colletotrichum*.

Diaporthe longicolla causes the black zone lines on the lower stems of mature soybean plants [26]. According to Preeti *et al.* [27], through mutualism, both plants and endophytic fungi

release some similar secondary metabolites. This could be an indication that the isolated endophytic fungus identified molecularly as *D. longicolla* can play a vital role regarding the chemical and pharmacological properties of *C. ramiflora* and offers protection from pathogens and grazing animals. It belongs to subkingdom Dikarya, phylum Ascomycota, subphylum Pezizomycotina, class Sordiaromycetes, subclass Sordiaromycetidae, order Diaporthales, family Diaporthaceae, and genus *Diaporthe*.

Phomopsis columnaris causes the twig dieback of *Vaccinium vitis-idaea* (lingon berry) [21]. The isolated endophytic fungus *P. columnaris* could promote growth and nutrient uptake capability of the plant *C. ramiflora*. *Phomopsis columnaris* belongs to subkingdom Dikarya, phylum Ascomycota, subphylum Pezizomycotina, class Sordiaromycetes, subclass Diaporthomycetidae, order Diaporthales, family Diaporthaceae, and genus *Phomopsis*.

Diaporthe pseudomangiferae was first reported causing inflorescence rot, rachis canker, and flower abortion in *Mangifera indica* in Puerto Rico [28]. Furthermore, the ethanol extract of *C. ramiflora* leaves has cytotoxic effects on HeLa, T47D, and WiDr cell-lines [29]. The cytotoxic properties of *C. ramiflora* could be due to the association with the endophytic fungus *D. pseudomangiferae*. Through mutualism, the plants and endophytic fungi were found to secrete some similar secondary metabolites [28]. *D. pseudomangiferae* belongs to subkingdom Dikarya, phylum Ascomycota, subphylum Pezizomycotina, class Sordiaromycetes, subclass Sordiaromycetidae, order Diaporthales, family Diaporthaceae, and genus *Diaporthe*.

On the other hand, like *C. karsti*, *C. acutatum* also causes anthracnose [30]. In another study, *C. acutatum* was isolated from anthracnose lesions in key lime, star fruit, mango, and leatherleaf fern [31]. The presence of endophytic fungi on the development of plants might be an indicator of potential medicinal properties of the plant. In addition, the relative family of *C. acutatum*, which is *C. gloeosporioides*, showed cytotoxic activity against numerous cell lines including MCF-7, NCI-H460, HepG-2, and SF-268 tumor cell lines [32]. *Colletotrichum acutatum* belongs to subkingdom Dikarya, phylum Ascomycota, subphylum Pezizomycotina, class Sordiaromycetes, subclass Hypocreomycetidae, order Gomerellales, family Glomerellaceae, and genus *Colletotrichum*.

Zang *et al.* [33] reported that the secondary metabolite isochromophilone X isolated from *Diaporthe* sp. was found to have moderate cytotoxic activities. Moreover, kampanol A, R-mevalonolactone, ergosterol, and ergosterol peroxide were isolated from the endophytic fungus *Phomopsis archeri* [34]. In addition, another isolated compound from *P. archeri*, phomoarcherin B showed antimalarial activity against *Plasmodium falciparum* with an IC_{50} value of 0.79 μg/ml. The isolated endophytic fungus *D. inconspicua*, associated with *C. ramiflora* leaves, is a close relative of *Diaporthe* sp. and *Phomopsis archeri*, which are all under the family Diaporthaceae. Therefore, it could be possible for *D. inconspicua* to have a cytotoxic and anti-malarial activity. *Diaporthe inconspicua* belongs to subkingdom Dikarya, phylum Ascomycota, subphylum Pezizomycotina, class Sordiaromycetes, subclass Diaporthomycetidae, order Diaporthales, family Diaporthaceae, and genus Diaporthe.

4. Conclusions

This study performed the isolation of endophytic fungi from the known medicinal plants in the Philippines namely, *C. ramiflora* and *W. pubescens*. With the application of modern biotechnological tools such as DNA barcoding in plants, the endophytes were identified with robust results and accuracy. The internal transcribed spacer (ITS) region was found to have a high accuracy for the identification of the broadest range of fungi. The isolated endophytic fungi in this

study are important materials to study on their secondary metabolites, close association with plants, and important enzymes, all of which may have biotechnological application and medicinal uses.

5. Acknowledgements

The authors would like to thank the people of the Tuklas Lunas Laboratory, and the Biotechnology and Analytical Laboratory of the Central Luzon State University, Science City of Muñoz, Nueva Ecija, Philippines. We also thank the Department of Science and Technology under the DOST-ASTHRDP (SEI) for providing financial support for BVL and assistance in the conduct of this study and the Commision on Higher Education (CHED)-GIA for research for the chemicals and reagents.

References

[1] Schulz, B. and Boyle, C., 2005. The endophytic continuum. *Mycological Research*, 109, 661-686.

[2] Romero, A., Carrion, G. and Rico-Gray, V., 2001. Fungal latent pathogens and endophytes from leaves of *Parthenium hysterophorus* (Asteraceae). *Fungal Diversity*, 7, 81-87.

[3] Strobel, G. and Daisy, B., 2003. Bioprospecting for microbial endophytes and their natural products. *Microbiology Molecular Biology Reviews*, 67, 491-502.

[4] Arnold, A.E., Mejia, L. C., Kyllo, D., Rojas, E. I., Maynard, Z., Robbins N. and Herre, E.A., 2003. Fungal endophytes limit pathogen damage in a tropical tree. *Proceedings of the National Academy of Science of the United Science of America*, 100, 15649-15654.

[5] Ratnaweera, P.B., De Silva, E.D., Williams, D.E. and Andersen, R.J., 2015. Antimicrobial activities of endophytic fungi obtained from the arid zone invasive plant *Opuntia dillenii* and the isolation of equisetin, from endophytic *Fusarium* sp.. *BMC Complementary and Alternative Medicine*, 15, 220, https//doi.org/10.1186/s12906-015-0722-4

[6] Haryoto, M., Azizaha, T., Indrayudha, P., Suhendi, A. and Heng, K.H., 2014. Antioxidant, cytotoxic activities and chemical constituents of *Cynometra ramiflora* L.. *International Journal of Indigenous Medicinal Plants*, 47, 1578-1586.

[7] Jittimanee, J., Panomket, P. and Wanrum, S., 2013. Inhibition of prostaglandin E2 by substances derived from *Wrightia pubescens* latex in LPS-activated RAW 264.7 mouse macrophages. *Journal of Medical Technology and Physical Therapy*, 25, 36-42.

[8] Delos Reyes, M.M., Oyong, G.G., Ng, V.A.S., Shen, C. and Ragasa, C.Y., 2018. Cytotoxic compounds from *Wrightia pubescens* (R.Br.). *Pharmacognosy*, 10, 9-15.

[9] Schoch, C.L., Seifert, K.A., Huhndorf, S., Robert, V. Spouge, J.L., Andre Levesque, L., Chen, W. and Fungal Barcoding Consortium, 2012. Nuclear ribosomal internal transcribed spacer (ITS) region as a universal DNA barcode marker for fungi. *Proceedings of the National Academy of Science of the United Science of America*, 109, 6241-6246.

[10] Wang, X., Liu, C., Huang, L., Bengtsson-Palme, J. Chen, H., Zhang, J., Cai, D and Li, J., 2014. ITS1: a DNA barcode better than ITS2 in eukaryotes? *Molecular Ecology Resources*, 15, 573-586.

[11] Hebert, P.D.N., Ratnasingham, S. and deWaard, J.R., 2003. Barcoding animal life*:* Cytochrome c oxidase subunit 1 divergences among closely related species. *Proceedings of the Royal Society B: Biological Science*, 270 (Suppl 1*)*, S96-S99.

[12] Mbareche, H., Veillette, M., Bilodeau, G. and Duchaine, C., 2020. Comparison of the performance of ITS1 and ITS2 as barcodes in amplicon-based sequencing of bioaerosols. *Peerj*, 8, e8523, https://doi.org/10.7717/peerj.8523.

[13] Gardes, M. and Bruns, T.D., 1993. ITS primers with enhanced specificity for basidiomycets-application to the identification of mycorrhizae and rusts. *Molecular Ecology*, 2, 113-118.

[14] White, T.J., Bruns, T., Lee, S. and Taylor, J., 1990. Amplification and direct sequencing of fungal ribosomal RNA genes for phylogenetics. In: M.A. Innis, D.H. Gelfand, J.J. Sninsky and T.J. White, eds. *PCR Protocols: A Guide to Methods and Applications*. San Diago: Academic Press, pp. 315-322.

[15] Altschul, S.F., Madden, T.L., Schaffer, A.A., Zhang, J., Zhang, Z., Miller, W. and Lipman, D.J., 1997. Gapped BLAST and PSI-BLAST: a new generation of protein database search programs. *Nucleic Acids Research*, 25, 3389-3402.

[16] Kumar, S., Stecher, G., Li, M., Knyaz, C. and Tamura, K., 2018. MEGA X: Molecular evolutionary genetics analysis across computing platforms. *Molecular Biology and Evolution*, 35, 1547-1549.

[17] Tamura, K. and Nei, M., 1993. Estimation of the number of nucleotide substitutions in the control region of mitochondrial DNA in humans and chimpanzees. *Molecular Biology and Evolution*, 10, 512-526.

[18] Stecher, G. Tamura, K. and Kumar, S., 2020. Molecular evolutionary genetics analysis (MEGA) for macOS. *Molecular Biology and Evolution*, 37(4), 1237-1239.

[19] Taheri, H., Javan-Nikkhah, M., Elahinia, S.A., Khodaparast, S.A. and Golmohammadi. M., 2016. Species of *Colletotrichum* associated with citrus trees in Iran. *Mycologia Iranica*, 3, 1-14.

[20] Yang, Q., Jiang, N. and Tian, CM., 2020. Three new Diaporthe species from Shaanxi Province, China. *MycoKeys*, 67, 1-18.

[21] Farr, D.F., Lisa, A., Castlebury, A.M.Y., Rossman, Y. and Putnam, M.L., 2002. A new species of *Phomopsis* causing twig dieback of *Vaccinium vitis-idaea* (lingonberry). *Mycological Research*, 106, 745-752.

[22] Peres, N.A., Timmer L.W., Adaskaveg, J.E. and Corell, J.C., 2005. Lifestyle of *Colletotrichum acutatum*. *Plant Disease*, 89, 784-796.

[23] Crous, P.W., Wingfield, M.J., Burgess, T.I., Hardy, G., Gené, J., Guarro, J., Baseia, I.G., Garcia, D., Gusmão, L., Souza-Motta, C.M., Thangavel, R., Adamčík, S., Barili, A., Barnes, C.W., Bezerra, J., Bordallo, J.J., Cano-Lira, J.F., de Oliveira, R., Ercole, E., Hubka, V., Groenewald, J.Z. 2018. Fungal planet description sheets: 716-784. *Persoonia*, 40, 240-393.

[24] Lima, N.B., Batista, M.V.D.A., De Morais, Jr., M.A., Barbosa, M.A.G., Michereff, S.J., Hyde, K.D. and Câmara, M.P.S., 2013. Five *Colletotrichum* species are responsible for mango anthracnose in northeastern Brazil. *Fungal Diversity*, 61, 75-88.

[25] Gangadevi, V. and Muthumary, J., 2008. Isolation of *Colletotrichum gloeosporioides*: a novel endophytic taxol-producing fungus from the leaves of a medicinal plant. *Justicia gendarussa*. *Mycologia Balcanica*, 5, 1-4.

[26] Olson, T.R., Gabreil, A., Micijevic, A., Bradley, C.A., Wise, K.A., Mueller, D.S., Chilvers, M.I. and Mathew, F.M., 2015. Association of *Diaporthe longicolla* with black zone lines on mature soybean plants. *Plant Health Progress*, 16, 118-122.

[27] Preeti, V., Ramesha, B.T., Singh, S., Ravikanth, G., Ganeshaiah, K.N., Suryanarayanan, T.S. and Shaanker, R.U., 2009. How promising are endophytic fungi as alternative sources of plant secondary metabolites? *Current Science*, 104, 178-182.

[28] Serrato-Diaz, L.M., Rivera-Vargas, L.I. and French-Monar, R.D., 2014. First report of *Diaporthe pseudomangiferae* causing inflorescence rot, rachis canker and flower abortion of mango. *Plant Disease*, 98, 1004-1005.

[29] Haryoto, H., Muhtadi, M., Indrayudha, P., Azizah, T. and Suhendi, A., 2013. Activity of sitotoksik ethanol extract plant growth (*Cynometra ramiflora* Linn) on heavy cell, T47D and WiDR. *Journal Penelitian Saintek*, 18, 21-28.

[30] Freeman, S., Shabi, E. and Katan, T., 2000. Characterization of *Colletotrichum acutatum* causing anthracnose of anemone (*Anemone coronaria* L.). *Applied and Environmental Microbiology*, 66, 5267-5272.

[31] Quirós, M.B., Peres, N.A. and Arauz, L.F., 2013. Presence of *Colletotrichum acutatum* and *Colletotrichum gloeosporioides* on leatherleaf fern, key lime, papaya, star fruit, and mango in Costa Rica and Florida (United States). *Agronomía Costarricense*, 37, 23-38.

[32] Liu, H.X., Tan, H.B., Chen, Y.C., Li, S.N., Li, H.H. and Zhang, W.M., 2018. Secondary metabolites from the *Colletotrichum gloeosporioides* A12, an endophytic fungus derived from *Aquilaria sinensis*. *Natural Product Research*, 32, 2360-2365.

[33] Zang, L.Y., Wei, W., Wang, T., Guo, Y., Tan, R.X. and Hui-Ming, G.E., 2012. Isochromophilones from an endophytic fungus *Diaporthe* sp. *Natural Products and Bioprospecting*, 2, 117-120.

[34] Hemtasin, C., Kanokmedhakul, S., Kanokmedhakul, K., Hahnvajanawong, C., Soytong, K., Prabpai, S. and Kongsaeree, P., 2011. Cytotoxic pentacyclic and tetracyclic aromatic sesquiterpenes from *Phomopsis archeri. Journal of Natural Products*, 74, 609-13.

Current Applied Science and Technology Vol. 21 No. 3 (July-September 2021)

Effects of Natural Sugar on Acidogenic Potential, Biofilm Biomass, and Antiseptic Resistance of Oral Streptococci

Pimpikar Kanchanadumkerng[1] and Karn Wongsariya[2]*

[1]Department of Food Chemistry, Faculty of Pharmacy, Mahidol University, Bangkok, Thailand
[2]Department of Biology, Faculty of Science, King Mongkut's Institute of Technology Ladkrabang, Bangkok, Thailand

Received: 8 August 2020, Revised: 13 January 2021, Accepted: 3 February 2021

Abstract

Natural sugar is deliberated as ordinary, non-chemical, and healthy alternatives. However, a diet rich in sugar is well documented as a causative agent for dental caries. The purpose of this study was to investigate the effects of natural sugars, including raw cane, palmyra palm and coconut sugar on the acidogenic profiles, biofilm formation and antiseptic treatment efficacy compared with refined sugar. The study was based on single-species and dual-species of *Streptococcus mutans* ATCC 25175 and *Streptococcus sobrinus* ATCC 33402. Our results showed that sucrose was a major component of all samples, with percentages of relative content higher than 89.0. Palmyra sugar gave the least pH change at 180 min of 4.84-4.93, which indicated it was the least acidogenic. Coconut sugar formed the lowest level of biofilm biomass compared to refined sugar ($p < 0.05$) and other samples. Antiseptic treatment was performed to study the level of percent eradication of bacterial plaque using MTT assay to determine cell viability under biofilm in each sugar medium. Biofilm derived from coconut sugar had a susceptibility to antiseptic treatment with 56.2-61.99% eradication which was higher than the biofilm from palmyra and raw cane sugar. As a result, this study points out the effects of various natural sugars (especially different sources of plant material) on cariogenic potential. However, further experiment should be done to confirm the results *in vivo* and further study the cariogenic effects of diet supplementation of these fermentable sugars.

Keywords: natural sugar; sweetener; dental caries; biofilm
DOI 10.14456/cast.2021.41

1. Introduction

Dental caries is widespread condition affecting about one-third of the global population at all ages and is considered to be the most common noncommunicable disease (NCD) worldwide [1]. This multifactorial disease is a biofilm-mediated, sugar-driven, and dynamic circumstance resulting in the phasic demineralization and remineralization of tooth surface. Acidogenicity is a consequence

*Corresponding author: Tel.: (+66)2-329-8400 Fax: (+66)2-329-8412
E-mail: karn.wo@kmitl.ac.th

of microbial sugar metabolism which accelerates demineralization and results in caries lesions [2]. Mutans streptococci (MS) has long been connected with dental caries in humans. Certain species, including *Streptococcus mutans* and *Streptococcus sobrinus*, have been shown to be related to the incidences and activities of dental caries [3]. These bacteria are able to efficiently utilize free sugars and thus promote the formation of cariogenic biofilm [4]. Biofilm is a matrix of polysaccharides synthesized by bacterial glucosyltransferase which produces extracellular polysaccharides (EPS) from dietary sugar. Biofilm further promotes bacterial adhesion, and generates a microenvironment which enhances the growth of acidogenic and cariogenic bacteria [5]. Recent research has established that a single specific cause of dental caries is free sugars [6, 7]. WHO recommends avoiding the excessive consumption of added sugars or "free sugars" to prevent dental caries. Free sugars can be defined as all the monosaccharides and disaccharides added to, and naturally present in, foodstuff [8, 9]. These sugars serve as the building block of EPS which is the core of biofilm or dental plaque. It is now commonly accepted that sucrose, or table sugar, is the most cariogenic sugar because it is readily metabolized by mutans streptococci yielding glucose and fructose, from which EPS is made up and acid is produced [5, 10, 11]. Recently, natural sugar has attracted interest as an alternative sweetener due to it being natural and unrefined, full-flavored and sweet-scented. It is generally used as sweetener for beverages and desserts, especially traditional dishes. These natural sugars are produced from several tropical plants including sugarcane (*Saccharum officinarum* L.), and several species of palms such as coconut palm (*Cocos nucifera* L.), palmyra palm (*Borassus flabellifer* L.), nipa palm (*Nypa fruticans* Wurmb.) [12, 13]. Sugarcane is primarily used to produce table sugar, also known as white sugar, which is a refined product containing up to 99.9% sucrose. Non-refined sugar alternatives have also attracted the interest of a range of people due to their nutritional and antioxidant properties [12-14]. Raw and brown sugar from sugarcane showed antioxidant activity which was directly related to the degree of refining, and was due to the retention of phenols and flavonoids [13]. Many studies have reported on palm sap sugar characteristics such as proximate analysis, aroma profile, reducing sugars content and antioxidant activity [12]. Moreover, recent work indicated that due to its antioxidant and nutritional properties, coconut sap, the material from which coconut sugar is derived, was a potential healthier sugar source which had a low glycemic index [15].

Therefore, natural sugar has become a popular non-refined sugarcane alternative to refined white sugar and a possible healthier candidate to be used instead of it. As for our knowledge, there is no report of these alternatives on their cariogenic potential. It remains unclear whether natural sugars have different cariogenic potentials to refined sugar. In this study, two palm sap-based sugars and two sugarcane-derived sugars were evaluated for their cariogenicity. Acidogenicity or glycolytic pH drop from sugar metabolization by cariogenic bacteria was evaluated. Biofilm biomass were determined using crystal violet staining. Moreover, antiseptic treatment of biofilm-induced from different sugars was studied to evaluate the robustness of the microbial matrix and metabolic activity was assessed using MTT assay. Our aim was to evaluate the cariogenic potential of natural sugars compared to that of refined sugar. Our research may well offer a base for further *in vivo* and dietary studies of these sugars versus refined sugar as causative agents of dental caries.

2. Materials and Methods

2.1 Microorganisms and sample preparation

Streptococcus mutans ATCC 25175 and *Streptococcus sobrinus* ATCC 33402 were cultivated on Brain Heart Infusion agar (BHI agar) in candle extinction jar (5% CO_2) for 48 h at 37°C. Pure refined, raw cane, coconut (*Cocos nucifera* L.), and palmyra palm (*Borassus flabellifer* L.) sugar

were purchased from local stores and supermarkets in Bangkok, Thailand. All samples were dissolved in deionized water and prepared as stock solution at concentration of 20% w/v.

2.2 HPLC analysis of monosaccharide and disaccharide in natural sugar

The analysis was performed using a Chromaster HPLC system (Hitachi High-Tech Corporation, Japan) and refractive index detector (RID) (Chromaster 5450 model). Samples were injected at the volume of 20 µl and separated using Benson polymeric (BP-800 H+) column at 35ºC with deionized water as mobile phase. The flowrate applied was 0.5 ml/min with a run time of 30 min. Standard sucrose solutions were injected to obtain the retention time. Sucrose content was determined based on peak area and calculated as % relative content.

2.3 Analysis of Acidogenic potential

Acidogenic potential was determined according to the method of Stegues *et al.* [16] with some modifications. A purified single colony of tested bacteria was inoculated into BHI broth (5 ml) and incubated in candle extinction jar at 37°C for 18 h. The overnight culture was centrifuged at 8,000 rpm for 10 min, and cell pellets were resuspended in a mixture solution of 50 mM KCl and 1 mM $MgCl_2$ (pH 7.4) in order to maintain pH value of the mixture in neutral range, which correlated with physiological pH in oral cavity. The cell suspension was required with the optical density at 600 nm of 1.0 (approximately 10^9 cfu/ml). For co-culture, the mixture of *S. mutans* ATCC 25175 and *S. sobrinus* ATCC 33402 was prepared in the ratio of 1:1. Then 2 ml of bacterial suspension was transferred to 50 ml conical centrifuge tube that contained 18 ml of mixture solution supplemented with 2% w/v of the tested sugar. The pH value was monitored at different time points for 180 min (0, 5, 10, 15, 20, 25, 30, 40, 50, 60, 90, 120, 150, and 180 min) using a polycarbonate electrode (Ionix instruments, Singapore). Time duration of 180 min was based on the duration that microorganism used to decrease the pH value from neutral pH to critical pH. The mixture solution of 50 mM KCl and 1 mM $MgCl_2$ (pH 7.4) was used as a negative control.

2.4 Biofilm formation of oral streptococci

The biofilm of oral streptococci was grown in 96-well polystyrene plate. *Streptococcus mutans* ATCC 25175 and *S. sobrinus* ATCC 33402 were cultured in BHI broth (5 ml) at 37°C for 18 h, and after that the turbidity of overnight cultures was adjusted to 0.1 at optical density 600 nm (approximately 10^7 cfu/ml). Twenty microliters of bacterial suspension were added into 180 µl of BHI broth supplemented with tested sugar at concentration of 2% w/v. For dual-species biofilm, the mixture of *S. mutans* ATCC 25175 and *S. sobrinus* ATCC 33402 was prepared in the ratio of 1:1. The plates were then incubated and biofilm was allowed to form at 37°C for 24 h. Time duration for 24 h was based on the time needed for biofilm to mature and become well-attached.

2.5 Quantitation of biofilm biomass

To assess biofilm biomass, crystal violet (CV) assay as previously described method of He *et al.* [17] with some modifications was used. First, the growth medium was softly removed. Then the 96-well polystyrene microplates were washed three times with sterile phosphate-buffered saline (PBS), pH 7.4. The biofilm was fixed with 200 µl of absolute ethanol for 15 min, and after that the fixed biofilm was stained by adding 200 µl of CV solution (0.01% w/v). In order to remove the excess dye, the wells were rinsed three times with sterile PBS and 200 µl of DMSO was then added to solubilize the bound CV. The solubilized solution was transferred to a new 96-well polystyrene

microplates and measured the absorbance at a wavelength of 590 nm by microplate reader (Biochrom EZ Read 2000, UK).

2.6 Antiseptic treatment of biofilm-induced by different sugars

Biofilms of *S. mutans* ATCC 25175, *S. sobrinus* ATCC 33402, and dual-species was performed in 96-well polystyrene microplates using BHI broth supplemented with 2% w/v of tested sugars along with the negative control (BHI broth). Then, each biofilm was subjected to treatment with 0.12% w/v of chlorhexidine gluconate according to the following procedure. After washing with PBS, chlorhexidine gluconate solution was added and incubated for 1 min. Then, the antiseptic solution was removed and gently rinsed twice with sterile PBS (pH 7.4) to remove the residual antiseptics and dead cells. The remaining biofilm was assessed for metabolic activity of viable cells under the biofilm using 3-(4,5-dimethyl-thiazol-2-yl)-2,5-diphenyltetrazolium bromide (MTT) assay according to the method of Zhong *et al*. [18] with some modifications. Briefly, 200 µl of MTT solution (1 mg/ml, MTT in PBS (pH 7.4)) was added to biofilm and incubated under light protecting condition at 37°C for 3 h to allow the metabolically active cells to reduce the MTT into formazan crystals. After the designated time, excess MTT solution was removed, and the formazan crystals were solubilized by adding 150 µl of DMSO. The solubilized solution was transferred to a new 96-well polystyrene microplate and the absorbance at 560 nm was determined using microplate reader (Biochrom EZ Read 2000, UK). The percentage of eradication was calculated using the equation as described below:

$$\%\ Eradication = \frac{A-B}{A} x\ 100 \quad (1)$$

A was defined as the average absorbance of untreated biofilm, B was defined as the average absorbance of treated biofilm.

2.7 Statistical analysis

All experiments were carried out independently in triplicate. Data were represented as mean value ± standard deviation. For statistical analysis, IBM SPSS statistics 21 was used to perform the one-way analysis of variance (ANOVA) followed by Dunnett test to compare the test groups with the control group. Level of significance at 5% ($p < 0.05$) was considered to indicate statistically significant difference.

3. Results and Discussion

3.1 Composition of monosaccharide and disaccharide in natural sugar

The type of monosaccharide or disaccharide which was the major component in selected natural sugars was determined by using HPLC. The retention times and chromatograms of samples compared with standard sucrose were presented in Figure 1. The major peaks of all samples and standard sucrose were detected after 10 min with retention time in the range of 10.60-10.610 min. The results showed that that sucrose was the main component of refined sugar, palmyra sugar, coconut sugar, and raw cane sugar with percentages of relative content at 99.85, 99.73, 93.08, and 89.03, respectively (Table 1). In addition, glucose and fructose were presented in small amount in coconut sugar and palmyra sugar, with approximate retention time at 12.1 and 13.1 min (data not shown). The high level of sucrose in natural sugar might be one of the crucial factors related to the cariogenic potential of oral pathogens.

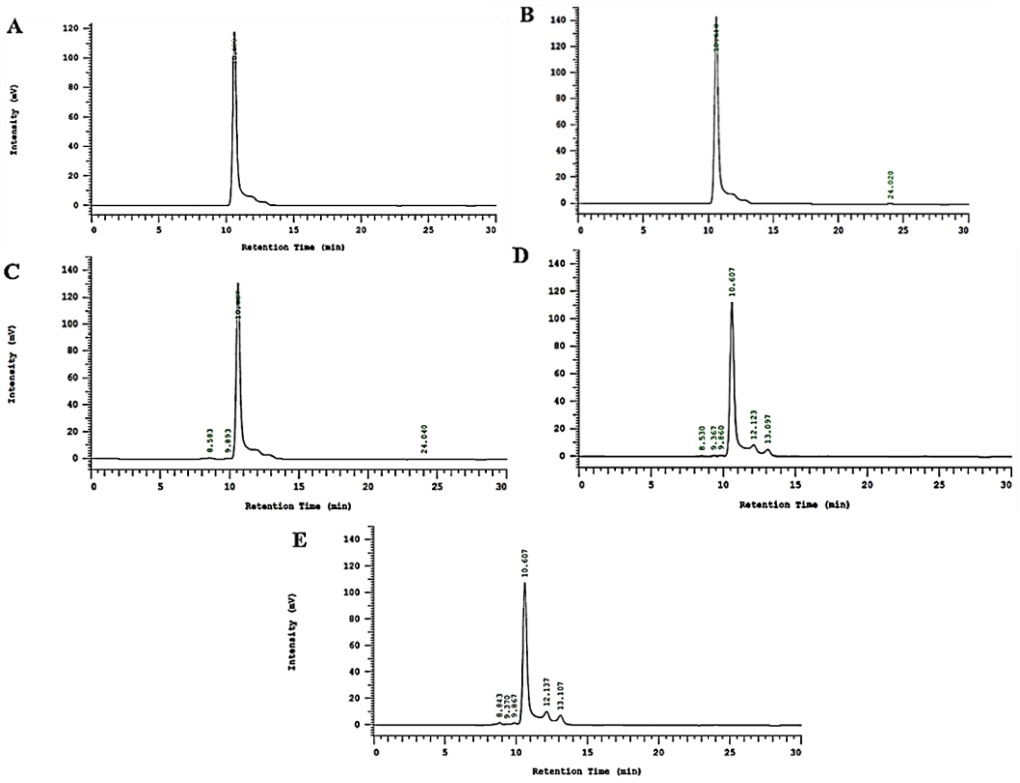

Figure 1. HPLC chromatographic profile of standard sucrose (A), refined sugar (B), raw cane sugar (C), coconut sugar (D), and palmyra sugar (E). The major peaks of standard sucrose, refined sugar, raw cane sugar, coconut sugar, and palmyra sugar were detected after 10 min.

Table 1. The HPLC analytical results of natural sugars

Samples	Retention time (min)	% Relative content of sucrose
Standard sucrose	10.600	100.00
Refined sugar	10.610	99.85
Raw cane sugar	10.607	99.73
Coconut sugar	10.607	93.08
Palmyra sugar	10.607	89.23

3.2 Acidogenicity

Glycolytic pH drop from sugar fermentation by cariogenic bacteria was shown in Figure 2. A similar pattern in pH fall curve was observed among various sugars in *S. mutans* ATCC 25175, *S. sobrinus* ATCC 33402 and co-culture. Significant difference of pH value for the four types of sugar was distinguished at 5 min ($p < 0.05$). Refined sugar showed significantly higher level of acidogenicity

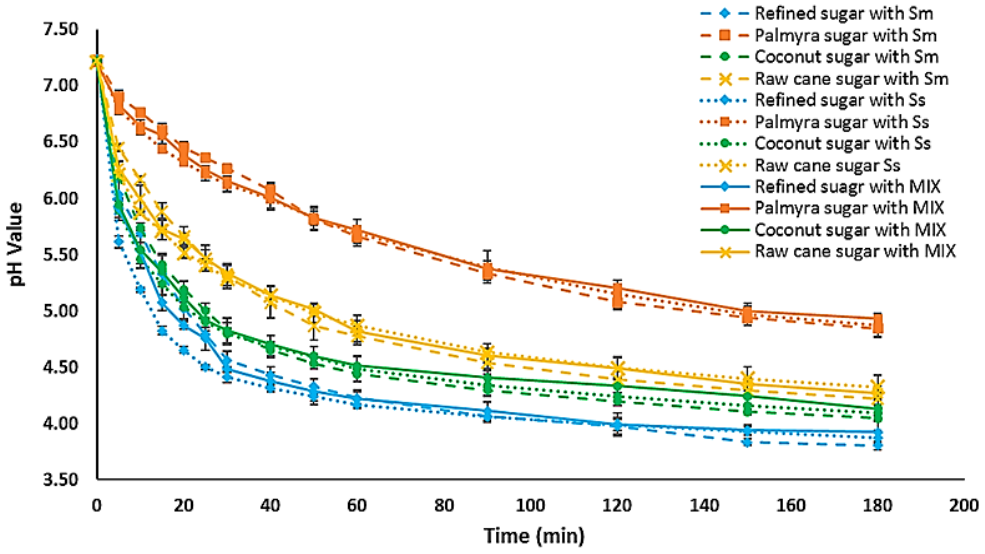

Figure 2. Acidogenic potential of *S. mutans* ATCC 25175 (Sm), *S. sorbrinus* ATCC 33402 (Ss), and co-culture (MIX) against refined sugar, raw cane sugar, coconut sugar, and palmyra sugar were presented as blue line, yellow line, green line, and brown line, respectively.

compared to other natural sugars in *S. mutans* ATCC 25175, *S. sobrinus* ATCC 33402 and co-culture at 5 min ($p < 0.05$), except that the variance between refined and coconut sugar in co-culture was observed for statistically difference at 15 min.

The presence of refined sugar influenced the pH fall the most, with the final pH values at 180 min of 3.80±0.04, 3.87±0.06 and 3.92±0.10 in *S. mutans* ATCC 25175, *S. sobrinus* ATCC 33402 and co-culture, respectively. Palmyra sugar resulted in the least pH change with the final pH values at 180 min of 4.84±0.07, 4.87±0.10 and 4.93±0.04 in *S. mutans* ATCC 25175, *S. sobrinus* ATCC 33402 and co-culture, respectively. Time to reach critical pH, which is acidic pH at 4.5-5.5 that affects the dental enamel of refined sugar fermentation faster than that of natural sugar fermentation. The slowest fermentation rate was found in palmyra sugar medium. It needed 90 min to reach a pH value of 5.3 whereas refined sugar took between 10 to 15 min. Hence, approximately about half of acidic end products were produced from glucose and sucrose [19]. According to the HPLC results, palmyra sugar showed the lowest sucrose content among the natural sugars resulting in the smallest pH dropping effect.

Even though sucrose is the major component of those natural sugars, brown color is from caramelization that occurs during production process from heat resulting in sucrose content reduction [12, 13]. As the same plant is the source of refined and raw cane sugar, it may well be that it is the degree of refining that results in different caloric nutrient or fermentable carbohydrate content in the sugar products. As reported by Seguí *et al*. [13], the sucrose contents in brown or non-refined sugarcane products ranged from 0.83 to 0.94 g per g product with low amount of glucose and fructose [13]. Moreover, retained components such as molasses and phenolic compounds in brown or non-refined sugarcane have been reported for their anti-mutans streptococci activities [20]. Recent study determined the sugar profile and total phenolic content of starting materials used for the production of natural sugars including sugarcane juice, coconut sap, and palm juice. Coconut sap had the highest monosaccharide and phenolic content [15]. As a result of this current study, sugar allocation in cariogenic bacteria may be one reason to explain the different effects of white and brown cane sugar on acidogenicity. In addition, it may primarily imply that impurities and

processing may affect some virulence factors of cariogenic microorganisms and more research is needed to clarify this.

3.3 Effect on biofilm biomass

The effect of sugar types on biofilm biomass based on crystal violet assay was shown in Figure 3 and Table 2. Compared to refined sugar, coconut sugar produced the least biofilm formation with statistically significance among all cariogenic biofilms ($p < 0.05$ in *S. mutans* ATCC 25175 and *S. sobrinus* ATCC 33402 biofilm and $p < 0.001$ in dual-species biofilm) whereas raw cane and palmyra sugar showed no significant difference from refined sugar. As describe above, the mono- and di-saccharide profile of tested sugar showed different sucrose content [15]. Sucrose influences pH change and promotes ecological and biofilm structural shift [11]. It is biologically described that external sucrose is used to produce extracellular polysaccharide (EPS), whereas internal sugars such as glucose or fructose are utilized for glycolysis and other mediated processes [21]. However, monosaccharide fructose plus glucose in combination can also cause caries [6]. On a dry basis, biofilm is mainly composed of cariogenic bacteria and EPS matrix which is created directly from sucrose substrate [22-24]. Previous study clearly demonstrated that sucrose formed cariogenic dental plaque to a greater degree than glucose plus fructose [10]. Duarte *et al.* [25] also reported that the polysaccharide matrix in sucrose supplementation was higher than in sucrose plus glucose supplementation. This suggests that the impurities in natural sugar provided less available substrate for EPS production, and this caused a decrease in the biofilm biomass which is consistent with the results of the current study.

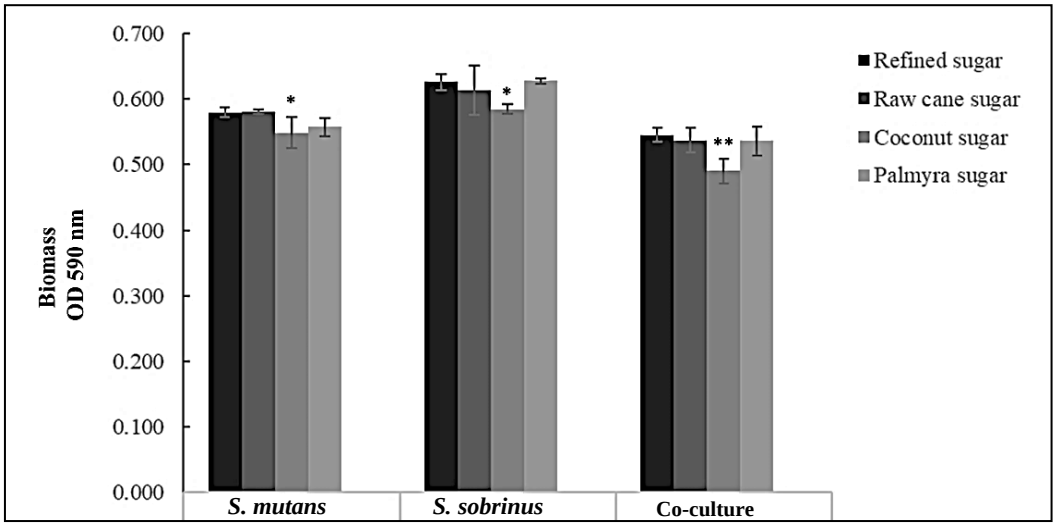

Figure 3. The effect of selected sugars (2% w/v) on biofilm formation of *S. mutans* ATCC 25175, *S. sobrinus* ATCC 33402, and co-culture. Statistical analysis was performed by one-way ANOVA followed by Dunnett t-tests by using refined sugar as control. Mean difference is significant at the level of significance: $p < 0.05$ (*) and $p < 0.001$ (**).

Table 2. Biofilm biomass based on crystal violet assay. Different superscript letters in the same column indicate significant differences at $p < 0.05$. Different capital letter in the same row indicates significant difference at $p < 0.05$ between bacterial individual and/or co-culture.

Biofilm formation (OD590 nm)	***S. mutans* ATCC 25175**	***S. sobrinus* ATCC 33402**	**Co-culture**
Refined sugar	0.580 ± 0.007^{aA}	0.626 ± 0.012^{aB}	0.545 ± 0.010^{aC}
Raw cane sugar	0.581 ± 0.003^{aA}	0.602 ± 0.041^{aB}	0.537 ± 0.019^{aA}
Coconut sugar	0.549 ± 0.023^{bA}	0.584 ± 0.007^{bB}	0.490 ± 0.019^{bC}
Palmyra sugar	0.557 ± 0.014^{aA}	0.628 ± 0.004^{aB}	0.536 ± 0.018^{aA}

Furthermore, the biofilm formation in the presence of coconut sugar yielded the lowest biomass level. This demonstrated that coconut sugar is not a suitable resource for biofilm formation of *S. mutans* ATCC 25175, *S. sobrinus* ATCC 33402, and co-culture when compared with refined sugar. This is preliminary data and human studies should be performed to confirm the effect of sugars on cariogenic plaque formation. In addition, the biofilm from *S. sobrinus* ATCC 33402 culture gave higher biomass than *S. mutans* ATCC 25175 and co-culture in all sugars. Acid by-products cause the micro-environment of dental plaque to be suitable for the growth of acid tolerant microbes. *Streptococcus sobrinus* strains are usually acidophilic and aciduric microbes [26, 27]. In addition, *S. sobrinus* can utilize glucose more efficiently than *S. mutans* [28]. In agreement with previous studies, *S. sobrinus* can produce more plentiful polysaccharide and may be more cariogenic than *S. mutans* [4].

3.4 Antiseptic treatment of biofilm

Palm-derived sugars gave less metabolically active microorganisms than refined sugar ($p < 0.05$ in co-culture biofilm in the presence of palm-derived sugars) (Table 3). The percentage of eradication was shown in Figure 4. After 1-min contact with 0.12% chlorhexidine, biofilm in the refined sugar medium was the most susceptible to antiseptic with 71.7% eradication of *S. sobrinus* ATCC 33402 biofilm while raw cane sugar dependent biofilm was the most resistant to antiseptic with 36.5% eradication of *S. mutans* ATCC 25175 biofilm.

Previous reports have mentioned that crude cane and molasses contained a protective agent that had an anticariogenic effect. In brown sugar, an anti-caries mechanism involved an enzyme inhibitor and its mineral content that reduced demineralization [29, 30]. This was contrary to our result in which raw cane sugar had more viability biofilm cells, and this may be due to the response to antiseptic of planktonic cells and microbes in biofilm being different. Usually, bacteria incorporated into biofilms are more resistant to antimicrobial agents than planktonic cells [31]. In addition, the different kinds of mono- or di-saccharide and other components in various natural sugars may affect the susceptible to antiseptics of cariogenic bacteria within biofilm. A different medium can have different effects on the bacterial growth, cell amount, glucosyltransferase (GTF) activity, and insoluble glucan yield [32].

Previous studies demonstrated that biofilm formed in sucrose media was significantly thicker than that in high fructose corn syrup media [33]. Moreover, the quality of unrefined sugars had variation based on source materials and non-standard processing technologies [34]. The analysis of compounds that responsible for the effect of microbial biofilm should be accomplished.

In addition, *S. sobrinus* can utilize glucose efficiently when compared to *S. mutans* [28]. In agreement with previous studies, *S. sobrinus* produced more plentiful polysaccharides and may be more cariogenic than *S. mutans* [4].

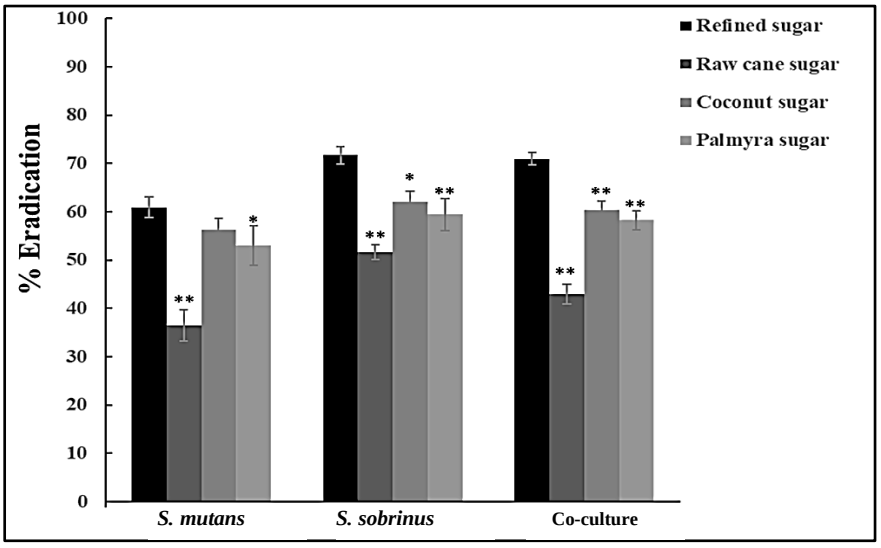

Figure 4. Percent eradication of viable cells under the biofilm after treated with antiseptic. Statistical analysis was performed by one-way ANOVA followed by Dunnett t-tests using refined sugar as control. Mean difference is significant at the level of significance: $p < 0.05$ (*) and $p < 0.001$ (**).

Table 3. Viable cell analysis of 24-h biofilm (before and after antiseptic treatment) by MTT assay. Different superscript letters in the same column indicate significant differences at $p < 0.05$.

Biofilm viable cell (OD560)	***S. mutans* ATCC 25175**		***S. sobrinus* ATCC 33402**		**Co-culture**	
	Untreated	Treated	Untreated	Treated	Untreated	Treated
Refined sugar	1.233 ± 0.025^{a}	0.482 ± 0.017^{a}	1.490 ± 0.062^{a}	0.422 ± 0.010^{a}	1.210 ± 0.031^{a}	0.351 ± 0.009^{a}
Raw cane sugar	1.189 ± 0.010^{a}	0.756 ± 0.043^{b}	1.414 ± 0.034^{a}	0.685 ± 0.014^{b}	1.200 ± 0.030^{a}	0.685 ± 0.007^{b}
Coconut sugar	1.210 ± 0.032^{a}	0.530 ± 0.043^{a}	1.433 ± 0.091^{a}	0.545 ± 0.013^{b}	1.130 ± 0.041^{b}	0.448 ± 0.008^{b}
Palmyra sugar	1.218 ± 0.019^{a}	0.573 ± 0.048^{a}	1.377 ± 0.043^{a}	0.559 ± 0.036^{b}	1.139 ± 0.030^{b}	0.476 ± 0.017^{b}

4. Conclusions

Natural sugar is commonly used in cultural dishes and desserts in Asia and South East Asia. However, fermentable carbohydrate, especially sugar, plays a pivotal role in the development of dental caries. This study aimed to clarify the cariogenic potential of various alternative natural sugars. The results of this study suggest that the palm-derived sugars, coconut and palmyra sugar, may have less acidogenic potential than refined sugars, and furthermore biofilm from palm-derived

sugars contained less metabolically active microorganisms than biofilm from refined sugar. Due to the variation in traditional processing and sources, sugar profile and presence of other compounds found in natural sugars need to be individually analyzed. Assuredly, analyses of virulence-related factors and biofilm such as confocal laser scanning microscopy and fluorescent staining should be conducted. Further studies included in *vivo*, and *in situ* investigations and studies involving human volunteers need to be performed to further discover and clarify the effects of sugar type on dental caries.

5. Acknowledgements

This research was kindly supported by Department of Biology, Faculty of Science, KMITL, Thailand and Department of Food Chemistry, Faculty of Pharmacy, Mahidol University, Thailand.

References

[1] Kassebaum, N.J., Smith, A.G.C., Bernabé, E., Fleming, T.D., Reynolds, A.E., Vos, T., Murray, C.J.L., Marcenes, W. and GBD 2015 Oral Health Collaborators, 2017. Global, regional, and national prevalence, incidence, and disability-adjusted life years for oral conditions for 195 countries, 1990-2015: a systematic analysis for the global burden of diseases, injuries, and risk factors. *Journal of Dental Research*, 96(4), 380-387.

[2] Pitts, N.B., Zero, D.T., Marsh, P.D., Ekstrand, K., Weintraub, J.A., Ramos-Gomez F, Tagami J, Twetman, S, Tsakos, G. and Ismail, A., 2017. Dental caries. *Nature Reviews Disease Primers*, 3(1), 1-16.

[3] Okada, M., Kawamura, M., Oda, Y., Yasuda, R.I.E., Kojima, T. and Kurihara, H., 2012. Caries prevalence associated with *Streptococcus mutans* and *Streptococcus sobrinus* in Japanese schoolchildren. *International Journal of Paediatric Dentistry*, 22(5), 342-348.

[4] Zhan, L., 2018. Rebalancing the caries microbiome dysbiosis: targeted treatment and sugar alcohols. *Advances in Dental Research*, 29(1), 110-116.

[5] Bowen, W.H., Burne, R.A., Wu, H. and Koo, H., 2018. Oral biofilms: pathogens, matrix, and polymicrobial interactions in microenvironments. *Trends in Microbiology*, 26(3), 229-242.

[6] Sheiham, A. and James, W.P.T., 2014. A reappraisal of the quantitative relationship between sugar intake and dental caries: the need for new criteria for developing goals for sugar intake. *BMC Public Health*, 14(1), 863.

[7] Giacaman, R.A., 2018. Sugars and beyond. The role of sugars and the other nutrients and their potential impact on caries. *Oral Diseases*, 24(7), 1185-1197.

[8] WHO, 2015. *Guideline: Sugars Intake for Adults and Children*. Geneva: World Health Organization.

[9] Moynihan, P., 2016. Sugars and dental caries: evidence for setting a recommended threshold for intake. *Advances in Nutrition*, 7(1), 149-156.

[10] Cury, J.A., Rebelo, M.A.B., Cury, A.D.B., Derbyshire, M.T.V.C. and Tabchoury, C.P.M., 2000. Biochemical composition and cariogenicity of dental plaque formed in the presence of sucrose or glucose and fructose. *Caries Research*, 34(6), 491-497.

[11] Leme, A.P., Koo, H., Bellato, C.M., Bedi, G., and Cury, J.A., 2006. The role of sucrose in cariogenic dental biofilm formation-new insight. *Journal of Dental Research*, 85(10), 878-887.

[12] Saputro, A.D., Van de Walle, D. and Dewettinck, K., 2019. Palm sap sugar: A review. *Sugar Tech*, 21(6), 862-867.

[13] Seguí, L., Calabuig-Jiménez, L., Betoret, N. and Fito, P., 2015. Physicochemical and antioxidant properties of non-refined sugarcane alternatives to white sugar. *International Journal of Food Science & Technology*, 50(12), 2579-2588.
[14] Phillips, K.M., Carlsen, M.H. and Blomhoff, R., 2009. Total antioxidant content of alternatives to refined sugar. *Journal of the American Dietetic Association*, 109(1), 64-71.
[15] Asghar, M.T., Yusof, Y.A., Mokhtar, M. N., Ya'acob, M.E., Mohd Ghazali, H., Chang, L. S. and Manaf, Y.N., 2020. Coconut (*Cocos nucifera* L.) sap as a potential source of sugar: Antioxidant and nutritional properties. *Food Science & Nutrition*, 8(4), 1777-1787.
[16] Stegues, C. G., Arthur, R. A. and Hashizume, L. N., 2016. Effect of the association of maltodextrin and sucrose on the acidogenicity and adherence of cariogenic bacteria. *Archives of Oral Biology*, 65, 72-76.
[17] He, Z., Huang, Z., Jiang, W. and Zhou, W., 2019. Antimicrobial activity of cinnamaldehyde on *Streptococcus mutans* biofilms. *Frontiers in Microbiology*, 10, 2241.
[18] Zhong, H., Xie, Z., Wei, H., Song, Y. and Wang, M., 2019. Antibacterial and Antibiofilm Activity of Temporin-GHc and Temporin-GHd Against Cariogenic Bacteria, *Streptococcus mutans*. *Frontiers in Microbiology*, 10, 2854.
[19] Aizawa, S., Miyasawa-Hori, H., Nakajo, K., Washio, J., Mayanagi, H., Fukumoto, S. and Takahashi, N., 2009. Effects of α-amylase and its inhibitors on acid production from cooked starch by oral streptococci. *Caries Research*, 43(1), 17-24.
[20] Takara, K., Ushijima, K., Wada, K., Iwasaki, H. and Yamashita, M., 2007. Phenolic compounds from sugarcane molasses possessing antibacterial activity against cariogenic bacteria. *Journal of Oleo Science*, 56(11), 611-614.
[21] Kawada-Matsuo, M., Oogai, Y. and Komatsuzawa, H., 2017. Sugar allocation to metabolic pathways is tightly regulated and affects the virulence of *Streptococcus mutans*. *Genes*, 8(1), 11.
[22] Razak, F.A., Baharuddin, B.A., Akbar, E.F.M., Norizan, A.H., Ibrahim, N.F. and Musa, M.Y., 2017. Alternative sweeteners influence the biomass of oral biofilm. *Archives of Oral Biology*, 80, 180-184.
[22] Koo, H., Xiao, J., Klein, M.I. and Jeon, J.G., 2010. Exopolysaccharides produced by *Streptococcus mutans* glucosyltransferases modulate the establishment of microcolonies within multispecies biofilms. *Journal of Bacteriology*, 192(12), 3024-3032.
[24] Gupta, P., Gupta, N., Pawar, A.P., Birajdar, S.S., Natt, A.S. and Singh, H.P., 2013. Role of sugar and sugar substitutes in dental caries: a review. *International Scholarly Research Notices*, 2013.
[25] Duarte, S., Klein, M.I., Aires, C.P., Cury, J.A., Bowen, W.H. and Koo, H., 2008. Influences of starch and sucrose on *Streptococcus mutans* biofilms. *Oral Microbiology and Immunology*, 23(3), 206-212.
[26] Coulter, J., Jakubovics, N.S., Preshaw, P.M. and German, M.J., 2019. An in vitro model to assess effects of a desensitising agent on bacterial biofilm formation. *Acta Biomaterialia Odontologica Scandinavica*, 5(1), 1-8.
[27] Conrads, G., de Soet, J.J., Song, L., Henne, K., Sztajer, H., Wagner-Döbler, I. and Zeng, A.P., 2014. Comparing the cariogenic species *Streptococcus sobrinus* and *S. mutans* on whole genome level. *Journal of Oral Microbiology*, 6(1), 26189.
[28] Homer, K.A., Patel, R.U.P.A.L. and Beighton, D.A.V.I.D., 1993. Effects of N-acetylglucosamine on carbohydrate fermentation by *Streptococcus mutans* NCTC 10449 and *Streptococcus sobrinus* SL-1. *Infection and immunity*, 61(1), 295-302.
[29] Jaffé, W.R., 2015. Nutritional and functional components of non centrifugal cane sugar: A compilation of the data from the analytical literature. *Journal of Food Composition and Analysis*, 43, 194-202.
[30] Jaffé, W.R., 2012. Health effects of non-centrifugal sugar (NCS): a review. *Sugar Tech*, 14(2), 87-94.

[31] Liu, C., Worthington, R. J., Melander, C. and Wu, H., 2011. A new small molecule specifically inhibits the cariogenic bacterium *Streptococcus mutans* in multispecies biofilms. *Antimicrobial Agents and Chemotherapy*, 55(6), 2679-2687.

[32] Wiater, A., Choma, A. and Szczodrak, J., 1999. Insoluble glucans synthesized by cariogenic streptococci: a structural study. *Journal of Basic Microbiology: An International Journal on Biochemistry, Physiology, Genetics, Morphology, and Ecology of Microorganisms*, 39(4), 265-273.

[33] Ma, R., Sun, M., Wang, S., Kang, Q., Huang, L., Li, T. and Xia, W.W., 2013. Effect of high-fructose corn syrup on the acidogenicity, adherence and biofilm formation of *Streptococcus mutans*. *Australian Dental Journal*, 58(2), 213-218.

[34] Lee, J.S., Ramalingam, S., Jo, I.G., Kwon, Y.S., Bahuguna, A., Oh, Y.S., Kwon, O.J. and Kim, M., 2018. Comparative study of the physicochemical, nutritional, and antioxidant properties of some commercial refined and non-centrifugal sugars. *Food Research International*, 109, 614-625.

Current Applied Science and Technology Vol. 21 No. 3 (July-September 2021)

Improvement in Plasticity Behavior of Residual Clay Soil via Bio-cementation Technique

Muttaqa Uba Zango[1,2]*, Khairul Anuar Kassim[1], Abubakar Sadiq Muhammed[1,3], Kamarudin Ahmad[1], Murtala Umar[4] and Jodin Makinda[1]

[1]School of Civil Engineering, Universiti Teknologi Malaysia, Johor, Malaysia
[2]Department of Civil Engineering, Kano University of Science and Technology, Kano, Nigeria
[3]Department of Civil and Water Resources Engineering, University of Maiduguri, Borno, Nigeria
[4]Department of Civil Engineering, Bayero University Kano, Kano, Nigeria

Received: 10 October 2020, Revised: 21 January 2021, Accpeted: 4 February 2021

Abstract

Enzyme-induced calcium carbonate precipitation (EICP) is a bio-inspired technique that uses urease to activate the urea-hydrolysis reaction to produce $CaCO_3$ precipitation. This study was conducted to assess the effect of cementation solution concentrations on the plasticity and swell behavior of residual clay soil. The findings showed that the plasticity behaviour of the residual soil was improved. The liquid limit of the residual clay soil decreased from 79% to 58.8%, plastic limit increased from 30% to 47.8%, plasticity index decreased from 49% to 11% and linear shrinkage limit decreased from 16 to 4.3%, and these results reflected an increase in calcium carbonate precipitation from 0% in the untreated soil to 4.09% in the EICP soil sample treated at 1.00 M concentration of cementation solution. The SEM and EDX results indicated the presence of $CaCO_3$ crystals in the treated residual soil, while XRD analysis confirmed the formation of calcite crystals in the treated soil.

Keywords: biocementation; plasticity behaviour; residual clay soil; enzyme-induced calcium carbonate precipitation (EICP)
DOI 10.14456/cast.2021.42

1. Introduction

Recently, research on soil improvement has shifted towards the use of green, environmentally friendly, and sustainable techniques [1-3]. Biocementation through either microbially-induced calcite precipitation (MICP) or enzymatically-induced calcium carbonate precipitation (EICP) is a green, environmentally friendly, and sustainable technique that utilizes ureolytic bacteria or free urease enzyme respectively, to synthesize calcium carbonate through the hydrolysis of urea and calcium-rich compounds [4-6]. The mechanism of MICP and EICP can be summarised in two equations (1 and 2), as shown below:

*Corresponding authour: Email: muttaqaubaz@yhoo.com

$$H_2N - CO - NH_2 + 2H_2O \xrightarrow{Urease} 2NH_4^+ + CO_3^{2-} \quad (1)$$

$$Ca^{2+} + CO_3^{2-} \rightarrow CaCO_3 \quad (2)$$

The majority of reported studies on biogeotechnology for soil improvement are centered around improvements in the strength, stiffness and permeability of granular soil via MICP [3, 7]. Despite several studies on MICP documented in various literature, only a few number of researches [8-12] were conducted on MICP in fine-grained soils. A limited number of studies on MICP in fine-grained soils is attributed to the inability of bacteria to pass through the pore throats of the soil, which are smaller than 0.4 μm [13].

In order to overcome treatment difficulties associated with MICP in fine-grained soils, enzymatically-induced calcium carbonate precipitation (EICP) has been adopted, which uses a free urease enzyme instead of urease produced by ureolytic bacteria [14, 15]. EICP has a similar mechanism to MICP, in which calcium carbonate is precipitated via ureolysis, as described in equations 1 and 2 above.

Previous studies conducted on EICP mostly focused mostly on improving strength the of sandy soils. For instance, Rohy *et al*. [16] adopted a one-phase injection method of various concentrations of EICP solution (urea, $CaCl_2$, and urease solution) at low pH to improve a uniformly graded silica sand. Almajed *et al*. [17] improved the strength of silica sand using an EICP solution that was modified with an organic stabilizer (non-fat milk). Simatupang and Okamura [18] used the EICP technique to improve the liquefaction resistance of a sandy soil prepared at various degrees of saturation. Other research works [19-22] utilized the EICP solution to increase the shear strength of sandy soils.

Although a small number of studies such as Chandra and Karangat [23] and Cuccurullo *et al*. [24] were conducted on the use of the EICP technique to improve the engineering and physical properties of fine-grained soils, the use of the EICP technique to improve the plasticity behavior of fine-grained soils has not been investigated. There is a need to investigate the effect of calcite formation via the EICP technique on the plasticity behavior of fine-grained soils, especially for the application in the design of compacted clay liner.

This work presents the effect of a biocement produced via the EICP technique on the plasticity and swelling characteristics of residual clay soil. The effect of varying the concentration of cementation solution (urea and $CaCl_2$) on the Atterberg limits of the residual clay soil was also investigated.

2. Materials and Method

2.1 Materials

The materials used to investigate the effect of enzymatically-induced calcite precipitation on the plasticity behavior of residuals are residual soil and EICP solution.

2.1.1 Tropical residual soil

The soil used for this work was retrieved through the disturbed sampling method from 1.5 m below the ground borrow pit at Universiti Teknologi Malaysia, Skudai Campus (1°33’35’’ N, 103°38’38’’E). The climate of the sampling area is a tropical rainforest and has a basement complex geologic formation.

2.1.2 EICP recipe

The EICP solution prepared for treating the residual soil consisted of free urease enzyme and the cementation solution. The free urease enzyme was extracted from the jack bean. The free urease enzyme was procured from Fischer Scientific Sdn Bhd, Malaysia. The urease activity of the enzyme was reported to be 3,500 U/g. The cementation solution was a mixture of urea ($CO(NH_2)_2$) and calcium chloride dihydrate($CaCl_2.2H_2O$). The concentration and composition of the EICP solution used in this study are presented in Table 1 below.

Table 1. Composition of EICP solution

Concentration (M)	Urease (g/l)	Urea (g/l)	$CaCl_2.H_2O$ (g/l)
0.25	3	15	36.6
0.50	3	30	73.2
0.75	3	45	109.8
1.00	3	60	146.4

The EICP solutions were prepared by first dissolving the amounts of urea ($CO(NH_2)_2$) and calcium chloride dihydrate($CaCl_2.2H_2O$) calculated as shown in Table 1 in a distilled and deionized water in Scott bottles. The dissolved urea and calcium chloride is herewith referred to as cementation solution. Then, equivalent free urease enzyme in powdered form was added to the cementation solution and the mixture was vigorously mixed until all the powdered urease enzyme were dissolved. The mixture of urea, calcium chloride and urease enzyme are known as EICP solution.

2.2 Methods

The work involved in this study involved mainly laboratory tests that have a connection with the plasticity behavior of a fine-grained soil. The tests were performed on both untreated natural soil and EICP treated soil.

2.2.1 EICP treatment

The soil to be treated with the EICP solution was initially prepared by oven drying and then sieving through a 425 µm sieve. About 500 g of the sieved soil was then mixed homogeneously with the EICP solution at different concentrations, as prepared in section 2.1.2 and presented in Table 1. The volume of the EICP solution taken for each mixture was 79% of the mass of dry soil, which corresponded to the liquid limit of the untreated soil. The procedure for the treatment was adopted from Osinubi *et al*. [25]. The soil-EICP solution mixtures (in paste form) were then cured for three days in a humidity chamber that was operating at 25 ± 2°C and 100% relative humidity. The soil-EICP pastes were then subjected to Atterberg limits tests, as explained in section 2.2.2.

2.2.2 Determination of index properties of the natural soil

The natural soil was characterized by conducting a particle size analysis, and Atterberg limits and specific gravity tests. The particle size analysis was conducted on the natural soil by combining wet and dry sieving, as outlined in British Standard Methods of test for soils for civil engineering purposes [26]. The retrieved natural soil from the borrow pit was initially air-dried. About 1 kg of the air-dried soil was then soaked in a solution of sodium metahexaphosphate for about 24 h. The wet soil was then washed through a 2 mm BS sieve. The soil retained on the 2 mm sieve was dried

in an oven and then sieved through a series of BS sieves from 28 mm down to 2 mm. The particle size analysis of wet soil passing through 2 mm and down to nanoscale was performed using a laser light scattering, automated particle size analyzer.

The Atterberg limits tests, including liquid limit, plastic limit and linear shrinkage tests on the natural and EICP treated soil were performed following the procedure enshrined in British Standard Methods of test for soils for civil engineering purposes [26]. The specific gravity of the natural untreated soil was determined by conducting a pyknometer test using small bottles as prescribed in British Standard Methods of test for soils for civil engineering purposes [26].

2.2.3 Determination of calcium carbonate content (CCC)

The dried samples after the Atterberg limits tests were used for the determination of calcium carbonate content. A gravimetric acid wash method, as reported in Choi *et al*. [27], was adapted for the determination of calcium carbonate content. The CCC was determined by allowing about 20 - 25 g each of the natural and treated soils to dissolve in a 4 M HCl solution for 24 h. The wet soils were rinsed and washed thoroughly with water for about 10 min and then filtered. The soils retained on the paper were oven-dried. The weight of the dried sample before acid digestion and the dried sample after acid digestion was determined. Equation (3) below was used to calculate the calcium carbonate content in the soil.

$$CCC = 100 - \left(\frac{B}{A}\right) \times 100 \tag{3}$$

CCC = Calcium carbonate content (%)
B = Mass of oven-dried soil post washing
A = Mass of oven-dried treated soil before washing

2.2.4 Microstructural analysis

In order to determine the morphology and molecular nature of the precipitation formed, microstructural analyses such as SEM, EDX and XRD were conducted on the natural and EICP treated soils at 0.50 M cementation solution. The XRD analysis was performed using a Rigaku SmartLab 9kW XRD machine, while a Hitachi SU8020 SEM machine was the instrument employed to conduct SEM-EDX analyses.

3. Results and Discussion

3.1 Index properties of the natural soil

The physical properties of the natural soil are summarised in Table 2. The soil is classified as gravelly clay of very high plasticity in the British Standard Classification System (BSCS). The dominant mineral in the soil is kaolinite as revealed by the XRD analysis conducted on the natural soil. The liquid limit and plastic limit of the natural soil are found to be 79% and 49%, respectively. It can be seen that the PI of the natural soil is higher than the recommended upper limit of 30% as suggested by Widomski *et al.* [28] and in Solid Waste Disposal Facility Criteria Technical Manual [29] for a compacted clay liner. As stated in EPA [29], clay soils with plasticity indices of higher than 30% tend to be challenging to work with when wet, and when dry, such soils could form hard clods that could provide a path for leachate to infiltrate. Therefore the soil plasticity index needs to be improved. One such method of improvement could be via enzymatically-induced calcium carbonate precipitation.

Table 2. Physical properties of the natural soil

Property	Quantity
Natural Moisture Content (%)	32.72
Percentage Passing 63 μm Sieve (%)	57
Gravel Fraction (%)	24.16
Sand Fraction	17.16
Liquid Limit (%)	79
Plastic Limit (%)	30
Plasticity Index (%)	49
Linear Shrinkage (%)	16
Specific Gravity	2.63
Loss on Ignition (LOI) (%)	12.28
BSCS Classification	CVG (Gravelly Clay of Very High Plasticity)
Colour	Reddish Brown
Clay Minerals	Kaolinte

3.2 Plasticity behaviour of EICP treated soil

Figure 1 shows the effect of concentration of cementation solution and calcium carbonate content on the Atterberg limits of treated soils. It can be seen from the graph that as the concentration of cementation solution increases, the liquid limit (LL), plasticity index (PI) and linear shrinkage limit (LS) decrease, while the plastic limit increases. The increase in the concentration of cementation reagents goes with the rise in calcium carbonate content formed in the treated soil. For instance, the natural soil has LL, PI, and SL of 79%, 49% and 16%, respectively. Upon treatment with EICP solution at 0.25 M concentration urea-$CaCl_2$, the values of LL, PI and LS drop to 64.5%, 22.59%, 10%. Further increments in the concentration of urea-$CaCl_2$ lead to continous decrease in the LL, PI and LS until the minimum values of 58.8%, 11.01% and 4.29%, respectively at 1.00 M urea-CaCl2 concetration are reached. Similar pattern of results were reported by Choobbasti *et al*. [30] and Yazarloo *et al*. [31]. Moravej *et al*. [32] also reported that the reduction of LL and PI from 42 to 34% and 19 to 10%, respectively was due to the bio-treatment of dispersive soil via MICP. Kannan *et al*. [33] also determined that LL and PI of treated marine clay decreased upon treatment via both biostimulation and bioaugmentation with MICP. Furthermore, an increase in plastic limits was also reported by Choobbasti *et al*. [30]. The reduction in the LL, PI and LS in EICP treated soils can be attributed to the reduction in the the thickness of the diffused double layer due to the replacement of hydrogen ions by the calcium from the calcium carbonate precipitation formed [30, 34]. The decrement in liquid limit is desirable in improving the plastic behavior of natural soils for compacted clay liner applications.

3.3 Relationship between Atterberg Limits and calcium carbonate content

Figure 2 shows the relationship between Atterberg limits and calcium carbonate precipitation formed in the EICP treated soils. The Figure also compared the results obtained in this study with those reported by Choobbasti *et al*. [30]. The reason for choosing Choobbasti *et al*. [30] for comparison with the results obtained in this research is to demonstrate that EICP treatment is equally viable in enhancing plasticity behaviour of soil as was the nano calcium carbonate from different

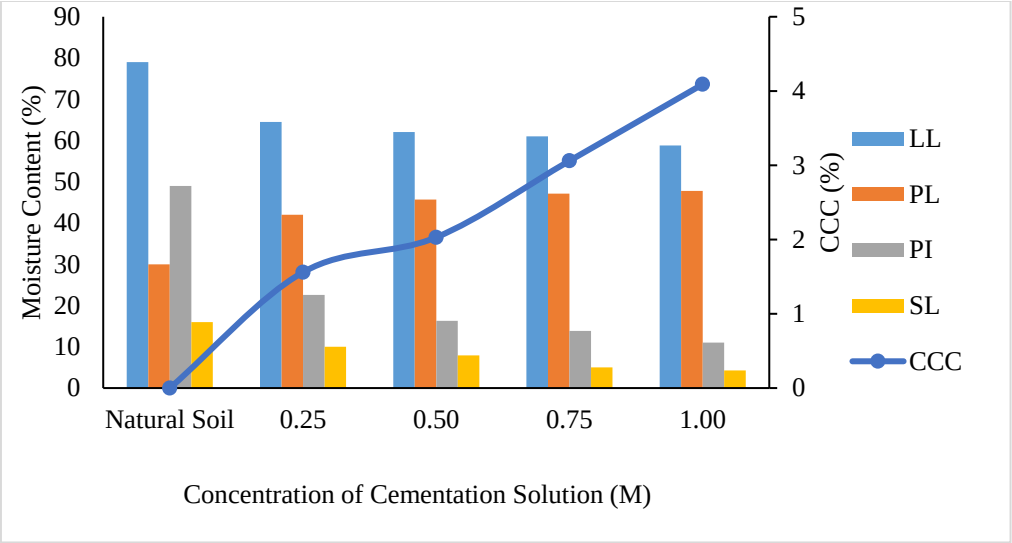

Figure 1. Variation of Atterberg limits with cementation solution and calcium carbonate content

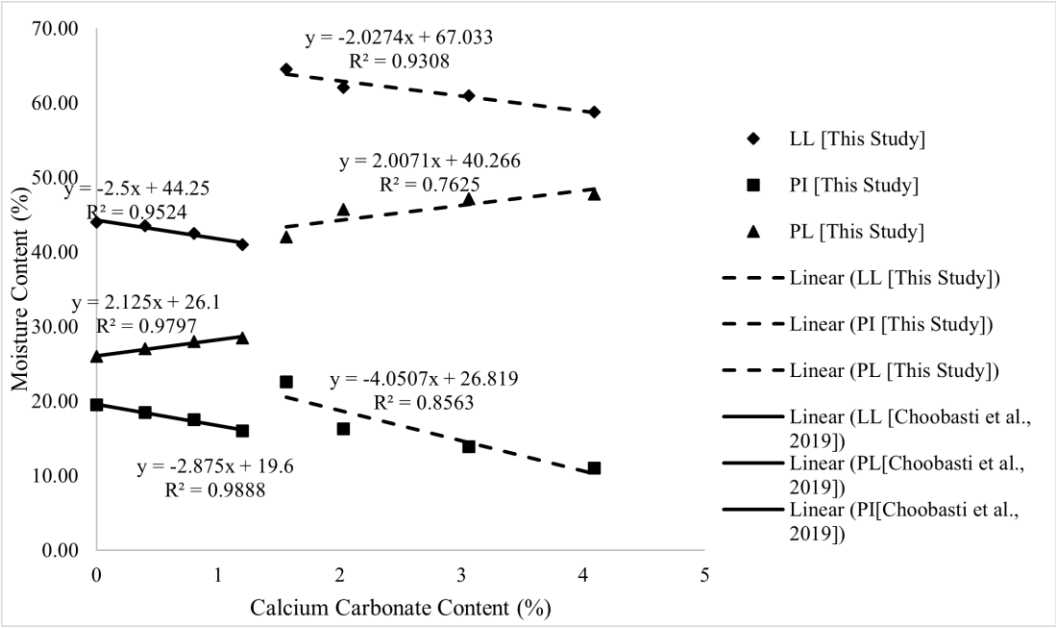

Figure 2. Relationship between Atterberg Limits with calcium carbonate content

sources of Choobbasti *et al*. [30]. As can be seen in the Figure, there is a linear inverse relationship between liquid limit and calcium carbonate precipitations formed. The variation between LL and CCC obtained is consistent with that reported by Choobbasti *et al*. [30]. The coefficient of regression for the variation of LL with CCC was found to be 0.9308 for this studies while that of Choobbasti *et al*. [30] was 0.952. The Figure also depicts that plastic limits increase with the increment in the

calcium carbonate precipitations as shown in this study and also PL rises with the increment in nano-calcium carbonate as reported in Choobbasti *et al*. [30]. It can also be seen in the Figure that plasticity index falls steadily with the increment in both calcium carbonate precipitations (as found in this study) and nano calcium carbonate as reported in Choobbasti *et al*. [30]. The variation between PI and CCC have R^2 values of 0.8563 and 0.9888 in this study and Choobbasti *et al*. [30], respectively. Similarly Musso *et al*. [35] and Howayek *et al*. [36] also reported decrease in liquid limit with increase in calcium carbonate. The decrease in LL and corresponding increase and decrease in PL and PI, respectively can also be explained in terms of cementation of soil particles through the action of calcium carbonate precipitates formed from biocementation technique [32]. Howayek *et al*. [36] also attributed increase in liquid limt and plasticity index of soil to the increase in surface area when cementation between, in this case carbonate, was removed from the soil aggregates. Thus, the decrease in LL and PL limits in this study can be associated with the formation of cementation between clay particles due to the formation of calcium carbonates via EICP.

3.4 Microstructure analysis

3.4.1 X-Diffraction (XRD) analysis

XRD analysis was conducted on both the untreated and treated EICP residual to determine the change in the mineral content due to EICP treatment. Figure 3 (a and b) depicts XRD patterns in both the untreated and EICP treated soil. Kaolinite was found to be the dominant mineral in the untreated soil, and the peaks showing the presence of calcite or calcium carbonate minerals detected as shown in Figure 3(a). XRD pattern depicted in Figure 3 (b) shows the presence of calcium carbonate and calcite minerals in addition to kaolinite mineral. Thus, EICP treatment resulted in the formation of calcite minerals in the soil. The presence of calcite minerals due EICP treatment was reported in sandy soils by Yasuhara *et al*. [19].

3.4.2 Scanning electron microscope (SEM) and electron dispersive X-ray (EDX)

The scanning electron microscope (SEM) and energy dispersive X-ray (EDX) analyses were performed on the natural soil and treated soil in order to confirm the formation of calcium carbonate in the EICP treated soil. Figure 4 shows the SEM and EDX analyses of both natural and treated soils. Calcium carbonate crystals were deposited on the treated soil (see Figure 4 (b)). The presence of calcium carbonate was confirmed by EDX analysis and is shown on the SEM images. As shown in Figure 4 (b), in addition to oxygen, calcium and carbon were detected in the treated soil which indicates the production of calcium carbonate as result of the biocementation via EICP technique, where as there was no detection of calcium and carbon in the untreated soil as depicted in Figure 4 (a). This indicates that $CaCO_3$ was responsible for the improvement in the plasticity behaviour of the EICP treated soil. The finding in this study is supported by studies reported by Almajed *et al*. [17] and Kavazanjian and Hamdan [37]. For instance, Kavazanjian and Hamdan [37] observed formation of visible white precipitates on the SEM images of EICP treated soil. The precipitations were verified to be $CaCO_3$ minerals by EDX analysis.

It should be noted that the amount of calcium carbonate content (CCC) determined using gravemetric acid for 0.50 M EICP treated soil was 2.03%, which was higher than the percentage of calcium, 1.7%, as determined by the EDX method. The reason for this discrepancy as explained by Choi *et al*. [27], could be that CCC determined from gravimetric acid wash of the EICP treated soil may tend to be overestimated due to dissolution of non-calcium carbonate substance. Nevertheless, the results obtained from gravimetric acid wash, XRD, SEM-EDX have confirmed the production of calcium carbonate precipitation due to EICP treatment.

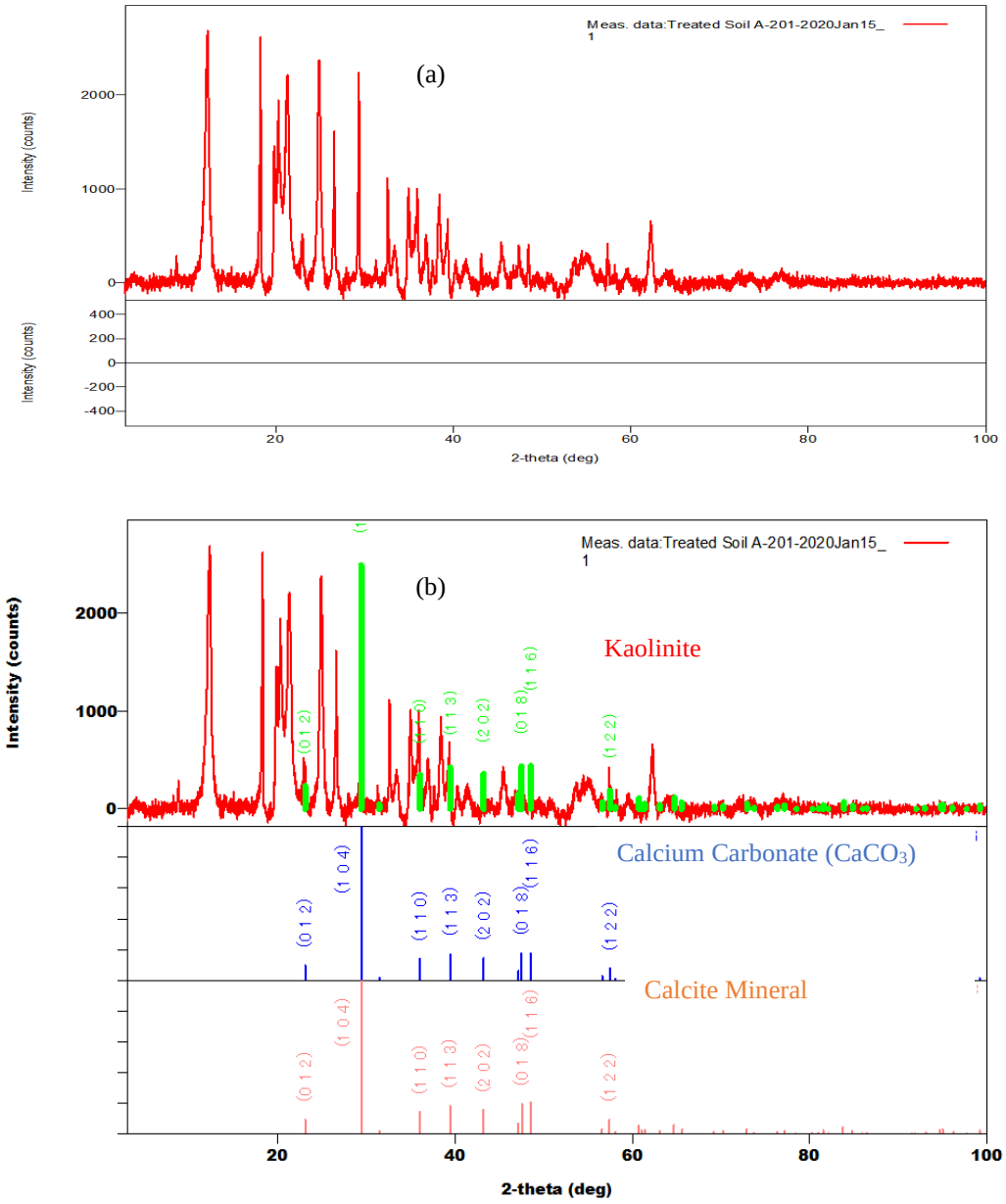

Figure 3. XRD pattern of (a) untreated residual soil and (b) EICP treated residual soil

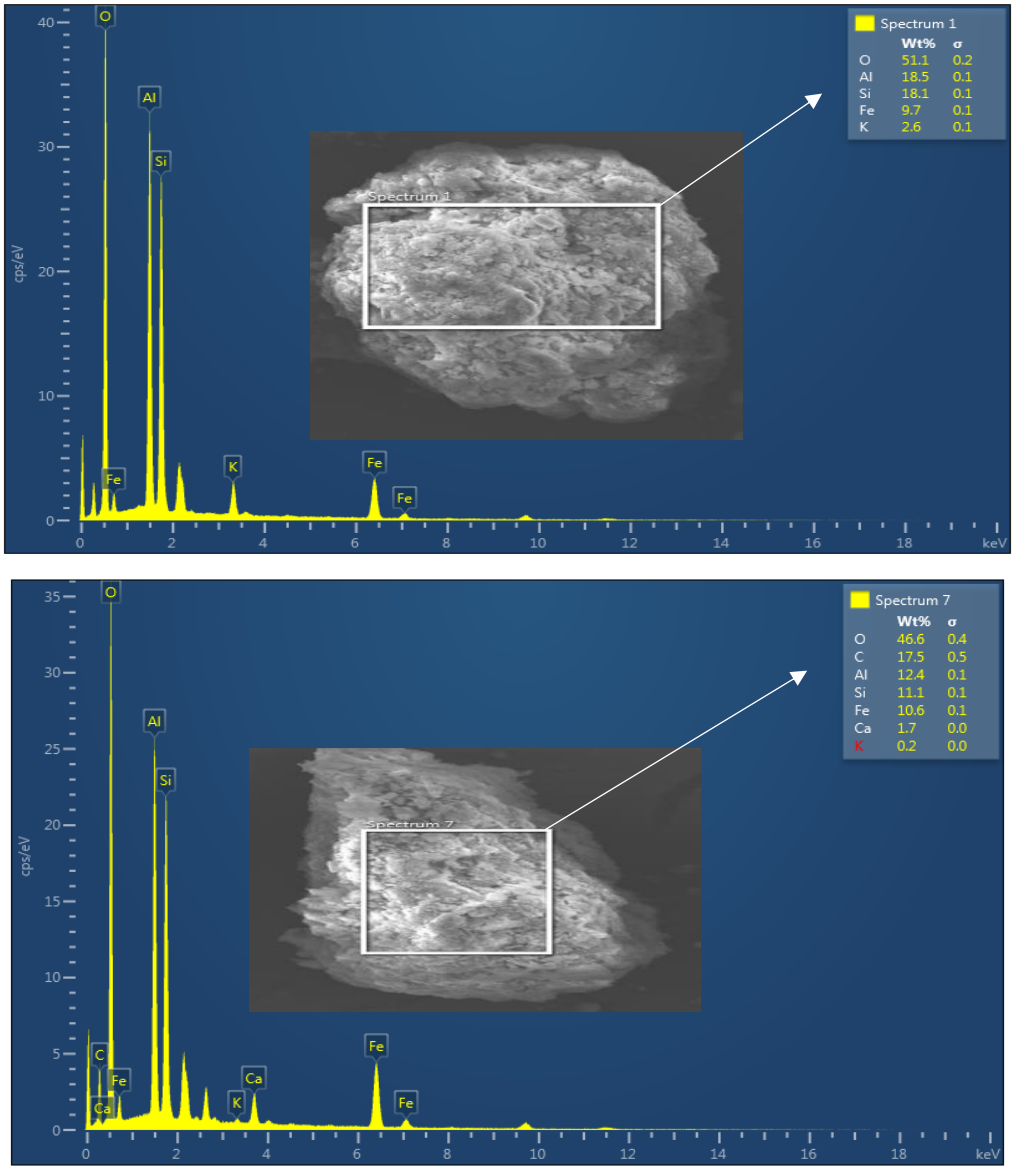

Figure 4. SEM and EDX analysis of (a) untreated residual, (b) EICP-treated soil at 0.50 M

4. Conclusions

In this study, an enzymatically-induced calcite precipitation technique for improving the plasticity and swelling behavior of residual clay soil was presented. The following conclusions are made:

i. It was found that due to the EICP treatment on the residual soil, the plasticity and swelling characteristics of treated soil were improved.

ii. The liquid limit, plasticity index and MFSI of the treated soil were found to decrease with an increase in the calcium carbonate content due to an increment in the concentration of cementation solution.
iii. The formation of calcium carbonate precipitation was confirmed via SEM and EDX analyses, and the formation of calcite was established through XRD analysis.

5. Acknowledgements

The authors gratefully acknowledge the financial support from the Malaysian Ministry of Higher Education (MOHE) through the Fundamental Research Grant Scheme (FRGS): (R.J130000.7851.5F256), GUP from UTM: Q.J130000.2522.20H21 and Q.J130000.2451.04G57 from UTM. The first and last authors also acknowledge the funding coming from the Nigerian Government through TETFUND.

References

[1] Achal,V., Mukherjee, A., Kumari, D. and Zhang, Q., 2015. Biomineralization for sustainable construction - A review of processes and applications. *Earth-Science Reviews*, 148, 1-17.
[2] Anbu, P., Kang, C.-H., Shin, Y.-J. and So, J.-S., 2016. Formations of calcium carbonate minerals by bacteria and its multiple applications. *Springerplus*, 5, 250, https://doi.org/10.1186/s40064-016-1869-2.
[3] Wang, Z., Zhang, N., Cai, G., Jin, Y., Ding, N. and Shen, D., 2017. Review of ground improvement using microbial induced carbonate precipitation (MICP). *Marine Georesources & Geotechnology*, 35(8), 1135-1146.
[4] Omoregie, A.I., Ngu, L.H., Ong, D.E.L. and Nissom, P.M., 2019. Low-cost cultivation of *Sporosarcina pasteurii* strain in food-grade yeast extract medium for microbially induced carbonate precipitation (MICP) application. *Biocatalysis and Agricultural Biotechnology*, 17(11), 247-255.
[5] Wen, K., Li, Y., Amini, F. and Li, L., 2020. Impact of bacteria and urease concentration on precipitation kinetics and crystal morphology of calcium carbonate. *Acta Geotechnica*, 15(1), 17–27.
[6] Umar, M., Kassim, K.A. and Chiet, K.T. P., 2016. Biological process of soil improvement in civil engineering: A review. *Journal of Rock Mechanics and Geotechnical Engineering*, 8(5), 767-774.
[7] Tian, Z.-F., Tang, X., Xiu, Z-L.. and Xue, Z.-J., 2020. Effect of different biological solutions on microbially induced carbonate precipitation and reinforcement of sand. *Marine Georesources & Geotechnology*, 38(4), 450-460.
[8] Liu, B., Zhu, C., Tang, C.-S., Xie, Y.-H., Yin, L.-Y., Cheng, Q. and Shi, B., 2020. Bio-remediation of desiccation cracking in clayey soils through microbially induced calcite precipitation (MICP). *Engineering Geology*, 264(11), 105389, https://doi.org/10.1016/j.enggeo.2019.105389.
[9] Morales, L., Garzón, E., Romero, E. and Sánchez-Soto, P.J., 2019. Microbiological induced carbonate ($CaCO_3$) precipitation using clay phyllites to replace chemical stabilizers (cement or lime). *Applied Clay Science*, 174(3), 15-28.
[10] Vail, M., Zhu, C., Tang, C.S., Anderson, L., Moroski, M. and Montalbo-Lomboy, M.T., 2019. Desiccation cracking behavior of MICP_treated bentonite. *Geosciences*, 9(9), 385, https://doi.org/10.3390/geosciences9090385

[11] Li, M., Fang, C., Kawasaki, S. and Achal, V., 2018. Fly ash incorporated with biocement to improve strength of expansive soil. *Scientific Report*, 8, https://doi.org/10.1038/s41598-018-20921-0

[12] Hataf, N. and Baharifard, A., 2020. Reducing soil permeability using microbial induced carbonate precipitation (MICP) method : A case study of Shiraz landfill soil. *Geomicrobiology Journal*, 37(2), 147-158.

[13] Mitchell, J.K. and Santamarina, J.C., 2005. Biological considerations in geotechnical engineering. *Journal of Geotechnical and Geoenvironmental Engineering*, 131(10), https://doi.org/10.1061/(ASCE)1090-0241(2005)131:10(1222)

[14] Hamdan, N., Kavazanjian, E. and O'Donnell, S., 2013. Carbonate cementation via plant derived urease. *Proceedings of the 18th International Conference on Soil Mechanics and Geotechnical Engineering*, Paris, France, 2013, 2489-2492.

[15] Almajed, A., Tirkolaei, H.K. and Kavazanjian, E., 2018. Baseline investigation on enzyme-induced calcium carbonate precipitation. *Journal Geotechnical and Geoenvironmental Engineering*, 144 (11), https://doi.org/10.1061/(ASCE)GT.1943-5606.0001973

[16] Rohy, H., Arab, M., Zeiada, W., Omar, M., Almajed, A. and Tahmaz, A., 2019. One phase soil bio-cementation with eicp-soil mixing. *Proceedings of the 4th World Congress on Civil, Structural, and Environmental Engineering*, https://doi.org/10.11159/icgre19.164

[17] Almajed, A., Tirkolaei, H.K., Kavazanjian, E. and Hamdan, N., 2019. Enzyme induced biocementated sand with high strength at low carbonate content. *Scientic Reports*, 9(1), 1135, https://doi.org/10.1038/s41598-018-38361-1

[18] Simatupang, M and Okamura, M., 2017. Liquefaction resistance of sand remediated with carbonate precipitation at different degrees of saturation during curing. *Soils and Foundations*, 57(4), 619–631.

[19] Yasuhara, H., Neupane, D., Hayashi, K and Okamura, M., 2012. Experiments and predictions of physical properties of sand cemented by enzymatically-induced carbonate precipitation. *Soils and Foundations*, 52(3), 539-549.

[20] Neupane, D., Yasuhara, H., Kinoshita, N. and Unno, T., 2013. Applicability of enzymatic calcium carbonate precipitation as a soil-strengthening technique. *Journal of Geotechnical and Geoenvironmental Engineering*, 139(12), 2201-2211.

[21] Zhao, Z., Hamdan, N., Shen, L., Nan, H., Almajed, A., Kavazanjina, E. and He, X., 2016. Biomimetic hydrogel composites for soil stabilization and contaminant mitigation. *Environmental Science and Technology*, 50(22), 12401-12410.

[22] Oliveira, P.J.V., Freitas, L.D. and Carmona, J.P.S.F., 2017. Effect of soil type on the enzymatic calcium carbonate precipitation process used for soil improvement. *Journal of Materials and Civil Engineering*, 29(4), https://doi.org/10.1061/(ASCE)MT.1943-5533.0001804

[23] Chandra, A. and Karangat, R., 2019. Effect of magnesium incorporation in Enzyme Induced Carbonate Precipitation (EICP) to improve shear strength of soil. In A. Prashant, A. Sachan, and C.S. Desai, eds. *Advances in Computer Methods and Geomechanics*, https://doi.org/10.1007/978-981-15-0890-5_28

[24] Cuccurullo, A., Gallipoli, D., Bruno, A.W., Augarde, C., Hughes, P. and Borderie, C.L., 2019. Advances in the enzymatic stabilisation of soils. *Proceedings of the XVII European Conference: Geotechnical Engineering Foundation of the Future*. September, 2019, https://doi.org/10.32075/17ECSMGE-2019-0987.

[25] Osinubi, K.J., Eberemu, A.O., Gadzama, E.W. and Ijimdiya, T.S., 2019. Plasticity characteristics of lateritic soil treated with Sporosarcina pasteurii in microbial-induced calcite precipitation application. *SN Applied Sciences*, 1, 829, https://doi.org/10.1007/s42452-019-0868-7.

[26] BS 1377-2, 1990. *Methods of Test for Soils for Civil Engineering Purposes-Part 2: Classification Tests.* London: British Standards Institute.

[27] Choi, S.-G., Park, S.-S., Wu, S. and Chu, J., 2017. Methods for calcium carbonate content measurement of biocemented soils. *Journal of Material and Civil Engineering*, 29(11), https://doi.org/10.1061/(ASCE)MT.1943-5533.0002064.
[28] Widomski, M.K., Stepniewski, W. and Musz-Pomorska, A., 2018. Clays of different plasticity as materials for landfill liners in rural systems of sustainable waste management. *Sustainability*, 10(7), 2489, https://doi.org/10.3390/su10072489
[29] EPA, 1993. *Solid Waste Disposal Facility Criteria. Technical Manual*. Washington D.C.: United States Environmental Protection Agency.
[30] Choobbasti, A.J., Samakoosh, M.A. and Kutanaei, S.S., 2019. Mechanical properties soil stabilized with nano calcium carbonate and reinforced with carpet waste fibers. *Constructions and Building Materials*, 211, 1094-1104
[31] Yazarloo, R., Katooli, F.A., Golestani, M., Asadi, M. and Ebrahimi, S., 2017. Adding calcite and nanocalcite to improving the plastic properties of the lean clay. *Proceeding of the 3rd World Congress on New Technology*, Rome, Italy, June 6-8, 2017, https://doi.org/10.11159/icnfa17.106.
[32] Moravej, S., Habibagahi, G., Nikooee, E. and Niazi, A., 2017. Stabilization of dispersive soils by means of biological calcite precipitation. *Geoderma*, 315, 130-137.
[33] Kannan, K., Bindu, J. and Vinod, P., 2020. Engineering behaviour of MICP treated marine clays. *Marine Georesources and Geotechnology*, 38(7), 761-769.
[34] Pei, X., Zhang, F., Wu, W. and Liang, S., 2015. Physicochemical and index properties of loess stabilized with lime and fly ash piles. *Applied Clay Science*, 114, 77-84.
[35] Musso, G., Chighini, S. and Romero, E., 2008. Mechanical sensitivity to hydrochemical processes of Monastero Bormida clay. *Water Resources Research*, 44(5), https://doi.org/10.1029/2007wr006533
[36] Howayek, A.E., Bobet, A. and Santagata, M., 2019. Microstructure and cementation of two carbonatic fine-grained soils. *Canadian Geotechnical Journal*, 56(3), 320-334.
[37] Kavazanjian, E. and Hamdan, N., 2015. Enzyme induced carbonate precipitation (EICP) columns for Ground Improvement. *Proceedings of the International Foundations Congress and Equipment Expo*, Texas, USA, https://doi.org/10.1061/9780784479087

Elicitation of Salicylic Acid on Secondary Metabolite Production and Antioxidant Activity of *In Vitro Musa acuminata* L. cv. 'Gros Michel' Shoots

Yaowapha Jirakiattikul[1]*, Panumart Rithichai[1], Kanokwan Songsoem[1] and Arunporn Itharat[2]

[1]Department of Agricultural Technology, Faculty of Science and Technology, Thammasat University, Rangsit Centre, Khlong Nueng, Khlong Luang, Pathum Thani, Thailand
[2]Department of Applied Thai Traditional Medicine, Faculty of Medicine, Thammasat University, Rangsit Centre, Khlong Nueng, Khlong Luang, Pathum Thani, Thailand

Received: 28 September 2020, Revised: 23 December 2020, Accepted: 12 February 2021

Abstract

In vitro Musa acuminata L. cv. 'Gros Michel' is a potential alternative source of secondary metabolites but low yield was obtained. Elicitation is used to increase secondary metabolite production by many plant species. The objective of this study was to investigate the effect of salicylic acid (SA), an elicitor, on secondary metabolite accumulation and antioxidant activity in shoot cultures of *M. acuminata* cv. 'Gros Michel'. Shoots of one centimeter in length were cultured for four weeks on Murashige and Skoog (MS) medium supplemented with 22.19 µM 6-benzyladenine (BA) and 0, 100, 200, or 300 µM SA. The results showed that SA was effective in enhancing the secondary metabolite production and antioxidant activity of *M. acuminata* cv. 'Gros Michel' shoots. The contents of secondary metabolites and antioxidant activity were significantly different among the treatments. Shoots treated with 100 µM SA exhibited the greatest accumulation of total saponins (263.86±0.42 mg diosgenin/ g dry extract), total phenolics (124.44±8.39 mg GAE/g dry extract), and total flavonoids (105.26±6.43 mg CE/g dry extract). These were 1.27, 1.25, and 1.34 times that of the control. The strongest antioxidant radical scavenging was also observed from 100 µM SA treated shoots (DPPH EC_{50} value of 9.79±0.86 µg/ml and ABTS EC_{50} value of 86.66±1.50 µg/ml).

Keywords: antioxidant; elicitor; phenolics; salicylic acid; saponins
DOI 10.14456/cast.2021.43

*Corresponding author: Tel.: (+66) 8545092
E-mail: yjirakia@tu.ac.th

1. Introduction

Musa acuminata belongs to family Musaceae. Its fruits are a rich source of secondary metabolites including vitamins, phenolics, carotenoids, biogenic amines and phytosterols. Some of these compounds perform as antioxidants and are useful for human health [1]. *Musa acuminata* is a wild species of banana distributed in tropical regions of South East Asia [2]. 'Gros Michel' is one of the triploid cultivars of *M. acuminata*, and has the genome AAA. It is a seedless cultivar and is usually eaten raw [1, 3]. Traditional doctors use *M. acuminata* fruit, peel, pseudostem, flower, leaf, and root for the treatment of cancer, allergies, fever, coughs, and diabetes mellitus [2]. Onyema *et al*. [4] reported that *M. acuminata* pseudostem had pharmaceutical value, containing flavonoids, phenolic compounds, saponins, tannin, alkaloids, oxalate, hemagglutinin, phytate, and cardiac glycoside. Saponins are secondary metabolites that normally accumulate in plants and are involved in plant defenses against pathogens, pests, and herbivores [5]. Biological and pharmacological properties of these compounds have been reported such as antiphlogistic, antihepatotoxic, hypoglycemic, and antiallergic [6]. Phenolic compounds and flavonoids are secondary metabolites with polyphenol structures and are also produced as defense mechanisms [7]. They possess several biological activities including antioxidant effects, anticancer [8, 9], anti-inflammatory, and cardio-protective effects [9].

Plant tissue culture has been used for mass propagation of several plant species of *Musa* [10-13]. This *in vitro* technique offers both plant multiplication and secondary metabolite production from cells and organs, as each cell maintains a complete genetic information [7, 14]. A single cell can develop into a new plantlet and is able to synthesize the same secondary metabolites as the parent plant grown under natural conditions [14]. Production of secondary metabolites from plant tissue culture offers shorter production cycles, a constant product supply, consistent quality and independence from climatic factors [7, 14]. Studies of medicinal plants have identified secondary metabolite contents with antioxidant properties, but production may be low [7, 15]. Elicitation is an effective technique for enhancing secondary metabolite production under aseptic conditions. Type and concentration of elicitor significantly affect elicitation. It is necessary to determine the optimum elicitor type and concentration for each plant species [16, 17]. Salicylic acid (SA) has been widely used as elicitor inducing defensive mechanisms in many plant species [16]. SA is a phenolic compound that is normally found as a phytohormone [18]. Enhancement of secondary metabolite accumulation by SA has been reported for *Taxus chinensis* [19], *Hypericum hirsutum* [20], *Jatropha curcas* [21], *Thevetia peruviana* [22], *Chlorophytum borivilianum* [23], *Fagonia indica* [24], *Centella asiatica* [25], and *Piper cumanense* [26]. However, SA has not yet been applied to *M. acuminata* cv. 'Gros Michel'. In this study, the effect of SA at different concentrations on enhancement of total saponins, total phenolic compounds, and total flavonoids including antioxidants was investigated using *in vitro* shoot cultures of *M. acuminata* cv. 'Gros Michel'.

2. Materials and Methods

2.1 Plant material and culture conditions

In vitro shoots of *M. acuminata* cv. 'Gros Michel' were subcultured at four week intervals on Murashige and Skoog (MS) medium supplemented with 22.19 µM 6-benzyladenine (BA) and 3% (w/v) sucrose until sufficient regenerated shoots were available. The medium pH was adjusted to 5.6-5.8 with 1 N NaOH prior to gelling with 0.8% (w/v) agar, followed by autoclaving at 121°C for 15 min. The cultures were incubated at 25±2° C with a photoperiod of 16 h under fluorescent lamps with light intensity of 3,000 lx.

2.2 Preparation of elicitors

A stock SA solution at a concentration of 0.1 M (BDH Prolabo, Belgium) was prepared following Wang *et al*. [19]. This was dissolved in absolute ethanol and diluted with distilled water. The solution was filter sterilized before adding to the culture medium through a 0.22 µm syringe filter.

2.3 Elicitation treatments

Four-week-old *in vitro* shoots of *M. acuminata* cv. 'Gros Michel' were used as the explants. Shoots were cut into samples approximately one centimeter in length and cultured on MS medium supplemented with 22.19 µM BA and 100, 200, or 300 µM SA for four weeks. MS medium supplemented with only 22.19 µM BA was used as a control. The experiment used a completely randomized design with four treatments and three replications. Shoots were harvested and the shoot fresh weight was recorded. The shoots were dried at 50ºC for 48 h and the dry weight was recorded. Extracts were prepared by powdering the dried sample with pestle and mortar. The ground samples were macerated with ethanol at the ratio of 1:3 (sample: ethanol) for three days. Extracts were filtered, evaporated in a hot air oven at 50ºC for 48 h, and kept at -20ºC until use.

2.4 Determination of total saponin content

Total saponin content was measured using a vanillin-sulfuric assay modified from Hiai *et al*. [27]. One milligram of plant extract was dissolved in 2 ml of absolute ethanol and sonicated for 1 min. A sample of 0.25 ml was mixed with 0.25 ml of 8% vanillin reagent and 2.5 ml of 72% H_2SO_4. The mixture was incubated in a water bath at 60ºC for 10 min then cooled to 25ºC for 10 min. Absorbance was measured at 544 nm using a microplate reader (PowerWave XS-BT-MQX200R). The total saponin content was reported as mg diosgenin/ g dry extract.

2.5 Determination of total phenolic content

Total phenolic content was measured using the Folin–Ciocalteu method, following Jirakiattikul *et al.* [28]. Plant extract solution at a concentration of 1 mg/ml was sonicated for 1 min. A sample of 20 µl was mixed with 100 µl of dilute Folin-Ciocalteu reagent and 80 µl of 7.5% (w/v) sodium carbonate solution. The solution was incubated at 25ºC for 30 min and the absorbance was measured at 765 nm using a microplate reader. The total phenolic content was reported as mg GAE/g dry extract (mg of gallic acid equivalents per g dry extract).

2.6 Determination of total flavonoid content

Total flavonoid content determined using a modified method of Zhu *et al*. [29]. Plant extract solution at a concentration of 1 mg/ml was prepared. A sample of 500 µl was mixed with 75 µl of 5% (w/v) $NaNO_2$ for 6 min, then 150 µl of 10% (w/v) $AlCl_3$ was added. After a 5-min reaction, 500 µl of 1M NaOH and 275 µl of distilled water were added. The solution was left for 15 min and the absorbance was measured at a wavelength of 510 nm. Flavonoid content was determined using a catechin standard calibration curve and the results were expressed as mg CE/g dry extract (mg catechin equivalents per g dry extract).

2.7 Determination of antioxidant activity

2.7.1 DPPH radical scavenging assay

The scavenging capacity was evaluated following Yamasaki *et al*. [30]. Plant extract solution was prepared at a concentration of 1 mg/ml, and 100 µl was mixed with 100 µl of $6x10^{-5}$ M DPPH. The solution was left in the dark for 30 min and absorbance was measured at a wavelength of 520 nm. Inhibition (%) was calculated as follows: % Inhibition = $[(Abs_{control} - Abs_{sample})/ Abs_{control}] \times 100$ where $Abs_{control}$ is the absorbance of the control and Abs_{sample} is the absorbance of the sample. EC_{50} values were calculated using a regression equation.

2.7.2 ABTS radical scavenging assay

The assay procedure was modified from Re *et al*. [31]. Twenty µl of 10 mg/ml sample solution was combined with 180 µl of ABTS reagent. The solution was left for 6 min in the dark and absorbance was measured at a wavelength of 734 nm. Inhibition (%) and EC_{50} values were calculated as mentioned above.

2.8 Statistical analysis

All tests were performed in triplicate. Data was analyzed using one-way ANOVA followed by Duncan's new multiple range test for mean comparison at $p \leq 0.05$.

3. Results and Discussion

3.1 Fresh and dry weight of shoots

SA at all concentrations affected shoot fresh and dry weight (Figure 1). The lowest fresh weight of 53.85±7.50 mg/shoot was recorded for 300 µM SA, while the 100 and 200 µM SA treated shoots had fresh weights of 77.12±8.76 and 74.96±12.07 mg/shoot, respectively. The control treatment had the greatest shoot fresh weight of 153.91±12.40 mg/shoot (Figure 1 A).

The dry weight of SA treated shoots was significantly lower than that of control (Figure 1 B). The dry weights of the 100-300 µM SA treated shoots were 6.82±1.04-9.11±1.47 mg/shoot, compared with 11.82±0.86 mg/shoot for control.

The growth response to SA is different in each plant species. At low concentrations, it promotes plant growth, as SA is a growth regulator. Sakhanokho and Kelley [32] reported that the shoot biomass of *Hibiscus acetosella* and *H. moscheutos* (cv. '*Luna Red*') was improved by low concentrations of SA (0.5 mM). In our experiment, however, SA had a negative effect on shoot biomass. The concentration used may have been insufficiently low to act as a plant hormone. This may have generated an imbalance condition [33] or have reduced primary metabolism [34]. This was in agreement with previous studies, which reported decreased growth of plant cells or organs such as the callus of root cultures of *Panax ginseng* [35], cell suspension of *Gardenia jasminoides* [36], root cultures of *Talinum paniculatum* [37], and shoot cultures of *Dioscorea membranacea* [38].

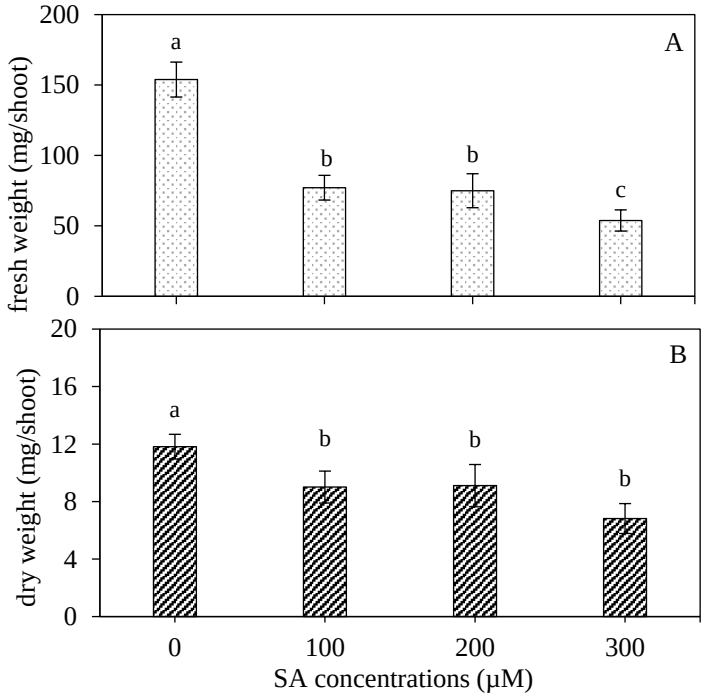

Figure 1. A) fresh weight, and B) dry weight of *Musa acuminata* cv. 'Gros Michel' shoots after treatment with salicylic acid at 0-300 µM for four weeks

3.2 Secondary metabolites and antioxidant activity

As can be seen from Figure 2 A, the total saponin contents of the 100 µM SA treated shoots (263.86±0.42 mg diosgenin/g dry extract) were not significantly different from that of the 200 µM SA treated shoots (261.81±2.61 mg diosgenin/g dry extract). These were 1.27 and 1.26 times that of control (208.31±0.42 mg diosgenin/g dry extract). The lowest total saponin content of 201.91±3.37 mg diosgenin/g dry extract was recorded in the 300 µM SA treated shoots.

A statistically significant difference in total phenolic contents was found among treatments (Figure 2 B). The highest total phenolic content (124.44±8.39 mg GAE/g dry extract) was recorded from the 100 µM SA treated shoots. This was 1.25 times that of control. The total phenolic content of the 200 µM SA treated shoots was 104.96±8.14 mg GAE/g dry extract, which was not significantly different from that of the control (99.66±7.65 mg GAE/g dry extract). The total phenolic content was lower when shoots were treated with SA at the highest concentration of 300 µM.

The effect of SA on total flavonoid content was similar to that on total phenolic content. The greatest content of 105.26±6.43 mg CE/g dry extract was observed in the 100 µM SA treated shoots. This was 1.34 times that of control (Figure 2 C). The total flavonoid content of the 200 µM SA treated shoots (81.84±3.68 mg CE/g dry extract) was not significantly different from that of the control (78.08±5.46 mg CE/g dry extract). The 300 µM SA concentration produced the lowest total flavonoid accumulation (54.49±2.68 mg CE/g dry extract).

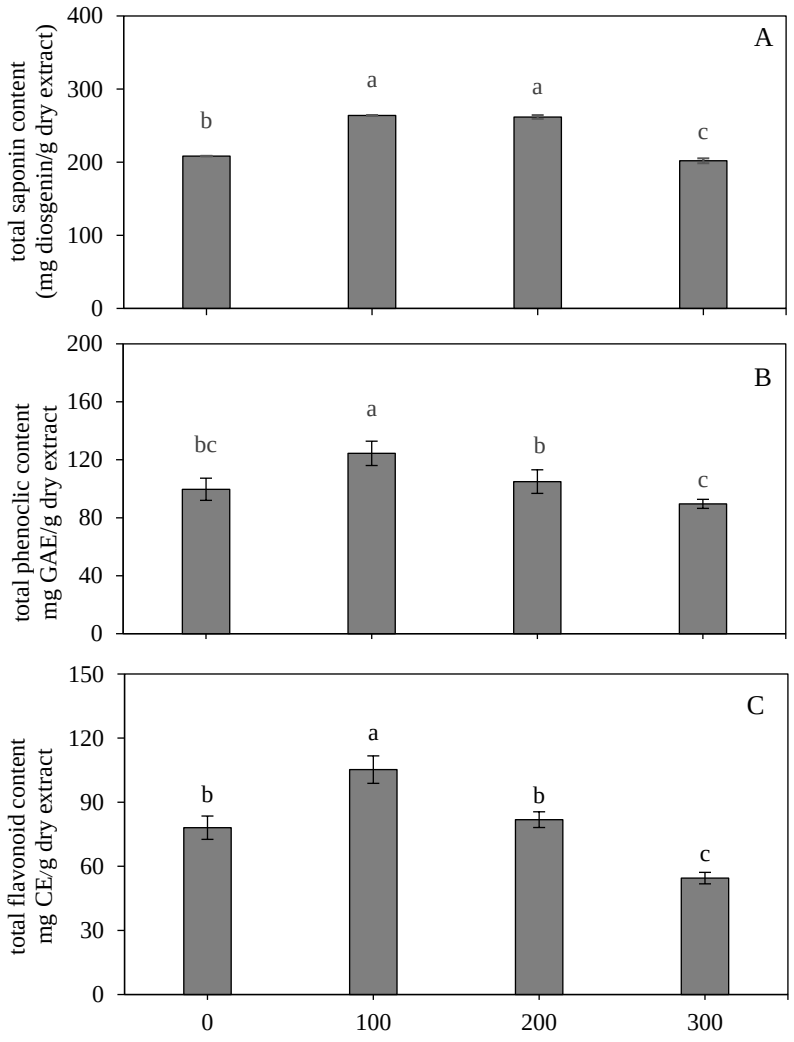

Figure 2. A) total saponin content, B) total phenolic content, and C) total flavonoid content after shoots were treated with salicylic acid at 0-300 µM for four weeks

The strongest DPPH radical scavenging was recorded for the 100 µM SA treated shoots, with an EC_{50} of 9.79±0.86 µg/ml (Figure 3 A). DPPH radical scavenging by the 200 and 300 µM SA shoots (EC_{50} values of 13.90±0.42 µg/ml and 17.44±0.96 µg/ml, respectively) was below that of control (EC_{50} of 11.99±0.73 µg/ml).

The 100 µM SA treated shoots exhibited the strongest ABTS radical scavenging, with an EC_{50} of 86.66±1.50 µg/ml (Figure 3 B). The weakest ABTS antioxidant (EC_{50} of 111.08±4.39 µg/ml) was exhibited by the 300 µM SA shoots, and was not significantly different from control (EC_{50} of 105.40±2.42 µg/ml).

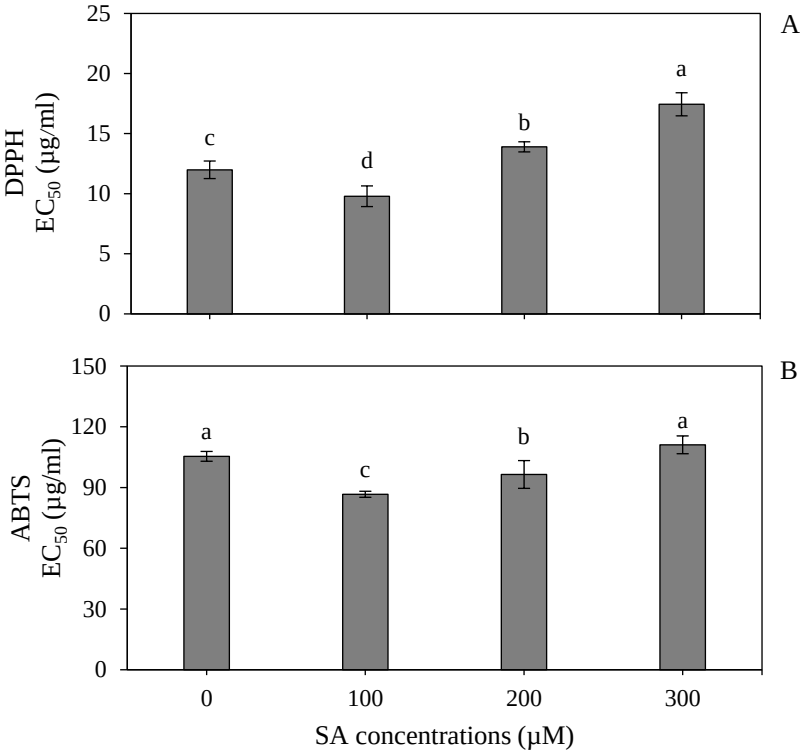

Figure 3. A) DPPH, and B) ABTS antioxidant scavenging activity after shoots were treated with salicylic acid at 0-300 µM for four weeks

From the results, SA at a concentration of 100 µM was most effective for enhancement of total saponin, total phenolics, and total flavonoids from *in vitro* shoots of *M. acuminata* cv. 'Gros Michel'. DPPH and ABTS radical scavenging assays were performed to analyze antioxidant activity. In both assays, the greatest antioxidant activity was observed from 100 µM SA treated shoots. This may reflect the greater accumulation of total phenolic compounds and flavonoids. These compounds have antioxidant properties, as their polyphenol structures scavenge free radicals [9]. SA at a concentration of 300 µM adversely affected secondary metabolite accumulation and antioxidant activity, perhaps through a toxic effect on plant cells. This result was consistent with that of Coste *et al*. [20] for *H. hirsutum*, and of Cai *et al*. [39] for *Changium smyrnioides*. In both cases, high concentrations of elicitor reduced accumulation of secondary metabolites. Therefore, elicitor concentration is a factor that must be considered for each specific case [16, 17, 40].

SA is a signaling molecule that triggers a defensive mechanism or systemic acquired resistance (SAR) when under pathogen attack [40-42]. It also induces expression of genes involved in biosynthesis of some secondary metabolites [40]. Many studies have successfully used SA to increase production of secondary metabolites including hypericin and pseudohypericin by *H. hirsutum* [20], phenolics, flavonoids, and antioxidants by *T. peruviana* [22], and polysaccharides, phenolics, and flavonoids by *Orostachys cartilaginous* [43].

4. Conclusions

Total saponin, total phenolic, total flavonoid accumulation, and antioxidant activity of *in vitro M. acuminate* cv. 'Gros Michel' shoots were enhanced by SA at a concentration of 100 μM. The results of this investigation will support further pharmaceutical study of *in vitro M. acuminate* cv.'Gros Michel' shoots.

5. Acknowledgements

The authors gratefully acknowledge the financial support provided by Faculty of Science and Technology, Thammasat University, Contract No. SciGR19/2563. The authors would also like to thank Mr. John Winward from Thammasat University for proof reading this manuscript.

References

[1] Singh, B., Singh, J.P., Kaur, A. and Singh, N., 2016. Bioactive compounds in banana and their associated health benefits. *Food Chemistry*, 206, 1-11.
[2] Nimisha, S.M. and Pradeep, S.N., 2017. Traditional uses, phytochemistry and pharmacology of wild banana (*Musa acuminata* Colla). *Journal of Ethnopharmacology*, 196, 124-140.
[3] Heslop-Harrison, J.S. and Schwarzacher, T., 2007. Domestication, genomics and the future for banana. *Annals of Botany*, 100, 1073-1084.
[4] Onyema, C.T., Ofor, C.E., Okudo, V.C. and Ogbuagu, A.S., 2016. Phytochemical and antimicrobial analysis of banana pseudo stem (*Musa acuminata*) Br. *Journal of Pharmacy Research*, 10, 1-9.
[5] Osbourn, A., Goss, R.J. and Field, R.A., 2011. The saponins: polar isoprenoids with important and diverse biological activities. *Natural Product Reports*, 28, 1261-1268.
[6] Lacaille-Dubois, M.A. and Wagner, H., 1996. A review of the biological and pharmacological activities of saponins. *Phytomedicine*, 2, 363-386.
[7] Matkowski, A., 2008. Plant in vitro culture for the production of antioxidants – A review. *Biotechnology Advances*, 26, 548-560.
[8] Saxena, M., Saxena, J. and Pradhan, A., 2012. Flavonoids and phenolic acids as antioxidants in plants and human health. *International Journal of Pharmaceutical Sciences Review and Research*, 16, 130-134.
[9] Tungmunnithum, D., Thongboonyou, A., Pholboon, A. and Yangsabai, A., 2018. Flavonoids and other phenolic compounds from medicinal plants for pharmaceutical and medical aspects: An overview. *Medicines*, 5, 93, https://doi.org/10.3390/medicines5030093
[10] Arinaitwe, G., Rubaihayo, P.R. and Magambo, M.J.S., 2000. Proliferation rate effects of cytokinins on banana (Musa spp.) cultivars. *Scientia Horticulturae*, 86, 13-21.
[11] Srangsam, A. and Kanchanapoom, K., 2003. Thidiazuron induced plant regeneration in callus culture of triploid banana (*Musa* sp.) 'Gros Michel', AAA group. *Songklanakarin Journal of Science and Technology*, 25, 689-696.
[12] Divakaran, S.P. and Nair, A.S., 2011. Somatic embryogenesis from bract cultures in diploid *Musa acuminata* cultivars from South India. *Scientia Horticulturae*, 131, 99-102.
[13] Nandhakumar, N., Kumar, K., Sudhakar, D. and Soorianathasundaram, K., 2018. Plant regeneration, developmental pattern and genetic fidelity of somatic embryogenesis derived *Musa* spp. *Journal of Genetic Engineering and Biotechnology*, 16, 587-598.

[14] Rao, S.R. and Ravishankar, G.A., 2002. Plant cell culture: chemical factories of secondary metabolites. *Biotechnology Advances*, 20, 101-153.
[15] Dias, M.J., Sousa, M.J., Alves, R.C. and Ferriera, I.C.F.R., 2016. Exploring plant tissue culture to improve the production of phenolic compound: A review. *Industrial Crops and Products*, 82, 9-22.
[16] Namdeo, A.G., 2007. Plant cell elicitation for production of secondary metabolites: A review. *Pharmacognosy Review*, 1, 69-79.
[17] Vasconsuelo, A.A. and Boland, R., 2007. Molecular aspects of the early stages of elicitation of secondary metabolites in plant. *Plant Science*, 172, 861-875.
[18] Hayat, Q., Hayat, S., Irfan, M. and Ahmad, A., 2010. Effect of exogenous salicylic acid under changing environment: A review. *Environmental and Experimental Botany*, 68, 14-25.
[19] Wang, Y.D., Yuan, Y.J. and Wu, J.C., 2004. Induction studies of methyl jasmonate and salicylic acid on taxane production in suspension cultures of *Taxus chinensis* var. *mairei*. *Biochemical. Engineering Journal*, 19, 256-259.
[20] Coste, A., Vlase, L. and Halmagyi, A., 2011. Effects of plant growth regulators and elicitors on production of secondary metabolites in shoot cultures of *Hypericum hirsutum* and *Hypericum maculatum*. *Plant Cell Tissue and Organ Culture*, 106, 279-288.
[21] Mahalakshmi, R., Eganathan, P. and Parida, A.K., 2013. Salicylic acid elicitation on production of secondary metabolite by cell cultures of *Jatropha curcas* L. *International Journal of Pharmacy and Pharmaceutical Sciences*, 5, 655-659.
[22] Mendoza, D., Cuaspud, O., Arias, J.P., Ruiz, O. and Arias, M., 2018. Effect of salicylic acid and methyl jasmonate in the production of phenolic compounds in plant cell suspension cultures of *Thevetia peruviana*. *Biotechnology Reports*, 19, e00273, https://doi.org/10.1016/j.btre.2018.e00273
[23] Chauhan, R., Keshavkant, S. and Quraishi, A., 2018. Enhanced production of diosgenin through elicitation in micro-tubers of *Chlorophytum borivilianum* Sant et Fernand. *Industrial Crops and Products*, 113, 234-239.
[24] Khan, T., Khan T., Hano, C. and Abbasi, B.H., 2019. Effects of chitosan and salicylic acid on the production of pharmacologically attractive secondary metabolites in callus cultures of *Fagonia indica*. *Industrial Crops and Products*, 129, 525-535.
[25] Buraphaka, H. and Putalun, W., 2020. Stimulation of health-promoting triterpenoids accumulation in *Centella asiatica* (L.) Urban leaves triggered by postharvest application of methyl jasmonate and salicylic acid elicitors. *Industrial Crops and Products*, 146, 112171, https://doi.org/10.1016/j.indcrop.2020.112171
[26] Rodríguez-Sánchez, L.K., Pérez-Bernal, J.E., Santamaría-Torres, M.A., Marquínez-Casas, X., Cuca-Suárez, L.E., Prieto-Rodríguez, J.A. and Patiño-Ladino, O.J., 2020. Effect of methyl jasmonate and salicylic acid on the production of metabolites in cell suspensions cultures of *Piper cumanense* (Piperaceae). *Biotechnology Reports*, 28, e00559, https://doi.org/10.1016/j.btre.2020.e00559
[27] Hiai, S., Oura, H. and Nakajima, T., 1976. Color reaction of some sapogenins and saponins with vanillin and sulfuric acid. *Plant Medica*, 29, 116-122.
[28] Jirakiattikul, Y., Rithichai, P., Songsri, O., Ruangnoo, S. and Itharat, A., 2016. *In vitro* propagation and bioactive compound accumulation in regenerated shoots of *Dioscorea birmanica* Prain & Burkill. *Acta Physiologiae Plantarum*, 38, 249, https://doi.org/10.1007/s11738-016-2268-6
[29] Zhu, H., Wang, Y., Liu, Y., Xia, Y. and Tang, T., 2010. Analysis of flavonoids in *Portulaca oleracea* L. by uv-vis spectrophotometry with comparative study on different extraction technologies. *Food Analytical Methods*, 3, 90-97.

[30] Yamasaki, K., Hashimoto, A., Kokusenya, Y., Miyamoto, T. and Sato, T., 1994. Electrochemical method for estimating the antioxidative effect of methanol extracts of crude drugs. *Chemical and Pharmaceutical Bulletin*, 42, 1663-1665.
[31] Re, R., Pellegrini, N., Proteggente, A., Pannala, A., Yang, M. and Rice-Evans, C., 1999. Antioxidant activity applying an improved ABTS radical cation decolorization assay. *Free Radical Biology and Medicine*, 26, 1231-1237.
[32] Sakhanokho, H.F. and Kelley, R.Y., 2009. Influence of salicylic acid on *in vitro* propagation and salt tolerance in *Hibiscus acetosella* and *Hibiscus moscheutos* (cv '*Luna Red*'). *African Journal of Biotechnology*, 8, 1474-1481.
[33] Cousins, M.M., Adelberg, J., Chen, F. and Rieck, J., 2009. Secondary metabolism-inducing treatments during *in vitro* development of turmeric (*Curcuma longa* L.) rhizomes. *Journal of Herbs Spices and Medicinal Plants*, 15, 303-317.
[34] Chen, H. and Chen, F., 2000. Effects of yeast elicitor on the growth and secondary metabolism of a high-transhinone-producing line of the Ti transformed *Salvia miltiorrhiza* cells in suspension culture. *Process Biochemistry*, 35, 837-840.
[35] Ali, M.B., Yu, K.W., Hah, E.J. and Paek, K.Y., 2006. Methyl jasmonate and salicylic acid elicitation induces ginsenosides accumulation, enzymatic and non-enzymatic antioxidant in suspension culture *Panax ginseng* roots in bioreactors. *Plant Cell Reports*, 25, 613-620.
[36] Liu, Z.B., Chen, J.G., Yin, Z.P., Shangguan, X.C., Peng, D.Y. and Lin, T.L.P., 2018. Methyl jasmonate and salicylic acid elicitation increase content and yield of chlorogenic acid and its derivatives in *Gardenia jasminoides* cell suspension cultures. *Plant Cell Tissue and Organ Culture*, 134, 79-93.
[37] Faizal, A. and Sari, A.V., 2019. Enhancement of saponin accumulation in adventitious root culture of Javanese ginseng (*Talinum paniculatum* Gaertn.) through methyl jasmonate and salicylic acid elicitation. *African Journal of Biotechnology*, 18, 130-135.
[38] Jirakiattikul, Y., Rithichai, P., Boonyeun, T., Ruangnoo, S. and Itharat, A., 2020. Improvement of dioscorealide B production by elicitation in shoot cultures of *Dioscorea membranacea* Pierre ex Prain & Burkill. *Physiology and Molecular Biology of Plants*, 26, 585-591.
[39] Cai, J., Ma, Y., Hu, P., Zhang, Y., Chen, J. and Li, X., 2017. Elicitation of furanocoumarins in *Changium smyrnioides* suspension cells. *Plant Cell Tissue and Organ Culture*, 130, 1-12.
[40] Zhao, J., Davis, L.C. and Verpoorte, R., 2005. Elicitor signal transduction leading to production of plant secondary metabolites. *Biotechnology Advances*, 23, 283-333.
[41] Angelova, Z., Georgiev, S. and Roos, W., 2006. Elicitation of plants. *Biotechnology and Biotechnological Equipment*, 20, 72-83.
[42] Patel, H. and Krishnamurthy, R. 2013. Elicitors in plant tissue culture. *Journal of Pharmacognosy and Phytochemistry*, 2, 60-65.
[43] Wen, T., Hao, Y.J., An, X.L., Sun, H.D., Li, Y.R., Chen, X., Piao, X.C. and Lain, M.L., 2019. Improvement of bioactive compound accumulation in cell cultures of *Orostachys cartilaginous* A. Bor. through elicitation with salicylic acid and effect of cell extract on bioactive activity. *Industrial Crops and Products*, 139(4), 111570, https://doi.org/10.1016/j.indcrop.2019.111570

Current Applied Science and Technology Vol. 21 No. 3 (July-September 2021)

Energy Efficiency Improvement in Micro-sized Food Processing Enterprises via Automatic Cooking Gas Control

Nakorn Tippayawong[1]*, Komkrit Thungkham[2], Thossaporn Onsree[1], James C. Moran[1] and Theeraphong Wongratanaphisan[1]

[1]Department of Mechanical Engineering, Chiang Mai University, Chiang Mai, Thailand
[2]JBK Technical, Co., Ltd., Chiang Mai, Thailand

Received: 11 August 2020, Revised: 8 December 2020, Accepted: 11 February 2021

Abstract

Food processing is a big industry in many countries. The industry consumes large amount of energy, primarily from liquefied petroleum gas (LPG). Food frying is conventionally controlled via the cooking oil temperature, which is regulated by controlling the amount of heat provided by the cooking gas burner, hence, consumption rate of LPG. For micro-sized food processing enterprises in Thailand, this is usually done manually by operators, resulting in poor energy efficiency and non-negligible amount of waste. To prevent such situations, it is necessary to control the food cooking process more precisely. The objective of this work was to develop a precise control system for a gas cooking stove used to fry rice crackers with an improved energy efficiency and fuel economy. This work reports on the development and testing of an automatic burner control system for an LPG cooking stove used to provide heat in frying Thai rice crackers. The system was based on low-cost sensing of the frying oil temperature and two-step control of gas valves. It was found that the automatic control system employed worked well and more precise control of the frying oil temperature could be achieved. Results of the experimental testing with and without automatic control of the LPG cooking stove in the laboratory setup indicated that better food processing control could give rise to almost 40% improvement in fuel economy for processing rice crackers.

Keywords: energy saving; process control; semi-automation; food engineering; LPG
DOI 10.14456/cast.2021.44

1. Introduction

Thailand has long been aiming to become the kitchen of the world. With fertile natural resources, it is a top 10 world leader in production of staple agricultural products including rice, cassava, sugarcane, palm oil, coconut, pineapple and natural rubber [1]. The country is among the world leaders in agricultural product suppliers, due mainly to its well-established food industry. The food industry is the country's 3rd largest industry, contributing nearly a quarter of the country's gross domestic product [2]. There are about 9,000 registered food processing firms in Thailand. Processed food exports contributed more than 50% of total food exports and accounted for about 15% of Thai manufacturing output [3]. Rising costs and energy consumption are crucial issues for the food processing sector [4, 5]. With continuous assistance from governmental offices, Thai manufacturing

*Corresponding author: E-mail: n.tippayawong@yahoo.com

companies have been investing substantial capital in research and development to increase their operational performances. Many firms are utilizing smart information and communications technology to control their manufacturing processes. This is particularly true for medium and large companies. However, for small and micro-sized enterprises, adopting advanced technologies remains a tremendous challenge. Development of food processing machinery and energy efficient equipment appropriate for these small and micro-sized enterprises is therefore of great importance [6].

Most people prefer cooking with gas [7] such as liquefied petroleum gas (LPG), since it is a clean-burning and efficient cooking fuel. It has been a fuel choice for many urban and rural households [8]. Consumption of cooking gas or LPG in Thailand is about seven million tons a year, in which the households sector (including small business operators) accounts for about a third (32%) or more than two million tons a year [9]. Thailand has been in the process of adjusting the retail LPG price structure to reflect actual capital costs, which hurts the household sector, as well as small and micro-sized food processing enterprises. Most related research on improvement in cooking stove efficiency is concerned with equipment redesign and modification [10-16]. To the authors' knowledge, there are no reports in existing literature on developing and applying automatic control to household gas cooking stoves.

Control of cooking is traditionally done manually and is rather inaccurate. This is especially true for small and micro-sized enterprises using deep fat frying for preparation of popular snacks such as rice crackers. The process is about the interaction between oil and food at high temperatures, which dehydrates and cooks the food, resulting in physical and chemical changes. A typical operation and end products are shown in Figure 1. This usually leads to the possibility of the product being over- or under-cooked, hence, defected products and high energy cost. Precise process control is therefore desirable to improve product quality, energy saving and reduce defects.

(a)  (b) 

Figure 1. (a) food frying operation; (b) produced rice crackers.

The objective of this work was to develop a cost effective, automatic burner control system for a gas cooking stove used to fry rice crackers. It was aimed at increasing the energy efficiency and reducing food waste by using a low-cost sensor for the frying oil temperature and two-step control of the gas valves. Control algorithms for LPG supply and cooking process stability were specifically designed for this application.

2. Materials and Methods

2.1 Frying process control

In the fast frying process of making rice crackers, cooking oil must be kept at high temperature, preferably around 200ºC. Dry precooked rice is cooked very quickly (about 20-30 s) by immersion in hot oil. Frying is a method that entails simultaneous heat and mass transfer, wherein frying oil acts as the heat transfer medium, while moisture moves outwards and the oil is engrossed into the food [17]. The process control model was developed (Figure 2), as follows;

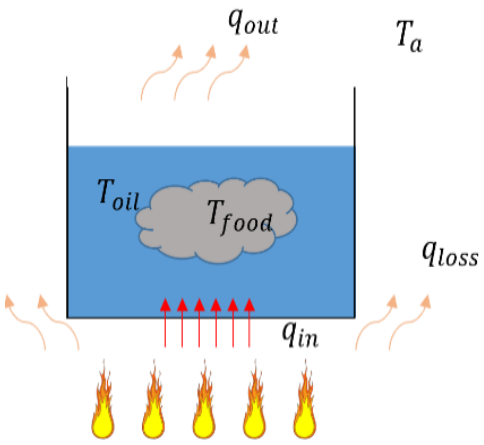

Figure 2. Physical model of food frying process.

From an energy balance:

$$q_{in} = q_{acc} + q_{out} + q_{loss} \quad (1)$$

where q_{in} *and* q_{loss} are heat input and heat loss. Accumulated heat (q_{acc}) and heat out to atmosphere (q_{out}) are:

$$q_{acc} = \frac{d}{dt}\left(m_{oil}C_{p,o}\left(T_{oil} - T_{oil,0}\right) + m_{food}C_{p,f}\left(T_{food} - T_{food,0}\right)\right)$$

$$q_{out} = hA(T_{oil} - T_a)$$

where m_{oil}, m_{food}, $C_{p,o}$, $C_{p,f}$, T_{oil}, T_{food}, $T_{oil,0}$, $T_{food,0}$ and T_a are masses, specific heat capacities, and instantaneous and initial temperatures of oil and food, and surrounding air temperature respectively. *A* and *h* are oil surface area and convective heat transfer coefficient. Then

$$\frac{d}{dt}\left(m_{oil}C_{p,o}T_{oil} + m_{food}C_{p,f}T_{food}\right) + hA(T_{oil} - T_a) + q_{loss} = q_{in}$$

Or

$$m_{oil}C_{p,o}\,\dot{T}_{oil} + m_{food}C_{p,f}\dot{T}_{food} + hAT_{oil} - hAT_a + q_{loss} = q_{in}$$

Let

$$Q_{predict} = m_{food}C_{p,f}\dot{T}_{food} - hAT_a + q_{loss}$$

Hence

$$m_{oil}C_{p,o}\,\dot{T}_{oil} + hAT_{oil} + Q_{predict} = q_{in}$$

Finally, the control equation for the heat input is:

$$q_{in} = Q_{predict} + u$$

where

$$m_{oil}C_{p,o}\,\dot{T}_{oil} + hAT_{oil} = u \quad (2)$$

This is a first order equation describing the oil temperature, with the heat loss (q_{loss}) as a disturbance. The relationship between the input (u) and output (T_{oil}) may be written as the following transfer function,

$$G(s) = \frac{T_{oil}(s)}{U(s)} = \frac{1}{m_{oil}C_{p,o}s + hA}$$

The transfer function, $G(s)$, represents a first-order dynamic system with time-constant (τ)

$$\tau = \frac{m_{oil}C_{p,o}}{hA}$$

For optimal control problems, on-off control law [18] ideally produces a solution in the shortest time. In practice, the on-off control system may be suitable for the first order system such as that seen in heat transfer.

2.2 Control system setup

Simple and cost effective control systems may be used to create step control action. In this simple setup, there are three levels of gas flow: no flow (off), medium flow and, high-flow which are implemented by a two-valve system. The automatic oil temperature control system was designed and built. This economical control system tailored made for gas cooking consists of a thermometer, a flame detector, a spark ignitor, two-stage main gas valve and regulator, connected to an electronic control board. The system is compact and can be easily installed on an existing gas cooking stove, shown in Figure 3.

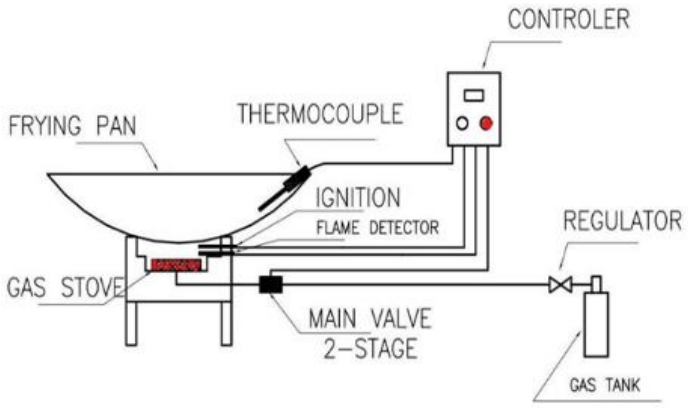

Figure 3. Schematic of the control system setup

The control system setup was based on industrial modular process controllers (Delta DVP16B for main PLC control, Siemens LMB 21.330C2 for burner control, and Fuji PXF4 for temperature control). A human operator can set up the program and monitor the process using a human machine interface (HMI). Control box diagram and hardware setup are shown in Figures 4 and 5.

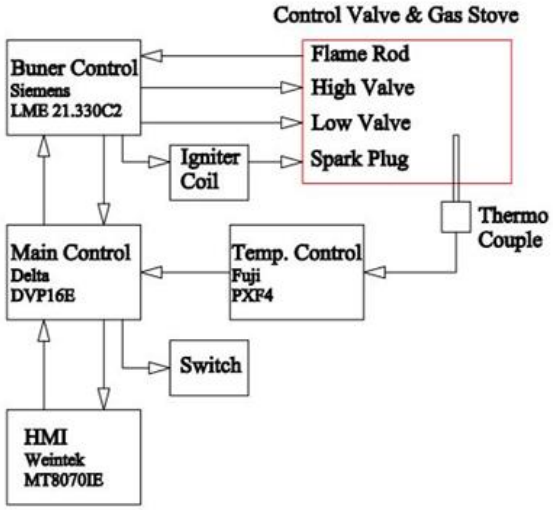

Figure 4. Control box diagram

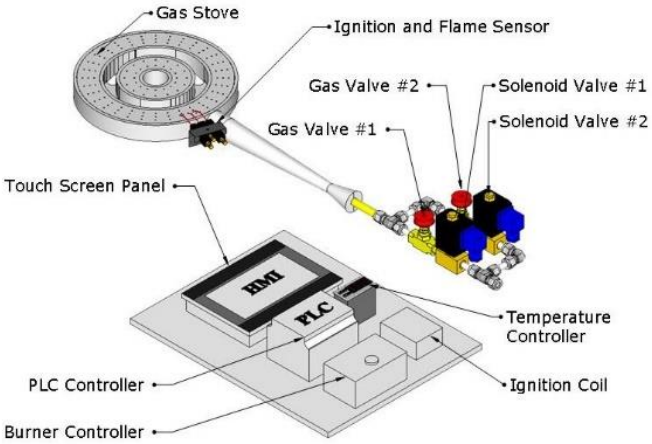

Figure 5. Hardware design for the control system setup

2.3 Test setup, procedure and evaluation

The control system was installed and experimentally tested on a gas cooking stove used in rice cracker frying. It was connected to an LPG cylinder and data logger. Figure 6 shows a laboratory setup for testing the control system with a frying set. The LPG mass was measured via a load cell with a full scale of 30-kg and 5-g resolution. The oil temperature was measured using a type-K thermocouple. For each run, about 10 liters of frying oil was initially used. The oil was started cold. For tests without the control system, the operator would adjust the main valve and ignite manually. Once the operator felt that the oil was sufficiently hot with oil temperature around 180-210^{o}C, he/she would then start

loading about 1 kg of dry precooked rice or raw rice crackers into the frying pan. When the rice crackers turned golden yellow and floated at the top of the oil layer, indicating that they were well cooked, they were then removed to a plate. For tests with the control system, the oil temperature was preset at 200°C. At the start, the control system would ignite and adjust the gas valves automatically. Once the preset temperature was reached, the operator would be notified, he/she would then start processing the snacks in a similar manner to the former case. The quantity of rice crackers, frying oil, and LPG before and after processing were monitored. About 300 kg of raw rice crackers were processed in about 20 test runs. Comparison between the manual and automatic systems was based on the following performance indicators; noise-to-signal ratio for oil temperature evolution, LPG consumption rate, specific energy consumption and potential reduction in greenhouse gas emission.

Figure 6. Setup for testing the control system with a gas cooking stove and a frying pan

The noise-to-signal ratio is the indicator used to identify a control factor and measure how the response varies relative to the target value. Here, it was used to evaluate the size of the temperature difference from the target (noise) or temperature fluctuation against the target temperature (signal).

$$N/S = \frac{\Delta T}{T} \quad (3)$$

Specific energy consumption (in $MJ/kg_{product}$) was the measure of energy requirement to process a unit of product. Here, it was determined from the cooking gas energy used per unit mass of processed rice crackers. The heating value of LPG used was 50 MJ/kg.

$$\text{SEC} = \frac{m_f HV_f}{m_p} \quad (4)$$

The reduction in greenhouse gas emissions (in $kg\text{-}CO_2/kg_{product}$) was a measure of the environmental benefit of the process by its reduced equivalent carbon emission. Here, it was determined from the amount of prevented CO_2 emission per unit mass of processed rice crackers.

$$R_{CO2} = \frac{m_{CO2}}{m_p} \quad (5)$$

3. Results and Discussion

For a typical frying operation of rice crackers, loading of the dry precooked rice and removing of the cooked rice crackers from the oil pan are carried out intermittently. The frying oil temperature drops when the dry precooked rice is loaded into the pan. The operator will normally increase the LPG feed to raise the oil temperature. If a large load of rice is put in at one time, a large drop in temperature is witnessed.

From these experiments, Figure 7 displays the variation of oil temperature with time during typical frying operation with and without the control system, respectively. Average temperature evolution is illustrated with error bars showing the standard deviation of data and dotted lines showing the trends. Both cases were carried out by the same experienced operator. For the former case, the frying oil temperature was intermittently adjusted manually via a main LPG valve by the operator, while for the latter case, the operator concentrated solely on the food products by allowing oil temperature regulation by the control system. During the initial heating up from room (30^{o}C) to target temperature (200^{o}C), both cases showed a similar heating rate and time of about 15 min, prior to the start of food frying. Short stabilization time was also allowed once the set temperature was reached before the start of each frying. As anticipated, it was found that larger error bar ranges were evident for experimental frying without automatic control. It was clear that with the automatic control system on, the frying oil temperature was able to stabilize mostly near the preset value of 200^{o}C with an average N/S ratio of around 5%. Larger variation in temperature was apparent for the manual control with maximum N/S ratio as large as 20%. The trend line (shown as dotted lines) for the case with automatic control was able to more closely follow the set temperature than the one with manual control.

Figure 8 illustrates LPG consumption rate during the frying with and without the control system. A number of test runs were carried out. Examples of several runs were shown here for operation with and without automatic control as square and round symbols, respectively. Their averages were displayed as solid lines. From the findings, it was found that operation with the control system consumed the fuel gas at a lower rate than that without the control system, from 0.185 g/s to about 0.120 g/s, a reduction of more than 35%. Taking into account the gas consumption used for heating up and processing from the start-to-finish, the overall fuel consumptions per unit mass of processed rice crackers were found to be 0.060 and 0.096 kg/kg for frying with and without the automatic control. The resulting SECs were 3.0 MJ/kg for operation with the automatic control, compared to 4.8 MJ/kg for operation with the manual control. This was a 37.5% saving in energy consumption. To justify its cost effectiveness, a simple period to positive cash flow or payback period analysis was estimated, taking into account the initial investment cost against the LPG cost saving. The term "simple" was used because no discount rate was considered here. The proposed control system required an investment of about 35,000 THB. For a small processed food vendor consuming 1200 kg of LPG a year, saving in fuel cost of about 10,800 THB could be obtained (with LPG price of 24 THB/kg). This gave rise to a simple payback period of about 3.2 years. With higher amount of LPG consumed or with governmental subsidy, the return on investment would be shorter.

With regards to potential CO_2 reduction, about 0.036 kg LPG was saved in processing 1 kg of rice crackers. According to the United Nations Intergovernmental Panel on Climate Change guidelines, released CO_2 from LPG usage is given as 3.12 kg CO_2/kg. Therefore, the reduced greenhouse gas emission was 0.112 kg CO_2/ kg product. With around 1,000 tons of yearly production of processed rice crackers, the anticipated reduction potential of CO_2 was approximated to be in excess of 110 tons per year in total.

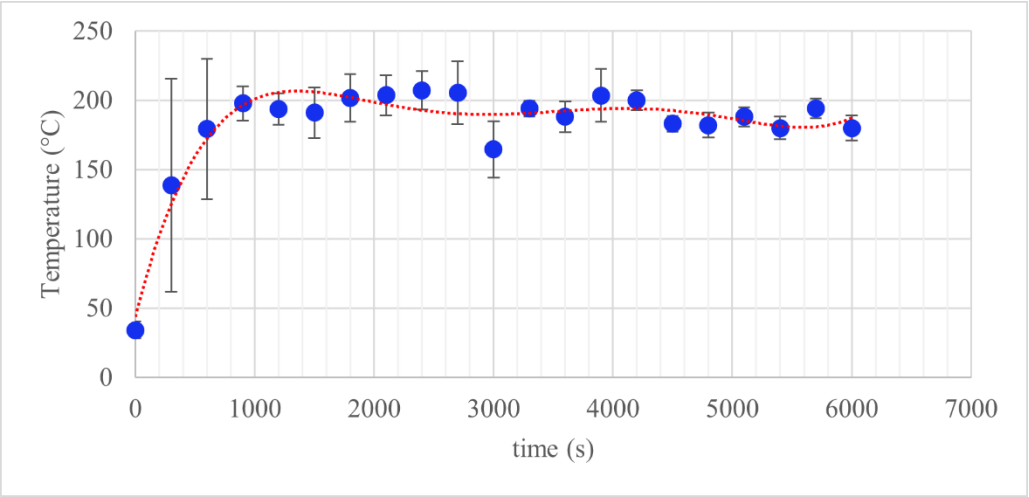

(a)

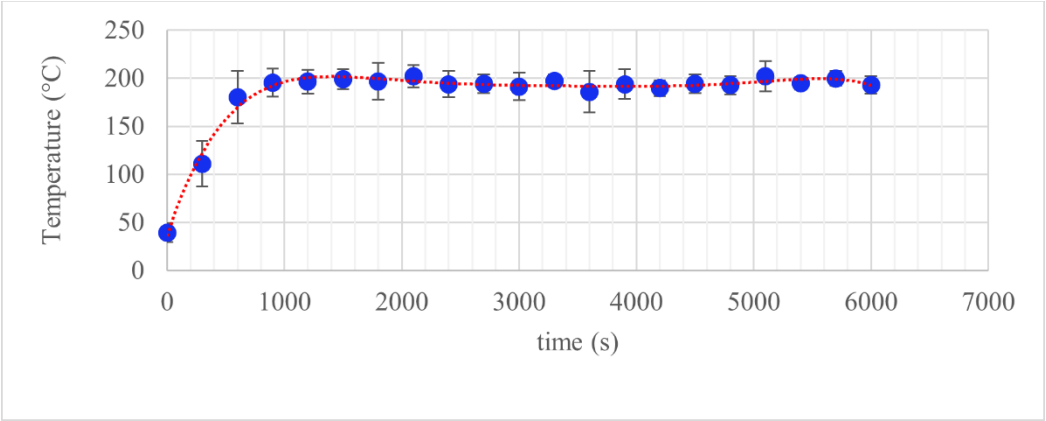

(b)

Figure 7. Change in frying oil temperature during typical food processing operation (a) without and (b) with control

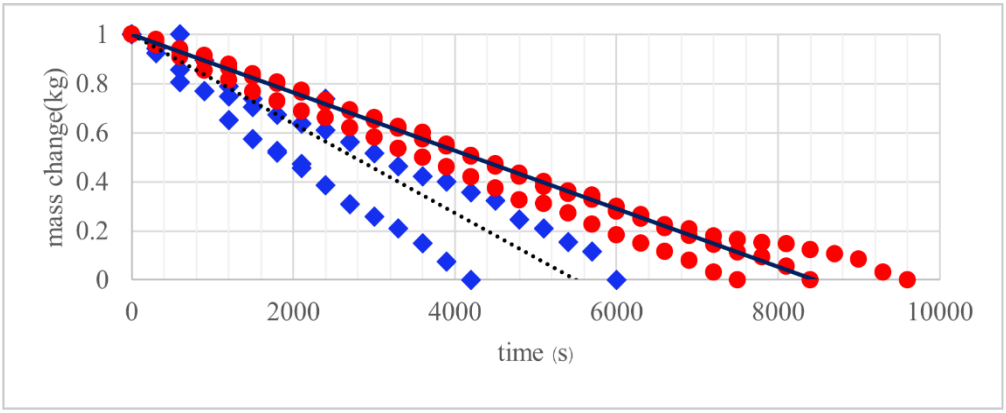

Figure 8. LPG consumption rate during a typical rice cracker frying operation with (diamond symbol) and without (round symbol) the control system

As far as the quality of food products was concerned, it was inspected and evaluated visually and sensually by experienced workers and entrepreneurs who have been in this business for many years. As anticipated, the product appearances, texture and taste were found to be similar and comparable between those obtained from both sets of tests, according to shop owners and food processing operators. From their personal assessment, they confirmed that the quality of the food products was satisfactory. However, based on the food processing point of view, any process modifications can affect product quality to varying degrees. Therefore, the assessments of color, texture, and other key quality aspects should be objectively and/or subjectively evaluated .For sensory evaluation, it requires at least 10-trained panelists or 30 non-trained panelists .The results, based from statistical analysis on quality aspects, must be acceptable. This exercise should be conducted in the future study. From general observation, a smoother operation was realized, but reduction in waste generation was rather marginal. Controlled food processing offered more savings in fuel and energy, compared to that without control. Switching from manual to automatic control was confirmed to improve productivity in terms of fuel economy, energy efficiency for this operation.

4. Conclusions

In this work, a cost effective, automatic burner control system was developed and designed specifically for micro- and small enterprises as well as household gas cooking stoves. It was based on regulating and stabilizing the temperature of the frying oil. Tests with rice cracker frying were conducted and the performance was compared between operating with and without the burner control system. Standard low-cost sensors and two-step control of gas valves proved to be acceptable, achieving smoother operation and a reduced LPG consumption during the trial runs. Energy efficiency was increased and food waste due to over- and under-cooked was reduced. Fuel saving, hence savings in the operating cost was successfully demonstrated. Cost analysis results showed that the control system may be feasible. Simple payback period was estimated to be about 3.2 years. Adoption of the gas burner control system appeared to give better process control, simpler operation, enhanced energy saving and potential reduction in CO_2 emissions for micro-sized food processing enterprises.

5. Acknowledgements

Support from the Fund for Energy Conservation Promotion, Ministry of Energy, and Chiang Mai University were acknowledged. This work was also part of the project "Industry 4.0 for SMEs" from the European Union's Horizon 2020 Research and Innovation program under the Marie Sklodowska-Curie Action grant agreement no. 734713. We would also like to thank Mr. Khajornsak Onlamnao and Mr. Wanchai Piluek for assistance in data collection and technical support.

References

[1] Office of Agricultural Economics, 2019. *Agricultural Economic Information*. [online] Available at: www.oae.go.th/view/1/Information.

[2] Federation of Thai Industries, 2020. *Knowledge Management*. [online] Available at: www.fti.or.th.

[3] National Food Institute, 2020. *Food Intelligence Center Thailand*. [online] Available at: www.nfi.or.th.

[4] Ladha-Sabur A., Bakalis, S., Fryer, P.J. and Lopez-Quiroga, E., 2019. Mapping energy consumption in food manufacturing. *Trends in Food Science & Technology*, 86, 270-280.

[5] Jagtap, S., Rahimifard, S. and Duong, L.N.K., 2019. Real-time data collection to improve energy efficiency: a case stury of food manufacturer. *Journal of Food Processing and Preservation*, 2019, https://doi.org/10.1111/jfpp.14338.

[6] Clairand, J., Briceno-Leon, M., Escriva-Escriva, G. and Pantaleo, A.M., 2020. Review of energy efficiency technologies in the food industry: trends, barriers, and opportunities. *IEEE Access*, 8, 48015-48029.

[7] Suwansri, S., Moran, J.C., Aggarangsi, P., Tippayawong, N., Bunkham, A. and Rerkkriangkrai, P., 2014. A biomethane solution to domestic cooking in Thailand. *Energy for Sustainable Development*, 23, 68-77.

[8] Grieshop, A.P., Marshall, J.D. and Kandlika, M., 2011. Health and climate benefits of cookstove replacement options. *Energy Policy*, 12(12), 7530-7542.

[9] Energy Policy and Planning Office -Ministry of Energy, 2020. *Annual Energy Statistics 2018*. [online] Available at: www.eppo.go.th.

[10] Jugjai, S., Tia, S. and Trewetasksorn, W. 2001. Thermal efficiency improvement of an LPG gas cooker by a swirling central flame. *International Journal of Energy Research*, 25, 657-674.

[11] Das, T., Subramanian, R., Chakkaravarthi, A., Singh, V., Ali, S.Z. and Bordoloi, P.K., 2006. Energy conservation in domestoc rice cooking. *Journal of Food Engineering*, 75(2), 156-166.

[12] Suwansri, S., Moran, J.C., Aggarangsi, P., Tippayawong, N., Bunkham, A. and Rerkkriangkrai, P., 2015. Converting LPG stoves to use biomethane. *Distributed Generation and Alternative Energy Journal*, 30(1), 38-57.

[13] Shinede, Y.H., Gudekar, A.S., Chavan, P.V., Pandit, A.B. and Joshi, J.B., 2016. Design and development of energy efficient continuous cooking system. *Journal of Food Engineering*, 168, 231-239.

[14] Ogedengbe, E.O.B. and Ajibade, F.D., 2017. Improved burner efficiency and fuel consumption in domestic cooking appliances. *Energy and Policy Research*, 4(1), 29-35.

[15] Kaushik, L.K., Deb, S. and Muthukumar, P., 2018. Energy saving and techno-economic assessment of self aspirated domestic LPG stove with porous radiant burner. *IOP Conference*

Series: Materials Science and Engineering, 377, 012194, https://doi.org/10.1088/1757-899X/ 377/1/012194.

[16] Mishra, N.K. and Muthukumar, P., 2018. Development and testing of energy efficient and environment friendly porous radiant burner operating on liquefied petroleum gas. *Applied Thermal Engineering*, 129, 482-489.

[17] Oke, E.K., Idowu, M.A., Sobukola, O.P., Adeyeye, S.A.O. and Akinsola, A.O., 2018. Frying of food: a critical review. *Journal of Culinary Science and Technology*, 16(2), 107-127.

[18] Lewis, F.L., Varabie, D.L. and Syrmos, V.L., 2012. *Optimal Control.* 3rd ed. Singapore: Wiley.

Current Applied Science and Technology Vol. 21 No. 3 (July-September 2021)

Impact of Wind Speed and Direction on Low Cloud Cover over Baghdad City

Zainab M. Abbood, Osama T. Al-Taai* and Wedyan G. Nassif

Department of Atmospheric Science, College of Science, Mustansiriyah University, Baghdad, Iraq

Received: 2 July 2020, Revised: 14 November 2020, Accepted: 17 February 2021

Abstract

Clouds are one of the best evidences for the continuous movement of the Earth's atmosphere, and they play a major role in the Earth's climate through their influence on the balance of solar radiation. Part of the falling solar radiation causes the heating of the Earth's surface. The statistical methods used in this study depend on the daily, monthly and seasonal mean of Low Cloud Cover (LCC), Wind Speed (WS), and Wind Direction (WD), with data taken from the European Center for Medium Range Weather Forecasts (ECMWF) for the year 2018 at the times of 00.00 am, and 12.00 pm over Baghdad Station. The highest values of low cloud cover were recorded during December, January and February, while wind speed was low. The highest values of wind speed were found during June and July at 12:00 pm. As for the seasonal analysis, it was noted that the LCC was high during winter and autumn. The relationship between wind speed and low cloud cover was also found to be inverse; the higher the wind speed, the lower the cloud cover.

Keywords: low cloud cover; wind speed; wind direction; ECMWF; Baghdad
DOI 10.14456/cast.2021.45

1. Introduction

Clouds are a collection of huge numbers of small droplets. There are about one hundred drops per cubic centimeter [1]. Clouds are formed when air cools and its temperature drop below the dew point and then water vapor condensation occurs. The cloud formation occurs in two ways. First, if the rise is slow, clouds that are predominant form the stratum shape. Second, if the rise is rapid, clouds of a cumulative shape tend to form [2]. Movement of clouds can be horizontal or vertical and does not remain in the places of their formation due to the movement of the air masses and wind directions. The movement of air currents is up and down and is affected by thermal changes and the resulting low or high pressures. Wind movement is from high pressure areas to low pressure areas, and winds moves clouds and clouds transfer the characteristics of the area passing over them from temperatures and humidity to other areas [3]. So, the direction of the wind is one of the main factors that determine the nature of clouds in terms of temperature, amount of moisture, height, and sometimes the shape and appearance of clouds [4]. Clouds have an important impact on the climate because they are source of rain and snow that fall on the surface of the earth [5]. The cooling and

*Corresponding author: Tel.: +964 7702642680
Email: osamaaltaai77@uomustansiriyah.edu.iq

heating depend on the height, thickness and water content of clouds. Clouds are classified according to their height and shape, and clouds are divided into three levels:

1) Low-rise clouds consist of drops of liquid water except for a period of cold winter storms and at an altitude of 2 km.

2) Medium-height clouds consist of water droplets, ice crystals or a mixture of the two, and are found in the middle levels of the troposphere; they form at an altitude between 2-6 km.

3) High-altitude clouds consist of snow crystals, and are at a freezing temperature and at a height of 6 km [6].

There are many studies that show the relationship between wind speed and direction of clouds in the city of Baghdad. Clouds play an important role in climate change, in predicting local weather or in the provision of flight safety. In the case of flight safety, the most important parameters are the height of the cloud base and the amount of cloud cover [7]. Using the T-Φ gram model over Baghdad, the calculation of absorption and heat radiation emission by cloud cover clarify the positive relationship between cloud water content and absorption; as the water content in the cloud increased, there was greater absorption. The relationship between the saturated vapor density in the cloud and the emissivity is also positive because an increase in the saturated vapor density in the cloud leads to a greater emission [8]. Some research has shown that the absorption of solar radiation by clouds, aerosols, and some atmospheric gases are affected by the composition of the atmosphere, location, season, and meteorological parameters (temperature, pressure, relative humidity, wind speed, wind direction, rain, and wavelength) as these factors can be very important in terms of volume of cooling and heating (surface and air) [9]. Abd [10] studied the frequency of winds in Iraq with its eight main directions and its relationship to the frequency of high, medium and low winds. It was concluded that wind directions have an effect on the formation of clouds and their types in the transitional seasons and the quality of the prevailing trends in each region.

The research aims to study the relationship between low cloud cover, wind speed, and wind direction at selected stations over Iraq for a whole year (2018).

2. Materials and Methods

2.1 The study aera

The work was carried out using daily data on Wind Speed (WS). Wind Direction (WD) and Low Cloud Cover (LCC) taken from the European Center for Medium Range Weather Forecasts (ECMWF) for Baghdad city (Lat. 33.24ºN, Long. 44.45ºE) [11]. This data was converted to monthly rates to show seasonally effects. The data were processed by MAT-LAB and drawn through the new version of SigmaPlot and Organics program [12]. Iraq map was drawn using a Geographical Information System (GIS) program, as shown in Figure 1.

2.2 Statistical analysis

2.2.1 Simple linear regression (SLR)

Simple linear regression is a statistical method that allows us to summarize and study the relationships between two continuous (quantitative) variables [13]. The basic concept and procedures for simple linear regression are according to the following equations [14]:

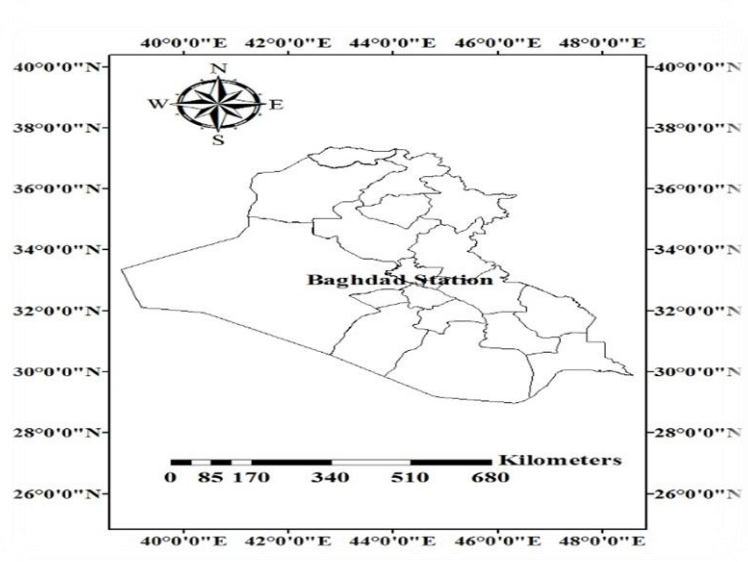

Figure 1. Baghdad city in Iraq

$$\bar{Y} = a + bx \tag{1}$$

$$b = \frac{\sum_{i=1}^{n}(X_i - \bar{X}) - (Y_i - \bar{Y})}{\sum_{i=1}^{n}(X_i - \bar{X})^2} \tag{2}$$

where b is the slope, and a is constant value.

2.2.2 Pearson's correlation coefficient ®

Pearson's correlation coefficient is a very useful statistical formula that measures the strength between variables and relationships. In the field of statistics, this formula is often referred to as the Pearson R test when performing a statistical test between two variables, and it is a good idea to perform a Pearson correlation value to determine how strong this relationship is between these two variables. The Pearson correlation coefficient r is used to measure the strength of the linear correlation between two variables; as r = 1 means full positive correlation and r = -1 means perfect negative correlation [15].

$$r = \frac{\sum_{i=1}^{n}(x_i - \bar{x})(y_i - \bar{y})}{\sqrt{\sum_{i=1}^{n}(x_i - \bar{x})^2}\sqrt{\sum_{i=1}^{n}(y_i - \bar{y})^2}} \tag{3}$$

3. Results and Discussion

3.1 The daily mean behavior of LCC, WS, and WD for Baghdad station

The daily means of LCC, WS and WD for Baghdad station, was observed at the times of 00:00 am and 12:00 pm. LCC was high during February, November and December while wind speed was

high during March and October at the time 00:00 am, wind speed was high during June and July at the time of 12:00 pm. Wind direction was high during July and August at the times of 00:00 am, and 12:00 pm. This was due to meteorological factors, pressure systems, astronomical factors through the seasons and surface nature. Low and high cloud cover affects the velocity of wind speed while reaching the Earth's surface as well as the effect on wind direction (Figure 2).

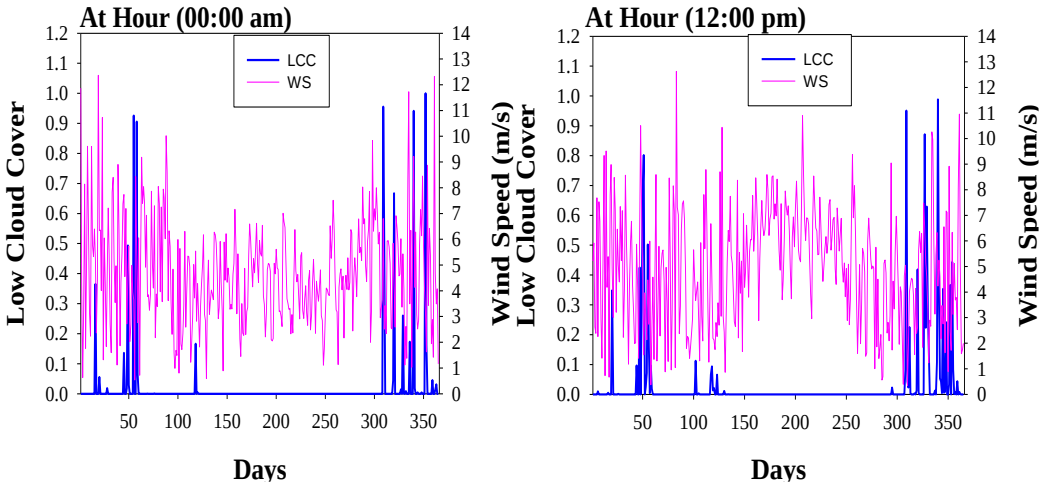

Figure 2. Behavior of the daily means of LCC, WS and WD for Bagdad station

3.2 Analysis of the daily means of wind direction for Baghdad station

Figure 3 shows that the wind is blowing from any direction, but the wind speed at 00.00am is faster than at 12.00pm. As for the direction, it changes more at 12.00 noon. The prevailing wind is the northwest wind, and the wind speed is greater than 5m/s. The wind direction is one of the main factors determining the nature of clouds in terms of temperature, height, and sometimes the shape of the clouds and their external appearance.

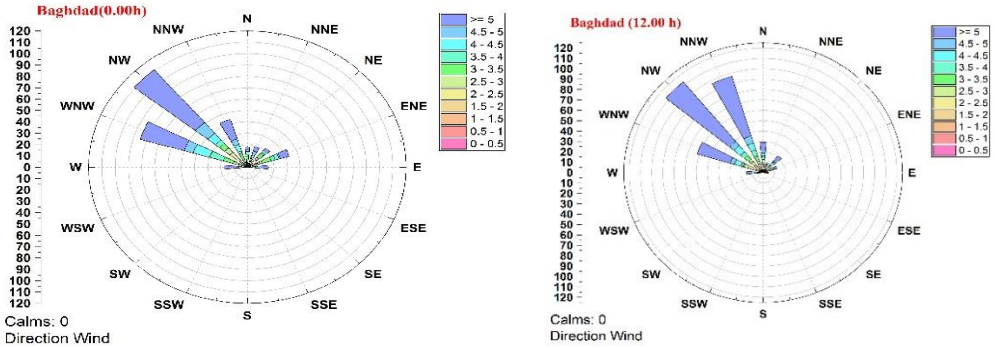

Figure 3. The analysis of the daily mean of winds (speed and direction) for Bagdad station

3.3 The relationship between the daily mean of LCC and WS for Baghdad station

Figure 4 and Table 1 present the type of relationship and the strength of the correlation between LCC and wind speed, LCC, and wind direction for Baghdad station at the times of 00:00 am and 12:00 pm over the year 2018. The relationship between LCC with wind speed and with wind direction is inverse because an increase in wind speed leads to a decrease in LCC, which is formed near the surface of the earth. The cooling and heating of the surface depends on the height, thickness and water content of the clouds. That is why the relationship between clouds and meteorological factors, especially speed and wind direction, is a very important relationship at all the time

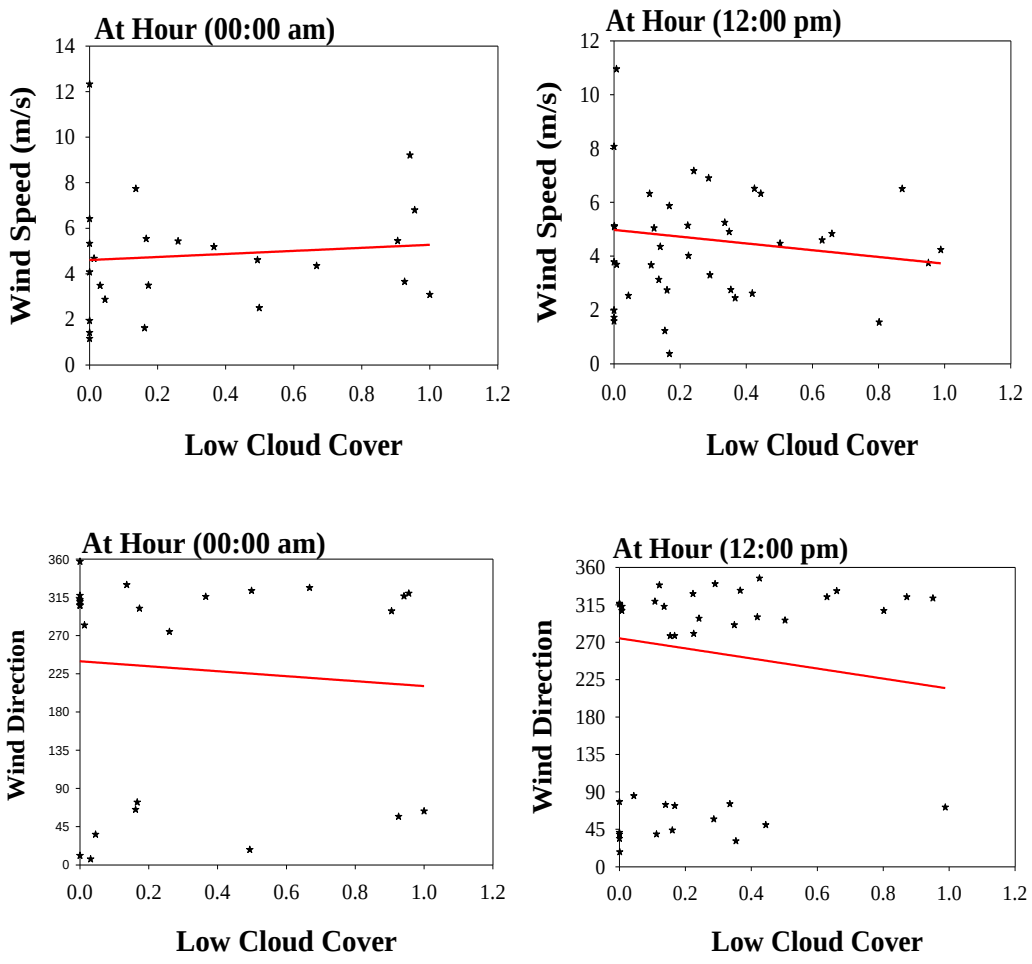

Figure 4. The relationship between the daily means of (LCC and WS), (LCC and WD) for Baghdad station

Table 1. Relationship and the strength of correlation coefficient between the daily means of (LCC and WS), (LCC and WD) at the times of 00:00 am -12:00 pm for Baghdad station

Relationship	Pearson's Test		Simple Linear Regression	
	r	Correlation	P-value	Interpretation
LCC vs. WS at 00:00 am	-0.1	Low inverse	0.001	**Linear**
LCC vs. WS at 12:00 pm	-0.2	Low inverse	0.002	**Linear**
LCC vs. WD at 00:00 am	-0.1	Low inverse	0.001	**Linear**
LCC vs. WD at 12:00 pm	-0.2	Low inverse	0.003	**Linear**

3.4 The monthly mean of LCC, WS and WD for Baghdad station

Figures 5 and 6 show the monthly means of LCC, WS and WD for Baghdad station. LCC was high during the months of December, January and February while speed and wind direction through these months was low due to various meteorological factors, which include low temperatures, high humidity, low solar radiation and low wind speed and wind direction. These conditions led to the formation of many low clouds such as cumulus, stratus, stratocumulus and cumulonimbus. While LCC was low during the months of June, July and August, speed and wind direction was high due to various meteorological factors including high temperatures, low humidity, high solar radiation, high speed and wind direction. These conditions led to the formation of many high clouds such as cirrus, cirrostratus and cirrocumulus. Low and high cloud cover affects the velocity of wind speed reaching the Earth's surface and consequently affects the wind direction.

3.5 The seasonal mean of LCC, WS, and WD for Baghdad station

Figures 7 and 8 show the seasonally means of LCC, WS and WD for Baghdad station as observed at 00:00 am -12:00 pm. LCC was high during winter and autumn while wind speed was high during winter and autumn at 00:00 am, but wind speed was high during summer at 12:00 pm. Wind direction was high during summer season at the times of 00:00 am-12:00 pm. This was due to meteorological factors, pressure systems and surface nature.

4. Conclusions

The relationship between LCC with wind speed and with wind direction was inverse as the higher the wind speed, the lower the LCC. LCC was high during December, January, February. The wind speed was high during the months of June and July at 12:00 pm which led to the absence of the formation of low clouds during these months. The wind speed was high during the summer at 12:00 pm and the wind direction was high during the summer season. This was due to the intensity of the solar radiation, which worked to heat the Earth's surface, and hence causing the air near the surface to warm, which in turn led to an increase in air moving in an upwards direction and an increase in wind speed. The increase and decrease in cloud cover affects the velocity of wind speed reaching the Earth's surface and consequently affects wind direction.

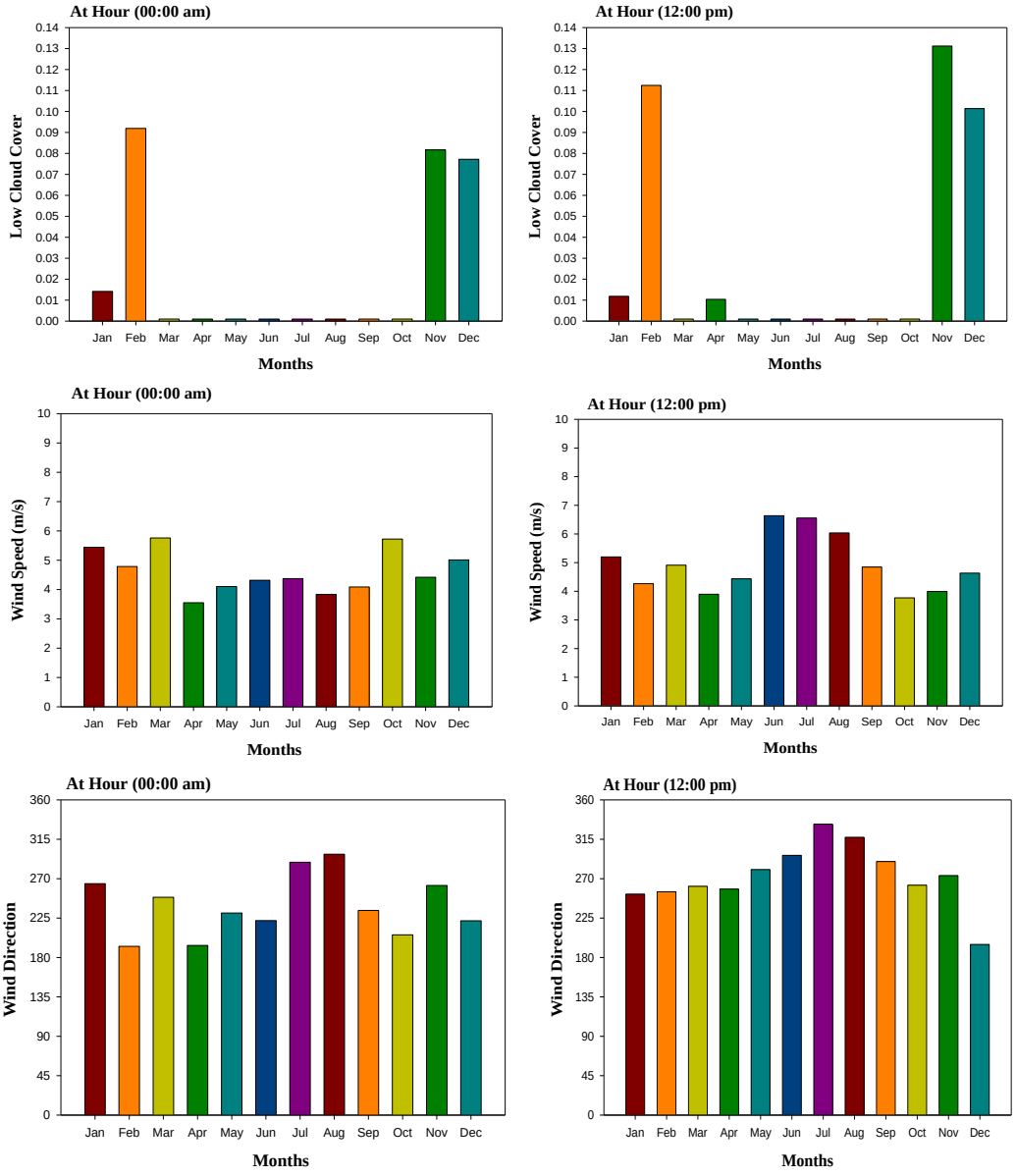

Figure 5. The monthly means of LCC, WS and WD at the times of 00:00 am -12:00 pm for Baghdad station

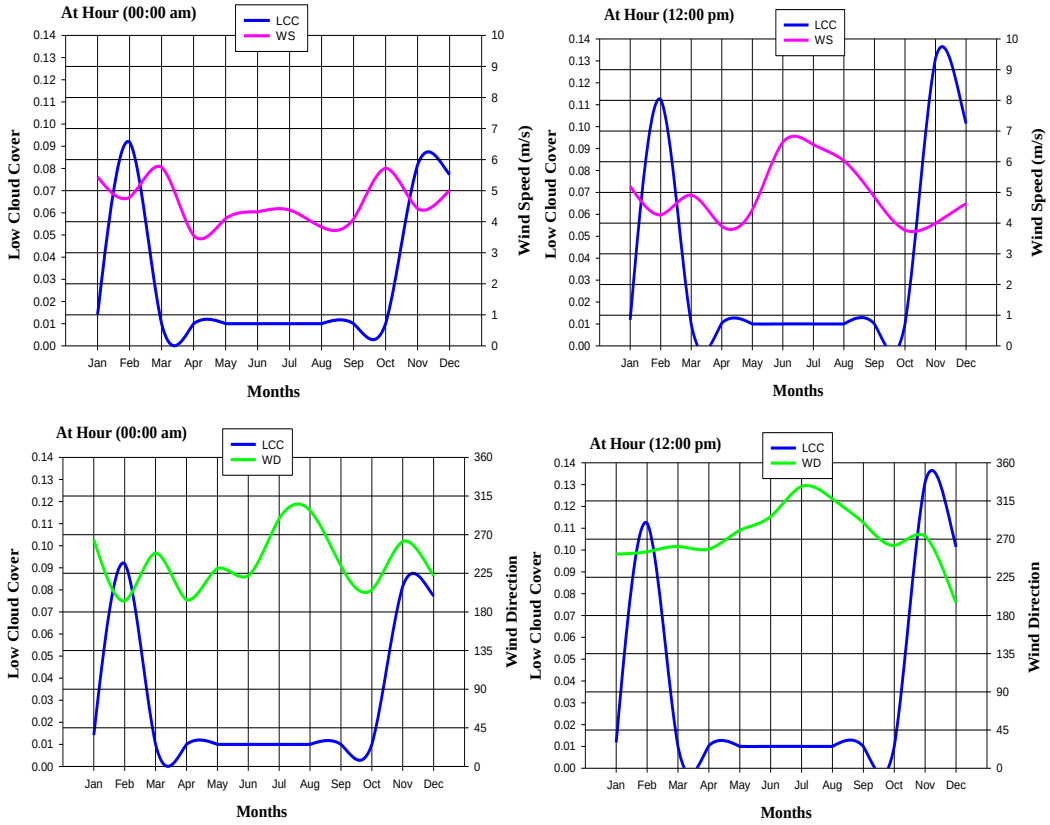

Figure 6. The monthly changes of (LCC and WS), (LCC and WD) at the times of 00:00 am -12:00 pm for Baghdad station

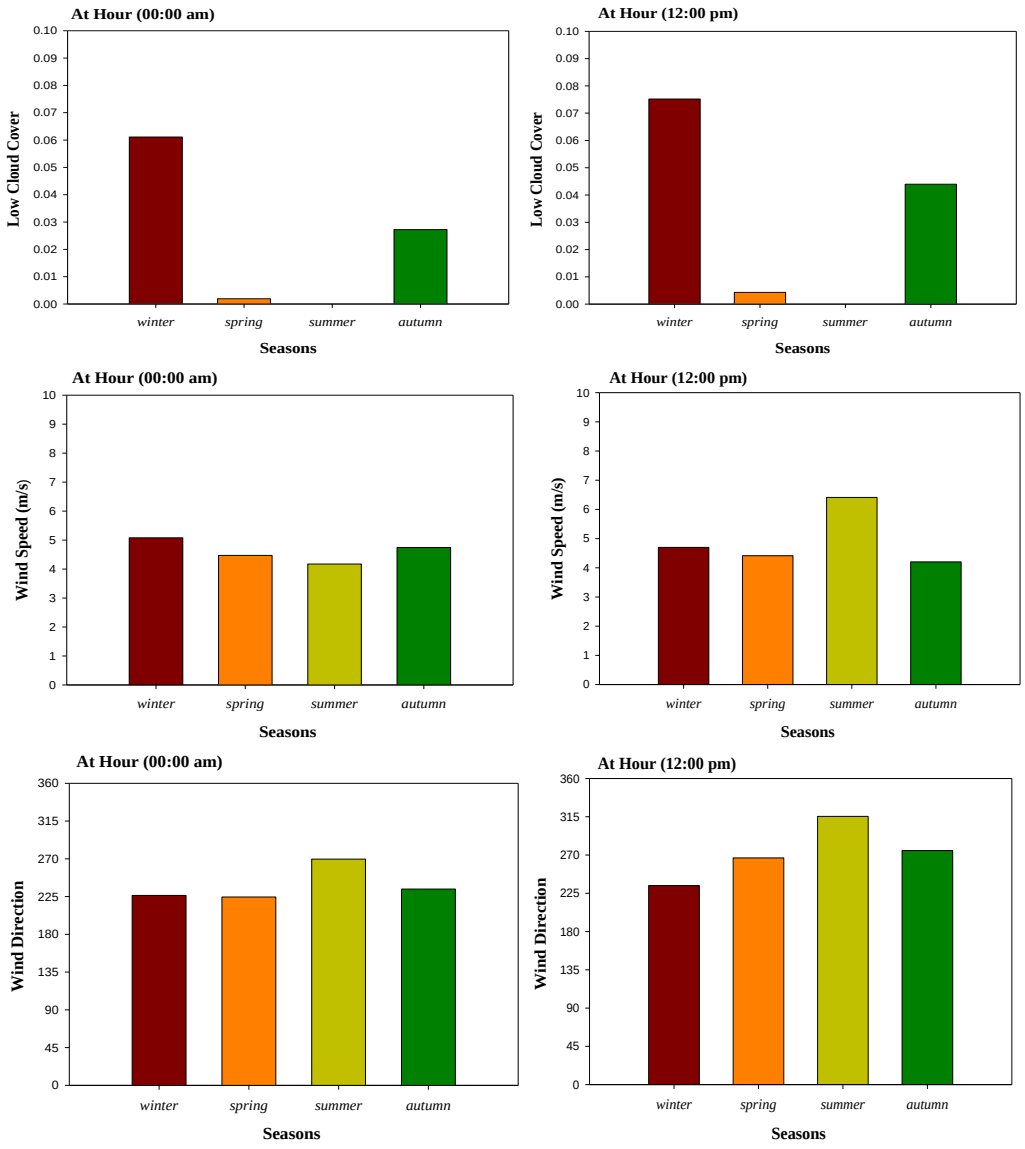

Figure 7. The seasonally means of LCC, WS and WD at 00:00 am -12:00 pm for Baghdad station

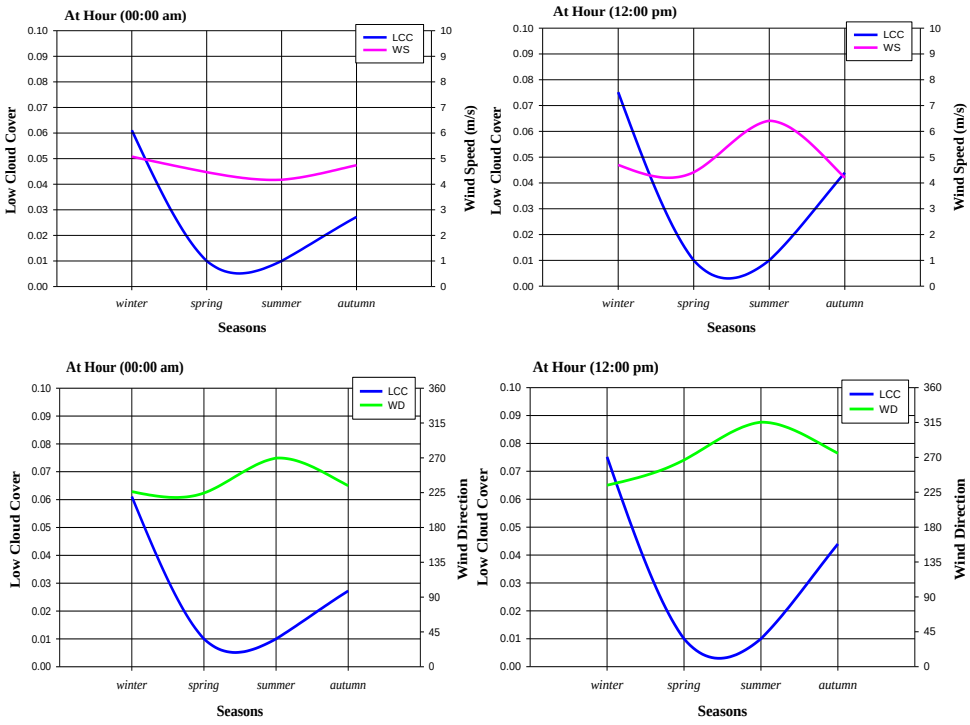

Figure 8. The seasonally change of (LCC and WS), (LCC and WD) at 00:00 am -12:00 pm for Baghdad station

5. Acknowledgements

The authors acknowledge the cooperation of the European Center Medium Weather Forecasts and are grateful for their provision of the data used in this study and sincere thanks to Mustansiriyah University.

References

[1] Yau, M.K. and Rogers, R.R., 1996. *A Short Course in Cloud Physics.* 3rd ed. Burington: Butterworth-Heinemann.

[2] Ahrens, C.D., 2011. *Essentials of Meteorology: an Invitation to the Atmosphere.* 6th ed. Boston: Cengage Learning.

[3] Orville, H.D., Farley, R.D. and Hirsch, J.H., 1984. Some surprising results from simulated seeding of stratiform-type clouds. *Journal of Applied Meteorology and Climatology*, 23(12), 1585-1600.

[4] Abodi, H., Thari, N. and Abbas, N., 2016. The relation between cloud cover and some atmospheric variable over Baghdad city. *Global Journal of Advanced Research*, 3(4), 283-289.

[5] Haberichter, K.M., 2017. *Comparison of Wind Speed, Soil Moisture, and Cloud Cover to Relative Humidity to Verify Dew Formation.* Meteorology Senior Theses. Iowa State University.
[6] Marlina, N. and Melyta, D., 2019. Analysis effect of cloud cover, wind speed, and water temperature to BOD and DO concentration using QUAL2Kw model (case study in Winongo river, Yogyakarta). *MATEC Web of Conferences*, 280, 05006, https://doi.org/10.1051/matecconf/20192800500.
[7] Janeiro, F.M., Carretas, L., Kandler, K., Wagner, F. and Ramos, P.M., 2014. Advances in cloud base height and wind speed measurement through stereophotogrammetry with low cost consumer cameras. *Measurement*, 51, 429-440.
[8] Abbood, Z.M. and Al-Taai, O.T., 2018. Calculation of absorption and emission of thermal radiation by clouds cover. *ARPN Journal of Engineering and Applied Sciences*, 13(24), 9446-9456.
[9] Abbood, Z.M. and Al-Taai, O.T., 2018. Study of absorbance and emissivity solar radiation by clouds, aerosols and some atmospheric gases. *Journal of Applied and Advanced Research*, 3(5), 128-134.
[10] Abd, H.F., 1997. *Frequences of Wind and Its Relationship to Cloud Cover in Geography Department.* Baghdad University.
[11] Dahiru, T., 2008. P-value, a true test of statistical significance? A cautionary note. *Annals of Ibadan Postgraduate Medicine*, 6(1), 21-26.
[12] Padua, D., 2000. The fortran I compiler. *Computing in Science & Engineering*, 2(1), 70-75.
[13] Williams, F. and Monge, P.R., 2001. *Reasoning with Statistics: How to Read Quantitative Research.*, 5th ed. Fort Worth: Harcourt College Publishers.
[14] Tuğran, E., Kocak, M., Mirtagioglu, H., Yigit, S. and Mendes, M., 2015. A simulation based comparison of correlation coefficients with regard to type I error rate and power. *Journal of Data Analysis and Information Processing*, 3, 87-101.
[15] Wang, G.J., Xie, C., Chen, S., Yang, J.-J. and Yang, M.-Y., 2013. Random matrix theory analysis of cross-correlations in the US stock market: Evidence from Pearson's correlation coefficient and detrended cross-correlation coefficient. *Physica A: Statistical Mechanics and Its Applications*, 392(17), 3715-3730.

Current Applied Science and Technology Vol. 21 No. 3 (July-September 2021)

Review article

Synthesis of Rare Earth Based Pyrochlore Structured ($A_2B_2O_7$) Materials for Thermal Barrier Coatings (TBCs) - A Review

J. Sankar and S. Suresh Kumar*

Department of Mechanical Engineering, Kalasalingam Academy of Research and Education, Krishnankoil, Tamil Nadu, India

Received: 11 Spetmber 2020, Revised: 7 December 2020, Accepted: 5 January 2021

Abstract

High temperature application requires protection coatings to ensure the optimal operating cycles to avoid the uncertainty caused by hot gases, foreign contaminates, ambient conditions and other occurrences. In general, protective coating materials can be ceramics, thermally grown oxides, silicates and some rare earth ores. For high-end applications such as gas turbines used in aviation, gas turbines surface are coated with a Thermal Barrier Coating to isolate the components thermally and protect the surfaces. Over the past four decades, those coatings have been employed with the inclusion of Yttrium Stabilised Zirconia (YSZ). The up growing developments on those areas require the coating, which can withstand temperatures above 1200°C. Due to this concern, the alternative to the YSZ based coatings finding has been accelerated. Rare earth oxides with pyrochlore structure ceramics are key interest to provide the coating properties comparatively more than YSZ-based coatings. In this paper, the preparation methods for pyrochlore structured ceramics are discussed. A solid state reaction method widely used for preparing the pyrochlore structure ceramics, but it requires higher temperature and long duration. Wet chemical methods such as precipitation, combustion and hydrothermal techniques produce the pyrochlores at lower temperature comparatively than that of solid state reaction-based methods. In coprecipitation method, intermediate hydrates are reduced into pyrochlores by calcinating at higher elevated temperature. Due to the heat treatment at higher temperature, agglomeration occurs. In the combustion synthesis, fuel-induced exothermic chemical reaction results in porous-structured powders. Upon heat treatment, it results in the porous pyrochlore- structured materials with the agglomeration of particles. Hydrothermal synthesis shows high energy efficiency, maximum yield, uniform particle size and morphology. It was understood that microwave-assisted hydrothermal synthesis requires shorter reaction time.

Keywords: thermal barrier coating; solid state reaction; hydrothermal synthesis
DOI 10.14456/cast.2021.47

*Corresponding author: Tel.: (+91) 9894665963
E-mail: sureshme48@gmail.com

1. Introduction

Thermal barrier coatings (TBCs) are generally used to safeguard the components of gas turbine power plants, gas turbine engines, and other hot sections where hot combustion gases with direct interaction [1-3]. Thermal protection coatings are employed to improve the life cycle of those components. Thermal barrier coating material needs to have a high melting temperature, good chemical stabilities from low temperature to high operating temperature, and it should not undergo phase transformation, and sintering during cyclic operation at higher temperature. Moreover, the material should have a low thermal conductivity at higher operating temperature, be well-adherable to substrates, and have a thermal expansion coefficient that matches with the bond coating [4]. Thermal barrier coating generally is employed with a nickel or cobalt-based metallic bond coat that improves the adhesion strength between the substrate and topcoat material. The coating materials are generally rare earth oxides, glasses, rare earth ores, and pyrochlores. A few of those coating materials that are widely used are as follows, zirconia (ZrO_2), alumina (Al_2O_3), lime (CaO), garnet ($Y_3Al_5O_{12}$), mullite, ceria (CeO_2), titanium oxide (TiO_2), lanthanum phosphate ($LaPO_4$), lanthanum aluminate ($LaMgA_{11}O_{19}$), barium zirconate ($BaZrO_3$), lanthanum zirconate ($La_2Zr_2O_7$) (LZ) and yttria stabilised zirconia (YSZ) [5]. Figures 1 and 2 show the melting temperature, the thermal expansion coefficient of the various above-discussed coating materials.

ZrO_2, CeO_2, and YSZ having high thermal expansion coefficient, which nearly match that of the NiCoAlY based Band Coat (BC) ($\alpha_{BC} = 17.5\times10^{-6}K^{-1}$) [6-8]. ZrO_2, YSZ, and Ba_2ZrO_3 having a higher melting temperature. YSZ, mullite, YSZ + CeO_2 coatings have excellent thermal shock resistance [9]. Silicates, alumina and mullite show higher corrosion resistance at higher working temperatures [10]. ZrO_2, YSZ, mullite, and alumina undergo phase transformation at higher temperature [11]. Mullite, alumina, $La_2Zr_2O_7$, and silicates have a very low thermal expansion coefficient [12]. ZrO_2, YSZ, and CeO_2 coating sinter at a higher temperature. ZrO_2 coating at higher temperatures shows a high level of oxygen transport to the BC, which causes thermally grown oxide (TGO) layer formation on the surfaces, leads to the spallation of ceramic coating and thus coating failure. YSZ has been commonly used as TBC material for the past four decades [13].

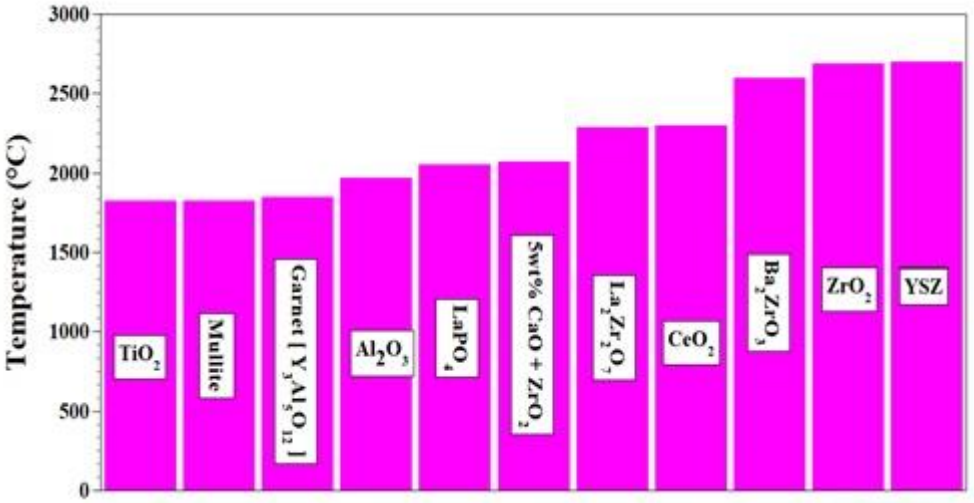

Figure 1. Melting temperature of various coating materials

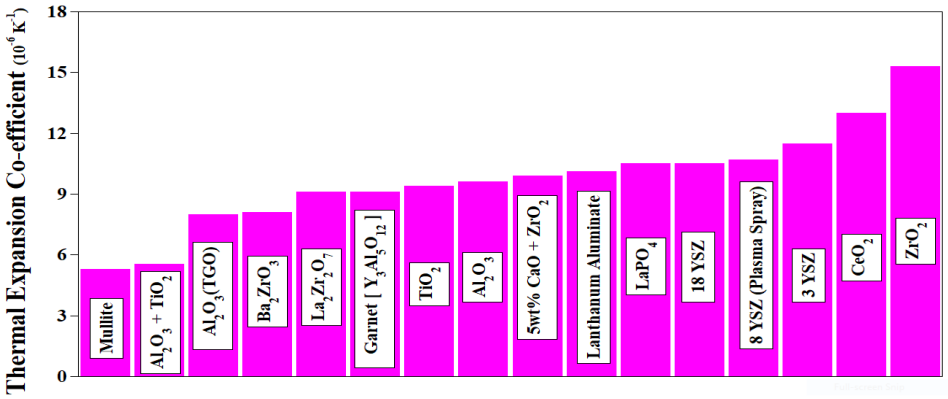

Figure 2. The thermal expansion coefficient of coating materials

At temperature beyond 1200°C, YSZ changes its crystal structure from tetragonal phase to tetragonal + cubic phase and then to monoclinic crystal structure [14]. As a consequence, at temperature above 1200°C, the volume of the coating material phase changes increases and sintering occurs due to this the reduction in thermal conductivity, which in turn leads to strain on the coating that results in cracking and prone to failure of coatings [15]. Undesirable phase transformation occurs at higher temperatures due to incomplete combustion of gases and air pollution [16].

For components operating under humid environment, and at low temperature, slow and spontaneous phase transformation from tetragonal to monoclinic at low temperature can occur. The above occurring phenomenon is known as low-temperature ageing degradation (LTAD) [17]. In the case of CeO_2 doped YSZ coating, the thermal stress generated at higher temperature closely matches the stress that develops on BC and shows higher and excellent thermal shock resistance, and the thermal expansion coefficient also increases more than YSZ [18]. Moreover, the CeO_2 doped YSZ coating reduces the hardness of the coating, and the vaporization of CeO_2 at higher operating temperatures leads to an accelerated sintering rate [19].

Pyrochlore structures are used in a vast range of applications such as catalysis, nuclear waste management, hydrogen production, sensors, and thermal barrier coatings. This is due to their unique crystal structure, thermal stability from room temperature to higher operating temperature, lower thermal conductivity at a higher temperature and good ionic conductivity. The pyrochlore structure belongs to the Fd-3m space group where A sites are occupied by mono, di and tri-valent rare earth cations and B sites are occupied by 3d, 4d and 5d transition metal cations. Among all the above oxidization states, $A^{3+}{}_2B^{4+}{}_2O_7$ species are widely preferred due to their stable ionic radius ratio [20].

Table 1 shows the various rare earth elements cationic radiuses in Å. Many of the rare earth elements have different RE^{3+} and RE^{4+} oxidization states, and those cationic radiuses are also mentioned in Table 1.

Lanthanum zirconates (LZ) contains two crystal structures that can be classified as ordered pyrochlore and disorder fluorite [21]. The type of crystal structure is based on the annealing temperature and the ratio of the crystal structure ionic radius of $r(Re^{3+})/r(Zr^{4+})$ [22]. In pyrochlore structures, the ratio lies between 1.46 and 1.78 [23]. LZ with the pyrochlore structure shows a longer thermal cycling life. The pyrochlore-structured materials have $A^{3+}{}_2B^{4+}{}_2O_7$ structure. Rare earth lanthanum, gadolinium, samarium, and neodymium can be substituted into "A" lattice site, and zirconium, cerium, and titanium may be situated on "B" sites. In recent days, researchers have also investigated co-doped pyrochlore for TBCs.

Table 1. Ionic radius of A^{3+} and B^{4+} cations

A cation	r(A^{3+}) in Å	B cation	r(B^{4+}) in Å
Yb	0.985	Ru	0.62
Er	1.004	Nb	0.68
Y	1.019	Ta	0.68
Dy	1.027	Hf	0.71
Gd	1.053	Zr	0.72
Eu	1.066	Ce	0.87
Sm	1.079	Y	0.90
Nd	1.109	Eu	0.947
Ce	1.143	Sm	0.958
La	1.16	Sc	0.745
Pr	1.126		

In this review work, the various possible synthesis routes available to prepare the rare earth-based pyrochlore structured materials for thermal barrier coatings are explored. The most widespread solid-state reaction is discussed initially with recently reported research work. In addition to this, the bottom-up wet chemical synthesis routes, namely coprecipitation, hydrothermal, sol-gel and combustion methods are discussed. Moreover, the thermomechanical properties of the synthesis materials are also explored in the article.

2. Preparation of Pyrochlore

The preparation of the pyrochlore structured TBC materials can be done by following methods: solid-state reaction, sol-gel method, solution reaction method, co-precipitation method, hydrothermal synthesis method and hydrazine methods [24]. The solid-state reaction method is widely used to synthesize pyrochlore in larger quantity, and the preparation of pyrochlore requires temperature above 900°C. Pyrochlore synthesized by the solid-state reaction displays heterogeneous mean particle size, and it gets easily agglomerated during heat treatment and sinters at very high temperatures. Wet chemical synthesis, on the other hand, involves synthesis of pyrochlore at the molecular level, so it provides powers with uniform particle size. Hydrothermal synthesis enables the preparation of pyrochlore at lower temperature than the solid-state reaction. Researchers also found the use of surfactants in hydrothermal synthesis that reduces the reaction temperature, pH, reaction time duration. Sol-gel methods, co-precipitate method, and hydrazine methods are also used to prepare the hydrates of the corresponding pyrochlore. Sintering process at higher temperatures results in the production of the required pyrochlore materials.

2.1 The solid state reaction method

In the solid-state reaction method (Figure 3), the rare earth oxide mixture at required stoichiometry is preheated to remove moisture and other impurities for about 120°C for 2 h. The resultant mixture is ball-milled for 15 min to form a uniform mixture immersion with distilled water or absolute ethanol. The resultant colloidal mixture heat treatment/calcination/sintering is carried out at above 1500°C to obtain the required pyrochlore structure. Researchers [25-27] also reported the ball milling and sintering process needed to be repeated a few times to obtain the required uniform pyrochlore structure.

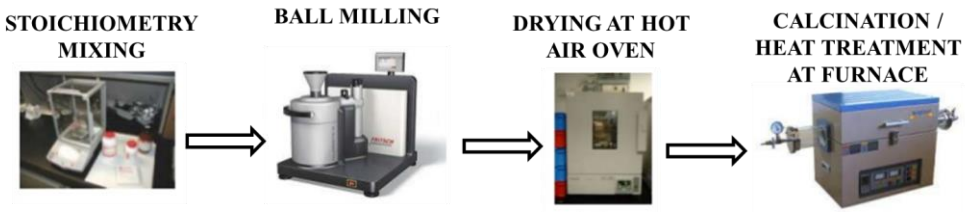

Figure 3. Pictorial representation of solid-state reaction method

Zhong *et al*. [27] prepared gadolinium zirconate (GL) pyrochlore powders through the solid-state reaction by sintering powder at 1500°C for 12h. Zhou *et al*. [28] prepared GZ pyrochlore for TBC using their respective oxides Gd_2O_3 and ZrO_2 stoichiometry and milled mixture dissolving in absolute ethanol, with a small amount of polyethyleneimine added after milling and the resultant mixture suspension diluted with 5 wt% of ethanol before coating. Lehmann *et al*. [29] prepared lanthanum rare earth element zirconate pyrochlore using a solid-state reaction method. Stoichiometric quantities of lanthanum oxides and ZrO_2 preheated at 1200°C for 2 h were taken at required composition and added to ethanol for ball milling for 24 h in a planetary milling using zirconia containers and balls. The resultant powder, after drying underwent a solid-state reaction at 1400°C for 24 h in zirconia crucible.

Ma *et al*. [25] prepared rare earth-codoped strontium zirconate pyrochlore by using a solid-state reaction. The rare earth oxides Y_2O_3, Yb_2O_3, $SrCO_2$, and ZrO_2 powders were mixed by milling for 24 h with 50 wt% water using zirconia balls. The milled powder water mixture was dried at 1450°C for 24 h and milled 15 min to avoid contaminations. The synthesis procedure was repeated until the required phase material had formed. Zhong *et al.* [30] prepared gadolinium zirconate by a solid-state reaction. Gd_2O_3 and ZrO_2 underwent a solid-state reaction at about 1500°C for 12 h. Ma *et al.* [31] prepared Ta_2O_5 and Yb_2O_3 codoped strontium zirconate using a solid-state reaction. The ball-milled powders were sintered at 1450°C for 24 h and the process was repeated three times to obtain the required phase material formation. The resultant powders were cold-pressed under a pressure of 30 MPa and the sintering process was carried out at 1700°C for 6 h in ambient air.

Li *et al*. [32] prepared lanthanum zirconate pyrochlore powder using a solid-state reaction. La_2O_3 and ZrO_2 powders were ball-milled for 24 h using zirconia balls with DI water and the resultant suspension was sintered at 1400°C for 12 h. Hu *et al*. [33] prepared Nd and Ce codoped $Gd_2Zr_2O_7$ pyrochlore ceramic using a solid state reaction. All the rare earth oxides were preheated at 120°C for 3 h to remove moisture and impurities, taken at the required ratio, and milled by grinding. The ground powder was compacted into pellet form under 10 MPa pressure and sintered at 1500°C for 72 h to perform the solid-state reaction. Mazilin *et al*. [34] prepared $Ln_2Zr_2O_7$ Zirconates using a solid-state reaction. Zirconium, neodymium, samarium, and gadolinium nitrate solutions were prepared separately and mixed gravimetrically. The mixture solution was fed into a spray reactor heated by hot air. The resultant powder was collected using a bag filter. Pasupuleti *et al*. [35] prepared lanthanum zirconate, lanthanum cerium zirconate, and cerium zirconate pyrochlore powder using a solid-state reaction. Table 2 shows the various rare earth-based pyrochlores' thermal expansion coefficients.

Wang *et al*. [36] prepared ytterbium cerium oxide by zirconate doping using a solid-state reaction involving sintering at 1500°C for 5 h. Yang *et al*. [38] prepared rare earth zirconate with cerium doping using a solid state reaction. The powders were preheated at 1000°C for 5 h, and then Yb_2O_3, ZrO_2, and CeO_2 were ball-milled with ethanol at the required composition using planetary ball mill for 12 h at 300 rpm and calcined at 1000°C for 5 h. Ma *et al*. [26] prepared strontium

Table 2. The thermal expansion coefficients of various pyrochlores prepared by solid-state reaction

Material	Coefficient of thermal expansion in ($\times 10^{-6}$ K^{-1})	Reference	Material	Coefficient of thermal expansion in ($\times 10^{-6}$ K^{-1})	Reference
$Gd_2Zr_2O_7$	10.4	[25]	$Yb_2(Ce_{0.5}Zr_{0.5})_2O_7$	11.4	[35]
$La_2Zr_2O_7$	9.1	[27]	YSZ	11	[35]
$La_{1.7}Dy_{0.3}Zr_2O_7$	8.8	[27]	$La_2Ze_2O_7$	9.1	[35]
$La_{1.4}Nd_{0.6}Zr_2O_7$	8.2	[27]	$Sr_2Zr_2O_7$	9.0 to 10.8	[36]
$La_{1.4}Eu_{0.6}Zr_2O_7$	9.3	[27]	$Yb_2Zr_2O_7$	11.1	[37]
$La_{1.4}Gd_{0.6}Zr_2O_7$	9.35	[27]	$Yb_2(Zr_{0.9}Ce_{0.1})_2O_7$	11.5	[37]
$Gd_2Zr_2O_7$ – 3 YSZ	10.6	[29]	$Yb_2(Zr_{0.7}Ce_{0.3})_2O_7$	11.75	[37]
$Yb_2Ce_2O_7$	11.8	[35]	$Yb_2(Zr_{0.5}Ce_{0.5})_2O_7$	12	[37]
$Yb_2(Ce_{0.9}Zr_{0.1})_2O_7$	11.7	[35]			

zirconate codoping with double rare earth oxide using a solid-state reaction. ZrO_2 and Yb_2O_3 underwent heat-treatment at 1000°C for 2 h and $SrCO_3$ was added and ball-milled for 24 h using zirconia balls with DI water. The resultant mixture was heat-treated at 1400°C for 24 h. The above ball milling and heat treatment was repeated until the single-phase pyrochlore structures were formed [38]. Pasupuleti *et al*. [39] prepared LZ, LC, and LZ – C zirconate using a solid-state reaction method.

2.2 Coprecipitation method

The coprecipitate method (Figure 4) is a wet chemical synthesis route and easy method to prepare pyrochlore structure after the solid-state reaction method. In this method, the rare earth nitrate salts were dissolved in DI water and the rare earth oxides were dissolved in acid and then the two solution were mixed. The pH was increased to about 9.0 to 11.0 for the above mixture using ammonia or sodium hydroxide, resulting in the formation of rare-earth complex hydrates. The heat treatment and sintering reduce the hydrates into uniform pyrochlore structures.

Zhang *et al*. [40] prepared amorphous lanthanum zirconate pyrochlore using a wet chemical co-precipitate method. Zirconate oxychloride and lanthanum nitrate salts were taken as starting materials, and ammonia was used as a pH stabilizer to raise pH to more than 9. The resultant solution stirring for 24 h resulted in a gel-like precipitate. The filtered and washed precipitates at pH 7 were initially dried at 80°C for 12 h and heat-treated at 300°C for 1 h. Liu *et al*. [41] prepared ytterbium and samarium oxide codoping zirconate pyrochlore using the co-precipitate method. The rare earth oxides of ytterbium and samarium were preheated at 900°C for 2 h to remove the impurities and dissolved in dilute nitric acid. Zirconia oxychloride was dissolved in DI water and all solution mixed with stirring then filtered. The filtered solution pH was increased by adding diluted ammonia solution with stirring resulting in the formation of gel-like precipitates. The resultant precipitates were rinsed and filtered with water and ethanol a few times. The resultant powder was dried and heat-treated at 800°C for 5 h in the air. The heat-treated powder underwent compacting and sintering at 1700°C for 10 h in the air. Zhou *et al*. [42] prepared rare earth codoping on lanthanum zirconate using the co-precipitate method. Lanthanum oxide was dissolved in hydrous nitric acid and zirconia oxychloride was dissolved in DI water mixed and the mixture was stirred for 30 min. Aqueous ammonia added to the above mixture solution to obtain a pH of 12.5, and

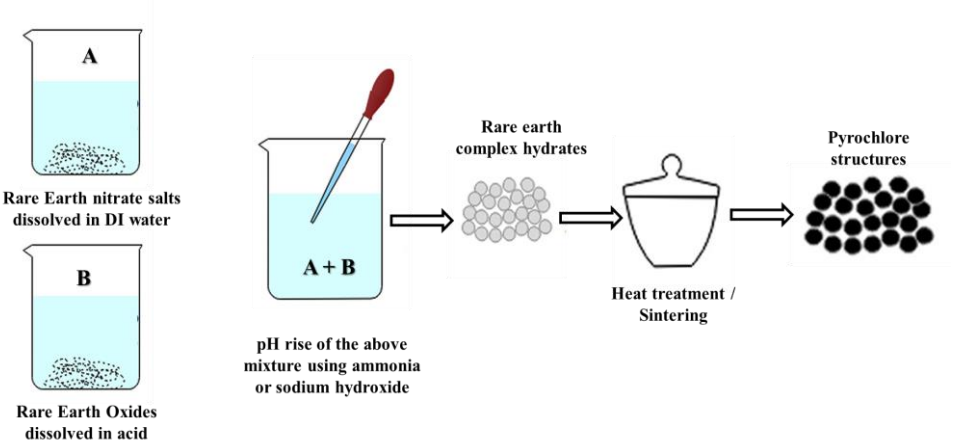

Figure 4. Pictorial representation of coprecipitation method

a gel-like precipitate formed. The precipitates was filtered, washed, and dried at 120°C for 12 h, heat-treated at 600°C for 10 h and calcinated at 1200°C for 5 h.

Gentleman *et al*. [43] prepared europium doped zirconate and YZ using the reverse co-precipitate method. Europium nitrate and yttrium nitrate salt solution, zirconium acetate solution were prepared in DI water. The mixture of all the solution resulted in the formation of a precipitate. The dried precipitates were heat-treated at 950°C and sintered at 1200°C for 2 h. Torres-Rodriguez *et al*. [44]. prepared $Ln_2Zr_2O_7$ (Ln = La, Nd, Dy, and Gd) pyrochlore powders using the co-precipitate method. Ln nitrate salts and zirconium oxychloride were dissolved separately in water with stirring for 30 min and then mixed with further stirring for 2 h. Aqueous ammonia solution used as the pH stabilizer to reach pH of 11 resulted in the formation of precipitates. The precipitates were rinsed with water and dried at 120°C for 12 h. Heat treatment was carried out at 1000°C in the air for 5 h to obtain the $Ln_2Zr_2O_7$ powder.

Bencina *et al*. [45] prepared $Bi_2Ti_2O_7$ pyrochlore using the co-precipitate method. $Bi(NO_3)_3{\cdot}5H_2O$ was dissolved in acetic acid with 20 min stirring and titanium isopropoxide was added to the above solution mixture and stirred for 5 min. Ammonium hydroxide solution was added dropwise to obtain a white-coloured precipitate. The precipitate was rinsed with water and dried at 100°C for 3 h. The dried powder was heat-treated at 550°C for 5-12 h. Gupta *et al*. [46] prepared Eu^{3+} doped $La_2Hf_2O_7$ using the co-precipitate method and MSS procedure with varying pH.

Kaliyaperumal *et al*. [47] prepared $Nd_2Zr_2O_7$ using the co-precipitation method. Neodymium nitrate, zirconium oxychloride were dissolved with Di water, and ammonia solution was added to adjust the pH to 11, which resulted in the formation of a precipitate. The precipitates was washed with water, ethanol and dried at 100°C and heat-treated at 800°C, 1000°C, 1200°C, and 1300°C. Pokhrel *et al*. [48] prepared pyrochlore Rare Earth Hafnate $RE_2Hf_2O_7$ (RE = La, Pr) using the co-precipitate method. Popov *et al*. [49] prepared $Ln_2M_2O_7$ (Ln = Gd, Tb, Dy; M = Ti, Zr) pyrochlore using coprecipitate method. Wang *et al*. [50] prepared rare earth-substituted $Ln_2Sn_2O_7$ pyrochlore (Ln = La, Nd and Sm) using the co-precipitation method. Rare earth nitrate and $SnCl_4{\cdot}5H_2O$ were dissolved in water, and NaOH aqueous solution added to the mixture to reach pH 9.5 ± 0.5 under vigorous stirring for 1hr. The resultant precipitate and mother liquor were aged at 50°C for 2 h and filtered. The filtered powder was washed and dried at 80°C for 12 h and then 120°C for 12 h before heat treatment at 900°C for 6 h in the air atmosphere. Table 3 shows the various rare

Table 3. Thermal conductivity, thermal diffusivity and hardness of pyrochlores prepared by coprecipitation

Material	Thermal conductivity in W/m·K	Thermal diffusivity in mm^2/s	Hardness in GPa	Reference
$Pr_2Zr_2O_7$	0.7	2.75	9.9	[48]
$Sm_2Zr_2O_7$	0.49	2.5	9.8	[48]
$(PrSm)_2Zr_2O_7$	0.38	1.25	8.9	[48]

earth-based pyrochlores' thermomechanical properties and significant pyrochlores suitable for thermal protection coatings.

2.3 Combustion method

The combustion method is similar to the precipitation technique described above; however, the use of fuel source and oxygen source results in auto-ignition and thus the production of pyrochlore powders. The fuel chemical agent was glycine, hydrazine, citric acid, and glycerol. The post-heat treatment of the fluffy powder removes the impurities and results in the required pyrochlore structure powders.

The combustion method (Figure 5) gives high efficiency, involves a simple reaction with low energy consumption, and produces powders with uniform morphology. The combustion method produces pyrochlore powder with a highly porous structure.

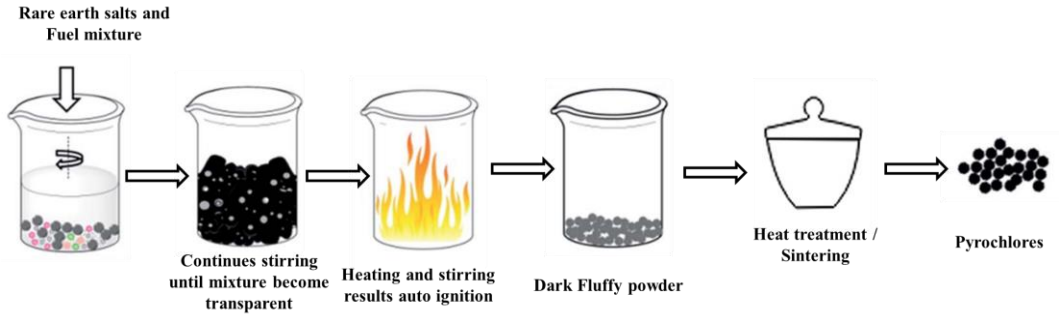

Figure 5. Pictorial representation of combustion method.

Matovic *et al*. [51] prepared lanthanum zirconate, dissolving lanthanum nitrate, zirconium chloride in glycine. The resultant solution was heat-treated at 950°C for 2 h then sintered at 1600°C for 4 h. Venkatesh *et al*. [52] prepared cerium zirconate using the combustion synthesis method. Cerium nitrate and zirconium nitrate solution were prepared by dissolving it in nitric acid and stirring for complete dissolving. Glycine was dissolved separately in DI water before adding dropwise to the cerium-zirconium mixture at a slow stirring rate and stirring was continued for 45 min with mild heat. This resulted in solution becoming transparent. The transparent solution was transferred to an alumina crucible and kept in a muffle furnace at 650°C for 10-15 min. the resultant powder was sintered at 1100°C to form $Ce_2Zr_2O_7$.

Li *et al*. [53] prepared $Gd_2Zr_2O_7$ transparent ceramic using the combustion synthesis method under vacuum sintering. $Gd(NO_3)_3{\cdot}6H_2O$ and $Zr(NO_3)_4{\cdot}5H_2O$ were dissolved in water and hydrous ammonia added to the mixture. The mixture was heated until the gelatine formed, and then

it was transferred to a muffle furnace and heated at 300°C until a fluffy grey powder formed. The powder was calcinated at 1200°C for 2 h and ball-milled for 24 h with DI water. The slurry was dried, pelleted and sintered at 1775°C, 1800°C, and 1825°C for 6 h in a vacuum and annealed at 1500°C for 5 h in the air. Jeyasingh *et al*. [54] prepared $Gd_2Ti_2O_7$ using the combustion process. Gd_2O_3 and TiO_2 were dissolved in nitric acid and mixed with distilled water and citric acid added with stirring for uniform mixing. Nitric acid and ammonium hydroxide were added to the above mixture to adjust the oxygen fuel ratio. The complex mixture at pH 7 was heated at 250°C. Dehydration followed by decomposition resulted in a dark form that auto-ignited, which resulted in voluminous and fluffy combustion powder. The fluffy combustion powder was calcinated at 600°C to remove the carbon residues.

Jeyasingh *et al*. [55] prepared $Dy_2Ti_2O_7$ pyrochlore oxide using combustion synthesis. Dy_2O_3 and TiO_2 were dissolved in nitric acid and mixed with diluted citric acid with stirring at room temperature. Ammonium hydroxide was added to increase the pH to 7 pH 7 and match the oxygen fuel ratio. Heating at 250°C resulted in auto-ignition and a dark fluffy powder. The powder was then calcinated at 700°C, pelleted and sintered at 1400°C for 4 h. $A_2Ti_2O_7$ (A = Gd, Dy and Y) pyrochlore oxide was also prepared using the combustion synthesis method. Ai *et al*. [56] prepared Ca–Co dually-doped lanthanum tin pyrochlore oxide using the combustion synthesis method. $SnCl_4 \cdot 5H_2O$ and $Co(NO_3)_3 \cdot 6H_2O$ were dissolved in DI water and heated at 80°C. Sodium hydroxide was added to the above mixture and this resulted in the white-coloured precipitate. $La(NO_3)_3 \cdot 6H_2O$ and $CaCl_2$ were dissolved in DI water and heated at 80°C. Sodium hydroxide was added to the above mixture and white colour precipitate formed. The above two precipitates were mixed, and pH adjusted to 10 by adding additional sodium hydroxide solution. CTAB was added at 1:1 ratio with metal ions by rapidly dissolving under sonication. The mixture was heated at 80°C for 5 h in an underwater bath and then heated at 80°C for 24 h. The precipitate was filtered and dried at 110°C overnight and calcinated at 900°C for 6 h in the air [57].

Quader *et al*. [58] prepared Nd–substituted $La_2Sn_2O_7$ pyrochlore using sol-gel auto combustion. $La(NO_3)_3 \cdot 6H_2O$, $Nd(NO_3)_3 \cdot 6H_2O$, $SnCl_4$ precursors, and fuel agents NH_2CH_2COOH and CH_4N_2O were dissolved separately in DI water with 2:1 ratio of fuel and precursors. The solution was mixed in a single beaker, heated at 90°C, and stirred at 300 rpm using a magnetic stirrer to obtain a viscous solution. The solution was further heated at 180°C to form paste-like colloid, and again increased up to 260°C which formed exothermic reaction that produced a fluffy powder. The fluffy powder was ground into a fine powder and calcinated at 600°C for 3 h. The calcinated powder was pelleted and sintered at 400°C for 1 h.

Zhang *et al*. [59] prepared a $(Gd_2\text{-}XCe_x)Ti_2O_7$ pyrochlore structure using the combustion method. Tetra butyl titanate, Gd_2O_3, $Ce(NO_3)_3 \cdot 6H_2O$ were used as precursors and glycerol was used as fuel. $Ce(NO_3)_3 \cdot 6H_2O$ was dissolved in water, Gd_2O_3 was dissolved in nitric acid and then heated to remove the excess amount of nitric acid and then all three prepared precursor solutions are combined. Tetra butyl titanate was added dropwise resulting in the formation of a precipitate. The appropriate amount of citric acid was added to the mixture solution and stirred until complete dissolution was achieved. The solution was heated at 200°C with stirring resulted in a gel-like solution and further dehydration resulted in auto-ignition that left behind voluminous powder. The resultant powder was calcinated at 1200°C for 2 h.

2.4 Hydrothermal method

In hydrothermal synthesis (Figure 6), the reaction precursors at required composition are dissolved with a suitable solvent, mixed by stirring and pH of the mixture solution is raised above 7 by using agents like ammonium hydroxide and sodium hydroxides. The clear transparent solution is then

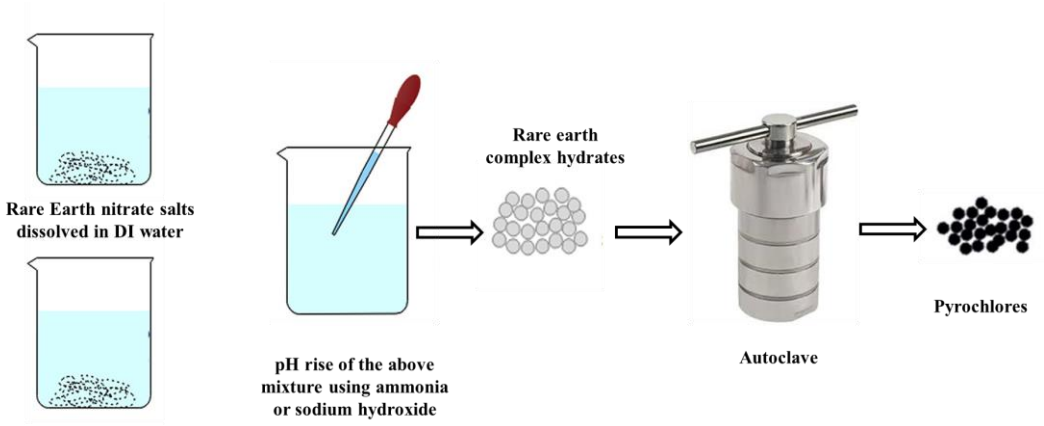

Figure 6. Pictorial representation of the hydrothermal synthesis method

transferred to the hydrothermal reaction chamber for the processing of hydrothermal synthesis. The hydrothermal synthesis method is the only method, which uses a lower reaction temperature (below 400°C) than other methods. The hydrothermal synthesis consumes long reaction duration, the reaction time depends on the pH of the solution. Surfactants are also used to reduce reaction time. Microwave-assisted hydrothermal synthesis features reduced reaction time.

Wang *et al*. [60] prepared $Sm_2Zr_2O_7$ pyrochlore using hydrothermal synthesis. SmO_2 and $ZrOCl_2{\cdot}8H_2O$ were dissolved in HNO_3 and stirred for 10 min. Aqueous ammonia was added to the above mixture to obtain pH 5-9, which resulted in the formation of a white precipitate. The precipitates was washed, and KOH solution was added with vigorous stirring and the mixture was transferred into a teflon-lined autoclave. A hydrothermal reaction was carried out at 100°C and 200°C. The resultant powder was washed and dried at a vacuum at 70°C for 18 h.

Hongming and Danqing [61] prepared lanthanum zirconates using lanthanum and zirconate nitrate salts, and NaOH was used to raise the pH to 11, and a hydrothermal reaction was then carried out at 200°C for 1 h. Huo *et al*. [62] prepared $Ce_2Sn_2O_7$ using hydrothermal synthesis. Cerium nitrate and sodium stannite hydrate were dissolved in DI water, and pH was adjusted by NaOH and stirring for 10 min. The mixture was transferred into a teflon-lined stainless steel autoclave for hydrothermal synthesis. Gadipelly *et al*. [63] prepared $Y_2Ti_2O_7$ pyrochlore structure using microwave-assisted hydrothermal synthesis. Y_2O_3 and TiO_2 were dissolved in preheated nitric acid, and the pH of the mixture increased to 12 by adding NaOH. The mixture underwent microwave-assisted hydrothermal synthesis for 4 min. The resultant precipitates was dried and calcinated at 800°C-1050°C for 3 h.

Sanjeewa *et al*. [64] prepared rare earth pyrochlore germinates $RE_2Ge_2O_7$ (RE = Yb and Lu) using high-temperature hydrothermal synthesis. RE oxides and germinate oxides were loaded into silver ampules and mineralizer solution added and then welded and sealed. The ampules were kept in a hydrothermal chamber and the remaining volume was filled with DI water, sealed, and heated at 600°C for 14 days. Trujillano *et al*. [65] prepared $Sm_2Sn_2O_7$ pyrochlore using accelerated microwave-assisted hydrothermal synthesis. $Sm(NO_3)_3{\cdot}5H_2O$ and $SnCl_4{\cdot}5H_2O$ were dissolved in water and mixed with NaOH solution to increase the pH to 9, resulting in precipitates. The precipitate slurry was mixed for 24 h at room temperature and transferred to a teflon container and hydrothermal synthesis was carried out at 200°C for 4 h. The resultant powder was dried at 40°C for 8 h and 140°C for two days.

2.5 Sol-gel method

The sol-gel method (Figure 7) is one of the wet chemical synthesis methods used to prepare porous-structured materials that are composed of three-dimensional polymeric chains for a wide range of applications. The sol-gel process, which involves hydrolysis followed by condensation, results in synthesis of a gel-like substance with a repentant polymeric matrix, and the drying heat treatment results in the dense powders.

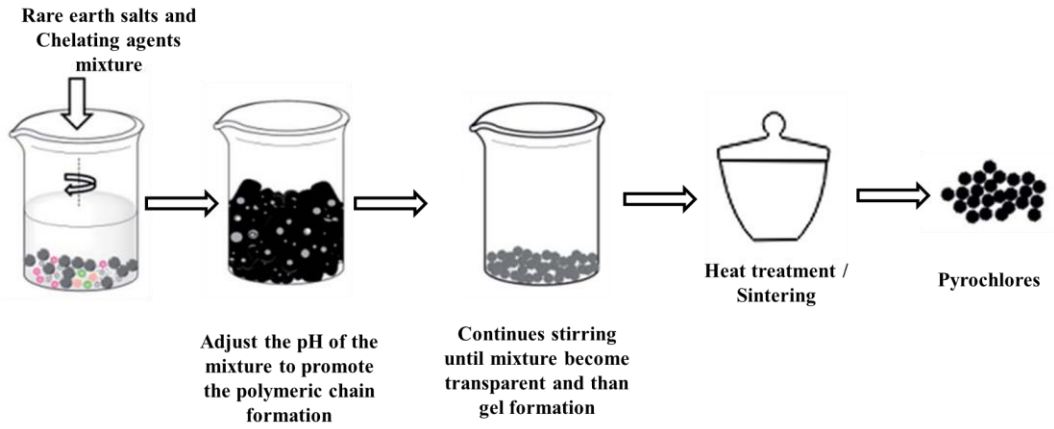

Figure 7. Pictorial representation of sol-gel method

Verma *et al*. [66] prepared rare earth titanate $RE_2Ti_2O_7$ (RE = Dy, Sm) crystal structure pyrochlore using the sol-gel method. $Ti(OiPr)_4$: EtOH : AcAc = 1: 27: 0.5 molar ratio and $RE(NO_3)_3 \cdot XH_2O$: EtHO = 1 : 10 molar ratio sol solutions were prepared separately by stirring for 30 min. The above two sol solutions were added together and stirred for 15 min and HNO_3 was added as a catalyst to promote hydrolysis. Additional DI water added to the above mixture to aid gel formation. The resultant gel was aged for 7 days and dried at 120°C for 48 h to obtain powder that was then annealed at 875°C for 4 h. Wang *et al*. [67] prepared $La_2Zr_2O_7$ pyrochlore using the sol-gel process and slurry. $ZrOCl_2 \cdot 8H_2O$ and $La(NO_3)_3 \cdot 6H_2O$ were dissolved in H_2O/EtOH solution mixed. Citric acid was added to the above mixture to achieve Zr^{4+} : La^{3+} : CA = 1: 1: 0.2. Chelating agent formamide (FA) and polyethylene glycol were added to the above mixture, which was then stirred at room temperature for 2 h to form uniform transparent sol solution. The resultant solution powder was put into a crucible and kept at 80°C for 20 h ageing, which resulted in gel formation. The resultant gel was dried at 110°C for 5 h and calcinated at 1200°C for 2 h in a muffle furnace to form homogeneous $La_2Zr_2O_7$ powders. Xia *et al*. [68] prepared Yb/Er/Eu: $Gd_2Ti_2O_7$ pyrochlore powders using the sol-gel method. Rare earth nitrate salts and titanium isopropoxide sol were prepared separately in DI water and mixed. Citric acid was separately mixed with ethanol and stirred for 30 min before adding to the above mixture with continuous stirring to obtain a transparent solution. The mixture solution was dried at 60°C and calcinated at 800°C for 3 h.

The comparison of all the synthesis processes based on various parameters are presented in Table 4.

Table 4. Synthesis process comparison

Parameters	Synthesis method				
	Solid state reaction	**Coprecipitation**	**Hydrothermal**	**Sol-gel**	**Combustion**
Approach	Top-down	Bottom-up	Bottom-up	Bottom-up	Bottom-up
Reaction parameters	Temperature, Time	pH, Temperature	Pressure, Temperature, pH	Surfactant, pH, Temperature	Fuel, Stabilizer, Temperature
Precursors	Rare earth oxides	Rare earth chloride and nitrate salts	Rare earth chloride and nitrite salts, rare earth oxides	Rare earth chloride and nitrate salts, rare earth isopropoxide	Rare earth nitrates
Particle size and shape	No uniform shape and size	Uniform shape not in uniform size	Uniform shape and size	No uniform shape and size	No uniform shape and size
Porosity	Low porosity	Low porosity	No porosity	Porous	Highly porous
Reaction duration	High	Moderate	Low	Moderate	Moderate
Calcination/ Heat treatment	Required	Required	Not required	Required	Required
Process reaction rate acceleration	Not possible	pH increase	Microwave assisted hydrothermal synthesis, pH	pH, surfactant	pH, stabilizer

3. Conclusions

The various synthesis techniques available to prepare the rare earth-based pyrochlore-structured materials have been discussed. Most of the commercial applications found use a solid-state reaction synthesis method, which is suitable for producing the larger quantity of the pyrochlores. The solid-

state reaction method produces pyrochlore-based material of a single phase. Drawbacks of this method are that this method consumes enormous time, produces no dimensional homogeneity and consumes a lot of energy. Wet chemical synthesis is an alternate method to solid-state synthesis, where the synthesis is possible at a lower temperature, and the synthesized powders have homogeneous particle distribution, unique crystalline structure with excellent physical as well as mechanical properties. Hydrothermal synthesis is one of the wet chemical methods in which the use of water at supercritical pressure can synthesize rare earth-based pyrochlores at less than 400°C with a uniform crystalline structure, and particle distribution with uniform morphology. The featured work was aimed for the mass production of rare earth-based pyrochlore-structured materials via hydrothermal synthesis possibilities for high efficiency and good yield.

References

[1] Zhang, J., Guo, X., Jung, Y.G., Li, L. and Knapp, J., 2017. Lanthanum zirconate based thermal barrier coatings: A review. *Surface and Coatings Technology*, 323, 18-29.

[2] Liu, B., Liu, Y., Zhu, C., Xiang, H., Chen, H., Sun, L., Gao, Y. and Zhou, Y., 2019. Advances on strategies for searching for next generation thermal barrier coating materials. *Journal of Materials Science and Technology*, 35(5), 833-851.

[3] Schmitt, M.P., Stokes, J.L., Rai, A.K., Schwartz, A.J. and Wolfe, D.E., 2019. Durable aluminate toughened zirconate composite thermal barrier coating (TBC) materials for high temperature operation. *Journal of the American Ceramic Society*, 102(8), 4781-4793.

[4] Cernuschi, F., Bianchi, P., Leoni, M. and Scardi, P., 1999. Thermal diffusivity/microstructure relationship in Y-PSZ thermal barrier coatings. *Journal of Thermal Spray Technology*, 8(1), 102-109.

[5] Cao, X.Q., Vassen, R. and Stöver, D., 2004. Ceramic materials for thermal barrier coatings. *Journal of the European Ceramic Society*, 24(1), 1-10.

[6] Garvie, R.C., 1970. Zirconium dioxide and some of its binary systems. *Refractory Materials*, 5, 117-166.

[7] Vassen, R., Cao, X., Tietz, F., Kerkhoff, G. and Stoever, D., 1999. $La_2Zr_2O_7$-a new candidate for thermal barrier coatings. *Proceedings of the United Thermal Spray Conference-UTSC'99*, DVS-Verlag, Düsseldorf, Germany, 1999, 830-834.

[8] Samsonov, G.V., 1982. *The Oxide Handbook*. New York: Springer.

[9] Ramaswamy, P., Seetharamu, S., Rao, K.J. and Varma, K.B.R., 1998. Thermal shock characteristics of plasma sprayed mullite coatings. *Journal of Thermal Spray Technology*, 7(4), 497-504.

[10] Xu, H., Guo, H., Liu, F. and Gong, S., 2000. Development of gradient thermal barrier coatings and their hot-fatigue behavior. *Surface and Coatings Technology*, 130(1), 133-139.

[11] Warshaw, I. and Roy, R., 1961. Polymorphism of the rare earth sesquioxides1. *The Journal of Physical Chemistry*, 65(11), 2048-2051.

[12] Chuanxian, D. and Zhaohe, T., 1992. Laboratory report-thermal spraying at the Shanghai Institute of Ceramics. *Journal of Thermal Spray Technology*, 1(3), 205-209.

[13] Chen, X., Zhao, Y., Fan, X., Liu, Y., Zou, B., Wang, Y., Ma, H. and Cao, X., 2011. Thermal cycling failure of new $LaMgAl_{11}O_{19}$/YSZ double ceramic top coat thermal barrier coating systems. *Surface and Coatings Technology*, 205(10), 3293-3300.

[14] Karthik, A., Srither, S.R., Dhineshbabu, N.R., Lenin, N., Arunmetha, S., Manivasakan, P. and Rajendran, V., 2019. Stabilization of tetragonal zirconia in alumina-zirconia and alumina-yttria stabilized zirconia nanocomposites: A comparative structural analysis. *Materials Characterization*, 158, https://doi.org/10.1016/j.matchar.2019.109964.

[15] Zhou, X., Song, W., Yuan, J., Gong, Q., Zhang, H., Cao, X. and Dingwell, D.B., 2020. Thermophysical properties and cyclic lifetime of plasma sprayed $SrAl_{12}O_{19}$ for thermal barrier coating applications. *Journal of the American Ceramic Society*, 103, 5599-5611.

[16] Northam, M., 2019. *Investigation of PS-PVD and EB-PVD thermal barrier coatings over lifetime using synchrotron X-ray diffraction.*MS. University of Central Florida.

[17] Gan, X., Yu, Z., Yuan, K., Xu, C., Zhang, G., Wang, X., Zhu, L. and Xu, D., 2018. Effects of cerium addition on the microstructure, mechanical properties and thermal conductivity of YSZ fibers. *Ceramics International*, 44(6), 7077-7083.

[18] Venkadesan, G. and Muthusamy, J., 2019. Experimental investigation of Al_2O_3/8YSZ and CeO_2/8YSZ plasma sprayed thermal barrier coating on diesel engine. *Ceramics International*, 45(3), 3166-3176.

[19] Keyvani, A., Bahamirian, M. and Kobayashi, A., 2017. Effect of sintering rate on the porous microstructural, mechanical and thermomechanical properties of YSZ and CSZ TBC coatings undergoing thermal cycling. *Journal of Alloys and Compounds*, 727, 1057-1066.

[20] Anantharaman, A.P. and Dasari, H.P., 2020. Potential of pyrochlore structure materials in solid oxide fuel cell applications. *Ceramics International*, https://doi.org/10.1016/j.ceramint.2020.10.012.

[21] Cao, X.Q., Vassen, R., Jungen, W., Schwartz, S., Tietz, F. and Stöver, D., 2001. Thermal stability of lanthanum zirconate plasma-sprayed coating. *Journal of the American Ceramic Society*, 84(9), 2086-2090.

[22] Lei, M.A., Weimin, M.A., Xudong, S.U.N., Jianan, L.I.U., Lianyong, J.I. and Han, S.O.N.G., 2015. Structure properties and sintering densification of $Gd_2Zr_2O_7$ nanoparticles prepared via different acid combustion methods. *Journal of Rare Earths*, 33(2), 195-201.

[23] Mandal, B.P., Shukla, R., Achary, S.N. and Tyagi, A.K., 2010. Crucial role of the reaction conditions in isolating several metastable phases in a Gd− Ce− Zr− O system. *Inorganic Chemistry*, 49(22), 10415-10421.

[24] Vaßen, R., Jarligo, M.O., Steinke, T., Mack, D.E. and Stöver, D., 2010. Overview on advanced thermal barrier coatings. *Surface and Coatings Technology*, 205(4), 938-942.

[25] Ma, W., Meng, X., Dong, H., Lun, W. and Zheng, X., 2013. Double rare-earth oxides co-doped strontium zirconate as a new thermal barrier coating material. *Journal of Thermal Spray Technology*, 22, 104-109

[26] Ma, W., Meng, X., Wen, J., Li, E., Bai, Y., Chan, W. and Dong, H., 2019. Aging effect on microstructure and property of strontium zirconate coating co-doped with double rare-earth oxides. *Journal of the American Ceramic Society*, 102, 2143-2153.

[27] Zhong, X., Zhao, H., Liu, C., Wang, L., Shao, F., Zhou, X., Tao, S. and Ding, C., 2015. Improvement in thermal shock resistance of gadolinium zirconate coating by addition of nanostructured yttria partially-stabilized zirconia. *Ceramics International*, 41(6), 7318-7324.

[28] Zhou, D., Mack, D.E., Bakan, E., Mauer, G., Sebold, D., Guillon, O. and Vaßen, R., 2020. Thermal cycling performances of multilayered yttria-stabilized zirconia/gadolinium zirconate thermal barrier coatings. *Journal of the American Ceramic Society*, 103(3), 2048-2061.

[29] Lehmann, H., Pitzer, D., Pracht, G., Vassen, R. and Stöver, D., 2003. Thermal conductivity and thermal expansion coefficients of the lanthanum rare-earth-element zirconate system. *Journal of the American Ceramic Society*, 86(8), 1338-1344.

[30] Zhong, X., Zhao, H., Zhou, X., Liu, C., Wang, L., Shao, F., Yang, K., Tao, S. and Ding, C., 2014. Thermal shock behavior of toughened gadolinium zirconate/YSZ double-ceramic-ayered thermal barrier coating. *Journal of Alloys and Compounds*, 593, 50-55.

[31] Ma, W., Lun, W., Dong, H., Wang, L., Song, F. and Zheng, X., 2011. Fundamental physical properties of Ta_2O_5 and Yb_2O_3 codoped strontium zirconate for thermal barrier coating applications. *Materials Research Innovations*, 15(5), 319-323.

[32] Li, J.Y., Dai, H., Zhong, X.H., Zhang, Y.F., Ma, X.F., Meng, J. and Cao, X.Q., 2008. Lanthanum zirconate ceramic toughened by $BaTiO_3$ secondary phase. *Journal of Alloys and Compounds*, 452(2), 406-409.

[33] Hu, Q., Zeng, J., Wang, L., Shu, X., Shao, D., Zhang, H. and Lu, X., 2018. Helium ion irradiation effects on neodymium and cerium co-doped $Gd_2Zr_2O_7$ pyrochlore ceramic. *Journal of Rare Earths*, 36(4), 398-403.

[34] Mazilin, I.V., Baldaev, L.K., Drobot, D.V., Marchukov, E.Y. and Akhmetgareeva, A.M., 2016. Composition and structure of coatings based on rare-earth zirconates. *Inorganic Materials*, 52(9), 939-944.

[35] Pasupuleti, K.T., Prasad, G.V., Akhil, M.P., Ramaswamy, P. and Murty, S.N., 2019. Adhesion strength studies on zirconia based pyrochlore and functionally gradient thermal barrier coatings. *Materials Today: Proceedings*, 19, 568-574.

[36] Wang, Y., Zhang, L., Wu, W. and Yang, J., 2019. Enhancement of thermal properties of ytterbium-cerium oxide by zirconium doping for thermal barrier coatings. *Philosophical Magazine Letters*, 99(9), 309-316.

[37] Ma, W., Meng, X., Wen, J., Li, E., Bai, Y., Chen, W. and Dong, H., 2019. Aging effect on microstructure and property of strontium zirconate coating co-doped with double rare-earth oxides. *Journal of the American Ceramic Society*, 102(4), 2143-2153.

[38] Yang, J., Zhao, M., Zhang, L., Wang, Z. and Pan, W., 2018. Pronounced enhancement of thermal expansion coefficients of rare-earth zirconate by cerium doping. *Scripta Materialia*, 153, 1-5.

[39] Pasupuleti, K.T., Ghosh, S., Dunna, U.M., Ramaswamy, P. and Murty, S.N., 2019. Influence of atmospheric plasma spray process parameters on crystal and micro structures of pyrochlore phase in rare earth zirconate thermal barrier coatings. *Materials Today: Proceedings*, 19, 731-736.

[40] Zhang, C., Zhao, J., Yang, L., Zhou, Y., Wang, Q., Chen, H., Yang, G., Gao, Y. and Liu, B., 2020. Preparation and corrosion resistance of nonstoichiometric lanthanum zirconate coatings. *Journal of the European Ceramic Society*, 40(8), 3122-3128.

[41] Liu, Z.G., Ouyang, J.H., Zhou, Y., Li, J. and Xia, X.L., 2009. Influence of ytterbium-and samarium-oxides codoping on structure and thermal conductivity of zirconate ceramics. *Journal of the European Ceramic Society*, 29(4), 647-652.

[42] Zhou, D., Mack, D.E., Bakan, E., Mauer, G., Sebold, D., Guillon, O. and Vaßen, R., 2020. Thermal cycling performances of multilayered yttria-stabilized zirconia/gadolinium zirconate thermal barrier coatings. *Journal of the American Ceramic Society*, 103, 2048-2061.

[43] Gentleman, M.M., and Clarke, D.R., 2005. Luminescence sensing of temperature in pyrochlore zirconate materials for thermal barrier coatings. *Surface and Coatings Technology*, 200(5-6), 1264-1269.

[44] Torres-Rodriguez, J., Gutierrez-Cano, V., Menelaou, M., Kaštyl, J., Cihlář, J., Tkachenko, S., González, J.A., Kalmár, J., Fábián, I., Lázár, I. and Čelko, L., 2019. Rare-earth zirconate $Ln_2Zr_2O_7$ (Ln: La, Nd, Gd, and Dy) powders, xerogels, and aerogels: preparation, structure, and properties. *Inorganic Chemistry*, 58(21), 14467-14477.

[45] Benčina, M. and Valant, M., 2018. $Bi_2Ti_2O_7$-based pyrochlore nanoparticles and their superior photocatalytic activity under visible light. *Journal of the American Ceramic Society*, 101(1), 82-90.

[46] Gupta, S.K., Zuniga, J.P., Ghosh, P.S., Abdou, M. and Mao, Y., 2018. Correlating structure and luminescence properties of undoped and Eu^{3+}-doped $La_2Hf_2O_7$ nanoparticles prepared with different coprecipitating pH values through experimental and theoretical studies. *Inorganic Chemistry*, 57, 11815-11830.

[47] Kaliyaperumal, C., Sankarakumar, A., Palanisamy, J. and Paramasivam, T., 2018. Fluorite to pyrochlore phase transformation in nanocrystalline $Nd_2Zr_2O_7$. *Materials Letters*, 228, 493-496.

[48] Pokhrel, M., Gupta, S.K., Wahid, K. and Mao, Y., 2019. Pyrochlore rare-earth hafnate $RE_2Hf_2O_7$ (RE= La and Pr) nanoparticles stabilized by molten-salt synthesis at low temperature. *Inorganic Chemistry*, 58(2), 1241-1251.

[49] Popov, V.V., Menushenkov, A.P., Ivanov, A.A., Yastrebtsev, A.A., Gaynanov, B.R., Acapito, F. and Puri, A., 2020. A XAFS investigation of amorphous-to-crystalline and fluorite-to-pyrochlore phase transitions in $Ln_2M_2O_7$ (Ln = Gd, Tb, Dy; M = Ti, Zr). *Radiation Physics and Chemistry*, 175, 108469.

[50] Wang, Z., Zhu, H., Ai, L., Liu, X., Lv, M., Wang, L., Ma, Z. and Zhang, Z., 2016. Catalytic combustion of soot particulates over rare-earth substituted $Ln_2Sn_2O_7$ pyrochlores (Ln= La, Nd and Sm). *Journal of Colloid and Interface Science*, 478, 209-216.

[51] Matovic, B., Maletaskic, J., Zagorac, J., Pavkov, V., Maki, R.S., Yoshida, K. and Yano, T., 2020. Synthesis and characterization of pyrochlore lanthanide (Pr, Sm) zirconate ceramics. *Journal of the European Ceramic Society*, 40(7), 2652-2657.

[52] Venkatesh, G., Subramanian, R. and Berchmans, L.J., 2019. Phase analysis and microstructural investigations of $Ce_2Zr_2O_7$ for high-temperature coatings on Ni-base superalloy substrates. *High Temperature Materials and Processes*, 38(2019), 773-782.

[53] Li, W., Zhang, K., Xie, D., Deng, T., Luo, B., Zhang, H. and Huang, X., 2020. Characterizations of vacuum sintered $Gd_2Zr_2O_7$ transparent ceramics using combustion synthesized nanopowder. *Journal of the European Ceramic Society*, 40(4), 1665-1670.

[54] Jeyasingh, T., Saji, S.K. and Wariar, P.R.S., 2017. Synthesis of nanocrystalline $Gd_2Ti_2O_7$ by combustion process and its structural, optical and dielectric properties. *AIP Conference Proceedings*, 1859(1), https://doi.org/10.1063/1.4990169

[55] Jeyasingh, T., Saji, S.K., Kavitha, V.T. and Wariar, P.R.S., 2018. Frequency dependent dielectric properties of combustion synthesized $Dy_2Ti_2O_7$ pyrochlore oxide. *AIP Conference Proceedings*, 1953(1), https://doi.org/10.1063/1.5032442

[56] Ai, L., Wang, Z., Cui, C., Liu, W. and Wang, L., 2018. Catalytic oxidation of soot on a novel active Ca-Co dually-doped lanthanum tin pyrochlore oxide. *Materials*, 11(5), 653, https://doi.org/10.3390/ma11050653.

[57] Jeyasingh, T., Vindhya, P.S., Saji, S.K., Wariar, P.R.S. and Kavitha, V.T., 2019. Structural and magnetic properties of combustion synthesized $A_2Ti_2O_7$(A = Gd, Dy and Y) pyrochlore oxides. *Bulletin of Materials Science*, 42(5), https://doi.org./10.1007/s12034-019-1878-1.

[58] Quader, A., Mustafa, G.M., Abbas, S.K., Ahmad, H., Riaz, S., Naseem, S. and Atiq, S., 2020. Efficient energy storage and fast switching capabilities in Nd-substituted $La_2Sn_2O_7$ pyrochlores. *Chemical Engineering Journal*, 396, https://doi.org/10.1016/j.cej.2020.125198

[59] Zhang, K.Q., Liu, C.G., Li, F.Z., Yang, D.Y., Chen, C., Wu, R.D., Peng, S.M., Li, Y.H. and Zhang, H.B., 2016. Study on the crystal structure of $(Gd_{2-x}Ce_x)Ti_2O_7$ ($0 \leq x \leq 0.8$) pyrochlore. *Advances in Applied Ceramics*, 115(7), 411-416.

[60] Wang, Q., Cheng, X., Li, J. and Jin, H., 2016. Hydrothermal synthesis and photocatalytic properties of pyrochlore $Sm_2Zr_2O_7$ nanoparticles. *Journal of Photochemistry and Photobiology A: Chemistry*, 321, 48-54.

[61] Hongming, Z. and Danqing, Y., 2008. Effect of rare earth doping on thermo-physical properties of lanthanum zirconate ceramic for thermal barrier coatings. *Journal of Rare Earths*, 26, 770-774.

[62] Huo, Y., Qin, N., Liao, C., Feng, H., Gu, Y. and Cheng, H., 2019. Hydrothermal synthesis and energy storage performance of ultrafine $Ce_2Sn_2O_7$ nanocubes. *Journal of Central South University*, 26(6), 1416-1425.

[63] Gadipelly, T., Dasgupta, A., Ghosh, C., Krupa, V., Sornadurai, D., Sahu, B.K. and Dhara, S., 2020. Synthesis and structural characterisation of $Y_2Ti_2O_7$ using microwave hydrothermal route. *Journal of Alloys and Compounds*, 814, https://doi.org/10.1016/j.jallcom.2019.152273.

[64] Sanjeewa, L.D., Ross, K.A., Sarkis, C.L., Nair, H.S., McMillen, C.D. and Kolis, J.W., 2018. Single crystals of cubic rare-earth pyrochlore germanates: $RE_2Ge_2O_7$ (RE= Yb and Lu) grown by a high-temperature hydrothermal technique. *Inorganic Chemistry*, 57(20), 12456-12460.

[65] Trujillano, R., Martín, J.A. and Rives, V., 2016. Hydrothermal synthesis of $Sm_2Sn_2O_7$ pyrochlore accelerated by microwave irradiation. A comparison with the solid state synthesis method. *Ceramics International*, 42(14), 15950-15954.

[66] Verma, S., Rani, S. and Kumar, S., 2018. Crystal structure, morphology and optical behaviour of sol-gel derived pyrochlore rare earth titanates $RE_2Ti_2O_7$ (RE=Dy, Sm). *Journal of Alloys and Compounds*, 750, 902-910.

[67] Wang, S., Li, W., Wang, S., Zhang, J. and Chen, Z., 2016. Deposition of SiC/$La_2Zr_2O_7$ multi-component coating on C/SiC substrate by combining sol-gel process and slurry. *Surface and Coatings Technology*, 302, 383-388.

[68] Xia, J., Lei, L., Dai, X., Ling, J., Li, Y. and Xu, S., 2018. Excitation-dependent multi-color emissions in Yb/Er/Eu: $Gd_2Ti_2O_7$ pyrochlore for anti-counterfeiting. *Materials Research Bulletin*, 107, 213-217.

Instructions for Authors

Current Applied Science and Technology journal contains research reports, articles concerning development work, reviews of the literature and research activities. The objectives are to publish and promote research contributions and innovative work in fields associated with applied science and technology. An electronic journal is provided on the website (https://www.tci-thaijo.org/index.php/cast/index). The editors reserve the right to require revision of the submitted manuscript as a condition for final acceptance.

The institute and the editorial board claim no responsibility for the contents or views expressed by the authors of individual articles. Copying is allowed provided that acknowledgement is made. All articles submitted for publication will be assessed by a group of distinguished.

Ethics:

The journal is committed to maintaining the high level of integrity in the content published and has a Conflict of Interest policy in place. The journal uses plagiarism detection software to screen the submissions. If plagiarism is found, the COPE guidelines on plagiarism will be followed. For more details, please see https://www.tci-thaijo.org/index.php/cast/navigationMenu/view/Publication_Ethics.

Page Charge: Free

Submission of Manuscripts:

Manuscripts must be written in English and submitted online. Manuscripts are to be reviewed (double blinded) by at least 3 referees specializing in relevant fields. Revised manuscripts have to be sent online.

All manuscripts should be submitted to: https://www.tci-thaijo.org/index.php/cast/index

Contact:

Editor of Current Applied Science and Technology
King Mongkut's Institute of Technology Ladkrabang
1 Soi Chalongkrung 1, Ladkrabang District,
Bangkok 10520, Thailand
Tel: 662-329-8136
Fax: 662-329-8221
Email: cast@kmitl.ac.th

Manuscript Preparation Guide:

General: Manuscripts must be typewritten using *Microsoft Word for Windows*, single-spaced with margin set-up (in page set up menu) as follows (see also the document template):

Top Margin	1.5"	Bottom Margin	1.5"
Left Margin	1.5"	Right Margin	1.5"

Good quality printouts using A4 paper size are required. Format should be a single column. Times New Roman font type is required. Font sizes for various text functions are as follows:

Text functions	Size *	Typeface
Title	14 (CT)	Bold
Author and co-authors	11 (CT)	Normal
Address for correspondence	11 (CT)	Normal
Abstract and main text	10 (LJ)	Normal
Section heading and number including "Abstract", "Acknowledgement", "References"	12 (CT)	Bold
Subsection heading and number	11 (LJ)	Bold

* CT = Center Text, LJ = Left Justified.

The corresponding author should be noted (included a Fax number and E-mail address) and indicated with an asterisk. Full postal addresses must be given for all co-authors, keyed to names (if required) by superscripted Arabic numbers.

Paper Length: Should not normally exceed 10 pages including figures and tables
Spelling: American English
Abstract: Should not exceed 250 words
Keywords: Should not exceed 8 keywords
Text: Authors are requested to use the following order when typing:-

All research reports (Full Length or Short Reports): Title, Authors, Affiliations, Abstract, Keywords, Introduction (in reserch papers this must be confined to relevant matters, and must not be a general review of cognate literature), Materials and Methods, Results and Discussion, Conclusions, Acknowledgements, References.

Reviews and Discussion Papers will be considered in any format appropriate to the purposes of the authors, although adherence to the general guidelines described above is encouraged.

Line Art Figures: Figures can be drawn using several packages such as Win Draw®, Auto CAD®, Corel Draw®, VISIO® etc.

Photographs: Actual size photographs are acceptable. However, they can also be put into a text stream using a good-resolution scanner. All photographs must be clear when printed in monochrome.

Graphs: Several packages available today can produce attractive and professional graph presentation. Some also provide curve-fitting function, which can be useful. However, two-dimensional bar charts are preferred. All graphs must be clear in monochrome printing.
Equations and complex expressions: Math CAD®, Math Writer® and Equation Editor® (included in Microsoft Word®) are acceptable for presentation of this type of material.

Citations: Citations in the text should be denoted by numbers between square brackets (i.e. [1, 2], [1-3], [1, 3-8]…) *in the order of first appearance in the text.*

References: References should be numbered to correspond with the text citations. References must be arranged as follows:

Books
Author's surname(s), Initials., Year. *Title of Book*. Edition. (only include this if not the first edition) Place of publication: Publisher.
Example:
[1] Einstein, A. 2019. *Relativity. The Special and the General Theory*. Ghaziabad: Samaira Book Publishers.

Chapters of edited books
Chapter author's surname(s), Initials., Year of book. Title of chapter. In**:** Book editor(s) initials. surnames, ed. or eds. *Title of Book*. Place of publication: Publisher, Chapter number or first and last page numbers.
Example:
[2] Smith, J.E., 2006. Public perception of biotechnology. In: C. Ratledge and B.Kristiansen, eds. *Basic Biotechnology*. Cambridge: Cambridge University Press, pp. 3-24.

E-books
Author's surname(s), Initials., Year, *Title of Book*. [e-book] Place of publication: Publisher. Available through: include e-book source/database, web address or URL.
Example:
[3] Willey, J., Sherwood, L. and Woolverton, C.J., eds. 2013. *Prescott's Microbiology*. 9th ed. [e-book] New York: McGraw-Hill. Available through: Libribook website < www.libribook.com>

Journal articles
Author's surname(s), Initials., Year. Title of article. *Full Title of Journal,* Volume number (Issue number), Page numbers.
Example:
[4] Ross, A.B., Junyapoon, S., Jones, J.M., Williams, A. and Bartle, K.D., 2005**.** A study of different soots using pyrolysis– GC– MS and comparison with solvent extractable material. *Journal of Analytical and Applied Pyrolysis*, 74(1-2), 494-501.

In case of online journal articles without page number:
Author's surname(s), Initials., Year. Title of article. *Full Title of Journal,* Volume number (Issue number), DOI**-**based link.
Example:
[5] Tanasupawat, S., Phongsopitanun, W., Suwanborirux, K., Ohkuma, M. and Kudo, T. 2016. *Streptomyces actinomycinicus* sp. nov., isolated from soil of a peat swamp forest. *International Journal of Systematic and Evolutionary Microbiology*, 66(1), https://doi.org/10.1099/ijsem. 0.000716.

Proceedings
Author's surname(s), Initials., Year. Title of article. *Full Title of Proceedings*, Place of Conference, Date, page numbers.
Example:
[6] Thanaboripat, D., Ruangrattanametee, V. and Srikitkademwat, K., 2010. Control of growth and aflatoxin production of aflatoxin producing fungi in corn by salts. *Proceedings of the 8th International Symposium on Biocontrol and Biotechnology*, Pattaya, Thailand, October 4-6, 2010, pp. 283-289.

Patent
Inventor surname(s), Initial(s)., Assignee, Year. *Title*. Place. Patent number (status, if an application).
Example:

[7] Leonard, Y., Super Sports Limited, 2008. *Tin Can Manufacture and Method of Sealing*. Canada. Pat. 12,789, 675.

Dissertation
Author's surname, Year of publication. *Title of Dissertation*. Level. Official name of University, Country.
Example:
[8] Sukcharoen, O., 2017. *Inhibitory Effect of Plant Essential Oils on Growth and Aflatoxin Production by Aspergillus flavus IMI 242684 and Aspergillus parasiticus IMI 283883.* Ph.D. King Mongkut's Institute of Technology Ladkrabang, Thailand.

Websites
Authorship or Source, Year. *Title of Document*. [online] Available at: include web site address/URL (Uniform Resource Locator).
Example:
[9] NHS Evidence, 2003. *National Library of Guidelines*. [online] Available at: http://www.library.nhs.uk/guidelines.

Acknowledgements: These should be as brief as possible.

Proofs:
Proofs will be sent to the corresponding author and *must* be returned as soon as possible. Corrections should be restricted to typesetting errors.

Copyright:

Page Numbering:
All pages must be sequentially numbered, preferably by using the automatic page numbering function on your computer.

Copyright Material:
It is the authors' responsibility to obtain written permission from the copyright holder (usually the book or journal publisher) to use copyright material, and to send a copy of this consent with the manuscript. This consent is not normally denied but it is an international legal requirement that it be obtained.

Note:

Please note that authors are urged to check their proofs carefully before returning, since the inclusion of late corrections cannot be guaranteed.

Author(s) are responsible for ensuring that the submitted manuscript fully meets the requirements specified in the above Instructions. Manuscripts which fail to do so will be returned unedited to the Author(s) for correction in accordance with the above requirements, before they can be submitted to the processes of Referee evaluation.

1.5"

TEMPLATE

Enter title here (14 PT type size, Title Case, Bold, Centered)

Author Information entered here:
Name (in full)

Affiliation
City
Country
(11 pt type size, upper and lower case, centered under the title)

How to Use This Document Template

Insert the information in your document in place of the text here. For the body of your document, use Times New Roman 10 pt. Font, upper and lower case, double-spaced. Allow an extra half space above a line containing superscripts and/or below a line containing subscripts. The whole text should be left-justified. The headings should be 12 pt size, uppercase, bold and centered.

1.5" 1.5"

Abstract (12pt)

Maximum 250 words here. (10 pt)
.....
.....
.....
.....
.....

Keywords: (10 pt)

Maximum of 8 words

1. Introduction (12 pt)

Clearly explain the nature of the problem, previous work, purpose, and contribution of the paper (10 pt).
.....
.....
.....
.....
.....

*Corresponding author: Tel.: ..... Fax: .....
E-mail: .....

1.5"

2. Materials and Methods (12 pt)

.....
.....
.....
.....

3. Results and Discussion (12 pt)

.....
.....…

4. Conclusions (12 pt)

Clearly indicate advantages, limitations and possible applications (10 pt).
.....
.....

5. Acknowledgements (12 pt)

A brief acknowledgement section may be included here (10 pt).
.....
.....

References (12 pt)

References must be numbered in the order cited in the manuscript and indicated in the text by a number in square brackets (e.g. [1, 2]) (10 pt).

Example of References must be arranged as follows:

[1] Barker, R. Kirk, J. and Munday, R.J., 1988. *Narrative Analysis*. 3rd ed. Bloomington: Indiana University Press.
[2] Samson, C., 1970. Problems of information studies in history. In: S. Stone, ed. *Humanities Information Research*. Sheffield: CRUS, pp. 44-68.
[3] Carlsen, J. and Charters, S., 2007. *Global Wine Tourism*. [e-book] Wallingford: CABI Pub. Available through: Anglia Ruskin University Library website <www.libweb.anglia.ac.uk>.
[4] Ross, A.B., Junyapoon, S., Jones, J.M., Williams, A. and Bartle, K.D., 2005. A study of different soots using pyrolysis–GC–MS and comparison with solvent extractable material. *Journal of Analytical and Applied Pyrolysis*, 74*(*1-2*)*, 494-501.
[5] Thanaboripat, D., Ruangrattanametee, V. and Srikitkademwat, K., 2010. Control of growth and aflatoxin production of aflatoxin producing fungi in corn by salts. *Proceeding of the 8th International Symposium on Biocontrol and Biotechnology*, Pattaya, Thailand, October 4-6, 2010, 283-289.

[6] Leonard, Y., Super Sports Limited., 2008. *Tin Can Manufacture and Method of Sealing*. Canada. Pat. 12,789, 675.
[7] Richmond, J., 2005. *Customer Expectations in the World of Electronic Banking: a Case Study of the Bank of Britain.* Ph.D. Anglia Ruskin University.
[8] NHS Evidence, 2003. *National Library of Guidelines*. [online] Available at: http://www.library.nhs.uk/guidelines

Note:

Tables and Graphs: Minimum of 10 pt type size, all captions should be upper and lower case, centered. Each table and figure must be on a separate page (or pages if required) , ***and must be embedded in the text.***

Illustrations and Photographs: Halftones, minimum of 10 pt type size, bold, captions should be in upper and lower case, centered. Images must be computer-designed with clearly visibility.

Contact

Editor of Current Applied Science and Technology
King Mongkut's Institute of Technology Ladkrabang
1 Soi Chalongkrung 1, Ladkrabang District
Bangkok 10520, Thailand
Tel: 662-329-8136 Fax: 662-329-8221
E-mail: cast@kmitl.ac.th
Website: https://www.tci-thaijo.org/index.php/cast/index

KING MONGKUT'S INSTITUTE OF TECHNOLOGY LADKRABANG
1 Soi Chalongkrung 1, Ladkrabang District Bangkok 10520, Thailand
Tel: 662-329-8136 Fax: 662-329-8221
E-mail: cast@kmitl.ac.th
Website: https://www.tci-thaijo.org/index.php/cast/index